A multi-level mechanical study of hypocotyl growth in the dark

Yuanjie Chen

Wolfson College, University of Cambridge

09/2018

This dissertation is submitted for the degree of Doctor of Philosophy

DECLARATION

This dissertation is the result of my own work and includes nothing which is the outcome of work done in collaboration except as declared in the Preface and specified in the text.

It is not substantially the same as any that I have submitted, or, is being concurrently submitted for a degree or diploma or other qualification at the University of Cambridge or any other University or similar institution except as declared in the Preface and specified in the text. I further state that no substantial part of my dissertation has already been submitted, or, is being concurrently submitted for any such degree, diploma or other qualification at the University of Cambridge or any other University or similar institution except as declared in the Preface and specified in the text.

It does not exceed the prescribed word limit of 60000 words for the Degree Committee for the Faculty of biology School of the Biological Sciences

SUMMARY

Dark-grown hypocotyls of *Arabidopsis thaliana* exhibit a striking wave of cell elongation which moves acropetally from the base to the tip of the organ over time. The combined effect of this wave of cell elongation is a pattern of organ elongation. It was aimed to understand the coordination of cellular growth and growth mechanisms through multi-level studies including modelling approaches, transcriptome analysis and hormone analysis.

The first aim of this thesis was to describe the hypocotyl growth at a cellular level, including cell length and diameter measures, over a 72-hour period after germination. It was observed that the 'wave of growth' is exhibited only in the cell length dimension, not in diameter. The precise position and magnitude of the elongation wave was quantified as a foundation for subsequent aims. Microtubules were quantified and co-ordinated transverse alignments at inner walls was found to be associated with cell growth rate.

In the second aim of this thesis a dynamic, intrinsic, model was built based on the physical factors controlling cell elongation, using a bottom-up approach. Using a chain of cell units, each modelled with a modified Lockhart model, hypocotyl elongation *in silico* mirrored experimental data. The model successfully simulated behaviours of cell size, turgor pressure and yield stress over time and it responded to simulated parameter changes (representing physical factors) reasonably well. The model performance was compared to experimental manipulations. A concept of 'bond energy distribution' was introduced to the model in relation to yield stress, and it suggested that a change in the cell wall structure, or bond distribution, can be an efficient way of controlling cell growth in comparison to change in physical factors. The model also implied that a quantitative 'chemical signal' may exist and can be involved in the initiation of cell growth and thus the acropetal wave.

For the next aim, an empirical model of hypocotyl cell growth was built based on data of cell sizes up to 72 hours post germination. Using data fitting and parameter extrapolation, the model predicted the progression of cell sizes until 196 hours post germination, when the hypocotyl elongation was terminating. The prediction fitted well with the measured hypocotyl growth at organ level. The Probit function had the best performance among the three sigmoidal functions selected for fitting and parameter extrapolation, which is a model describing the transition from cellular to organ level growth.

The fourth aim of this thesis was to investigate which genes, related to physical growth parameters, were related to cell growth. An RNAseq experiment was conducted and analysed which yielded differentially expressed genes from slow and fast-elongating regions of the hypocotyl (non-wave vs

wave) at three time points (24/36/48HPG). Several groups of genes that were involved in cell wall modification and hormones were studied in detail and those with differential expression within the wave were identified.

The final aim of this thesis involved investigating a hormonal signal for the acropetal wave and cell growth initiation. The intrinsic cell model in Aim 2 indicated the need for a growth signal to start cell elongation. Hormones are strong candidates for growth signals and the transcriptome analysis in Aim 4 indicated that gibberellin may be a good candidate. GA levels were examined in the hypocotyl using the nlsGPS1 GA-biosensor. It was found that the level of sensor emission ratio qualitatively correlated well with the cellular growth rates, indicating the existence of global control on cell growth through chemical signals.

ACKOWLEDGEMENTS

Firstly, I would like to express my sincere gratitude to my supervisor Dr. Siobhan Braybrook for the continuous support of my Ph.D study and related research. Her guidance helped me in all the time of research and writing of this thesis.

My sincere thanks also goes to Dr Firas Bou Daher, who guided me in all aspects of my research. I thank everyone in the Braybrook Group, for the stimulating discussions and all the fun we had in the last three years.

Besides the Braybrook Group, I would like to thank Dr Sebastian Ahnert, who behaved as my first supervisor and provided support for me at Cambridge after Siobhan and the Braybrook Group moved to UCLA in 2017.

I would also like to thank Dr Alexander Jones and Dr Annalisa Rizza, who provided me an opportunity to join their team at SLCU in 2018, and who gave access to the material and research facilities. Without their precious support it would not be possible to conduct this research.

Last but not the least, I would like to thank my family and friends, for supporting me spiritually throughout writing this thesis and my life in general.

PUBLICATION

Daher FB, Chen Y, Bozorg B, Clough J, Jonsson H, Braybrook S. Anisotropic growth is achieved through the additive mechanical effect of material anisotropy and elastic asymmetry. *Elife*. 2018;7:e38161:316364. doi:10.1101/316364

Table of Contents

LIST OF ABBREVIATIONS 12

CHAPTER 0: INTRODUCTION 13

OVERVIEW OF THE THESIS 13

GROWTH OF THE DARK-GROWN HYPOCOTYL AND EPIDERMAL CELLS 13

ROLE OF THE PRIMARY CELL WALL IN CELLULAR GROWTH 14

MODELLING PLANT GROWTH 14

TRANSCRIPTOME ANALYSES OF THE DARK-GROWN HYPOCOTYL 14

LEVEL OF GA IN THE DARK-GROWN HYPOCOTYL 15

CHAPTER 1: THE GROWTH CHARACTERISTICS OF THE *ARABIDOPSIS THALIANA* HYPOCOTYL 16

SUMMARY 16

INTRODUCTION 16

The *Arabidopsis thaliana* hypocotyl 16

Light-grown vs Dark-grown seedlings 17

Structure of the primary cell wall 17

Microtubule and cellulose orientations 18

Xyloglucan and the XTH activities 19

METHODS 20

Sample preparation 20

The Inducible *PME5* over-expressor 22

Characterising organ level growth 22

Characterising the cellular level growth 24

Chemical treatments 24

Characterising the Microtubule (MT) orientations 24

Generation of the *XTH* transgenic lines 27

Verifying the inducible *XTH* genes (by L. Dedow, Braybrook Lab, UCLA) 28

RESULTS 28

Stiffer cell walls reduced organ growth rate and final length 28

The cellular level growth profile showed a progressive, acropetal wave of growth 31

The acropetal wave of growth was anisotropic 34

The acropetal wave of growth travelled uniformly and increased its magnitude over time 36

The microtubules were dynamic over time, and their predicted ‘strength’ in both longitudinal and transversal directions affected growth anisotropy 38

Estradiol induced XTHs showed a phenotype of longer hypocotyl in dark only 5 days post germination 40

DISCUSSION 42
The organ level hypocotyl growth possesses a non-symmetric sigmoidal pattern 42
The quantified cellular wave of growth of the dark-grown hypocotyl 43
Anisotropic growth starts at the beginning of the wave 43
Important role of the pectin chemistry 43
The role of microfibrils in the plant cell wall 44
The function of XTH in the cell wall 45
Problems of quantifying the cell wall properties using the microscope images 45
The 'pause' in the growth from 18 HPG till 24 HPG may due to growth in radial direction 46
CHAPTER 2: AN INTRINSIC MODEL OF PLANT GROWTH AT THE CELLULAR LEVEL 47
SUMMARY 47
INTRODUCTION 47
Physical deformation of the cell wall 47
Turgor pressure 48
The cell wall 48
Linking wall composition to mechanics 49
Existing growth models 50
METHODS 52
Turgor pressure measurement and calculation 52
Atomic force microscopy (Experiment performed by F. Bou Daher) 54
Young's modulus calculation 54
Modelling 54
RESULTS 60
Hypocotyl epidermal cells exhibited a sigmoidal-like elongation pattern in length but not in width 60
Turgor Pressure decreased over time, with a large reduction during the fast elongation period 61
The cell wall became softer during the fast elongation period 62
The model simulates the dynamic patterns of cell size, turgor pressure and the wall stiffness 64
The cell wall stiffness showed a positive correlation with the turgor pressure and a negative correlation with the growth rate, when being modified artificially 66
Growth is inhibited when the turgor pressure is slightly reduced 69
A bond energy distribution with a sharper peak is more resistant to change in bond energy 70
Mimicking the behaviour of cellulose reorientation by changing irreversible bonds in the cell wall slows down the growth 72
Increasing the wall thickness leads to reduced growth 72
DISCUSSION: 73

Is hypocotyl epidermal cell growth perfectly sigmoidal? 73
Turgor vs cell wall, how do they coordinate cell growth? 74
Insights from the model: The physical properties of the cell wall and the role played by the bond energy distribution 77
Limitations of the model 78
Beyond the hypocotyl epidermal cells 79
CHAPTER 3: AN EMPERICAL MODEL OF THE WAVE OF GROWTH OF THE HYPOCOTYL EPIDERMAL CELLS 80
SUMMARY 80
INTRODUCTION 80
The Three Sigmoidal Functions 81
METHODS 81
The Four Parameters (coefficients) 82
Fitting the sigmoidal function 83
Parameter extrapolation 83
Prediction validation 83
RESULTS 84
The initial fitting of the lower hypocotyl cells re-demonstrated the cellular wave of growth 84
Value of the parameters were stable for cells with indices<11 86
Constraining parameter $\boldsymbol{c}$, a sigmoidal growth curve for the hypocotyl was predicted 87
A linear extrapolation was more appropriate than a polynomial extrapolation for parameter $\boldsymbol{a}$ and $\boldsymbol{b}$ 89
The Logistic function and its parameter extrapolation did not attain a good prediction of hypocotyl growth 92
The Loglog function was unable to outperform the Logistic function 93
The Probit outperformed the other two sigmoidal functions 94
The Probit model can be further improved by reducing extrapolated parameters 96
DISCUSSION 98
The Probit-fitted data of cellular growth predicts a hypocotyl growth closely matched with the measured data. 98
The pattern of cell-level growth may not imply the same pattern for the organ growth 98
The hypocotyl cellular acropetal wave of growth increases in magnitude 99
Cell growth interval by index is not linear in time 100
Why is there a wave of growth? 100
CHAPTER 4: A STUDY OF DARK-GROWN HYPOCOTYL GROWTH AT THE TRANSCRIPTOME LEVEL 102
SUMMARY 102
INTRODUCTION 102

METHODS:.....104
Sample harvesting and RNAseq preparation.....104
Sample similarity verification.....106
Counts normalisation verification.....106
Agrigo and GO analysis.....106
Categorisation approach 1: RNA levels across three time points.....107
Categorisation approach 2: Study across the two regions, top and bottom.....111
FAMILIES OF GENES RELATED TO GROWTH.....114
GA genes.....114
Introduction.....114
The GA related genes tend to be more expressed over time.....116
The GA related genes tend to be more expressed in the fast-growing region of the hypocotyl120
GA biosynthesis genes expressed slightly before the cell growth wave.....122
GA receptors are expressed slightly behind the growth wave.....127
GA catabolism genes are not highly active during the early hypocotyl elongation phase.....128
Discussion.....130
The Auxin-related genes.....133
Introduction.....133
The TAA1 became less expressed at the bottom region over time, and all the TARs were less expressed.....136
Most of the YUC genes were more expressed at the top region of the hypocotyl.....137
The *AO* showed different expression pattern with the *TAA1* and *YUC* genes.....138
The TIR1/AFB and ABP1 genes were not differentially expressed between the two regions in general.....139
Most of the Aux/IAA genes were more expressed at the bottom region, and increased in expression level over time.....141
Most of the ARF genes were more expressed at the top region, and their expression at the bottom region decreased over time.....141
The auxin up-regulated genes were more active at the bottom region of the hypocotyl.....143
No consistent expression pattern was seen for the *PIN* genes.....145
The PILS genes were more expressed at the bottom region, and increased in expression level over time.....145
Discussion.....146
The *PECTIN METHYLESTERASE* Genes.....148
Introduction:.....148
PME and PMEI genes tend to be more expressed in the growing region.....149

Genes encoding type I PME had higher expression in the dark-grown hypocotyl during our experiment compared to those encoding type II PME 151
Discussion 153
The *CELLULOSE SYNTHASE* genes 155
Introduction: 155
The CESAs involved in cellulose biosynthesis in the primary cell wall possess consistent expression pattern 156
Discussion 157
The *XYLOGLUCAN ENDOTRANSGLUCOSYLASE/HYDROLASE(XTH)* Genes 158
Introduction 158
The *XXT* genes were downregulated over time at the bottom region but not at the top region 159
Most of the highly active XTH genes were more expressed at the bottom region, and highly expressed during the rapid elongation period 160
Discussion 161
GENE ONTOLOGY ANALYSIS 162
Categorisation approach 1: Identifying interesting categories 162
Genes up-regulated over time 163
Genes downregulated over time 163
Genes with changing expression pattern over time 164
Genes act as a growth trigger 166
Genes with expression pattern correspond to the rapid acceleration phase 167
Discussion 169
Categorisation approach 2: Identifying interesting categories 171
Genes expressed more at bottom only at early time (category b23) 172
Discussion 174
Gene expression corresponding to a wave travelling early and fast (category b22) 175
Inversed expression pattern with b22 (category b6) 175
Gene with expression pattern a step ahead of the growth wave (category b26 and b25) 175
Inversed expression pattern with b26, b25 (category b2, b3) 177
Gene with expression pattern a step behind the growth wave (category b18) 178
Inversed expression pattern with b18 (category b10) 180
Discussion 181
Genes expressed more at the bottom region (category b27) 183
Genes expressed more at the top region (category 1) 184
Discussion 186
FINAL DISCUSSION ON TRANSCRIPTOME ANALYSES 188

CHAPTER 5: THE GIBBERELLIN IN THE DARK GROWN HYPOCOTYL 191
SUMMARY 191
INTRODUCTION 191
METHODS 192
Seedling preparation: 192
Imaging with fluorescence microscopy 192
Image processing and analysis: 193
Extraction and ontology of genes supporting how GA regulate growth 193
RESULTS 194
The patterns of GA-level over time show spatial patterns along the hypocotyl 194
The GA level across the hypocotyl corresponds well with the local cellular growth rate 195
GA appears to act as a precursor to growth, correlates with growth rates within 12 hour windows and correlation decays by 24 hours 198
The GA level had the closest match with the cellular relative growth rate in the interval from 6 hours before to 6 hours after its measurement 200
Fast growing regions of dark-grown hypocotyls share common gene expression profiles with seeds at germination 202
DISCUSSION 204
The level of GA is a good indicator of cellular growth rates 204
Activities of GA responsive genes in the hypocotyl 205
Is GA the 'chemical signal' regulating the growth? 206
CHAPTER 6: FINAL DISCUSSIONS 208
The anisotropic growth of hypocotyl cells 208
The sigmoidal growth curves from plant cells to plant organs 208
Heterogeneous growth of the epidermal cells 210
Function of cell wall modification enzymes 210
Can we build a perfect intrinsic model of plant cell growth? 212
The chemical signal revisited 212
How can we 'squeeze' the most out of our current data? 213
Further questions 216
BIBLIOGRAPHY 218
APPENDICES (Supplementary) 231

LIST OF ABBREVIATIONS

mYFP: Myristoylated-Yellow Fluorescent Protein

GA: Gibberellic acid

PME/PMEI: PECTIN METHYLESTERASE/PECTIN METHYLESTERASE INHIBITOR

CESA: CELLULOSE SYNTHASE

XTH: XYLOGLUCAN ENDOTRANSGLUCOSYLASE/HYDROLASE

XXT: XYLOGLUCAN XYLOSYLTRANSFERASE

KAO: ENT-KAURENOIC ACID OXIDASE

GID: GA INSENSITIVE DWARF

TAR: TRYPTOPHAN AMINOTRANSFERASE RELATED

IPA: Insole-3-pyruvic acid

IPD: IPA DECARBOXYLASE

IAA: Indole-3-acetic acid

Aux/IAA: AUXIN/INDOLE ACETIC ACID

TAA: TRYPTOPHAN AMINOTRANSFERASE OF ARABIDOPSIS

AO: ALDEHYDE OXIDASE

ARF: AUXIN RESPONSE FACTOR

ABP: AUXIN-BIDING PROTEIN

PIN: PIN-FORMED

PILS: PIN-LIKES

DMSO: dimethyl sulfoxide

CHAPTER 0: INTRODUCTION

OVERVIEW OF THE THESIS

Elongation of the dark-grown *Arabidopsis thaliana* hypocotyl is studied in this thesis. The thesis aims to understand this growth at different levels: from the single cell to the complex multi-tissue organ. Each chapter corresponds to a different aspect of growth of this. In Chapter 1, growth is characterised in detail at the cell level, and the cell wall properties and structures are discussed in relation to growth. In Chapter 2, an intrinsic model of physical factors involved in single cell expansion is constructed. In Chapter 3, an empirical model is built for the hypocotyl elongation, based on growth of epidermal cells. In Chapter 4, transcriptome analyses are performed on slower and faster growing regions of the hypocotyl, and selected genes directly involved in growth are studied and discussed. In Chapter 5, the level of gibberellic acid, a potential 'growth signal' in dark-grown hypocotyl is quantified over time.

A better multi-level understanding of the hypocotyl growth is gained from this study. As the study was conducted from different angles, detailed introduction is provided in each of the chapters, and a broad background of this study is presented here.

GROWTH OF THE DARK-GROWN HYPOCOTYL AND EPIDERMAL CELLS

Hypocotyl elongation starts immediately after germination, and its successful growth is crucial to the plant's establishment. The *Arabidopsis* hypocotyl was chosen as the key organ to be studied, characterized and modelled in this thesis. The hypocotyl has been used as a model organ and its growth was quantified[1]. However, the growth was not quantified in detail at the cellular level. Non dividing files of epidermal cells exist in the hypocotyl and their growth can be used as a reflection of regional hypocotyl growth[1]. An acropetal wave of growth was observed in the hypocotyl[1]: basal hypocotyl epidermal cells grow first right after germination, and the upper cells start growing later. The position, and travelling speed of the wave was not known. Furthermore, how this wave of growth affected each cell in terms of their growth rate and final length was also not known.

Hypocotyl epidermal cells grow anisotropically, in a cylindrical shape. It was proposed that such anisotropic growth was mainly due to the orientation of cellulose microfibrils[2][3][4][1]. Yet, cell growth anisotropy was not quantified in detail nor was cellulose orientation, and it was not clear whether cellulose microfibrils were the only factor controlling the growth anisotropy.

ROLE OF THE PRIMARY CELL WALL IN CELLULAR GROWTH

The cell wall is a stiff material which resists turgor pressure but also controls growth by adjusting its mechanical properties[5][6]. The structure of the primary cell wall is complex, and cell growth can be controlled by modifications in isotropic pectin chemistry[7] as well as the alignment of cellulose microfibrils[2][3]. Other components in the primary cell wall, such as hemicellulose, were proposed to be functional in tethering the cellulose[4], but the role they play in regulating plant cellular growth is not clear. It was shown that wall modifying enzymes can greatly affect pectin matrix gelling and hence change the growth at both cellular and organ level[5][8][9], and hence the chemistry and structure of the cell wall is important in growth rate and growth anisotropy.

MODELLING PLANT GROWTH

A variety of models were built for plant growth which could be related to hypocotyl elongation. At the single cell level, modelling focused on the relationships between turgor and wall properties[10][11],thermodynamics equilibrium[12], energy conservation[13], fibre layers[14], mechanical properties and geometrical transformations[15][16][17][18], etc. Yet there was no growth model aimed to investigate the change of physical growth factors over time and how they would affect cell growth rates.

At the organ level, many sigmoidal functions have been used to fit plant growth[19][20][21], aimed at capturing the behaviour of plant growth: an initial exponential acceleration phase, a linear elongation phase, and a saturation phase. There was no predictive model of organ growth based on cell data, and there was no model focused on the acropetal wave of growth in the hypocotyl.

TRANSCRIPTOME ANALYSES OF THE DARK-GROWN HYPOCOTYL

In the dark-grown hypocotyl, changes in gene expression levels over time in whole seedlings were studied previously using microarray analysis at 45, 48, 52 and 55 hours post incubation[22]; this study investigated the transcriptome level difference around two days post germination, and identified overexpression of cell wall remodelling genes during the growth acceleration. Another transcriptome analysis focused on gibberellic acid (GA) identified GA-regulated and GA-response genes during *Arabidopsis* seed germination[23], indicating the importance of GA in seedling development. Yet differentially expressed genes between fast-growing and slow-growing regions of the hypocotyl were

not revealed by either experimental design. No analysis at the transcriptome level had been conducted to address the mechanisms behind the hypocotyl's wave of growth and to date no one has taken advantage of this wave to study differentially expressed genes in different regions of the hypocotyl.

LEVEL OF GA IN THE DARK-GROWN HYPOCOTYL

GA is an important hormone found in plants, fungi and bacteria. In higher plants, it regulates important aspects of growth including seed germination and flowering. Previously the level of GA was quantified using the nlsGPS1 sensor[24] in both dark and light-grown seedlings at 3 days post incubation. In the dark, a gradient of GA level in the epidermal cells was seen along the hypocotyl, with basal cells having higher nlsGPS1 emission ratio, and it was proposed that there was a positive relationship between the bioactive GA and the cell size[24]. How the level of GA presented early during elongation was not explored, nor was GA change over time, and the non-reversibility of the sensor did not allow exact level of GA to be detected precisely once the level of GA decayed.

CHAPTER 1: THE GROWTH CHARACTERISTICS OF THE *ARABIDOPSIS THALIANA* HYPOCOTYL

This work has been partially published in eLife[7]. All work contained here was performed by Yuanjie Chen unless otherwise indicated.

SUMMARY

The dark-grown *Arabidopsis* hypocotyl is the fundamental organ studied in this thesis, and its growth is characterised in this chapter. Hypocotyl growth was characterised using an automatic length extraction program on sequences of image data. Cell wall elasticity was found to be a major factor affecting hypocotyl elongation. A stiffer wall induced a significant suppression of growth. The cellular level growth of the hypocotyl epidermis was characterised using a yellow-fluorescent membrane marker. Elongation of the hypocotyl epidermal cells progresses as a 'wave of growth' in cell length alone. The position and magnitude of the wave was quantitatively defined. As a proxy for cellulose orientation, microtubule orientations were also studied and the 'strength' in both longitudinal and transversal orientations affect the growth anisotropy, where the 'strength' of alignment was computed from the microtubule alignments and orientations. Fast elongating cells tends to have lower strength in the longitudinal orientations.

It was also shown that the xyloglucan endotransglycosylase/hydrolase (XTH) activities may promote hypocotyl elongation at later growth stages.

INTRODUCTION

The *Arabidopsis thaliana* hypocotyl

The hypocotyl is an organ that allows the seedlings to extend in height, pushing the shoot tip out of the soil shortly after germination[25]. Its successful growth is key to establishing the plant after germination, The *Arabidopsis* hypocotyl elongation is accomplished by cell elongation, unlike many other organs where the growth is accomplished by cell division[26][27]. It was suggested that the very few cell divisions were limited to stomata formation in older hypocotyls[1]. Heterogenous epidermal cell growth in the dark was observed where elongation of basal hypocotyl cells began earlier than cells located at middle or upper parts of the hypocotyl[1]. Observations made during this thesis indicated that stomatal-producing cell files exhibit transverse anti-clinal divisions after germination[7].

A file of non-dividing hypocotyl cells contains 17±2 cells (experimental observation, n>200). The non-dividing files of cells were analysed in this thesis allowing the behaviour of each cell at defined positions of the hypocotyl over time to be characterised.

Light-grown vs Dark-grown seedlings

Arabidopsis hypocotyls normally grow for 5-7 days, with the fastest growth occurring between 48-96 hours post germination (HPG)[1]. The light-grown *Arabidopsis* hypocotyls behave very differently from those grown in the dark. In a normal light-grown condition, the final length a hypocotyl reaches is about 1.7mm with the longest cells (about 0.13mm in length) located in the middle of the hypocotyl[1]. In contrast, hypocotyls grown in the dark can grow faster and longer, reach approximately 20mm in 5-7 days[1]. The differences in length among epidermal cells are also bigger for the seedlings grown without the light. I focus on the dark-grown seedlings as the data is more evident, with smaller relative errors, and there is an acropetal wave of growth in the dark-grown hypocotyl but not in the light-grown hypocotyl. In the dark, images were taken with infra-red images (low resolutions) or under green light (higher resolution), as plants were less sensitive to green light spectrum (500-600nm)[28].

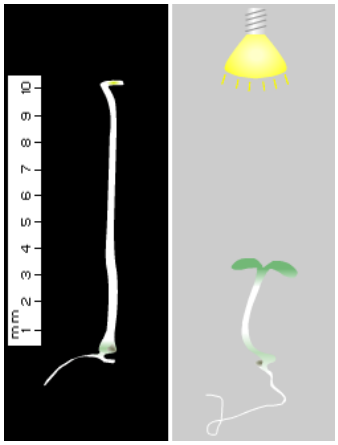

Figure 1.1 Left: Hypocotyl elongation is different in the dark and the light, post germination. Left: Hypocotyl grown in the dark. Right: Hypocotyl grown in the light. Adapted from[29].

Structure of the primary cell wall

The cell wall has a special role in the plant: it is strong enough to resist the high turgor pressure but also it needs to allow cell growth at the right time. The growing cell wall has crystalline cellulose

microfibrils that are embedded in a matrix of complex polysaccharides[30]. One class of important matrix polysaccharide are pectins which are complex polysaccharides consisting mainly of esterified D-galacturonic acid resides in an alpha-(1-4) chain[31]. Pectin gelling is largely affected by changes in the degree of methyl-esterification of the pectin backbones and the availability of calcium ions[32]. De-methylation makes the chains negatively charged and then Ca^{2+} ions are able to bond to two chains and facilitate pectin backbone cross-linking via Calcium Bridges[5]. Ca^{2+}-cross-linked pectin gels exhibit strain stiffening and this process makes the cell wall harder to expand[33]. PECTIN METHYL ESTERASE (PME) is a cell wall modifying enzyme that removes methyl groups from pectin. PME has diverse roles in plant development: it is involved in cell separation, seed germination, root tip elongation, leaf growth polarity, internode stem growth and so on[34]. Most importantly here, PME is involved in changing in cell wall stiffness which is supposed to retard growth. It was shown that PECTIN METHYLESTERASE 5 leads to decreased pectin methyl-esterification[5], whereas PECTIN METHYLESTERASE INHIBITOR 3 leads to increased methylesterification[5]. As such, changes in the pectin matrix gelling can have large effects on growth[8][9], such as the meristem formation[5].

Microtubule and cellulose orientations

Unlike pectin, cellulose microfibrils (MF) do not provide isotropic strength. Cellulose microfibrils are embedded in the pectin matrix and they provide strength and mechanical rigidity to the cell wall. The cellulose microfibril is a fine fibril which forms to increase cell strength during growth, and eventually wraps the cell in a microfibril layer[35][4][36]. The MF are generally considered to be strong and inextensible[37][36], providing strength in the direction where they are aligned[38][39]. Cellulose is deposited in the cell wall through the action of cellulose synthase complexes located on the cell membrane[40]. Cellulose synthase enzyme synthesises cellulose by catalysing the chemical reaction to form a chain of (1⟶4)-β-D-glucosyl residues[41]. MF are bonded to the pectin matrix via H-bonding to xyloglucans[6], and it plays an important role holding the cell wall together as well as maintaining the anisotropy. Inhibition of cellulose synthesis by DCB inhibits hypocotyl elongation but promotes the radial expansion[42], and epidermal cells cannot maintain their anisotropy (Fig. S1.4). Mutants loss function of cellulose synthase shows growth defect in the dark[42].

With a few exceptions[43][44][45][46], cortical microtubules (MT) are believed to direct cellulose biosynthesis by guiding the trajectories of cellulose synthase complexes in the plasma membrane[47], since the two seem to be correlated in most cases[3][2][39][48]. As imaging cellulose orientation dynamically is difficult, one can image MT orientation as a proxy[3][2]. Microtubules are a component of the cytoskeleton and they are important in a number of cellular processes including maintaining

the cell structure, provide platforms for intracellular transport and control the chromosome separation[49]. The orientation of microtubules of an *Arabidopsis* hypocotyl cell can be seen using *35::GFP MICROTUBULE ASSOCIATED PROTEIN4 (35::GMAP4)*.

Previous studies showed a change of MT orientation over time in the hypocotyl epidermis of 2- and 3-day old seedlings[3], differences of MT orientations at different locations of a hypocotyl[50], and differences of the MT orientation between the inner face and outer face of an epidermal cell [2]. It was suggested that the MT alignment on the inner wall was a more stable predictor of growth anisotropy, whereas outer-wall alignment was more sensitive to elongation rate[2]. In onion bulb epidermal cells, growth rate changed corresponding with a changed MF orientation[51]. Yet correlation between net MF and degree of growth anisotropy is poor[51].

Xyloglucan and the XTH activities

Xyloglucan is the main component of hemicellulose in *Arabidopsis* cells[52]. Xyloglucan binds at the surface of the cellulose microfibrils[53][54], and provides tension resistance to the cell wall together with the cellulose microfibrils after forming a tethered network[47][30]. It was previously reported that the majority of cellulose was natively coated with xyloglucan[55][53] but more recent experiments showed that only <8% cellulose surface area was coated with xyloglucan[4]. It was shown using a creep test that a minor part of structurally important xyloglucan was tightly contacted between microfibrils and served as load-bearing tether[56]. During the cellular growth, division and differentiation, the primary cell wall needs to be remodelled[57] and the XYLOGLUCAN ENDOTRANSGLUCOSYLASE/HYDROLASES (XTHS) are important enzymes modifying the architecture of the cell wall structure during wall synthesis[58]. Xyloglucan is cut and re-joined by through endotransglucosylase action[59] or the hydrolase action[60], and cell expansion can be affected by both of the actions. Many evidence has suggested connections between the XTH activity and cell growth[61][62][63][64], and the expression of *XTH* genes are often found to be high at sites where cell elongation or division process is rapid[65][66]. In addition, XTHs may also play a role in integrating the newly synthesised xyloglucans into the cell wall[67]. In addition to elongation growth, XTHs also appear to be involved in other developmental processes such as response to wind or touch[68], cell wall degradation[69], mobilization of seed reserves[70], formation of vascular tissue[65][60], etc.

METHODS

Sample preparation

Seeds were sterilised using 70% and 100% ethanol, then transferred to ½ Murashige & Skoog media (MS, 2.2g B5 vitamins, 15g sucrose, 8g plant agar, per 1L, pH:5.7), wrapped in foils and placed at 4°C for 2-4 days. Seeds were then transferred to a 20°C room with 16 hours light per day, for 24-26 hours to allow germination. Seedlings were then selected using a microscope, seedlings at germination (t_0) were selected and transferred into ½ MS+1.5%sucrose media. They were left to grow in the dark condition until time of imaging.

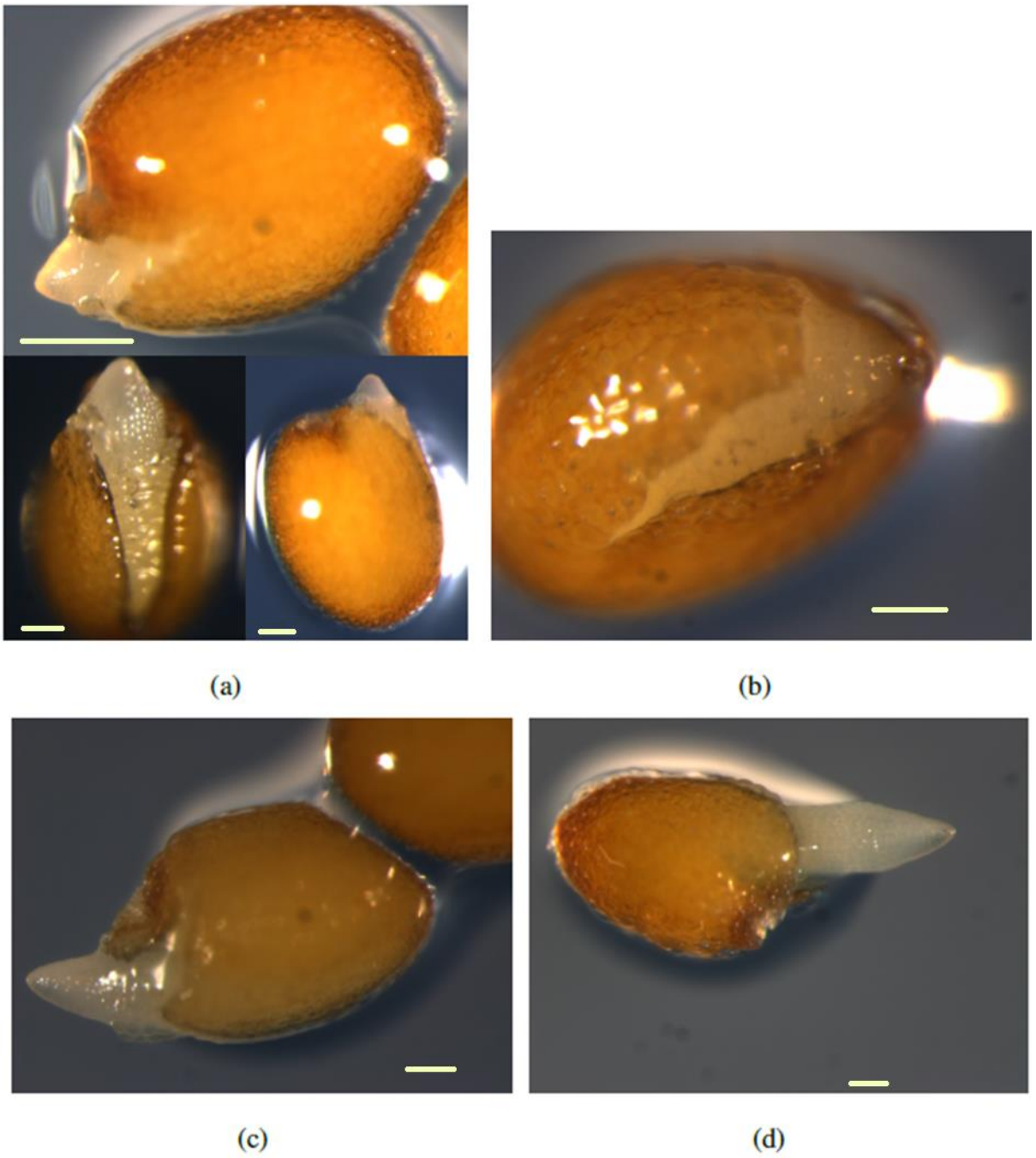

Figure 1.2 a: *Arabidopsis* seeds at time of germination (t_0), endosperm and seed coat have ruptured and the root starts to pop out. **b**: seedling just before germination. **c**: 1 hour after seed germination. **d**: 3 hours after seed germination. Images taken by F. Bou Daher, Braybrook Lab, UCLA, scale bar=100 µm

The Inducible *PME5* over-expressor

As mentioned earlier, in the growing plant cell, the major carbohydrates are cellulose, hemicellulose and pectin. The activity of PME may result in a more rigid gel by removing methyl groups from pectin, allowing calcium cross-links to form. In this genotype, an extra *PME* gene with an inducible promoter has been added. The expression level of the *PME5* is regulated by a promotor which is turned on by ethanol[8][71]. For the induction, a tube containing 400ul of 50% EtOH was placed in the petri dish to provide vapour ethanol for ethanol inducement of the transgene[7] (Fig 1.3). Seeds were induced after germination (t_0) to not interfere with endosperm softening and rupture.

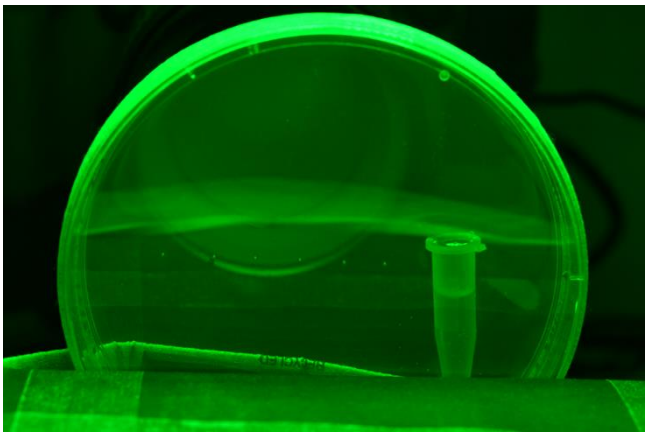

Figure 1.3 Inducible PME over-expressor *Arabidopsis* seeds in a petri dish with a microfuge tube containing 50% ethanol

Characterising organ level growth

Plates were fixed vertically on a stand to allow for orientation of growing hypocotyls along the gravity vector. Images were taken in a dark room, with constant green lights on the top of the petri dish containing the seedlings. A camera with 60mm lens and 36mm extension tube was used for imaging. Images were taken every five minutes for five days, controlled by the Smart Shooter software (Francis Hart, Kuvacode Oy) (Fig. 1.4). The sequences of images were analysed in Matlab (MATHWORK 2016). A script (Script1) was written to automatically identify the hypocotyl and extract the length from each image using image erosion and skeleton extraction. (Fig. 1.5, script written as part of my Master's degree[72])

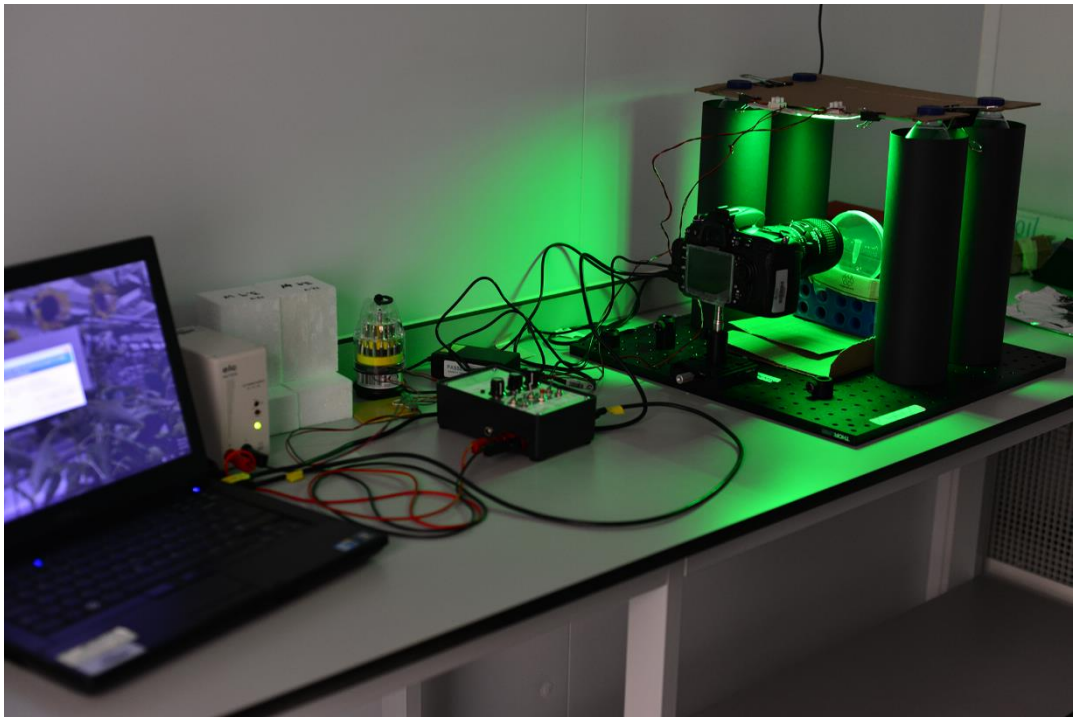

Figure 1.4 Imaging acquisition of the hypocotyl growth in a dark room. The laptop controls the camera and the light controller controls the green light. A cover was placed on during the acquisition to reduce the light effect from the laptop. (Nikon D90 Camera, F8, iso=100, shuttle speed=1 second. Image resolution 4280 x 2840 pixels. Scale=5.6 μm/pixel)

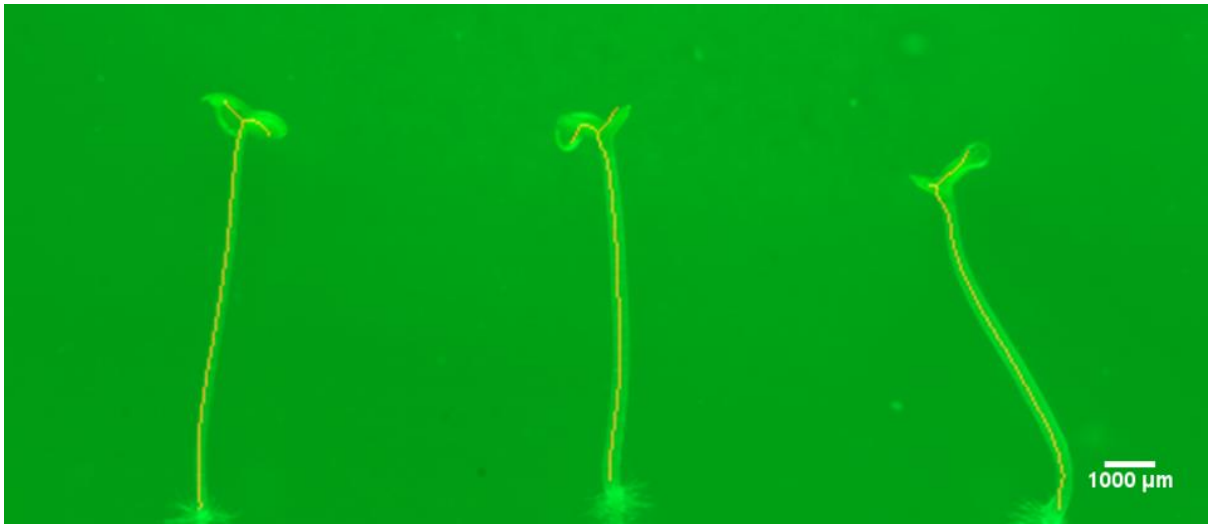

Figure 1.5 Three 48 HPG seedlings, yellow lines are the length automatically extracted in Matlab.

Characterising the cellular level growth

A confocal microscope (Leica SP8, Leica Microsystems) was used to examine the size of individual cells. Unlike the hypocotyl, continuous cellular level data for a seedling cannot be captured as exposure to the confocal laser stopped elongation. Instead, the seedlings of Myristoylated-Yellow Fluorescent Protein (mYFP)[73] as membrane markers were grown in dark until time of imaging. At 13 different time points (0 HPG to 72 HPG, with 6 hours interval), 20 seedlings were transferred to glass slides, submerged with sterilised water, and covered with cover slips for imaging. The confocal microscope was set with: Argon laser on (10%), Objective: 25X Water (0-24 HPG) or 10X (30-72 HPG), absorption emission spectrum in the range of 514nm-535nm, image resolution 1024x1024, line average=1, zoom factor=0.75, rotation angle was set to fit the screen, z-stack step size=1µm, normally a stack of 17-40 layers per image taken to cover the epidermal cells. A non-dividing file normally consists 15-19 epidermal cells; Non-dividing files of cells were identified by calculating the number of cells in a file. Cell lengths were measured in ImagJ (Fiji), using the straight line tool joining the two ends of a cell in the direction of elongation. Widths were measured similarly, with a line crossing the midpoint of the cell. n>20 hypocotyls were used for cell size quantification, n>34 cells/hypocotyl, error bar=propagated standard error.

Chemical treatments

To disrupt the cellulose, seedlings were grown on media with 1 μM isoxaben, 10 μM isoxaben, 1 μM DCB (2,6-Dichlorobenzonitrile) and 10 μM DCB. Chemicals were prepared in dimethyl sulfoxide (DMSO) and mock controls were included. (Results in Supplementary S1.3, S1.4)

Characterising the Microtubule (MT) orientations

Images were acquired from *35S::GFP-MICROTUBULE ASSOCIATED PROTEIN* (*GMAP4*), a microtubule marker. Dark-grown seedlings were prepared as before, and the basal cells were imaged with the Leica SP8 confocal microscope using a 63X oil objective. For the outer epidermis wall, 7 time points were studied: 18, 24, 30, 42, 48, 54 and 72 HPG. For the inner epidermis wall, 4 time points were studied: 42, 48, 54 and 72 HPG. n>80 cells for each time points were used for quantification from 10 hypocotyls.

The microtubule orientation was quantified using the ImageJ plug-in Fibriltool[74]. For each cell, the growth axis was defined and Fibriltool generated two values: anisotropy, which is an indicator of how

well the microtubules within the cell were aligned; angle, which measured the angle between the net MT orientation and the growth axis. (Fig 1.6)

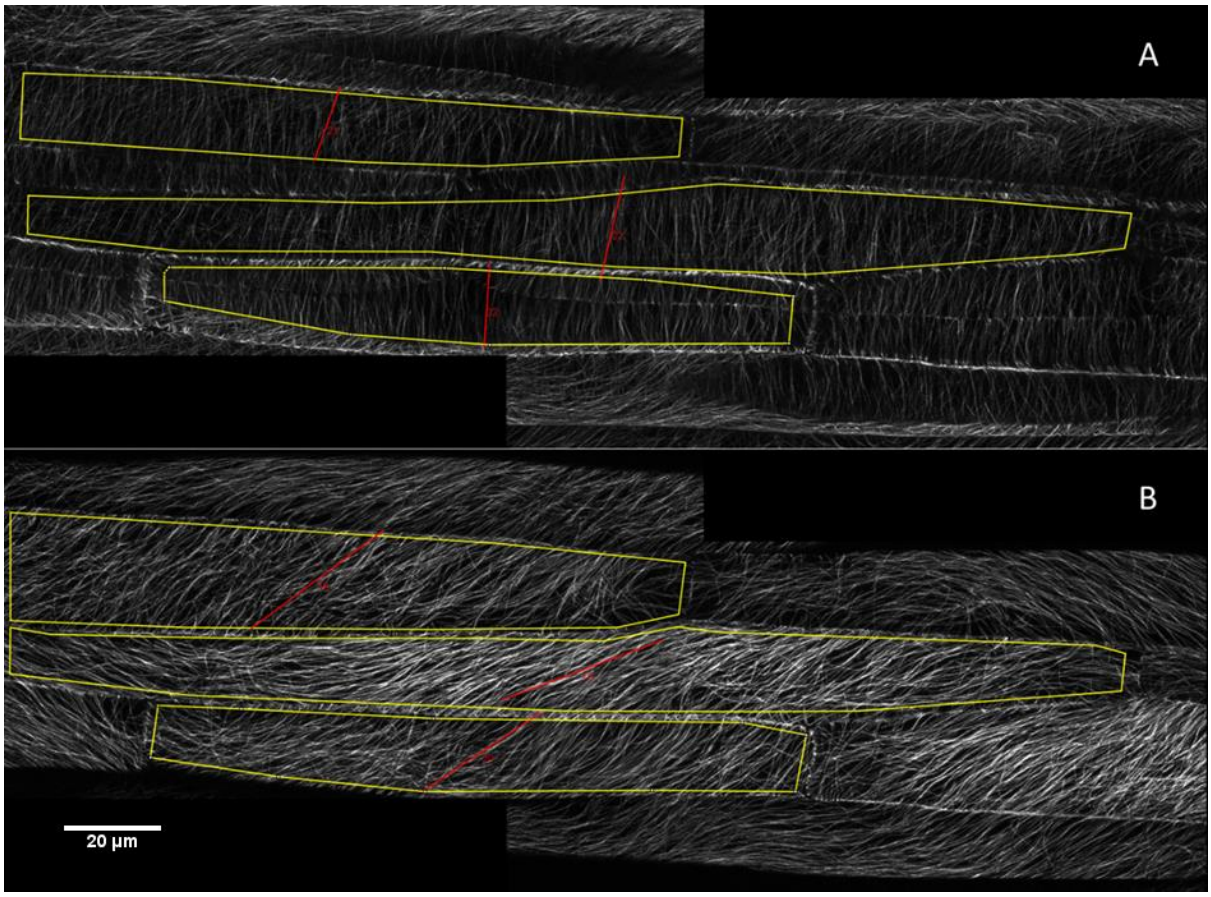

Figure 1.6 Measuring the MT using the Fibriltool. Regions of interest (cells) are enclosed by yellow lines. Red line points to the direction of the net MT orientation, and its length represent the anisotropy value (alignment). A: Inner epidermis wall of three basal cells from a 48 HPG seedlings B: Outer wall of the same three cells.

None of the two values (anisotropy, angle) generated by Fibriltool was enough to describe the state of the MT. They need to be merged to be studied together. The concept of longitudinal and transversal 'strength' were introduced as a measure of how much stiffness the microfibril (MF) were providing in the two directions. A higher value of strength in the transversal direction suggested that it was more difficult for the cell to expand in the transversal direction, and vice versa.

The orthogonal decomposition approach was used to merge the two values. However, it was not fully understood how much strength would the unaligned microfibrils provide, two sets of formulae were developed based on different assumptions.

Assumption 1:

The strength is provided by all the present microfibrils, independent of their alignment. Therefore in the ideal situation when all microfibrils are perfectly aligned (orientation either longitudinal or transversal), the strength would be either 1 or 0 depending on the orientation. In the situation when all microfibrils are not aligned or randomly aligned, the strength would be contributed by each fibril using orthogonal decomposition and equals to $\frac{\sqrt{2}}{2}$ towards both orientations. Based on these, the following formulas were constructed.

Longitudinal strength:

$$F_l = \left[sin^2\left(\frac{\pi}{2} - k\alpha\right) + \sin(\frac{\pi}{2} - \theta)\, sin^2(k\alpha)\right] \cdot (m\alpha + \frac{\sqrt{2}}{2})$$

Transversal strength:

$$F_t = \left[sin^2\left(\frac{\pi}{2} - k\alpha\right) + \sin(\theta)\, sin^2(k\alpha)\right] \cdot (m\alpha + \frac{\sqrt{2}}{2})$$

Where α is the anisotropy value, ranges between [0,1]. θ is the absolute angle from the growth (longitudinal) axis, ranges between [0, $\frac{\pi}{2}$]. In a typical confocal image, α ranges between [0, α_{max}] where $\alpha_{max} < 1$ due to the noise-signal ratio of the image. k and m are normalisation parameters accounting for this ratio such that $k * \alpha_{max} = \frac{1}{2}\pi$, and $m * \alpha_{max} + \frac{\sqrt{2}}{2} = 1$. This way, both F_l and F_t range between [0,1]. For the outer epidermal wall, $\alpha_{max} = 0.6$, $k = \frac{5\pi}{6}$, and $m = \frac{10-5\sqrt{2}}{6}$. For the inner epidermal wall, $\alpha_{max} = 0.35$ $k = \frac{10\pi}{7}$ and $m = \frac{20-10\sqrt{2}}{7}$

Assumption 2:

The strength is provided only by the aligned microfibrils, the randomly-oriented microfibrils have limited contribution to the strength. Therefore unlike Assumption 1, non-aligned microfibrils result in small values of strengths, independent to overall microfibril orientation.

Longitudinal strength:

$$F_l = \sin\left(\frac{\pi}{2} - \theta\right)\frac{\alpha}{\alpha_{max}}$$

Transversal strength:

$$F_t = \sin(\theta)\frac{\alpha}{\alpha_{max}}$$

Where definitions of α, θ, and α_{max} are the same as in Assumption 1.

Generation of the *XTH* transgenic lines

Seedlings of *35S::GMAP4* were transformed with estradiol inducible XTH18, XTH20 and XTH22 constructs. Constructs were generated by S.Braybrook and S.Boyen de Noyer (Braybrook Lab) by amplifying cDNA sequences and cloning them into the pER8 binary vector[75], modified for Kanamycin screening in plants and containing a seed expressed GFP for additional visual screening[76].

Bacteria containing each construct were grown in LB media with 10ug/ml of Rifampicin (genomic antibiotic resistance) and 50ug/ml of Spectinomycin (bacteria resistance) for 2 days at 28 degrees. Then one colony of bacteria was transferred into 3ml liquid LB media with same concentration of antibiotics and left to grow for another day. 1ml of bacterial was then added to 400ml LB with the same concentration of antibiotics at the next day, and left overnight in a 28 degree chamber with constant shaking, until the optical density of the bacteria at 600nm reached 0.8-1. Then bacteria were transferred to centrifuge bottles and spun at 4000rpm for 10 minutes. The bacteria pellet was then resuspended in with 500ml of a 5% sucrose solution to which 250 μm silwett (a surfactant) was added before submerging the plants into the solution for 45-60 seconds.

The dipped plants were grown at normal conditions, and their seedlings were selected using antibiotics followed by genotyping for cDNA clones in genomic DNA extractions (details see table below).

Name	Forward primer	Reverse primer	cDNA length (bp)	gDNA length (bp)
XTH18	CACCATGAAGCTTTCT TGTGGTACAAG	TTAACTGCACTCTACA GGAACACCTCG	853	1045
XTH20	CACCATGGTGTCATT TTGCGGTAG	TTAACTGCACTCTGG AGGAGCACCTT	853	1078
XTH22	CACCATGGCGATCAC TTACTTGCTTC	CTATGCAGCTAAGCA CTCTTTAGGAAGACC	859	944

Successfully transformed *XTH* seedlings should have kanamycin resistance, such seedlings were genotyped with corresponding *XTH18/XTH20/XTH22* primers to confirm the existence of inserted *XTH* genes.

Verifying the inducible *XTH* genes (by L. Dedow, Braybrook Lab, UCLA)

The induction of transgenes was checked on 7-day-old seedlings grown with 0.5 μm estradiol with qPCR, and it was found that all the *XTH* lines selected were successfully induced by estradiol, with >2 fold change in *XTH18* expression, >50 fold change in *XTH20* expression, and >100 fold change in *XTH22* expression.

RESULTS

Stiffer cell walls reduced organ growth rate and final length

The *PME5* over-expressor was previously shown to make cell wall stiffer by removing the methyl group from the pectin and allowing calcium crosslinks to from[7]. The WT and PME5 over-expressor were grown and compared. The hypocotyls had similar behaviours in the first 36 HPG, where length increased for ~0.2cm. Later, the seedlings with induced *PME5* expression did not grow fast, and reached a final length of approximately 0.4cm (Fig. 1.7b). In contrast, hypocotyls of the control (without ethanol) launched a fast elongation period after 24 HPG, and reached a length of approximately 1 cm after 72 HPG, and the hypocotyl was still elongating after 100 HPG (Fig. 1.7a). Note that the actual hypocotyl length might be slightly shorter, because the fitted length in Fig. 1.7 from Matlab included the cotyledon, as the automatic fitting algorithm was unable to exclude cotyledon from hypocotyl. Similar data can be found in[7].

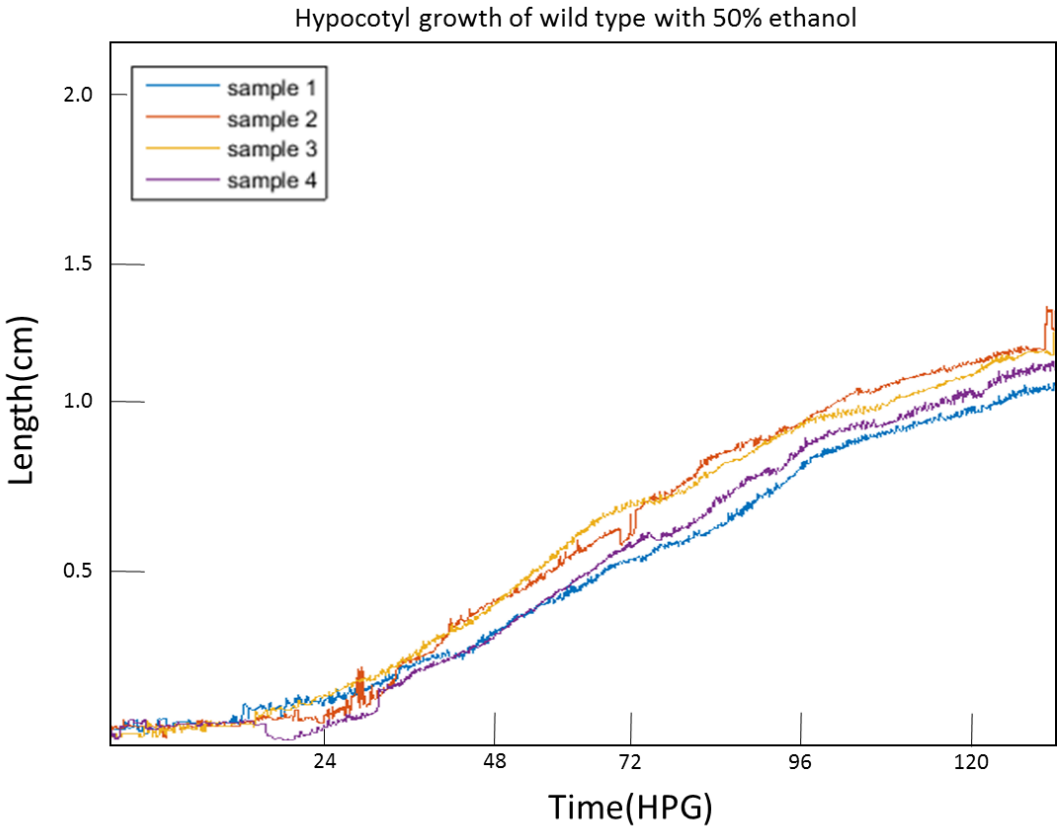

Figure 1.7 (a) Growth of four hypocotyl growth of *Columbia* control hypocotyls, with 50% ethanol induction, imaged by InfraRed set-up

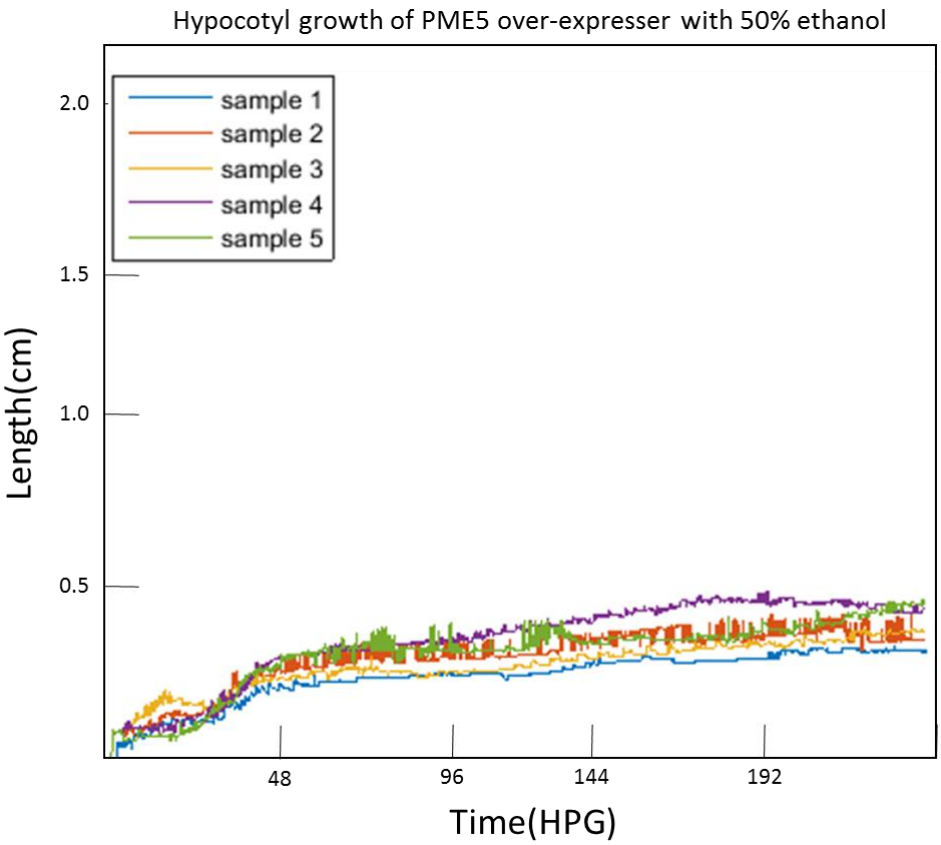

Figure 1.7 (b) Growth of five hypocotyl growth of *PME5* over-expressor hypocotyls, with 50% ethanol induction, imaged by InfraRed set-up

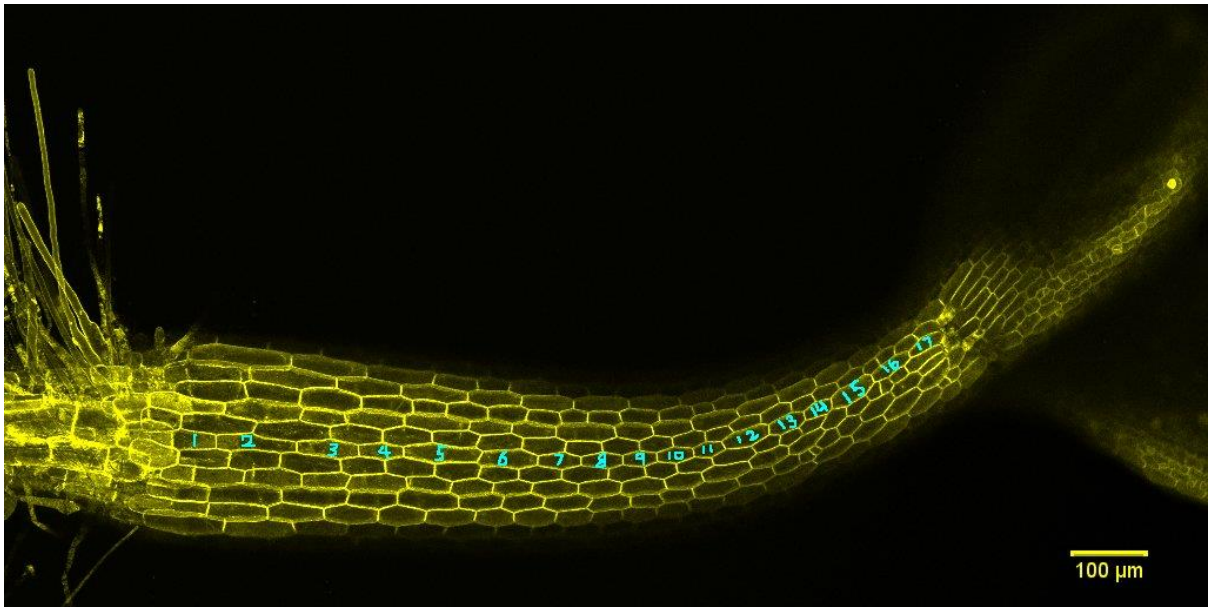

Figure 1.8 Image of a 30 HPG *mYFP* dark-grown hypocotyl. Cells of a non-dividing file are indexed.

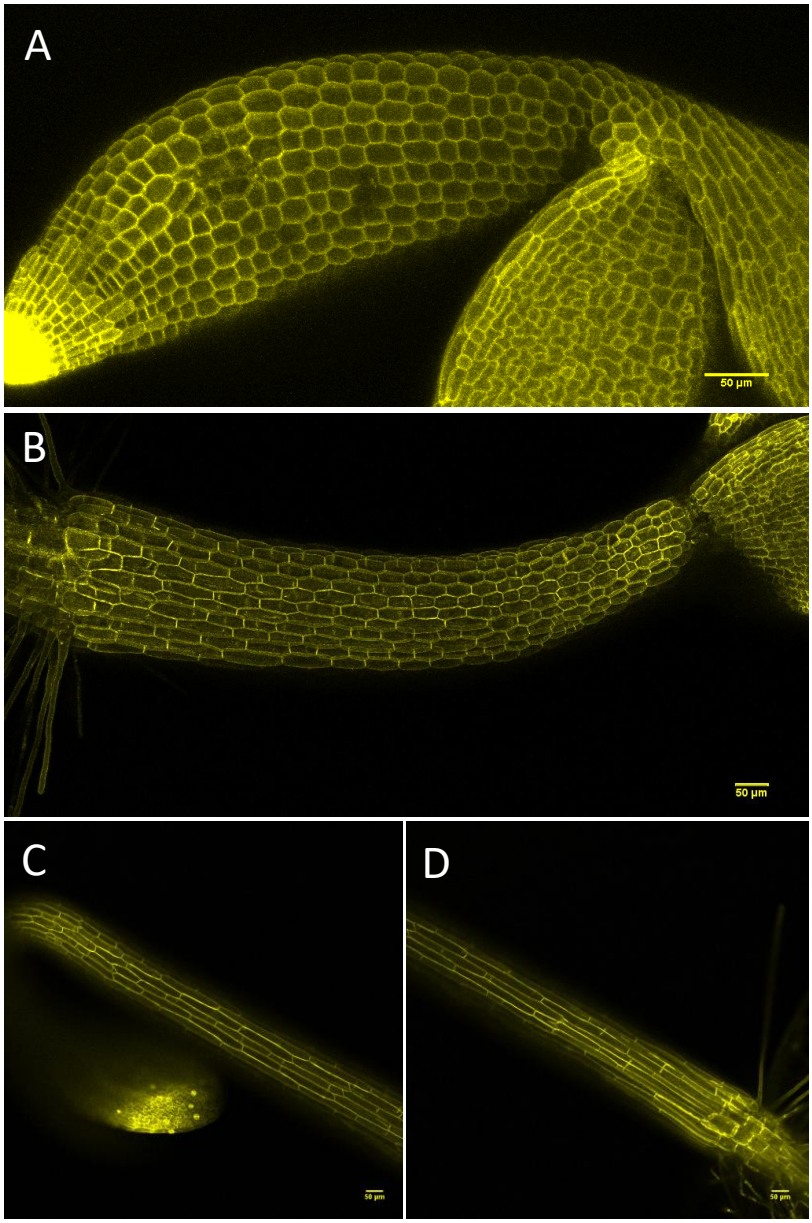

Figure 1.9 Images of seedlings expressing 35S::mYFP at different time points, imaged with confocal microscopy. **A**: 0 HPG, **B**: 24 HPG, **C**: 48 HPG, top part, **D**: 48 HPG, bottom part

The cellular level growth profile showed a progressive, acropetal wave of growth

The growth at the cellular level is more complex than the growth at the organ level: In the beginning, bottom cells start to expand in a fixed, anisotropic direction and top cells remain more isotropic (Fig. 1.9A). Eventually, the expansion extends to the topmost cells in a wave of growth (Fig. 1.9B,C,D). When examining cell size during this process heterogeneity was observed, indicating an underlying growth heterogeneity at the cell level. To quantify this wave of growth in hypocotyl, I studied the non-dividing

files of epidermal cells, whose elongation was a reflection of the hypocotyl elongation since plant cells are permanently attached to each other. Seedlings expressing *mYFP* were grown in the dark until imaging, and the experimental resolution was taken at a 6 hours interval from 0 HPG till 72 HPG.

Upon germination, cells in a hypocotyl were small and more isotropic (Fig. 1.9A). After a day, all cells increased in size. Bottom cells showed more evident size increment and anisotropy in shape compared to the top cells (Fig. 1.9B). After two days, the hypocotyl enlarged 40 times in length (versus germination), with the largest cells being the basal ones (Fig. 1.9C,D). At each of the time points length and width of cells in non-dividing files of cells were measured (n>20 hypocotyls, n>34 cells/hypocotyl)

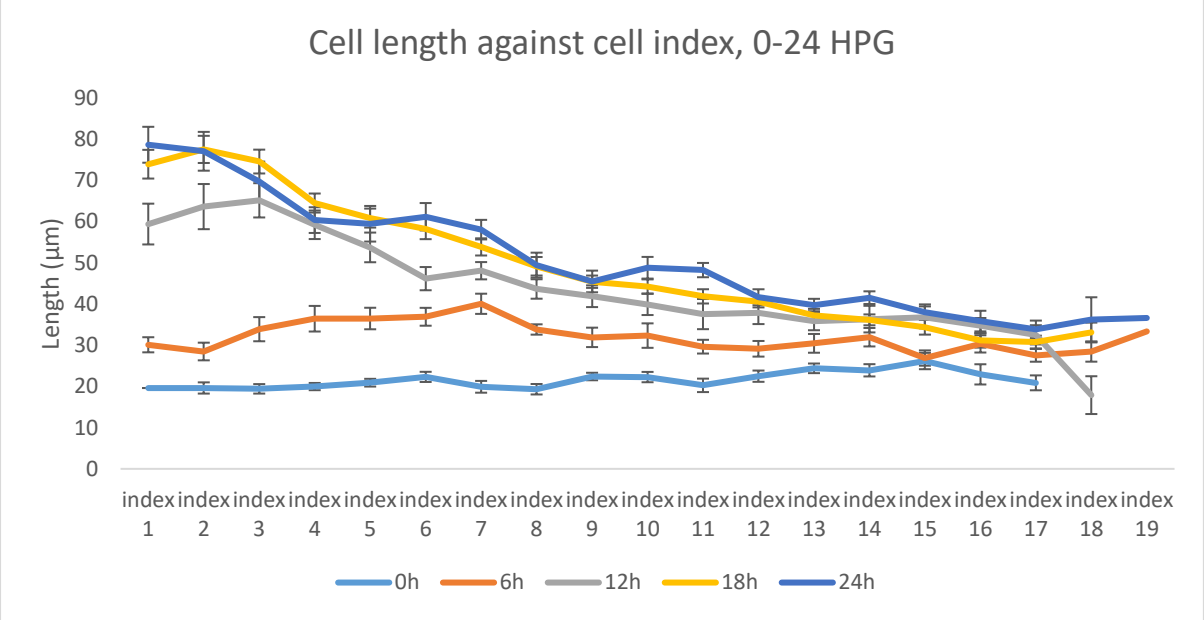

Figure 1.10a Length of hypocotyl cells, at 0, 6, 12, 18 and 24 HPG, plotted against cell indices (see Fig. 1.8; index of 1 is near the collet, index of 19 near cotyledons). Error bar=standard error (n>20 hypocotyls, n>34 cells from at least two files per hypocotyl)

Fig. 1.10(a) shows how length of cells differ depending on their position on the hypocotyl at five distinct time points within the first day after germination. Cells with small indices were closer to the bottom part of the hypocotyl and cells with larger indices were closer to the top part. The initial length of a hypocotyl epidermal cell was around 20 µm. In the first day, all cell extended for approximately 10 µm in the first 6 hours, followed by a faster elongation for the basal cells from 6-12 HPG. Cells with indices 1-3 doubled their length in this period. In the meantime, all other cells grew for approximately another 10 µm. Cells kept extending but slowed down from 12 HPG to 24 HPG. This erratic

phenomenon was also seen in the organ level growth, where hypocotyl growth paused in length but not in width, just before the fast acceleration of growth.

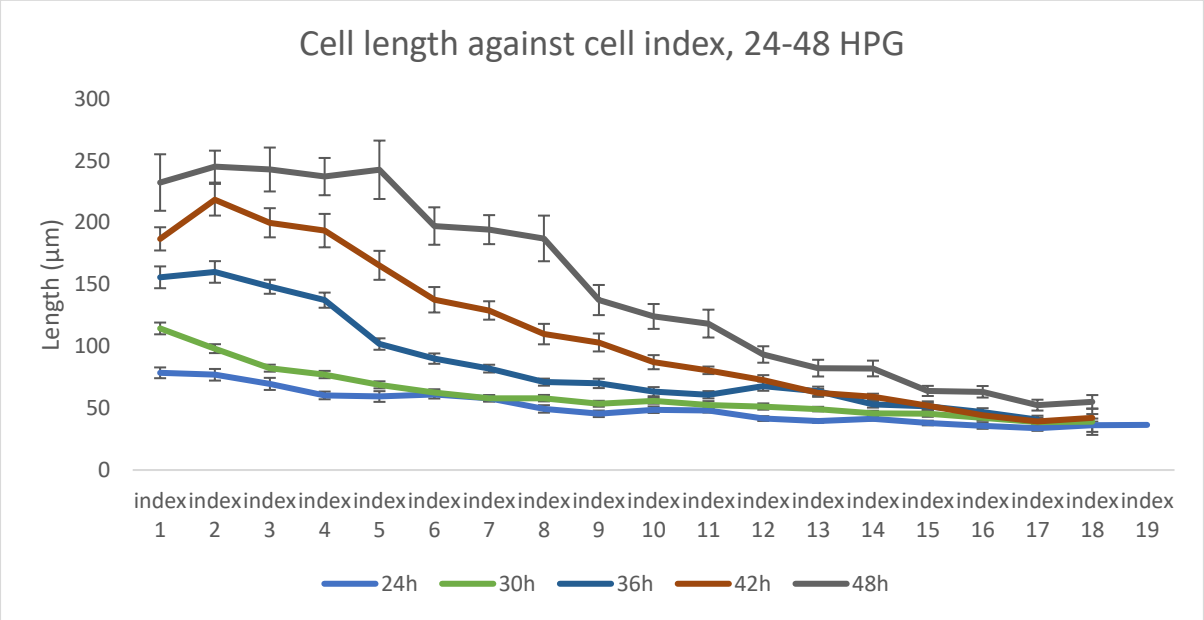

Figure 1.10b Length of hypocotyl cells, at 24, 30, 36, 42 and 48 HPG, plotted against cell indices. (n>20 hypocotyls, n>34 cells from at least two files per hypocotyl)

In the second day post germination (Fig. 1.10b), the cellular extension was slow from 24-30 HPG, but since 30 HPG, the basal cells elongated for approximately 50µm in every 6 hours until 48 HPG, which was faster than other cells in the first day. Also, a noticeable more rapid growth was observed for cells with indices 1-4, from 30-36 HPG, as well as cells with indices 6-8, from 42-48 HPG. So the elongation rate of the basal cells had slowed down and this was the evidence of the growth 'wave' transferring to cells with larger indices. Cells with indices>13 were still growing very slowly.

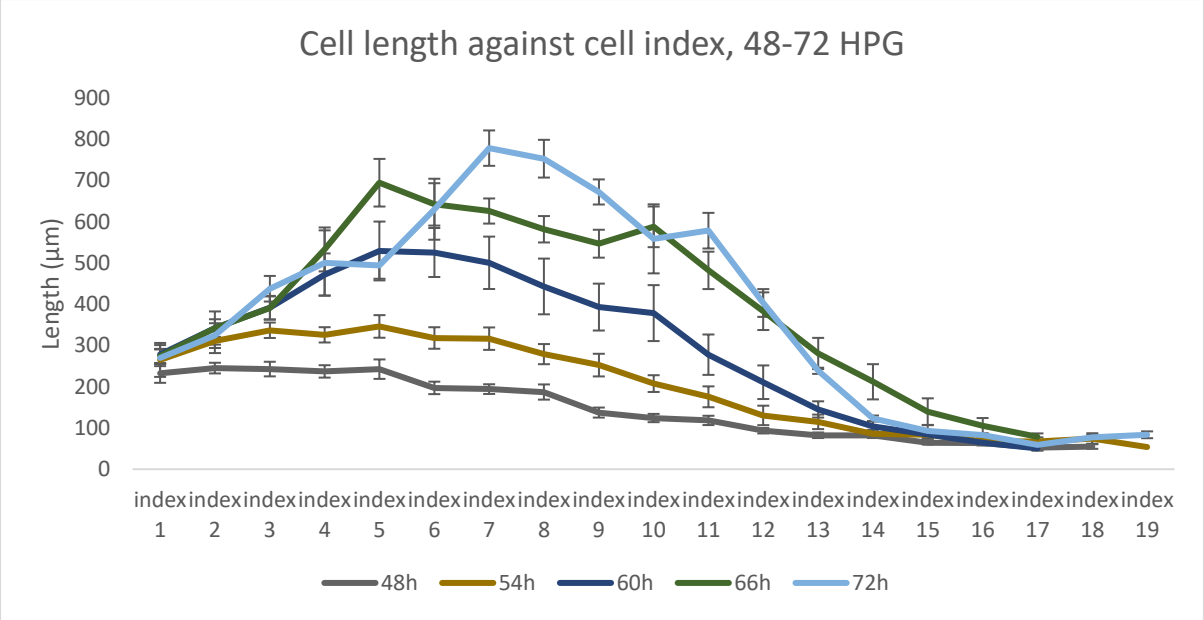

Figure 1.10c Length of hypocotyl cells, at 48, 54, 60, 66 and 72 HPG, plotted against cell indices. Error bar=standard error (n>20 hypocotyls, n>34 cells from at least two files per hypocotyl)

In the third day post germination (Fig. 1.10c), cells had huge differences in their lengths. At 72 HPG, cells with indices 6-8 were more than twice as long as the basal cells, which were not growing anymore. Differences in final lengths of these cells implied the heterogeneity in cells. From 48-60 HPG, cells with indices 4-10 had the fastest growth rate, with a length increment of approximately 300 µm and doubled their lengths. From 60-72 HPG, basal cells (indices 1-3) almost cease the growth, and cells with indices 12-15 started to elongate.

The acropetal wave of growth was anisotropic

Turgor pressure, the driving force for cell expansion, is applied on the cell wall isotropically. Yet the anisotropic properties of the cell wall forces the cell to grow significantly in the longitudinal direction but not as much in the radial direction[7]. Indeed, when cell diameter was plotted against cell index, no 'wave of growth' was observed (Fig. 1.11[7]). All cells increased in their diameter uniformly, and slowly over time, from approximately 15 µm at germination to 25 µm at 72 HPG. The anisotropic cell elongation was clearly observed when the ratio of $\frac{\text{cell length}}{\text{cell diameter}}$ was plotted over cell indices from 0-72 HPG (Fig. 1.12[7]). After 48 HPG, most epidermal cells of the hypocotyl had the ratio $\frac{\text{cell length}}{\text{cell diameter}}$>5.

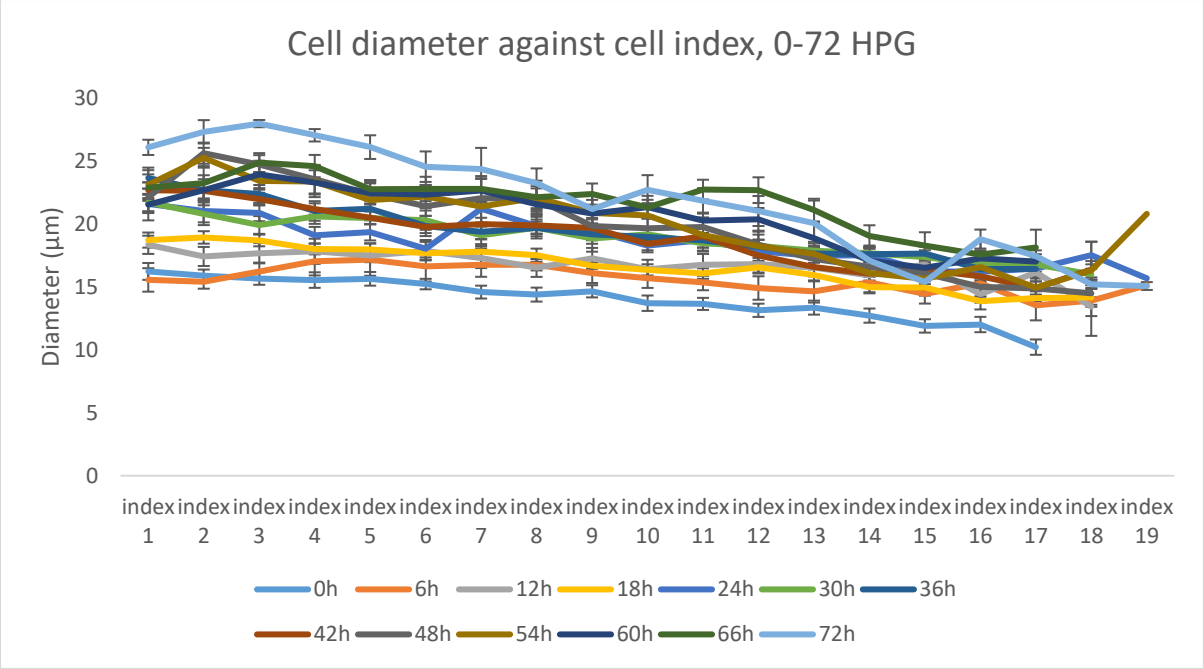

Figure 1.11 Diameter of hypocotyl cells, from 0-72 HPG, plotted against cell indices. Error bar=standard error (n>20 hypocotyls, n>34 cells from at least two files per hypocotyl)

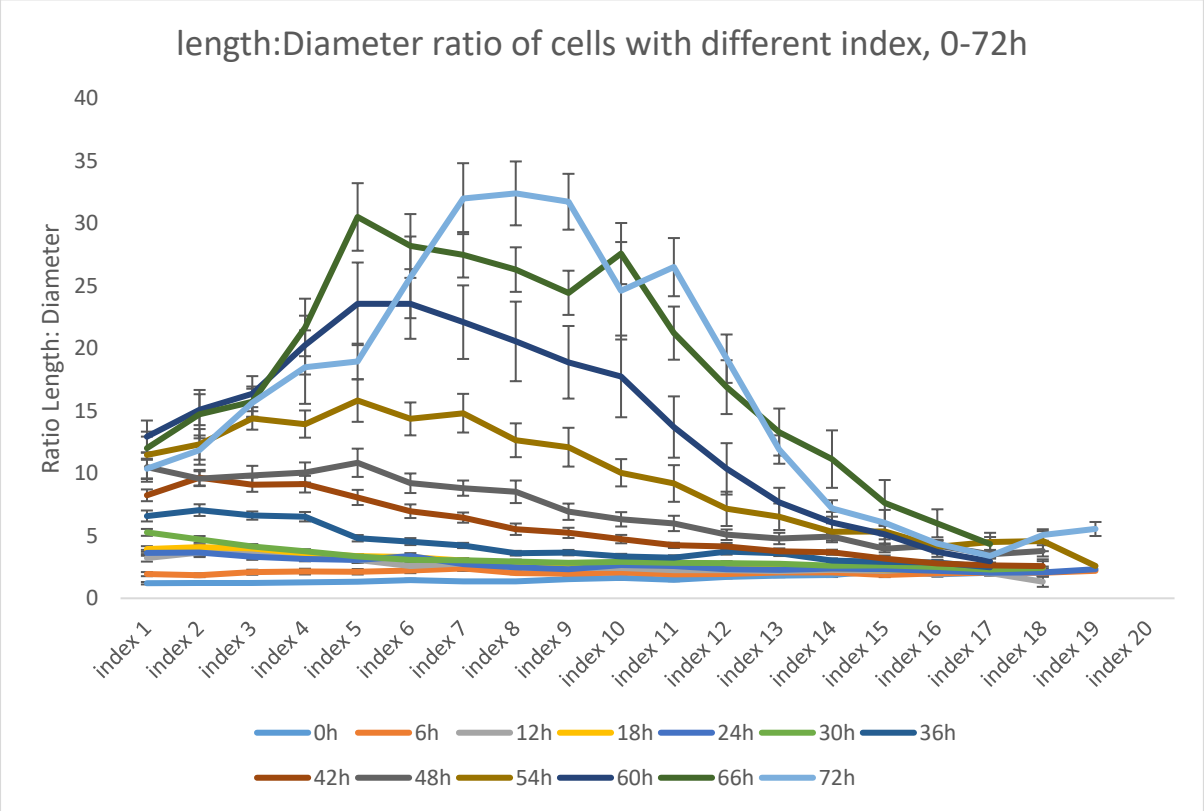

Figure 1.12 Ratio of $\frac{Length}{Diameter}$ of hypocotyl cells in µm, from 0-72 HPG, plotted against cell indices. Error bar=standard error (n>20 hypocotyls, n>34 cells from at least two files per hypocotyl)

The acropetal wave of growth travelled uniformly and increased its magnitude over time

To quantify the wave of growth, RGR (Relative growth rate, defined as the growth rate relative to current cell size, $\frac{1}{t_2-t_1}\ln(\frac{L_2}{L_1})$, where L_1 is length at t_1, and L_2 is length at a later time t_2 of cells were plotted against cell indices (Fig. 1.13[7]). The RGR of cell lengths was always increasing at higher rates than cell diameter, and RGR for cell length by position demonstrated the movement of the acropetal wave, beginning at around 24 HPG and positioned at middle cells (index 7 ± 2) at around 60 HPG. The higher RGR in length and suppressed RGR in diameter at early time intervals (0-12 HPG) was likely to due to the expansion of collet cells at the hypocotyl-root junction and so the quantification of the cellular wave of growth began at 24 HPG, when the rapid cellular elongation was about to start.

Defining the 'position' of the wave as cell with the largest index i whose relative growth rate is qualitatively larger than that of cell with index $i+1$. The apparent position of the wave based on the data (Fig. 1.10) was summarised in Table 1.1, and plotted in Fig. 1.14a. A linear trend was seen in position of the wave over time, which meant that the acropetal wave of growth travelled uniformly in time.

Similarly, defining the 'magnitude' of the wave as the size of the largest elongating cell at any given time. The magnitude was summarised in Table 1.1, and plotted in Fig. 1.14b. The magnitude of the wave increased significantly over time, from 100 at 24 HPG to 800 at 72 HPG. However it was difficult to conclude whether the increase in magnitude over time had a linear trend or not.

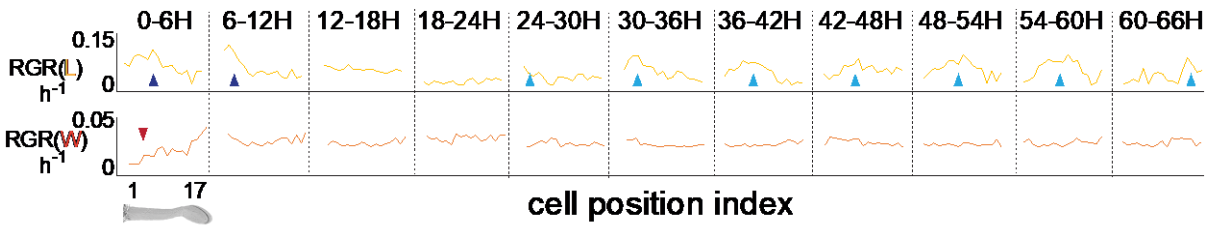

Figure 1.13 Relative growth rate of cell growth in length (L) and diameter (W), from 0-66 HPG, in 6 hours windows. Blue arrowheads point to early-pulse growth adjacent to the collet, red arrowheads to early growth suppression, light blue arrowheads trace the maximal RGL and proxy the acropetal wave. Reproduced from [7].

Time (HPG)	Position of the wave (Cell index)	Magnitude of the wave (μm)
24	2	78.6
30	3	114.4
36	4	160.1
42	4	218.4
48	8	242.7
54	7	346.2
60	9	525.5
66	10	626.1
72	11	752.8

Table 1.1 Apparent position and magnitude of the wave, determined from Fig.1.10

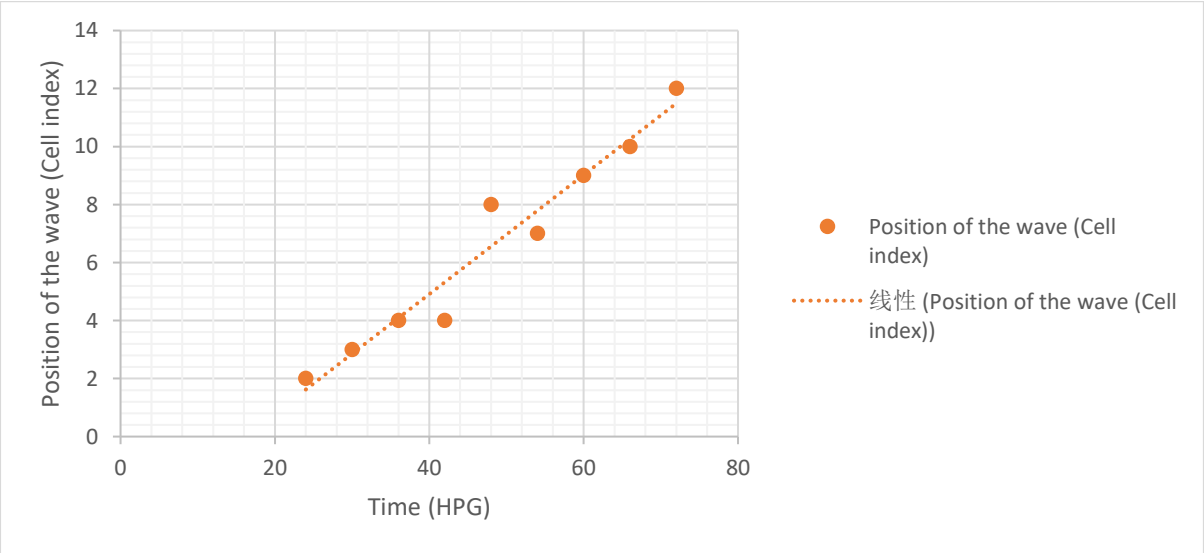

Figure 1.14a Apparent position of the wave over time

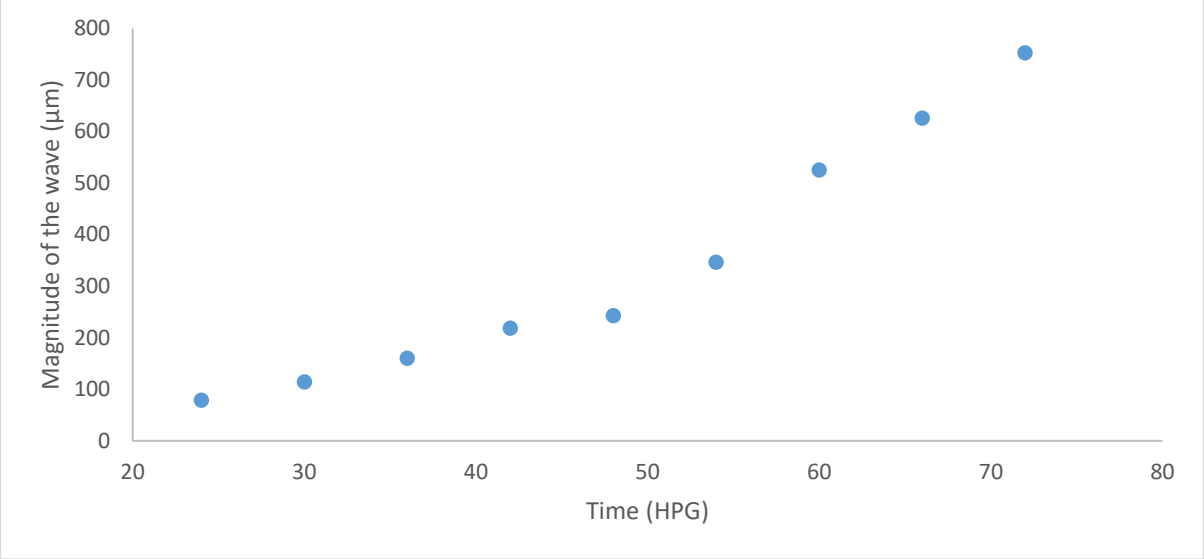

Figure 1.14b Apparent magnitude of the wave over time

The microtubules were dynamic over time, and their predicted 'strength' in both longitudinal and transversal directions affected growth anisotropy

Epidermal cells of the dark-grown hypocotyl were found to grow anisotropically, likely due to the anisotropic properties of the cell wall. The cell wall anisotropy at the inner and outer surface was studied using the *35S::GFP-MICROTUBULE ASSOCIATED PROTEIN(GMAP4).*

Our previous examinations indicated that epidermal cells of the hypocotyl display transversely oriented microtubules after the onset of rapid elongation has begun[7]. Here, I chose to examine MT orientation in more depth, at both outer and inner epidermal walls; transgenic plants carrying a 35S:GFP::MAP4 construct were time sampled at 18 HPG, 24 HPG, 30 HPG, 42 HPG, 48 HPG, 54HPG and 72 HPG and imaged using confocal microscopy. The resulting images were analysed using FibrilTool[74] to obtain anisotropy values and average angles of MTs. These values were then used to calculate a contribution to strength in longitudinal and transverse directions. As previously observed[7], microtubules were not visible at the inner epidermal face early during growth and in this case only became visible at 42HPG. In order to provide anisotropic information from this layer early I chose to extrapolate the 42HPG data backwards as a benchmark for future modelling. Consistent with the previous findings[3], MTs in the inner epidermal wall were more transversely aligned than those in the outer wall at all times. To quantify the strength provided by MF based on the MTs, two different sets of equations were developed: 1) All the fibrils contribute to the strength in its current direction, and by the principle of orthogonal decomposition, a strength in the longitudinal direction and a

strength in the transversal direction is computed (Fig. 1.15 AB). 2) The aligned fibrils are considered to be more effective in providing strength, and the non-aligned fibrils are less significant (Fig. 1.15 CD).

When considering all the fibrils using orthogonal decomposition (A,B), less difference was seen between Fl (Strength in the longitudinal direction) and Ft (Strength in the transversal direction). When only aligned fibrils were considered (C,D), this difference was exaggerated. In outer epidermal wall, calculated strength in the longitudinal direction was always substantially higher than the one in the transversal direction, except at 30 and 42 HPG, when the values were similar. Inner wall microtubule signals could not be seen before 42 HPG, where at 42 HPG the transversal strength was significantly higher than the longitudinal strength. From 42 to 72 HPG, the strength in the longitudinal direction gradually overtook and became significantly higher than the strength in the transversal direction.

Both methods of quantification gave similar outcomes. In the outer epidermal wall, the strength favoured slightly to the longitudinal direction in the beginning (18-24 HPG), and it was roughly equal in the two directions during the rapid elongation phase (30-42 HPG). Eventually it favoured the longitudinal direction again when the growth was slowing down. In the inner epidermal wall, the strength in the transversal direction is a lot higher than that in the longitudinal direction during the rapid elongation phase (42 HPG). Then the longitudinal strength gradually overtook the transversal strength and eventually became a lot higher (72 HPG), corresponding to the cease of the growth when MTs were mostly longitudinally aligned.

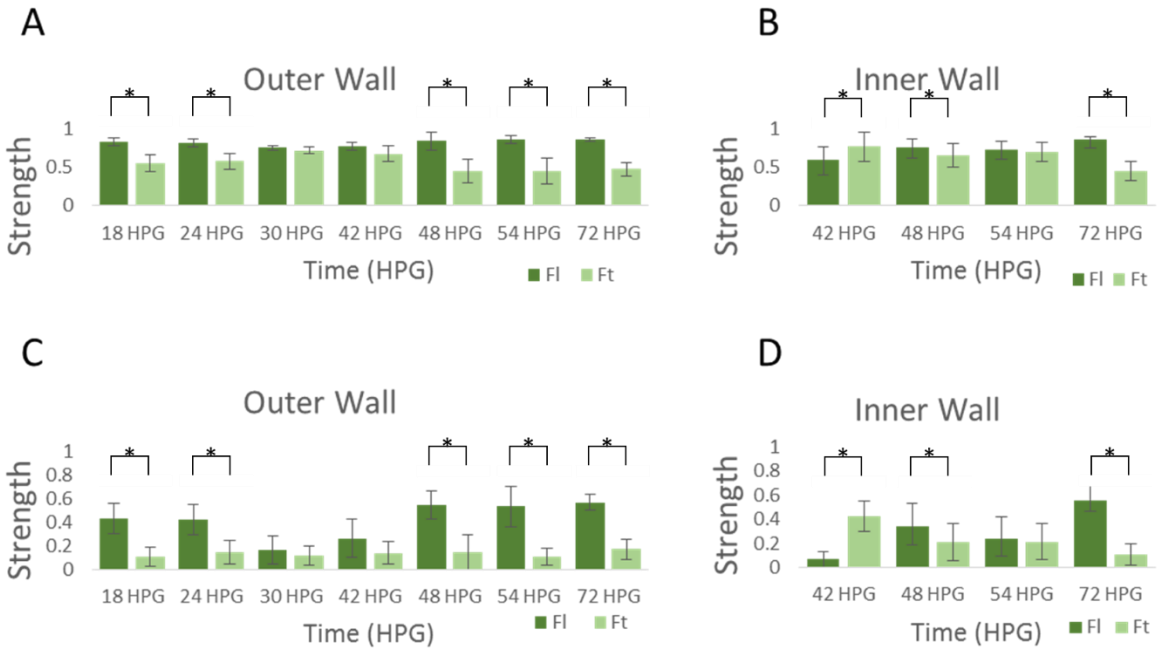

Figure 1.15 The strength provided by cellulose microfibril (approximated using MT) was calculated with two different sets of equations. When considering all the fibrils using orthogonal decomposition (A,B), and when only aligned fibrils were considered (C,D). n>80 basal cells for each time points, error bar= propagated standard error, for all the pairwise statistical test with significant differences (marked as *), p-value< 2.152e-7.

Estradiol induced XTHs showed a phenotype of longer hypocotyl in dark only 5 days post germination (qPCR and, hypocotyl measurement experiment by L. Dedow, Braybrook Lab, UCLA)

Apart from cellulose microfibril, the function of xyloglucan, the major hemicellulose in *Arabidopsis*, was studied. Three XTH genes were transferred into GMAP4 background and homogeneous lines were selected. The induction was tested with qPCR (by L.Dedow), where all three XTH genes were significantly up-regulated. (>2, >50, and >100 fold changes for *XTH18, 20* and *22*, respectively, Fig. S1.6). Two replicates were run with 1 µM estradiol at three time points (24 HPG, 48 HPG and 72 HPG), but no significant difference in length was found between the mock and estradiol treatment, and no difference in hypocotyl diameter (width) was found between the mock and estradiol treatment. Two more replicates were run with 1 µM estradiol for longer time points (3, 5 and 7 days post germination, by L.Dedow). The background (GMAP4) did not show any difference between the mock and estradiol treatment. Length was significantly increased at 5 days and 7 days post germination when *XTH20* and

XTH22 were induced (Fig. 1.16A). A slight reduction in the hypocotyl width was observed at 5 days post germination but not at earlier or later times (Fig. 1.16B) for XTH20. Overall there was an increment in volume expansion (Fig. 1.16C) and hypocotyl anisotropy (Fig. 1.16D) at 5 and 7 days post germination for induced *XTH20* and *XTH22* lines.

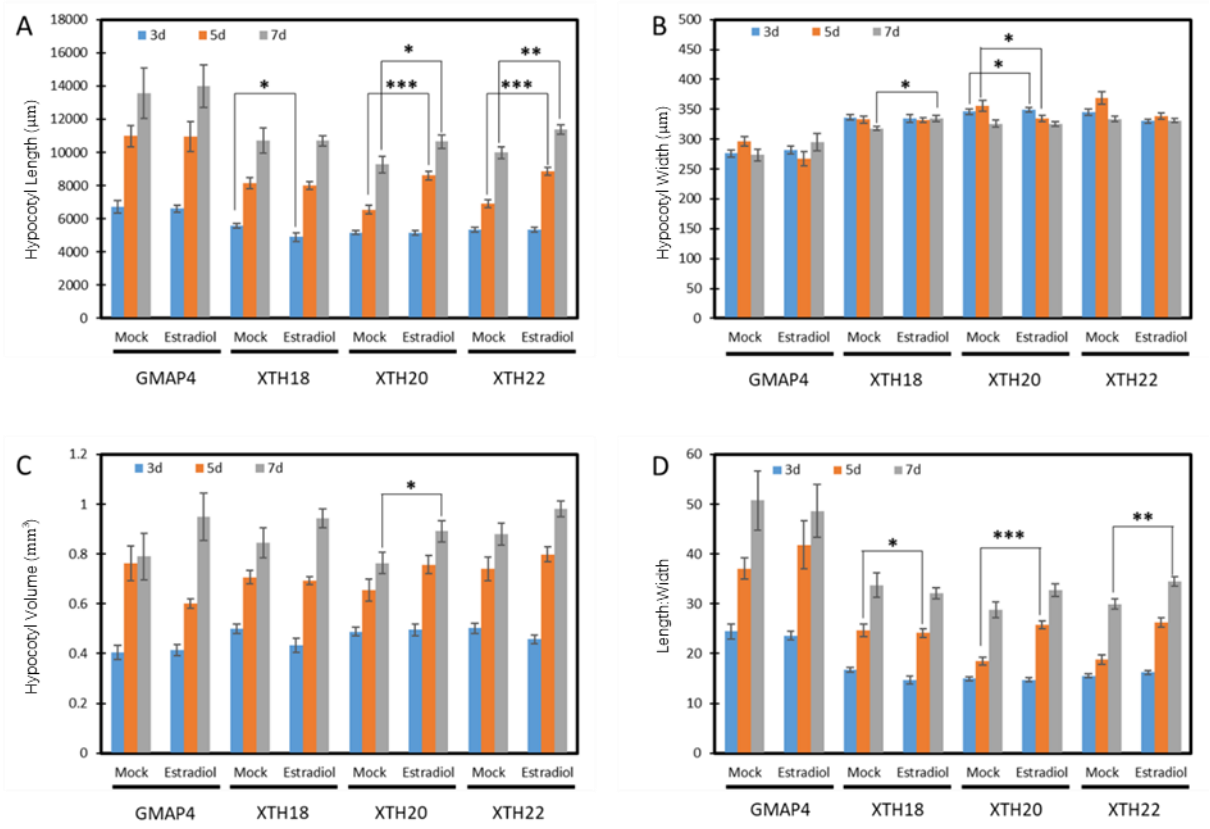

Figure 1.16 Hypocotyl length at 3,5 and 7 days post germination, for the GMAP4 (background) and the estradiol inducible XTH lines. A: Hypocotyl length; B: Hypocotyl width; C: Hypocotyl volume; D: Length:Width ratio. (n=20 seedlings per time point per line, from two biological replicates, error bar= standard error, Student's T-test used between mock and estradiol treatment, where * $p<0.05$, ** $p<0.01$, and *** $p<0.001$)

DISCUSSION

The organ level hypocotyl growth possesses a non-symmetric sigmoidal pattern

In this Chapter, the hypocotyl growth was studied at cellular and organ levels. At the organ level, it was found that the hypocotyl growth over time is sigmoidal over time, but not symmetrical.

A sigmoidal pattern was observed for the hypocotyl growth[1] (Fig. 1.7) However, this sigmoidal shape did not look like a symmetric sigmoidal function, such as the Logistic function, being symmetric with respect to its middle point. Rather, the hypocotyl growth was more like an exponential acceleration followed by linear growth rate elongation (Fig. 1.7). This is consistent with many of the functions used to describe growth in crops, such as the beta function proposed by Yin[19], or other classic growth equations (Richards et al[77], Gompertz et al[20], Weibull et al[21]). Such equations provide more flexibility in fitting and are able to capture the asymmetrical sigmoidal patterns through parameter adjustments.

Like many other plant organ's lifecycle, the growth of hypocotyl can be divided into three sub-phases: an early accelerating phase; a linear phase; and a saturation phase. Different growth mechanisms associated with the three sub-phases are possible causal of the asymmetric growth. Whether this asymmetric growth corresponds to similar asymmetric growth patterns at the cellular level is still unclear and will be studied in later chapters.

Growth of the dark-grown hypocotyl was tracked automatically with a continuous imaging kit setup. The extracted hypocotyl lengths were not precise enough for three reasons: 1) Movements of seedlings in the plates during the experiment would cause some part of the roots being misidentified as hypocotyl. 2) The automatic length extraction was unable to distinguish between cotyledons and hypocotyls, and hence the length of cotyledons was often included in the hypocotyl length. 3) When the seedling loses its seed coat during hypocotyl elongation, the seed coat is attached to the hypocotyl and its size is sometimes included as part of the hypocotyl. Errors caused by these three facts became relatively small when the seedling grew large, and these errors were difficult to overcome. They made initial hypocotyl size extraction inaccurate (before 24 HGP) and hence in the later chapters (Chapter 3), when a precise size of hypocotyl was necessary to be compared with modelling prediction, the hypocotyl size was measured manually at distinct time points. Manual measures were made for [7] as well.

The quantified cellular wave of growth of the dark-grown hypocotyl

Cellular level hypocotyl growth is more complex than the organ level growth. Quantified cell growth over cell indices reveals a progressive wave of growth over time, yet the full picture of hypocotyl cell growth profile is still unclear at this stage.

The level of regional organ growth can be visualised by the growth of non-dividing file of epidermal cells. The size of these cells was quantified in the first 72 hours post germination. The RGR of these cells revealed an acropetal wave of growth travelling along the hypocotyl uniformly in time, with increasing magnitude. The magnitude of the wave was defined as the longest cell which was still growing, i.e. within the growth wave. The increasing magnitude over cell numbers (Fig. 1.14b) implies that cells with larger indices grow with faster growth rates. In addition, cell with larger indices elongate for longer periods of time compared to those with smaller indices, resulting in huge differences in their final length. Due to technical difficulties, cell size beyond 72 HPG was unable to be acquired. Elongation of hypocotyls lasts for around 8 days, and how growth progresses at the cellular level beyond 72 HPG is still not clear. The position and magnitude of the wave seem to follow some positive trends over time/cell indices, and these will be studied further and modelled in Chapter 3.

Anisotropic growth starts at the beginning of the wave

Our evidence shows that the material anisotropy is observed before the travelling wave of growth of the hypocotyl cells. Both cell length and diameter were increasing during hypocotyl elongation according to the data presented (Fig. 1.10, Fig. 1.11), and anisotropic growth of cells can be estimated by assessing these data. The data imply that anisotropic growth starts from the time of germination (Fig. 1.10a, Fig. 1.11). This is supported by our previous findings that the axial walls were more elastic when compared with transverse walls at 4 HPG and 24 HPG[7], and hence anisotropic growth is a result of both cellulose orientation and pectin asymmetry. At germination, no MT could be observed in the epidermal cell until 18 HPG, and no strongly transversally aligned MT observed until 42 HPG. Before 42 HPG, the anisotropic growth is more likely to be controlled by pectin chemistry and wall material anisotropy.

Important role of the pectin chemistry

Cell growth rate and growth anisotropy can be greatly affected by cell wall modifications through changes in pectin chemistry. Pectin methylation was proposed to play an important role in the pectin

chemistry and its mechanical properties, and hence anisotropic growth of hypocotyl cells[7]. Overexpressing *PME5* leads to pectin de-methylation; cell walls are less elastic and rapid elongation is suppressed. However, role of each of the PME families is not well understood, and PME activity has been reported to be associated with both increased[78] and decreased cell elongation[79][5]. PMEs may have different activities resulting in HG chains be more likely to cross link or more likely to degrade[7], depending on the pH[80][81] and patterns of demethylation on HG chains[82] and the activity of other enzymes involved in pectin degradation like pectate lyases and polygalacturonases[83][84]. We have also recently shown that induction of a PECTIN METHYLESTERASE INHIBITOR has the opposite effect to PME on hypocotyl elongation and cell anisotropy[7].

The role of microfibrils in the plant cell wall

Microfibirls play important roles in cell growth rate and growth anisotropy, and two equations were built attempting to quantify and distinct the two. The two sets of equations implied different assumptions depending on relationships between MF and rest of the cell wall. The first (Assumption 1) was more appropriate if the MFs load most of the force to hold the cell wall together. The difference of strength in the two directions controls the anisotropy. This would imply that the anisotropic growth rate depends mostly on pectin chemistry, since the difference in strength provided by microfibrils are relatively small compared to the difference in growth rate at the axial and transversal directions. The second (Assumption 2) method was more appropriate if the pectin loads most of the force, and the cellulose need to be aligned to control the anisotropy. This would imply that the anisotropic growth rate is mostly regulated by the microfibril alignment and orientations. Currently, it is still unclear how cellulose and pectin work together and how they coordinate the anisotropic growth during a cell deformation.

MT was used as an approx. for the MF but with exceptions[43][44][45][46], variation in the seedling MT-labelled fluorescence intensity and the variation in the MT density, it is difficult to compute the true MF alignment, density and an accurate anisotropic strength tensor provided by the MF. The linkage between growth rate and MF orientations was seen earlier[51][3]. I hypothesise that the strength provided by the MF acts as a growth limiter, and controls the growth together with the material synthesis/secretion rate, turgor pressure and the pectin stiffness.

The function of XTH in the cell wall

The function of XTH in cell wall modification is discussed here based on limited experiments and current knowledge. Miedes et al[85] found that induced XTH18 and XTH20 lines stimulated hypocotyl growth and that, the hypocotyls were more extensible and grew longer compared to the wild type. Interestingly, it was found that our induced induced XTH20 and 22 lines showed longer hypocotyl after 5 days post germination but not the XTH18 lines (Fig. 1.16), possibly due to the proteins not being translated or not active. It is not known why the phenotype is seen only at late times, and there can be two possibilities: 1) The upper cells, growing later in time, were affected by the XTHs and grew bigger in size. 2) All the cells were slightly bigger due to the presence of XTHs, but only became quantitatively significant at later time. A follow-up test to this could be testing the diameter of cells whose microfibrils has already turned longitudinally orientated, to see if XTHs affect hypocotyl cells only at late times.

At early time points (before 3 days post germination), no phenotype in hypocotyl size was seen. This could be either because the effect of XTH in hypocotyl growth was minor so that the relative difference in hypocotyl length was small and only became observable when hypocotyl became long. Another possibility was the time of the XTH expression was not correct for changes in hypocotyl length at early time points. Previous studies showed differences in hypocotyl extensibility depending on the acidity of environments (pH from 5.0 to 6.0)[86][85] and phenotypes in hypocotyl length was observed only after 3 days post germination for the XTH overexpression lines, which means the function of XTH may only be effective at certain environmental conditions. It is not known whether XTH activities loose or stiffens the cell wall, but it is more likely to promote growth according to our data. The role of XTH in the cell wall will be revised in Chapter 6 (Final discussion)

Problems of quantifying the cell wall properties using the microscope images

The MT orientation and alignments were studied and quantified using the *35S::GFP-MICROTUBULE ASSOCIATED PROTEIN.* Due to the nature of images, a globally comparable quantification method was difficult to be achieved. The biggest issue was that at different time points (0H, 24H and 65H) the signal intensity was different, and the intensity for MT on the outer epidermal cell was different from that of the inner cell. Hence different laser intensities or values of gain was used during image acquisition, giving different signal-to-noise ratios. The difference in the signal-to-noise ratio affected the parameter output from Fibriltool. For a test of straight parallels lines, Fibriltool gave an anisotropy value of 0.97 out of 1 (means highly aligned), but only 0.38 when artificial noise was added.

(Supplementary Fig. S1.5). Further, fibril length and density also had an effect on Fibriltool's output, although not as significant, (data not shown). This means images of cells walls from different positions of the hypocotyl (upper, lower), from different locations of the cell (inner, outer) and different ages of the cell (younger, older) are not directly comparable. To compare the 'strength' from microfibrils in this chapter, two sets of equations were introduced and a rough normalisation method was used based on estimation of peak alignment based on observation. It is difficult to improve this normalisation method. Currently, deep convolution neural networks are popular in image denoising methods[87], yet, a quantified signal-to-noise normalisation method which can be applied to microtubule images has not been developed. The biggest challenge is that one cannot find a benchmark of degree of normalisation from an image itself.

The 'pause' in the growth from 18 HPG till 24 HPG may due to growth in radial direction

An unexpected pause was observed in the cell growth at 18-24 HPG (Fig. 1.10a). But the expansion in cell diameter did not seem to be paused during this period (Fig. 1.11). The observed 'pause' in the cell/hypocotyl elongation at early stage is possibly a result of expansions in cell/hypocotyl diameters. This was verified at the organ level where hypocotyl length was measured, and the results were consistent: the hypocotyl elongation seemed to slow down at 18-24 HPG (Fig. S1.1) whereas the hypocotyl diameter kept increasing (Fig. S1.2). This may be physically explained by the MT orientations: At 18 and 24 HPG the MT in the outer wall of epidermal cells tends to be longitudinally orientated, and at 30 HPG the MT starts to reorient and show no clear longitudinal/transversal tendency (Fig. 1.15). As a result, the cell expands in diameter from 18-24 HPG but not much in length, which might be the cause of increased hypocotyl diameter. So in fact the growth was not 'paused', only the length was. Due to this abrupt behaviour of basal cell growth at early time, the wave of growth was thought to start at 24 HPG from the basal cells[7]. The expansion in the basal cells at very early time intervals (0-12 HPG) is potentially a holdover from germination due to the expansion of collet cells.

CHAPTER 2: AN INTRINSIC MODEL OF PLANT GROWTH AT THE CELLULAR LEVEL

All work contained here was performed by Yuanjie Chen unless otherwise indicated.

SUMMARY

Turgor pressure, cell wall stiffness, cellulose orientation and chemical signals act together to govern the growth rate of a plant cell. Hypocotyl cells are cylindrical and the non-dividing epidermal cells expand anisotropically, in the axial direction. To date, no model has been proposed which explores the growth of a hypocotyl cell over a long period. Studying the hypocotyl epidermal cells of *Arabidopsis thaliana*, I investigated and quantified the behaviour of cell size, turgor pressure and wall stiffness over time. I then developed an intrinsic model linking these factors, based on the Lockhart model[10] of cell growth and including the concept of an energy bond stress distribution function and energy dissipation within the cell wall itself. Using this bottom-up approach, the model described the relationships among length, pressure and yield stress with mathematical equations and simulated them over time. It successfully captured the experimentally observed behaviour when one or more of those parameters were altered. In addition, a sensitivity analysis was performed to provide insight into a potential role of stress distribution (bond energy distribution). This model provides a new way of studying and understanding the growth pattern of a cell in walled organisms including plants, bacteria, fungi and many algae.

INTRODUCTION

Physical deformation of the cell wall

Plant cells are embedded in a stiff shell; the cell wall. The growing cell wall is a thin, strong layer of cellulose microfibrils embedded in a matrix of complex polysaccharides and a small amount of structural proteins[36]. In order for the cell to grow, the cell wall has to yield; this means linkages among cellulose, hemicellulose, polysaccharide chains and chemical bonds would break. In plants, the presence of a cell wall creates two important physical realities: firstly, for a cell to grow its cell wall must change to allow plastic deformation; secondly, the cell wall connects neighbouring cells such that the behaviour of any cell may be controlled locally but has global impact and feedback. For

simplification, each plant cell is considered as its own physical unit with a rigid cell wall and high internal pressure (turgor pressure).

Turgor pressure

Turgor pressure is the force maintaining cell turgidity and driving its volumetric expansion[88]. In plants, it is caused by the osmotic flow of water: the inflow of water, due to a solute concentration difference across the plasma membrane pushes the membrane against the cell wall[89]. As the driving force for cell expansion, the magnitude of turgor pressure may impact the rate of cellular growth. In plants, diffuse growth is evenly distributed over the cell's surface and tip growth occurs at the tip of an elongating cell. In maize coleoptiles (diffuse growth), the growth rate was affected when turgor pressure was changed artificially[90]. Whereas in growing lily pollen tubes (tip growth), no correlation was found between turgor pressure and growth rate[91]. It is possible that diffuse growth, throughout the cell volume, is more reliant of pressure magnitude than the very localised tip-growth. Water potential describes the potential energy of water movement and in plant cells, $(\psi) = \psi_\pi + P$[25]. Where ψ_π is the osmotic pressure caused by dissolved ions inside the cell. P is the turgor pressure, which pushes the plasma membrane against the cell wall. The presence of turgor pressure is important for a healthy plant cell to maintain turgidity and to provide the force for cell enlargement.

The cell wall

The cell wall is a very tough, flexible and sometimes fairly rigid layer that surrounds each cell and acts as a physical constraint on pressure. It is strong enough to resist the high turgor pressure but also it needs to allow cell growth at the correct time. A cell expands when force created by turgor pressure is greater than a yield threshold; this threshold depends on the cell wall material properties[10].

The cell wall is composed of crystalline cellulose microfibrils that are embedded in a matrix of complex polysaccharides[34][92]. Cellulose microfibrils provide strength and mechanical rigidity to the cell wall. They also contribute to material anisotropy through coordinated alignment[38][39]. Cellulose is deposited in the cell wall through the action of cellulose synthase complexes located on the cell membrane[40]. Cellulose synthase enzyme synthesises cellulose by catalysing the chemical reaction to form a chain of (1⟶4)-β-D-glucosyl residues[41].

Another class of important cell wall polysaccharides are the matrix pectins and xyloglucans. In *Arabidopsis*, these complex polysaccharides consist mainly of esterified D-galacturonic acid resides in

an alpha-chain, homogalacturonan (HG)[5]. Pectin forms hydrated gels that may act to push cellulose microfibril apart, ease their slippage during cell enlargement[8] and lock them in place when growth ceases. HG gelling is largely affected by changes in HG degree of methyl-esterification and the availability of calcium ions. Pectin is delivered to the cell wall highly methyl-esterified in a form which does not gel well[84]. De-methylation makes the chains negatively charged and Ca^{2+} ions are able to bond to chains, forming a cross-linking via a calcium bridge[71][5][9]. Ca^{2+} cross-linked pectin gels exhibit strain stiffening making the cell wall harder to expand[9][93].

Linking wall composition to mechanics

Xyloglucan, together with cellulose (more rigid), and the chemical bonds inside the pectin (more elastic), form a load-bearing network in the cell wall. When a cell enlarges in size, some of those bonds in the cell wall are constantly broken and reformed, resulting in microstructure rearrangements[94]. Considering the fluid mechanical properties of the cell wall, the widely accepted $k-\varepsilon$ fracture model can be applied: $\mu = C_v k^2 \varepsilon^{-1}$, where μ is the viscosity of the fluid, k is the energy and ε represents the energy dissipation rate[95]. C_v is some constant range between 0.0785 and 0.09 (commonly accepted value)[95]. And viscosity μ is a function of bond density ρ, i.e. $\mu = \mu(\rho)$.

Cellulose is widely accepted to bear the load in the cell wall[34][92][39][48]. More recently, pectin has been shown to be involved in maintaining cell shapes[7]. However, the way that pectin and cellulose limit growth is fundamentally different: Pectin forms Ca^{2+} bridges, which stiffens the wall. The bridge can be broken and polysaccharides can slip apart, free Ca^{2+} ion can re-form bridges once broken[96][97]. In contrast, cellulose is inextensible, and only stiffens the wall in the direction along its length, if extended. It is proposed that hemicellulose (xyloglucan) tethers cellulose at 'hot spots'[98], which provides irreversible linkage at the axis of cell expansion. So for directions orthogonal to cellulose fibres when aligned, wall stiffness may be contributed by pectin and the bonds between hemicellulose and cellulose. The orientation of cellulose is important for the dark-grown hypocotyl epidermis[2]. At germination, the orientation is random when there is no rapid anisotropic growth[7][99] (Chapter 1). Later, during rapid anisotropic elongation, the stiffness in the radial expansion contributed from the pectin is not sufficient with a high turgor, and cellulose transversely orientates to help the cell to retain the radial expansion[7]. At this time the vertical stiffness is only provided by the pectin (reversible bonds) and hemicellulose (irreversible bonds) and the cell achieves fast anisotropic elongation in the longitudinal direction[2][7]. The process of cellular elongation does not continue indefinitely. The cellulose eventually becomes longitudinally oriented to provide stiffness

in the growth axis direction and growth then ceases (Chapter 1). Radial stiffness is still high as enough transversely aligned cellulose is embedded in the pectin already.

Existing growth models

Numerous growth models have been developed for plant cells. Many of these models have focused on a limited set of factors affecting cellular growth, a necessary reduction to further our understanding. These may broadly be split into two categories: models of growth itself and models which incorporate material anisotropy and geometry. With respect to growth models, Lockhart[10] was the first to raise the idea of a relationship between pressure and yield threshold. He developed mathematical equations describing cylindrical cell elongation in relation to cell wall extensibility and osmotic pressure. He assumed that the turgor was relatively steady during growth, and had a linear relationship with irreversible strain (growth) if it exceeded a yield stress. Wall extensibility was not addressed in detail and assumed to be a constant. Later, Green et al[100] modelled the plant with a similar governing equation to the one used by Lockhart, but he simplified the equation by introducing a varying threshold Y (yield). He showed that Y responded to an artificial change in turgor pressure. Fitting experimental data, an empirical non-linear equation of Y over time was established.

Cosgrove et al[101] mathematically determined how pressure should change over time, and investigated the effect of pressure perturbation on cellular growth rate. Later, it was found that the water potential in pea stems did not vary when growth rates were altered (over a 20-fold change) and hence growth was concluded to be mainly controlled by the yielding properties of the wall[102]. A theoretical analysis of pressure decay during growth was performed and the in vivo stress-relaxation tests (which measure wall visco-plasticity) were supportive[102]. Ortega[103][104][105] augmented Lockhart's equation by considering the non-steady state, i.e. a changing force. He also introduced an elastic modulus to the system and different conditions where turgor pressure and wall extensibility can change, and discussed the measurement based on the mathematical formulation. Theoretical turgor pressures for *Nitella* and *Phycomyces* based on the equations were measured, and it was found that both a large step-up and step-down in the turgor pressure reduce the growth rate[104][105].A potential limitation of this study lies in the assumption that too many parameters were constant, which may not be the case in reality. In addition, the cell wall was treated as a static material rather than a part of a live growing cell.

McCoy et al[13] developed an axial plant growth model based on the law of energy conservation, where all forces driving plant growth were assumed to be known; internal chemical potential energy

and kinetic energy associated with the aqueous phase and non-aqueous phase were estimated. Theoretical solutions were given but the energy lost was neglected and some parameter details lack justification in terms of a plant growth model. Wold et al[14] assumed the cylindrical cell wall was made of layers with aligned fibres, a constant fibril orientation distribution of new wall synthesis, and strain rates being the same in each layer. By considering axial, transverse, and shear strain and stress, the model derived how strain rate could be affected. As mentioned previously, Cosgrove et al[101] modelled growth after studying the time dependency of turgor in detail; this growth model also attempted using conservation of energy law[13] and equilibrium of thermal dynamics[12], where extensibility had a more chemically relevant basis within the cell wall. In Cosgrove's model, the focus of the thermodynamics was the elasticity of macromolecules and hydrogen bonds and he derived the same governing equation as previously assumed by Lockhart. This approach opened up the utility of thermodynamic descriptions of the wall as they relate to growth, and left room for exploration of anisotropy and pectin dynamics within this framework.

Recently, modellers have shifted their interests to material anisotropy, mechanical properties and geometrical transformations, and many highly dynamical cellular models have been created. Cave et al[106] developed an anisotropic elasticity model of the plant cell wall assuming the wall comprised an anisotropic fibrillary cellulose component and an isotropic matrix component. Starting with Hook's law and using the stress tensor, a relationship between the longitudinal Young's modulus and the mean microfibril angle was established. Ahlquist et al[107] took a similar approach to modelling growth in the fungus, *Phycomyces*. He considered a number of different factors including wall thickness, variable microfibril orientation, variable microfibril spacing and microfibril overlap. The organ was pulled in a tensile test and some relationships between stress and strain were plotted and discussed, yet the mathematical process was not fully explained. Sellen et al[15] developed a theoretical stress-strain relationship when there is an elastic deformation on a cylindrical cell, and he showed how longitudinal, transverse and shear strain are different as a result of the cylinder geometry. Wu[16] investigated the effect of cell wall elastic properties on the shear modulus of the wall material, and a non-linear pressure-volume relationship was identified for spherical and cylindrical-shaped cells. Chaplain[108] agreed with Wu and simplified the theory by characterising the elastic properties of an ideal cell wall in terms of a more general strain energy function which can describe the non-linear pressure-volume relationship exhibited in cell expansion. Dumais et al[18] modelled discrete tip growth by considering the cell wall thickness and extensibility distribution over a tip geometry. Dyson et al[17] constructed a theoretical model of a growing cell, representing the primary cell wall as a thin axisymmetric fibre-reinforced viscous sheet. Her model reaffirmed the traditional Lockhart model but provided insights into the geometric parameters and discussed solutions with different fibre angle and

extensibilities. So far, no computational model has been built to study the dynamics and relationships among the growth factors.

In this chapter I introduce a new dynamical model considering the key factors affecting cell growth: turgor pressure, growth signals, cell wall stiffness and bond stress distributions. I studied those factors in dark-grown hypocotyl epidermal cells of the *Arabidopsis thaliana* and used them to test the modelling outcome. I focused on the bottom epidermal cells and modelled them as being cylindrical shaped.

METHODS

Turgor pressure measurement and calculation

mYFP (and *PME x mYFP*, *PMEI x mYFP*) seedlings were used to find the osmotic pressure in hypocotyl cells during growth. Seedlings were prepared as before (Chapter 1) and harvested at 24, 48 and 72 HPG. For PME and PMEI induction, 400ul of 50% EtOH in a tube was placed in the petri dish for ethanol inducement of the transgenes[7](Chapter 1). At the desired time points, seedlings were taken from the dark environment, seed coats were removed and a shallow scratch was made on the hypocotyl from bottom to top using a fine needle; scratching was necessary to disrupt the cuticle and allow for fast exposure of hypocotyl cells to osmotic treatments. Seedlings were then placed into Mannitol solutions of different concentration (range from 0.2M to 0.7M) for 10 minutes and then imaged. Images were taken using the Leica SP8 confocal microscope with a 25 x water objective. Each cell was then classified as being non-plasmolysed (cell membrane do not detach from the cell wall, sharp edge), plasmolysed (cell membrane just start to detach from the cell wall) (Fig. 2.1(a)) or over-plasmolysed (cell membrane completely detach from the cell wall, round edges)(Fig. 2.1(b)), depending on their plasmolysis status. (n>40 per time point)

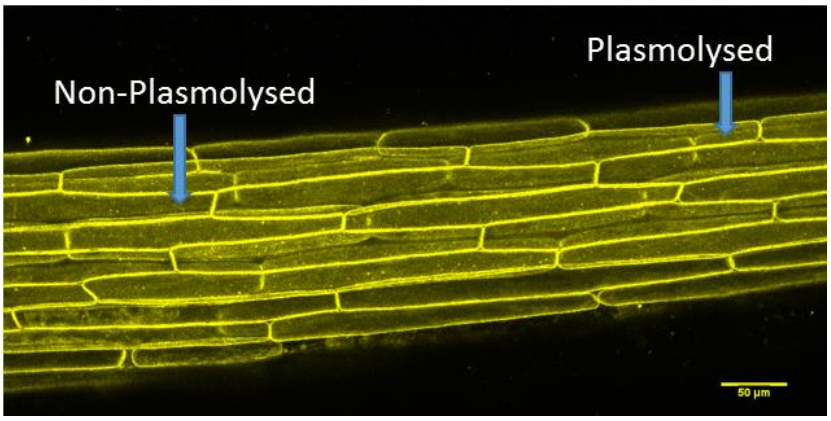

Figure 2.1(a) An mYFP-expressing seedling where both non-plasmolysed and plasmolysed cells are seen. Incipient plasmolysis is best seen as the slight rounding of cell-cell junctions and corners

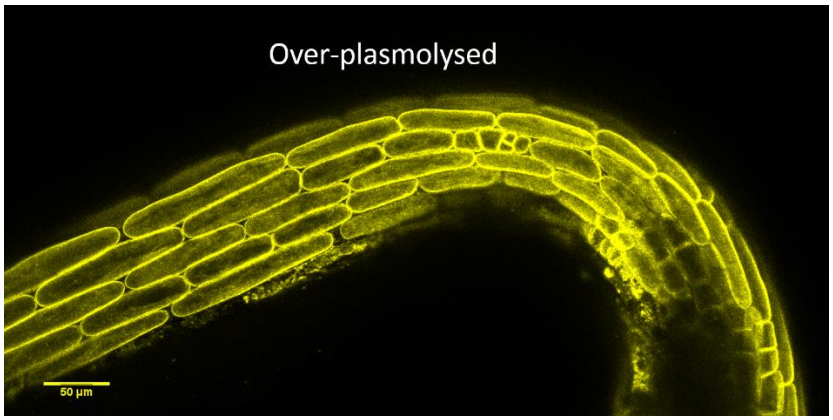

Figure 2.1(b) An mYFP-expressing seedling where most cells are over-plasmolysed

The osmotic strength of the 1/2MS media was estimated according to the major salts in the solution, and with the formula:

$$\pi = i \cdot \phi \cdot C \cdot R \cdot T$$

Where π was the osmotic potential, *i* was the ionization constant, ϕ was the osmotic coefficient, *C* was the concentration in mol/liter, *R* was the universal gas constant, 0.083145 L·bar/moles·K, and *T* was the absolute temperature in Kelvin. The osmotic potential for the 1/2MS media was calculated to be 0.2442 MPa (detailed calculation see supplementary). Using the same formula, the osmotic potential for the mannitol solution was also calculated.

At plasmolysis, there was assumed to be no net water flow across the cell membrane, and hence the turgor pressure could be estimated: $-P = \pi_{out} - \pi_{in} = \pi_{mannitol} - \pi_{media}$, and the absolute value of the turgor pressure was calculated[96]. (For detailed calculations see supplementary)

Atomic force microscopy (Experiment performed by F. Bou Daher)

AFM-based nano-indentation experiments were designed and performed according to Braybrook[109] (by F. Bou Daher). Dissected and plasmolysed (0.55M mannitol; minimum 15 min) hypocotyls were indented using a Nano Wizard 3 AFM (JPK Instruments, DE) mounted with a 5 nm diameter pyramidal indenter (Windsor Scientific, UK) on a cantilever of 45.5N/m stiffness; cantilever stiffness was calibrated by thermal tuning. For each hypocotyl, a basal cell area (cell index 1-4) was indented with 32x32 points. Indentations were performed with 500 nN of force yielding an indentation depth range of 250-500nm. At each of the three time points (24 HPG, 48 HPG, 72 HPG), sample numbers were as follows: 24 HPG, n=15 cells from 6 seedlings; 48 HPG, n=20 cells from 20 seedlings, 72 HPG, n=30 cells from 20 seedlings. *PME/PMEI* at 48 HPG, n=15 cells from 6 seedlings. Sample image in Fig. S2.4.

Young's modulus calculation

JPK SPM Data Processing software (JPK Instruments, DE, v.spm 6.0.69) was used to extract data and analyse the force indentation approach curves. Young's modulus (indentation modulus[7]) maps were then imported into Matlab (MATLAB 2016a, MathWorks, Inc., USA) (See supplementary code) and values were selected from anticlinal cell walls. For each grid area, 10-50 points were chosen from anticlinal side walls and used for subsequent analyses, representing data from 3-10 cells depending on cell length in the scan area. Mann-Whitney tests for significant differences were performed as distributions were non-normal.

Modelling

Here I introduce a physical growth model of an anisotropic cylindrical plant cell, based on the internal bond energy of the wall and the turgor pressure. The growth of a cell is a complex process. In previous models, cell wall expansion was often viewed as a purely viscous flow of a fibreglass-like material. While growing cell walls possess viscoelastic properties, the viscoelastic properties change slowly but growth could be controlled quickly without concomitant changes in viscoelasticity[110]. Hence,

identifying the starting and ending mechanisms of growth for a cell is important, and the following parameters are chosen:

S: Material Synthesis rate. This is the signal for growth, travelling through the hypocotyl from the bottom to the top in an acropetal wave[7][1]. On average, the fast elongation phase was delayed for approximately 5 hours for every cell index away from the bottom[7]. S≠0 is essential for growth to begin. Here S is modelled as a unipolar continuous sigmoid function: $S(t) = \frac{1}{1+e^{-t+(5Index+c_1)}}$ when t is small and $S(t) = \frac{1}{1+e^{t-(5Index+c_2)}}$ when t is large. c_1 and c_2 are a delay constant depending on the cell position. (c_1=10, and c_2=52 according to experimental data (Chapter 1), in order to produce a wave)

P: the turgor pressure of the cell

p: a proportion of bond to break for cell wall to yield

H1: a proportion of the sum of the irreversible energy per unit area of the cell wall, mainly from the newly synthesised cellulose and hemicellulose. H1 is anisotropic, depending on the orientation of the newly synthesised cellulose

H2: a proportion of reversible bond energy per unit area inside the cell wall, mainly from the calcium cross links in the pectin gel. H2 is assumed to be isotropic.

V: Volume of the cell

$Width$: Diameter of the cell

TW: Thickness of the cell wall

L: Length of the cell, equals $\frac{V}{\pi*(\frac{Width}{2})^2}$, assuming the cell is perfectly cylindrical

Y: The total bond energy inside the cell wall, Y= TW*(H1+H2)

Stress: the stress caused by the turgor pressure, calculated by $(\frac{P*Width}{2*TW})$ for a cylindrical cell

$yield\ stress$: a value determined by the total bond energy (Y), the energy distribution, and the proportion of bond energy that the stress need to exceed for the growth to happen.

The parameters vary with time and are dependant on one another. Here a feedback model is constructed to capture the relationships among all those factors inside the cell wall. A flow chart is presented to indicate the mechanism of the model simulation.

Flow chart of the model

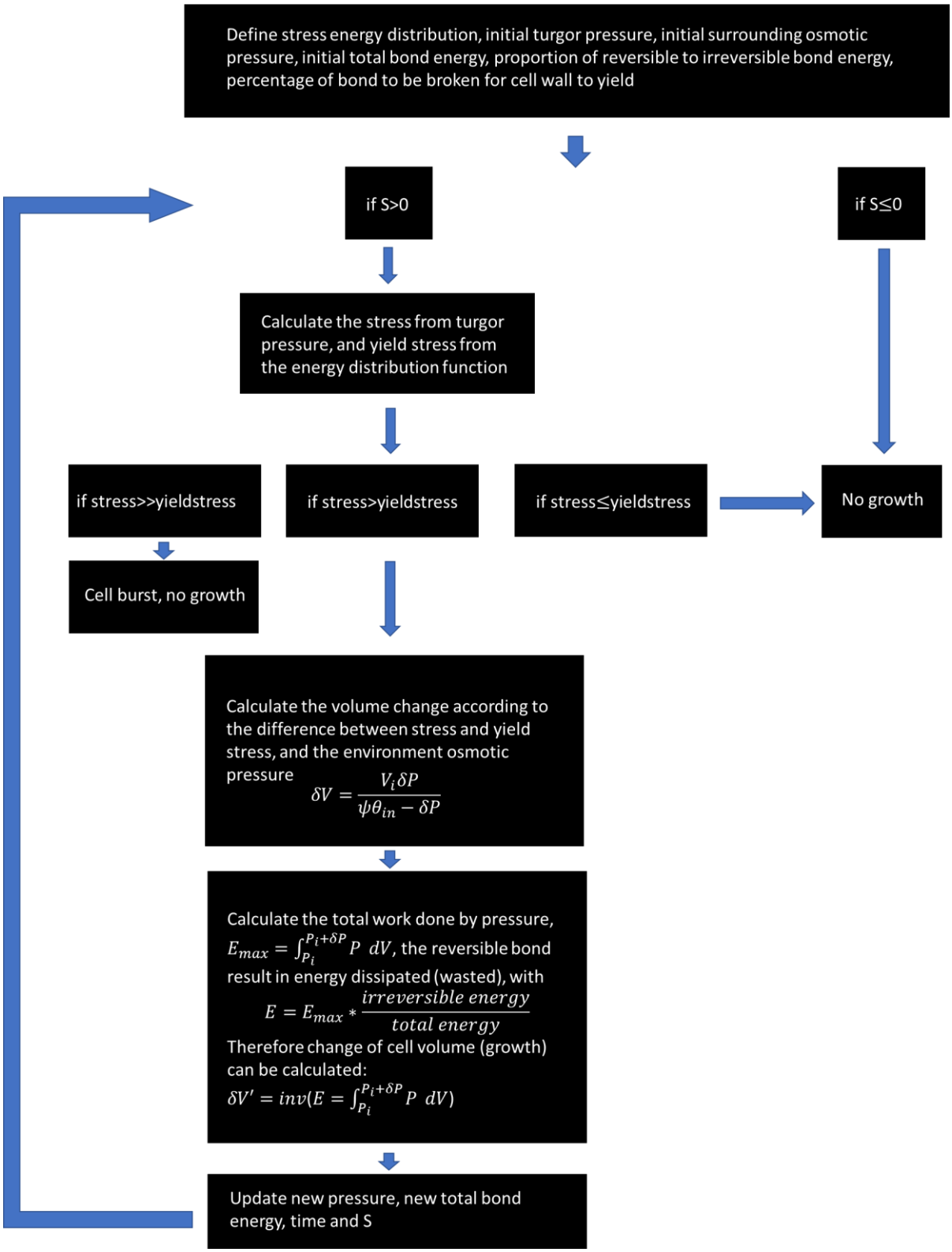

Flow chart 1 A brief summary of the model

The concept of the bond energy distribution function is introduced: Not all bonds in the cell wall are subject to the same force; some may experience larger forces to hold the cell wall and some may experience smaller ones due to their nature or position inside the cell wall. This gives a stress distribution of bonds, where the x-axis is the stress a single bond is subjected to and the y-axis is the number of bonds. The area under the distribution curve therefore represents the total bond energy. Given that a number of bonds needs to be broken for the wall to yield, the actual yield stress is different with different shapes of bond energy distributions. It is difficult to determine what distribution it is, due to the existence of different types of bonds and the complex structure of the bond network. This distribution may also change with the cell size, wall thickness, and the ratio of different types of bonds within the wall. For simplicity, the probability distribution function of gamma distribution with parameter [α =7, λ=1.2] is set as default (Equation 1). The gamma distribution is a continuous representation of a Poisson distribution, and its shape can be modified with its parameters for further investigation (Supplementary Fig. S2.2).

$$B(x) = \begin{cases} \frac{\lambda(\lambda x)^{\alpha-1}e^{-\lambda x}}{\Gamma(\alpha)} & x > 0 \\ 0 & x \leq 0 \end{cases} \quad (1)$$

Where $B(x)$ is the bond energy distribution, and $\Gamma(z) = \int_0^\infty x^{z-1}e^{-x}dx$, for $z > 0$, is the Gamma function. Hence the total bond stress energy function, $B_c(x)$ is the cumulative distribution function of $B(x)$.

The growth of a cylindrical hypocotyl cell is modelled as the sum of many discrete growth cycles. In each cycle, the turgor pressure (P) increases with a rate according to the Noyes-Whitney equation or decreases exponentially[102][111] as the water moves in and the cell expands in volume. The stress in the cell depends on the pressure as well as the cell geometry:

$$stress = \frac{P*Width}{2*TW} \quad (2)$$

Where Width is the diameter of the cell and TW is the thickness of the cell wall. Both Width (=16.17) and Wall thickness (=1) are constants for simplicity in the model.

A cell can grow when its stress exceeds a yield stress, where some bonds would break. The yield stress is determined by a proportion of bonds with high stress which need to be broken for the wall to yield. The initial proportion of bond to be broken is set to be 0.005. The yield stress also depends on the total bond energy (Y) and the total bond energy distribution, and so we have:

$$yield\ stress = inv(B_c(\frac{p}{(Y/L)}) \quad (3)$$

Where p is the proportion of bond need to be broken, L is current length of the cell, and Y is the total bond energy of the cell wall. i.e. Higher bond energy density (Y/L) of the cell wall results in larger yield stress but higher proportion of bond breakage results in lower yield stress. During simulation, the bond energy distribution ($B(x)$) has three parameters, in addition to α and λ, a third parameter l changes the location of the function, which was selected so that values of the x-axis are in the same scale with the stress calculated from turgor pressure.

Similarly to Lockhart[10] it was assumed that the growth rate is proportional to the difference between stress and the yield stress, and this difference gives a potential change in the turgor pressure:

$$\delta P=\frac{2*TW*(stress-yield\ stress)}{Width} \quad (4)$$

But it is known that:

$$P = \pi_{in} - \pi_{out} = i\emptyset RT(\theta_{in} - \theta_{out}) \ (5)$$

where $\pi_{in} - \pi_{out}$ is the difference in osmotic potential across the cell wall, i is the ionization constant, $\emptyset$ is the osmotic coefficient (unitless, equals one in most cases), $\theta_{in},\ \theta_{out}$ are the concentrations in mol/liter, R is the universal gas constant, 0.083145 L·bar/moles·K, and T iss the absolute temperature in Kelvin. When a cell enlarges, water comes in and concentration inside the cell is $\theta = \frac{V_i\theta_{in}}{V_i+\delta V}$. Hence $\delta P = P(\theta = \theta_i) - P(\theta = \theta)$, where $P_i = P(\theta = \theta_i)$, the initial turgor pressure at the start of the cycle, and $P = P(\theta = \theta)$, the current turgor pressure. Rearrange to get the maximum increment in volume due to this change in turgor:

$$\delta V = \frac{V_i\delta P}{\psi\theta_{in}} \quad (6)$$

Where $\psi = i\emptyset RT$ according to the definition of osmotic potential. Therefore the maximum potential work that can be done by this turgor is:

$$E_{max} = \text{Force} * \text{Distance} = \text{Pressure} * \text{Volume}$$

$$= \int_{P_i}^{P_i+\delta P} P\ dV = \delta V\psi((\theta_i - \theta_{out}) + \theta_i \log\left(\frac{\delta V+V_i}{2\delta V+V_i}\right)) \ (7)$$

During growth, energy is dissipated into the cell wall[94], and this process is modelled differently depending on the proportion of fracture of polymer chains, reversible crosslinking and pullout of fibres. The hemicellulose and other polymer chains are irreversible and fragile (evolution of H1 during growth), the ionic calcium cross links are reversible and extensible (evolution of H2 during growth). Depending on the ratio of irreversible bonds and reversible bonds in the cell wall, the mechanical energy dissipated is calculated according to the Lake–Thomas theory:

$$\Gamma_f = 2U_f N_f h$$

$$\Gamma_{dc} = 2U_{dc} N_{dc} h \quad (8)$$

where U_f is the energy required to rupture a bond, N_f is the number of bonds fractured per unit volume, and h is the thickness of the process zone (cell wall). U_{dc} is the mechanical energy dissipated per decrosslinked polymer chain, N_{dc} is the number of decrosslinked polymer chains per unit volume of the dissipation zone, and h is the thickness of the dissipation zone (cell wall). So the dissipated energy is proportional to the total reversible energy, and a simplified estimation of work done by turgor is given by:

$$E = E_{max} * \frac{irreversible\ energy}{total\ energy} \quad (9)$$

Then, the real volume increment in this growth cycle is calculated by solving the inverse function of (7), i.e.:

$$\delta V' = inv(E = \int_{P_i}^{P_i+\delta P} P\ dV) \quad (10)$$

The breaking of bonds in the cell wall allows water to enter the cell, balancing the osmotic potential and reducing turgor pressure. In the meantime, the ionic bonds re-form in the pectin matrix (evolving H2), and this ends a growth cycle. The volume of a cell, pressure and bond energy is updated before a new cycle starts.

Since the process of water uptake is proposed to happen fast, a few seconds at the single cell level[112], this time is considered to be insignificant when calculating the overall growth rate.

In this computational model, the growth of a cell is slowed down or terminated by two different mechanisms: 1) If the growth signal (S) is ended, no new material is synthesised, no ion is exchanged through the plasma membrane, the turgor pressure becomes stable and the cell can no longer enlarge. 2) The cellulose can re-orient and limit the growth. Growth is stopped once the bond energy is high enough that the potential stress caused by the turgor pressure is unable to yield the cell wall.

RESULTS

Hypocotyl epidermal cells exhibited a sigmoidal-like elongation pattern in length but not in width

Cell-level elongation profiles of dark-grown hypocotyls have been reported to undergo sigmoidal growth[1]. Seedlings growing in the dark possess longer epidermal cells and smaller outer wall curvature compared to those growing in the light[1][113] so they can be modelled as cylindrical. I have previously conducted a confocal-based analysis of cell length and width during the first 72 hours of growth after germination in order to accurately describe anisotropic elongation in the dark-grown hypocotyl system (Chapter 1). Here, the same dataset was used but cells were grouped according to their position on hypocotyl, and the length/width was plotted against time rather than position. The average growth pattern of basal hypocotyl epidermal cells over 72 hours at 6-hour intervals was plotted in Fig. 2.2. After germination, defined here as the time of the radicle emergence from both the seed coat and the endosperm, there was a phase of a slow increase in cell length (0 to 12 hours post germination (HPG)) followed by a pause (12 to 24 HPG) after which the rapid expansion phase began (24 to 66 HPG); from 66 to 72 HPG the growth in length slowed considerably (Fig. 2.2A). The growth was slightly discontinuous at 12 to 24 HPG when a pause was seen, probably due to the transition from root growth to hypocotyl elongation. Data for cells from the middle and upper portions of the hypocotyl were displayed in Fig. S2.1. These patterns of cell dimension fit well with those previously described for length[1] and here serve as a benchmark for the model fitting: I attempted to generate a model growth curve with such sigmoidal behaviour.

Consistent with the earlier analyses[7], there was little change in cell diameter over these intervals (Fig. 2.2B). Interestingly, between 12 HPG and 24 HPG where cell elongation was paused, cell diameter was still increasing.

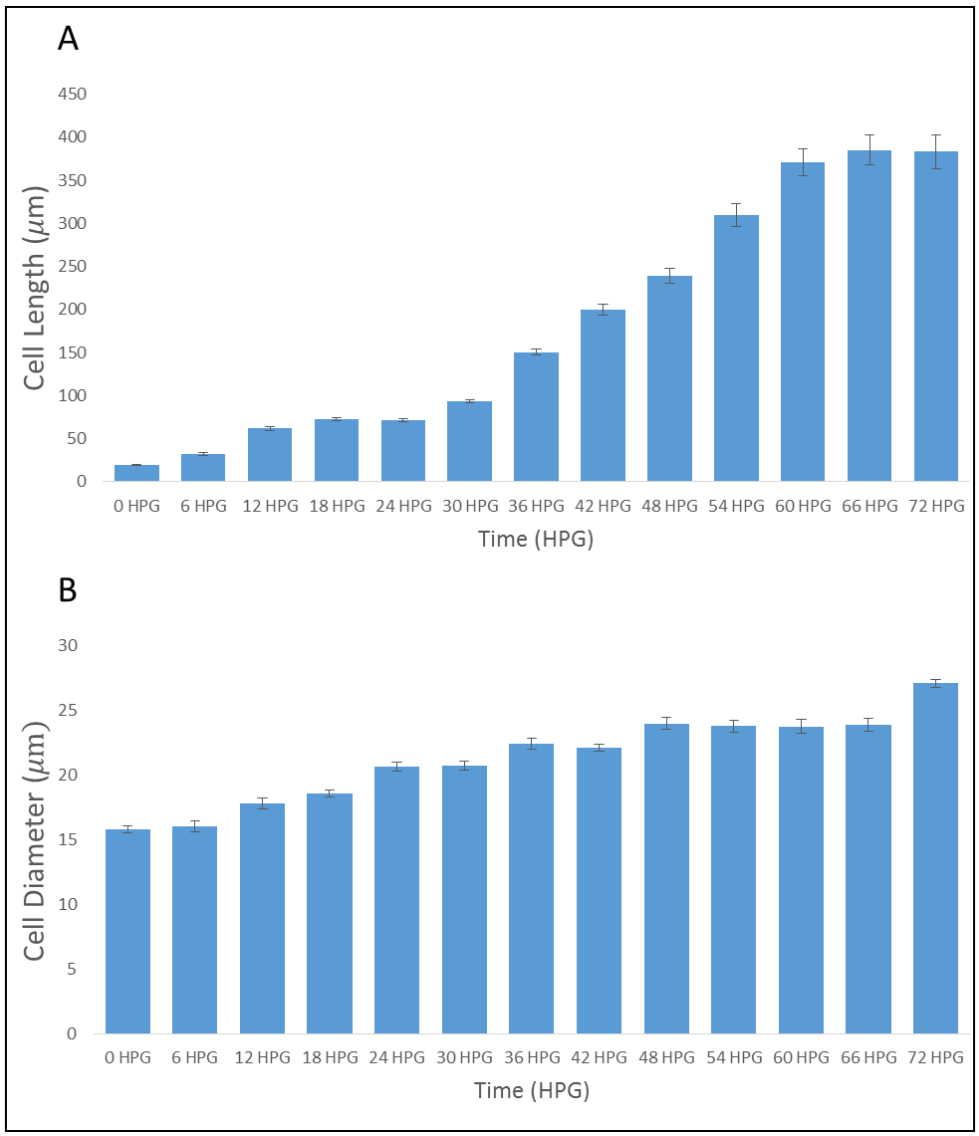

Figure 2.2 Basal epidermal cells (index 1-4) in the hypocotyl grow anisotropically. **A:** Average basal cell length. A sigmoidal pattern in the first 72 hours post germination (HPG), with a rapid elongation phase starts at 24 HPG and slows down at 60 HPG. After 72 HPG the basal cells are about 15 times longer on average than at 0HPG. **B:** Average basal cell diameter: Increases slowly over time, and only has a 50% expansion in the first 72HPG. Its relative growth rate is constantly small. (n>20 hypocotyls, n>34 cells/hypocotyl, error bar=propagated standard error)

Turgor Pressure decreased over time, with a large reduction during the fast elongation period

Turgor pressure generates the force required for the wall to yield[36][10]. In the plant roots, it has been suggested that no obvious difference in pressure exists between non-elongating and elongating cells[114]. In order to examine if pressure changed during basal cell hypocotyl elongation, the

plasmolytic method[115] was used to obtain turgor estimates for the 4 most basal cells (index 1-4) during elongation at 24 HPG, 48 HPG, 72 HPG and 96 HPG. In examined conditions, plasmolysis of seedlings was observed after 10 minutes in plasmolysing mannitol solutions (Fig. 2.1). Similar kinetics were observed upon cuticle disruption before exposure to plasmolytic solution(where a shallow scratch is made along the hypocotyl) indicating that the non-destructive method was not affected by the presence of cuticle (Supplementary Fig. S2.3). It was observed that plasmolysis points were variable between cells and as such a weighted thresholding mechanism for determining the average plasmolytic point for a time point was used, and the error bar represented maximum variation observed).

Initially, the average turgor was 1.1±0.05MPa at 24 HPG for the basal cells (Fig. 2.3A, max value=1.15 MPa, min value=0.95 MPa). Average turgor pressure decreased over the next 72 hours, quickly from 24 to 48 HPG (Fig. 2.3A, max value=0.79 MPa, min value=0.62 MPa, average 0.7±0.09MPa), and more slowly from 48 to 72 HPG (Fig. 2.3A, max value=0.63 MPa, min value=0.5 MPa, average 0.57±0.06MPa). From 72 HPG to 96 HPG the turgor stayed stable. These data led to a conclusion that turgor decreased with increasing cell length. Cells in the upper part of the hypocotyl had the same pattern of pressure decrease (S1), where the pressure decreased to a slightly lower value than the basal cells.

The cell wall became softer during the fast elongation period

The presence of turgor pressure is necessary for a cell to grow but turgor pressure cannot expand the wall on its own without the wall yielding[89]. Cell wall stiffness plays a major role in controlling growth[7]. The pectin matrix, cellulose and hemicellulose are assembled in a complex network[112], forming a rigid cell wall. Different types of bonds such as chemical bonds (some are reversible) and physical tethers (mostly irreversible) provide both elastic and viscoelastic properties to the cell wall[5]. A mechanical model that describes the plant cell wall perfectly has not yet been developed. Some viscoelastic models capture behaviours of the cell wall but their parameters could not be easily interpreted[116][5]. Here, Young's modulus (YM) was used for a representation of plant cell wall elasticity, which was proportional to the stiffness by definition.

Our previous examination of hypocotyl growth indicated that epidermal cell wall elasticity decreased over time[7]. In order to provide a full and quantitative analysis of this possibility, AFM-based elasticity tests in basal regions of hypocotyls at 24HPG, 48HPG, 72HPG were performed. The indentation modulus of elongating axial cell walls decreased between 24 and 48 HPG from 37.89±2.48 to 18.06±1.70, then to 17.37±1.88 by 72HPG (Fig. 2.3B, blue and orange lines are two possible regression

lines given the three time points). These data indicated that cell wall stiffness decreased over the rapid growth phase and remained more elastic afterwards.

Compared to the observed pattern in turgor pressure (Fig. 2.3A), the YM had a similar decreasing pattern from 24 HPG to 72 HPG, indicating a potential correlation between the two. In traditional models, the strain (growth) rate was proportional to the difference between P and Y[10][102], where P was defined as the turgor pressure and Y as the yield threshold. This concept of 'excess of turgor pressure over a wall threshold' has been widely used[10][12][100][103][104]. The data was normalised against the reference value at 24 HPG and the ratio of $\frac{\text{Pressure}}{\text{YM}}$ was compared (Fig. 2.3C). The ratio of normalised $\frac{\text{Pressure}}{\text{YM}}$ was higher at 48 HPG, corresponding to a faster relative elongation rate calculated in the previous section.

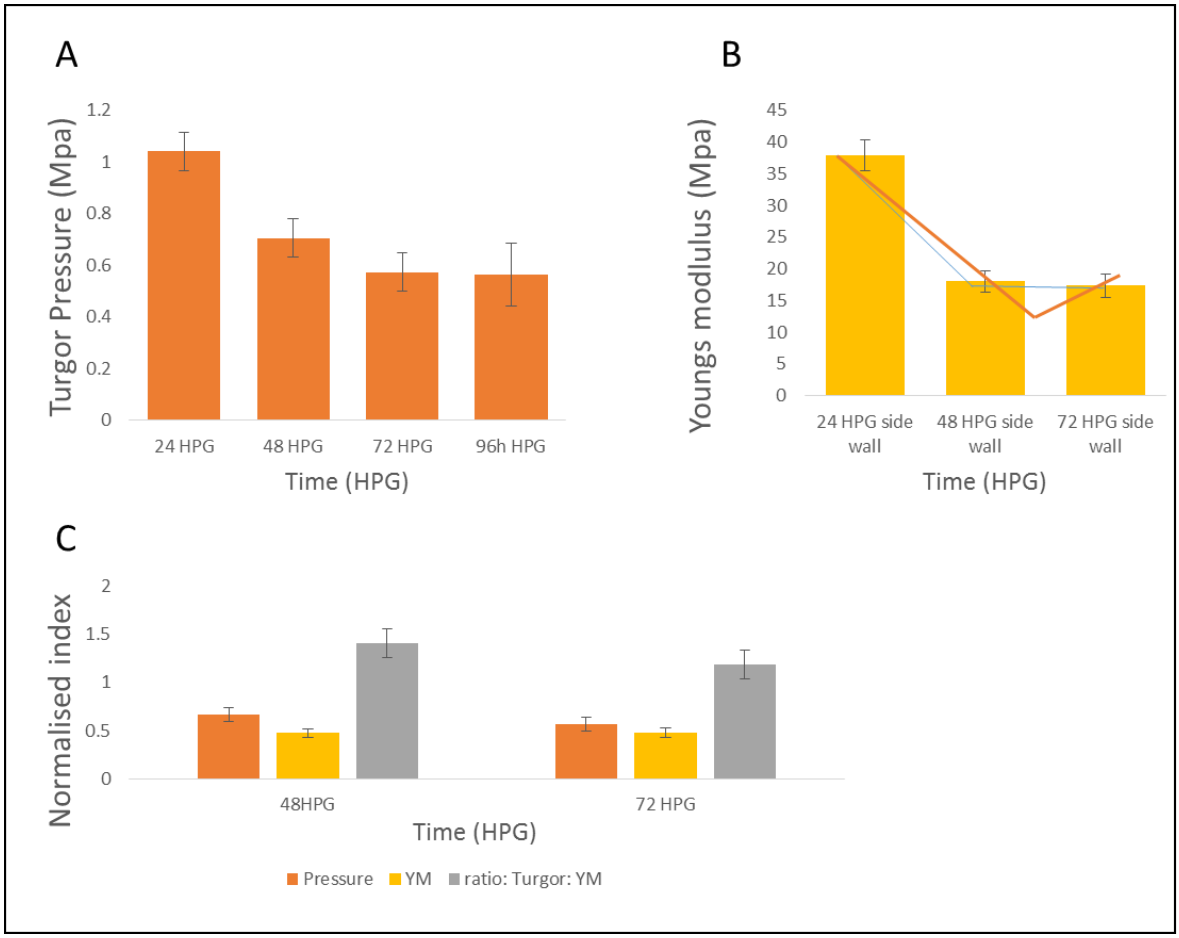

Figure 2.3 Both turgor pressure and wall stiffness decrease over time, following a similar pattern. **A:** The average calculated turgor pressure of basal cells at 4 time points after germination shows a decrease in the turgor pressure over time. (n>40 cells from 5 hypocotyls, bars=maximum variation of concentration of mannitol used for cell plasmolysis, ANOVA test, p-value=4.92E-06) **B:** The average Young's modulus of the basal epidermal axial cell walls at 3 time points after germination. The red and

blue lines represent two possible patterns based on the data from three time points. (n>6 seedlings for each time points, >20 points from the AFM data extracted for analysis from each seedling, bars=standard error, Mann Whitney test, p-value=2.56E-07) **C:** Normalising the pressure and the YM to their value at 24 HPG

The model simulates the dynamic patterns of cell size, turgor pressure and the wall stiffness

An intrinsic and dynamic model of cellular growth was built, based on a current understanding of the physical factors involved in cell elongation. The model specifies the initial turgor pressure, energy of irreversible bond H1 (e.g. cellulose, xyloglucan linkages), the energy of reversible bond H2 (e.g. chemical bonds), and the energy distribution function in the cell wall. The model output consists of cell size, pressure, and yield stress (wall stiffness) over time. Many of the initial parameters are chosen according to real experimental data (e.g. width of the cell wall, osmotic potential of the media, etc) and many others are generated artificially with arbitrary units (e.g. the rate of chemical secretion and the rate of change of turgor due to the chemical secretion). (Supplementary Table S2.1) This model aims to investigate the relationships among physical factors of growth, by comparing their simulated pattern over time. The simulations of single cell volume, length, pressure and yield stress using the default set of parameters were plotted in Fig. 2.4. The simulated patterns of growth, pressure and yield stress were the same as the experimental data. The model gave a sigmoidal behaviour in volume (Fig. 2.4A), and then using the cell diameters acquired earlier (Chapter 1, Fig.1.11), the volume was divided by the cell cross-section area to get cell length (Fig. 2.4B). Because the expansion in diameter was relatively small, the length over time had a similar pattern with the volume over time, only slightly less curved in the beginning. The simulated sigmoidal pattern of the length over time was very similar compared to Fig. 2.2A or Fig. S2.1A, Fig. S2.1C, where the growth rate gradually increased in the beginning, remained linear during the fast elongation period and slowed down quickly in the end.

Simulated pressure decreases over time and the rate of change of pressure decreases over time (Fig. 2.4C), just like the experimental data (Fig. 2.3A). This is likely due to the water inflow during cell expansion (Eq.6), which lowers the turgor pressure in each growth cycle. The simulation also suggests a decreasing yield stress over time during the growth (Fig. 2.4D). The experimental data acquired earlier suggested a more exponential behaviour of the pressure, which was not seen in the simulation. This might be due to a non-constant synthesis rate (S) over time in the real hypocotyl: a slower synthesis rate would cause a slower change in the pressure and a slower growth rate. Another possibility could be a positive relationship between the rate of change of pressure and the difference

in the osmoticum across the plasma membrane, which was not included in the model; in a living cell the osmoticum could reasonably change over time.

It was difficult to measure the yield stress, and hence the YM, wall elasticity (stiffness), was measured as a reference. Although YM is not yield stress but quite likely they are correlative parameters. Overall, the simulated yield stress decreased over time with some variation in the rate of decrease. The value of yield stress depends on the total bond energy in the cell wall but it also depends on the bond energy (stress) distribution function. This dependency on the stress distribution resulted in the non-smoothness of the yield stress (Fig. 2.4D). In reality, middle and upper cells would have similar patterns but delay in the time. The synthesis rate S, and the initial values of P and Y might also be different with the basal cells, which would give faster/slower growth rates and longer/shorter final lengths.

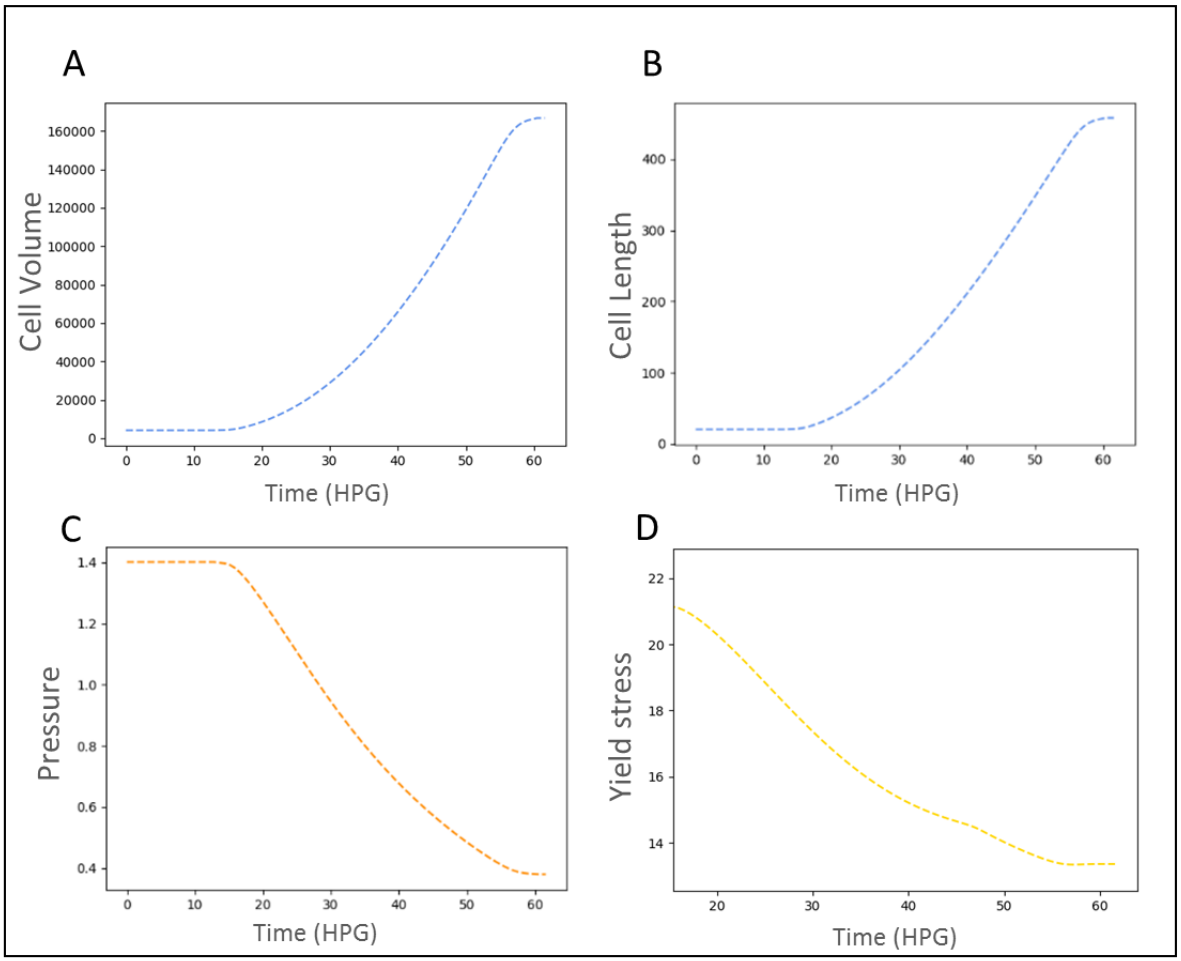

Figure 2.4 The simulated results of the model give correct trends of the length, pressure and yield stress for the basal hypocotyl epidermal cells over time. Units of the y-axis are arbitrary, scaled to a sensible range. **A, B:** The volume and length has a sigmoidal growth pattern. **C:** The turgor pressure drops over time during the elongation, slower than a linear rate. **D:** The yield stress exhibits a similar pattern to the turgor pressure. The pattern very much depends on the stress distribution function.

The cell wall stiffness showed a positive correlation with the turgor pressure and a negative correlation with the growth rate, when being modified artificially

As the cell wall is an important component in cell growth, wall-related parameters were varied experimentally and in simulations. PECTIN METHYL ESTERASE (PME) is a cell wall modifying enzyme that removes methyl groups from the pectin homogalacturonan. It allows more calcium cross links to form and makes the wall stiffer[7][5]. PECTIN METHYLESTERASE INHIBITOR (PMEI) proteins acts as inhibitors of PME proteins, keeping pectin in a methylated state. EtOH-inducible overexpression of PME5 and PMEI3 were used to modify the cell wall during growth[7][92]. We have previously showed that this line of PME5 over-expressor reduced cell size and increased Young's modulus compared to the mock, and oppositely for the PMEI3 over-expressor[7]. In order to test my model, I used the same system to induce walls with higher stiffness and lower stiffness. The PME over-expressor (*PME*) had a higher Young's modulus (Fig. 2.5C, 24.19±1.54 MPa), and a reduced length and diameter (Fig. 2.5A Fig. 2.5B, Basal cell length: 130.53±7.71 um, Basal cell diameter: 18.59±0.78) at 48 HPG[7]. On the other hand, the estimated pressure was significantly higher in the PME over-expressor compared to that of the *PMEI*. It remained high throughout the growth period and never went below 1 MPa (Fig. 2.5D). The *PMEI* behaved just like the *mYFP* used earlier, with a reduced pressure over time.

A stiffer wall and a softer wall were simulated and compared. To mimic what happened when seedlings were grown with inducible PME, the reversible bond energy H2 was increased (0.01 for softer wall and 0.025 for stiffer wall, unit nJ/μm^3), and also the parameter *a* in the stress distribution from 7 to 7.15, which mimicked a slightly higher proportion of bonds loading higher stress. Changing both is necessary for the yield stress generated to be in the correct range. The simulated length, pressure and yield stress over time was plotted in Fig. 2.6. Growth was slower with a stiffer wall, which resulted in a shortened final length. The simulated pressure had a sharp increment in the beginning when growth started. This indicated that the initial value for pressure was not sufficient to start growth, so it was increased to exceed the yield stress. For a stiffer wall, the simulated turgor pressure remained high and tended to experience less reduction over time (Fig. 2.6B). This was consistent with the turgor pressure in the plasmolysis experiment when comparing the inducible PME and PMEI (Fig. 2.5D Similarly, the yield stress started with a higher value and remained high over time during growth (Fig. 2.6C). With a stiffer wall, more bonds were available to load high stress, and this could increase the yield stress. Further, more bonds were initially under low stress but became available to load more stress when some bonds were broken during the growth, which could also result in a higher yield stress.

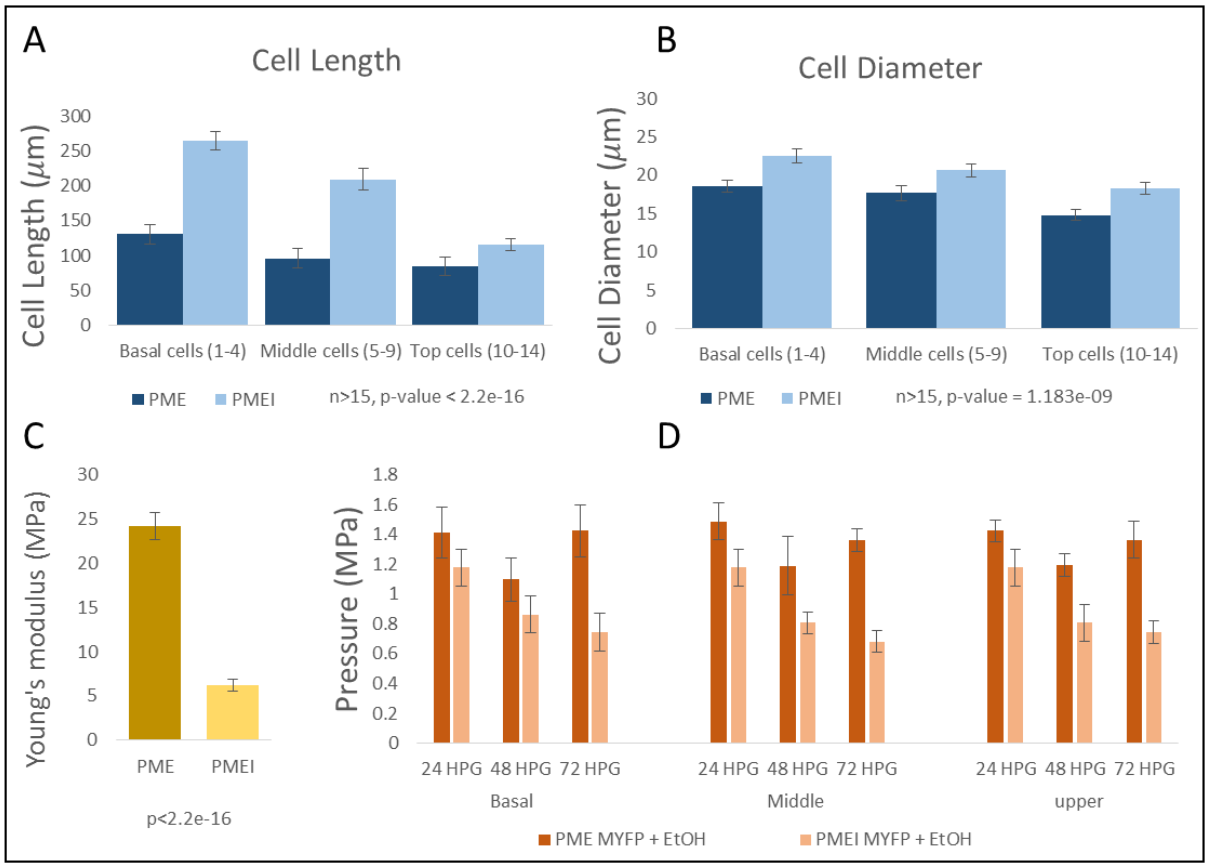

Figure 2.5 The wall stiffness had an effect on the growth parameters, resulting in different growth outcomes. The wall stiffness was altered using the inducible PME/PMEI, where there were more/less calcium cross links in the cell wall. **A,B**: At 48 HPG, the inducible PME had a significant reduction in cell length and diameter compared to the inducible PMEI. (ANOVA test, p<1.18e-09) **C:** The effect on wall stiffness was verified using the AFM. The indentation modulus (Young's modulus) of the basal PME hypocotyl cells is significantly higher than that of the basal PMEI hypocotyl cells. (t-test, p<2.20e-16) **D:** Turgor pressure was also affected. Cells with stiffer walls tended to have a higher turgor pressure, which was maintained high over time. Cells with softer walls tended to have a lower turgor pressure, which dropped over time during growth. (ANOVA test, p<2.33e-05)

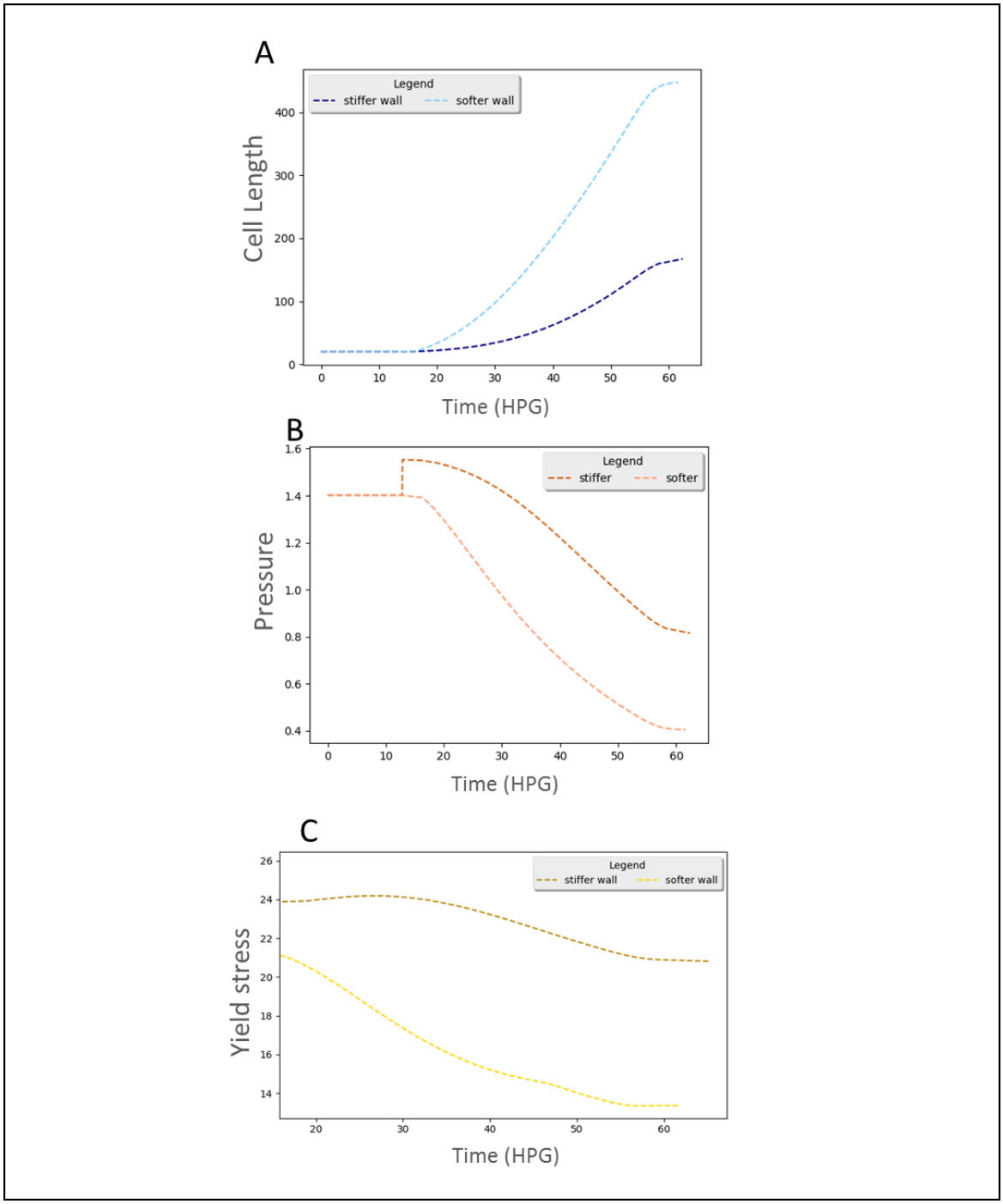

Figure 2.6 The simulated Length, Pressure and Yield stress matched to the earlier observation (Fig. 2.5). The reversible bond energy and the stress distribution function was altered to model a stiffer wall. **A:** With a stiffer wall, the growth rate was reduced; the final length was shorter. **B:** With a stiffer wall, the initial pressure was higher when the growth started. The pressure still dropped during growth but the rate was not as fast as that from a softer wall. **C:** The yield stress was directly affected by a change in the bond energy and stress distribution, and it was higher in a stiffer wall. During the growth it was not reduced as much compared to that from a softer wall.

Growth is inhibited when the turgor pressure is slightly reduced

Turgor pressure is one of the important factors involved in cell enlargement, and it is not easy to modify the turgor directly. The effect of turgor pressure on growth was studied and simulated in this section. Since turgor pressure is a result of the osmotic flow across the plasma membrane, theoretically, it can be changed slightly by raising the osmotic pressure in the media. In order to manipulate turgor, seedlings were grown in media with sorbitol; sorbitol provides an osmotic force without being metabolised as other sugars, e.g. sucrose. With extra sorbitol the surrounding osmotic pressure was increased, the osmotic difference across the plasma membrane was decreased, resulting in a reduced turgor pressure. In hypocotyls grown on media with increasing amounts of sorbitol, the overall organ length reduced proportionately. (Supplementary Fig. S2.5) Based on this experiment, a concentration of 1.60% sorbitol, equivalent to the 0.216 MPa osmotic force provided by 3% sucrose, was chosen for further experiments. Average cell lengths and diameters were reduced for seedlings growing in media with extra sorbitol (Fig. 2.7A, Fig. 2.7B). This is consistent with reduced turgor pressure. Unfortunately, this reduction in turgor pressure was too small, and unable to be tested using the plasmolysis method (the theoretical reduction in turgor was only 10% of the plasmolysis experimental resolution). Since the sorbitol was not involved in plant metabolism and a reduced hypocotyl/cell sizes were seen, it was reasonable to assume that turgor was reduced with the presence of the sorbitol.

In the simulation, theta2, a parameter representing the concentration of dissolved ions in the surrounding medium, was increased to simulate the extra osmoticum provided by sorbitol in the previous experiment. The simulation showed a slight reduction in growth rate, which became more obvious at later times as widening gap in final cell length (Fig. 2.7C). The relative decrease in the cell size was small, similar to the measured data (Fig. 2.7), yet they were not quantitatively comparable, as many parameters in the model had arbitrary units.

Although plants have abilities to adjust their internal pressure to compensate for the loss of turgor, it was reasonable to expect an overall reduced pressure due to the presence of additional surrounding osmoticum. This reduction in pressure was unable to test using the plasmolytic method due to the resolution issues. The reduction was more obvious in cell 4 to 7 and less obvious in cell 2 and 3, suggesting basal cells are more resistant to a decrease in pressure. This might also imply a delayed or slowed growth due to the reduced pressure.

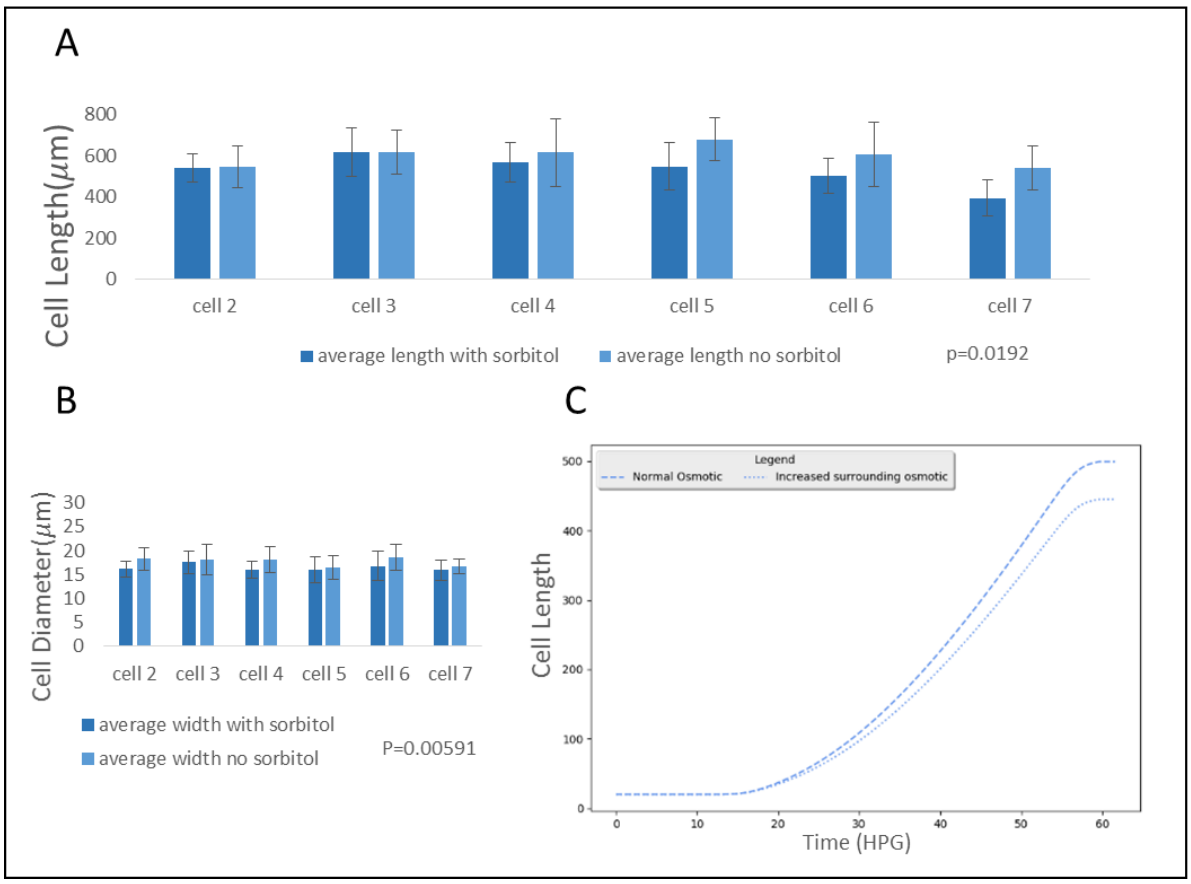

Figure 2.7 A,B: Hypocotyl elongation with altered osmoticum. Both cell length and diameter of seedlings growing in sorbitol (concentration equivalent to osmotic pressure provided by 3% sucrose) were significantly reduced at 48 HPG (n=60, paired t-test). The reductions were not intense because the extra osmotic pressure provided by the sorbitol was only ~ 0.2 MPa in magnitude, and going into a higher concentration might affected plants in other ways. n=60, Error=standard deviation. **C:** Simulating this by changing the osmotic pressure equivalent to the previous experiment outside the cell, a slightly reduced growth rate was seen.

A bond energy distribution with a sharper peak is more resistant to change in bond energy

In the model, the cell wall is characterised by its internal reversible/irreversible bonds and their energy distribution of bonds under different stress. When the stress exceeds the yield stress, a proportion of the bond break and the cell enlarges. A sensitivity analysis is performed here to investigate how the growth changes with respect to a change in bond energy and the bond energy distribution.

Growth is very sensitive to slight changes in the parameters related to the energy distribution (shape parameter: '*α*', location parameter: '*l*'). To investigate how the shape of the energy distribution function could affect growth, two combinations of '*α*' and '*l*' were selected to give similar growth and

yield stress starting points (Fig. 2.8B) and very similar growth patterns (Fig. 2.8C) with very different underlying energy distributions (Fig. 2.8A): A more spread-out distribution (‘*a*’=7, ‘*l*’=0), and a distribution with a sharp peak (‘*a*’=2, ‘*l*’=8). The distribution with sharp peak is thought to be more resistant to change in the bond energy. When the value of H2 is changed so that the wall is artificially stiffened, a cell with a sharp-peaked energy distribution has less reduction in growth rate and final length, hence it is less affected by the change in the bond energy (Fig. 2.8D).

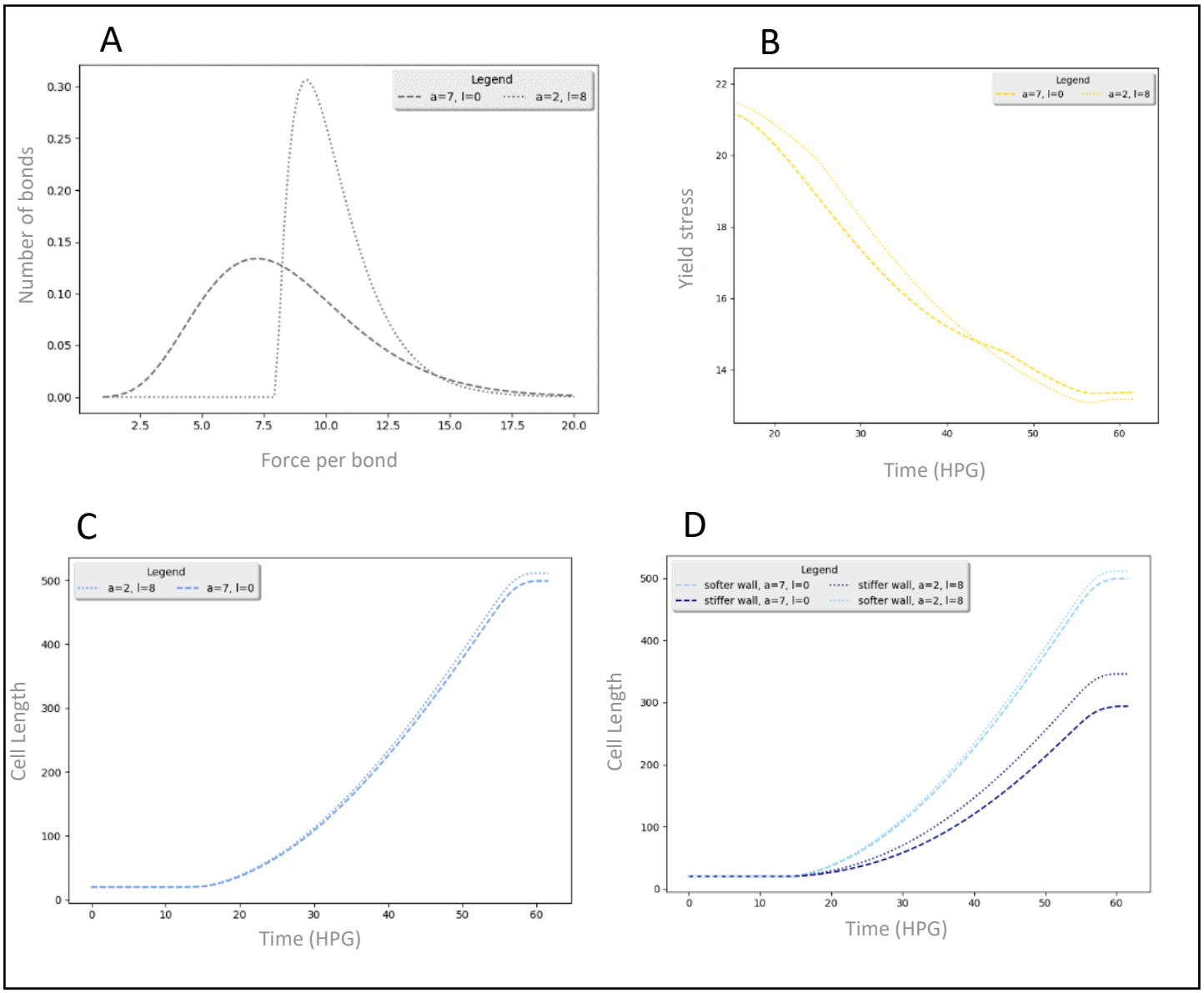

Figure 2.8 A change in the stress distribution function causes the wall to have different resistance against changing in wall properties. **A:** Energy distribution function (gamma) with parameter [*a*=7, *l*=0] and [*a*=2, *l*=8]. **B:** The simulated yield stress over time for the two energy distributions had similar patterns. **C:** The simulated cell length using the two sets of parameters in Fig. 2.8A This two sets of parameters are chosen so that the simulated growth over time is very similar, despite the obvious difference in the pattern of the two energy distributions. **D:** With different stress distribution, wall

reacts differently against changing bond energy. When the wall is stiffer, a more significant impact on the growth reduction is seen with the distribution with [α=7, l=0].

Mimicking the behaviour of cellulose reorientation by changing irreversible bonds in the cell wall slows down the growth

As discussed in Chapter 1, the orientation of cellulose changes over time, with the most transversely aligned microtubules seen at 42 HPG, in both inner and outer walls. This can be incorporated into the model by modifying the irreversible energy over time, since the tethering among cellulose (by hemicellulose) is physically structured, and cannot reform once broken. It was suggested that the newly synthesised wall is more likely to be under stress[3][2]. Between 48 and 60 HPG, hypocotyl epidermal cells still grow anisotropically despite the displaying a large proportion of longitudinally aligned microtubules[7]. This suggested either the older cellulose microfibrils in transverse directions were still under stress, or, that isotropic bonds such as pectin-calcium cross links formed in the cell wall when cellulose is reoriented. Either way, there must have been an increase in the total bond energy, or the cell would experience a significant expansion in diameter during cellulose reorientations. An extra trigonometrical function was added to represent the additional bond energy in the cell wall (Fig. 2.9A)

The simulation gave a reduced growth rate when the reorientation started. It could therefore be concluded that cells can regulate their growth rate by altering the total bond energy in the cell wall, via changing the orientation of the cellulose microfibril. This might be more easily achieved than altering the turgor pressure.

Increasing the wall thickness leads to reduced growth

The stress of a plant cell at a given location was determined by the turgor pressure, its geometry and wall thickness. The dynamics of wall thickness was not addressed in this model[113] and was assumed to be constant; however, wall thickness does change during hypocotyl cell elongation[113][117] and so it seemed prudent to assess its effect on growth in the model. When growth was simulated with an increased cell wall thickness, 6.5% thicker, (Fig. 2.9B) a significantly reduced growth rate was found.

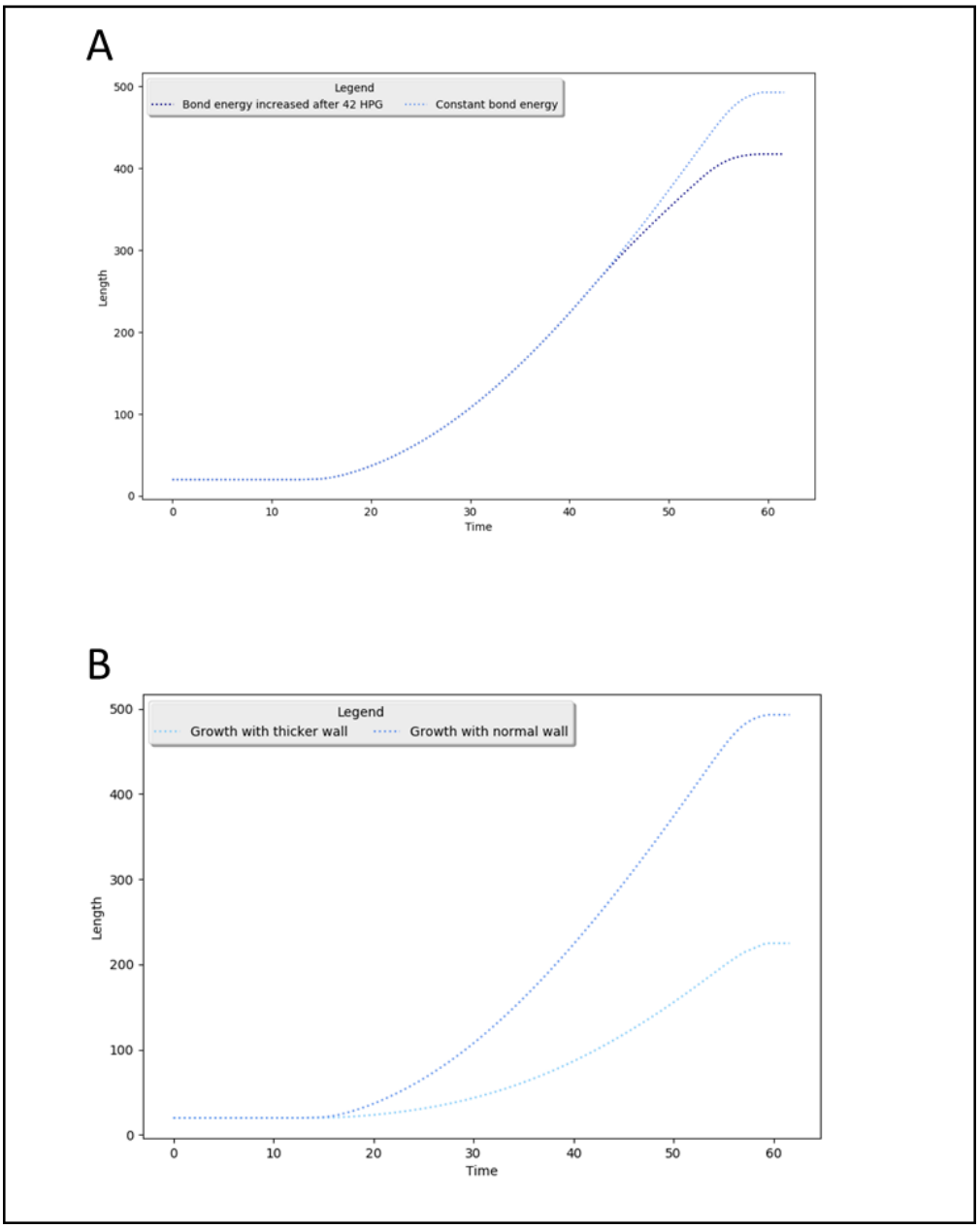

Figure 2.9 **A**: Increasing the bond energy after 42 HPG, the simulated growth rate and the final length was reduced. **B**: The simulated growth rate and final length were reduced with a thicker cell wall.

DISCUSSION:

Is hypocotyl epidermal cell growth perfectly sigmoidal?

In this Chapter, an intrinsic model was built aimed to investigate the growth mechanisms and how physical factors behave during cell growth. The study shows that even at the cellular level, the growth over time is unlikely be symmetrical. The growth of cylindrical plant cells, like those in the hypocotyl

epidermis, is often referred to as 'sigmoidal' over time[1][7]. But how close is the growth pattern to a perfect sigmoidal curve (described by $S(t) = \frac{1}{1+e^{-t}}$, symmetric with respect to the middle point)? The pattern is similar to a sigmoidal curve (slow-fast-slow over time), but the cellular growth is too simplistic to be described by just a standard sigmoidal function, as the growth initiation, fast elongation and termination are contributed by a number of different factors, e.g. cellulose orientation, turgor pressure, hormones, etc. In this chapter, evidence was presented which contradicts the perfect symmetric sigmoidal model. Firstly, the growth of basal cells starts at 0 HPG but between 12 HPG and 24 HPG a pause in length increase was seen while a steady increase in width was observed, indicating that growth was ongoing but the degree of anisotropy changed (Fig. 1.12) It is possible that the early increase in length (0-12 HPG) was an artefact due to collet expansion during germination; collet cells just basal to the hypocotyl elongate during germination to push the radicle out of the seed[118].

Secondly, the existence of a wave of growth means different cells grow at different times. Findings in Chapter 1 also suggest that different cells have very different growth rates and final lengths. Depending on the environmental conditions (e.g. light) or local hormone concentrations (e.g. GA), different cells are unlikely to possess the same growth pattern. They might follow different sigmoidal patterns but growing and stopping at different times means that it is difficult to produce a perfect symmetric sigmoidal pattern.

Thirdly, the MFs are involved in maintaining the cell anisotropy at the beginning, but later they may also be involved in the cellular growth rate[7]. The dynamic orientation of MFs is difficult to completely incorporate into the model, and the change of cellular growth rate may be affected, resulting in variations in the sigmoidal pattern, which are likely to break the symmetry. Overall, the growth of a cylindrical plant cell is achieved through a number of different mechanisms; it looks like a sigmoidal pattern but many of the growth characteristics are not captured by symmetric sigmoidal curves.

Turgor vs cell wall, how do they coordinate cell growth?

Simulated turgor pressure and yield stress have decreasing patterns over time, and their relationships are discussed here. Both turgor pressure and the cell wall stiffness are important factors involved in cell expansion. In the model, cell enlargement happens when the stress (generated by the turgor) exceeds the yield stress. This was inspired by the traditional Lockhart model[84][7][93][119] where growth rate was linearly proportional to the difference between turgor pressure and a yield threshold. The data of the ratio for turgor: YM (Fig. 2.3C) supported the idea that growth rate was proportional to the difference between turgor and wall stiffness in the traditional models. On the other hand, if the

pressure was too low, or the wall was too rigid, the cell was unable to expand[84][7][93][119] (Chapter 1). Hence a tight relationship must exist between the turgor and the wall properties of a plant cell. A healthy plant cell controls the two to achieve expansion or to retain its shape accordingly. Previous evidence suggested that turgor was essential for the growth to happen whereas the growth rate was more likely to be controlled by the wall properties[11][117](Fig. 2.3B).

Turgor pressure was estimated by a plasmolytic approach; however, as pointed out earlier[120], the flow rate of water depends on the difference in concentration of dissolved ions across the plasma membrane, as well as membrane permeability. In addition, plant cells are capable of adjusting their internal osmoticum with ion channels[121]. All these factors affect the time it takes for seedlings in the plasmolytic solution to exhibit plasmolysis. Together with an approximated osmotic potential in the media and errors in the calculation, the estimated turgor pressure may be different from the real one. Fortunately, these errors are unlikely to have significant effects on the overall pattern of turgor pressure or the change of pressure over time.

Although a negative correlation between turgor and cell size was seen, there was a positive correlation between the change in pressure and the relative growth rate of cells. From 24 to 48 HPG, the basal cells had a relative growth rate of 0.0504 hr^{-1} (Chapter 1), with a turgor difference of 0.35 MPa between this two time points. From 48 to 72 HPG, the relative growth rate was 0.0196 hr^{-1}, with a turgor difference of 0.11 MPa (Fig. 2.3). A larger decrease of turgor corresponded to a bigger relative growth rate over a period. In a short time, because the volume of water intake and the decrease in osmotic pressure could be related by a simple equation: $\delta V = \frac{V_i \delta P}{\psi \theta_{in}}$, the change of turgor pressure was linearly proportional to the volume increase of the cell. But in the long term, this was weakened due to the deposition of new wall material and the exchange of ions. In some other organs where secretion rate was high and volume expansion is small, the pressure would stay relatively constant and this pressure-volume relationship might not be seen in the long term[114][91].

In the hypocotyl epidermis, the turgor pressure typically ranged from 0.5 MPA to 1.5 MPa over time(Fig. 2.4, Fig. 2.5). Being the force driving the cellular growth, turgor pressure should have a positive correlation with cellular growth rate. This was confirmed both experimentally and by model simulation (Fig. 2.7), where a reduced turgor resulted in a slower growth rate. But this was no longer true when wall properties were also modified: A softer wall results in faster growth rate but lower pressure (Fig. 2.5, Fig. 2.6). Plants have the ability to adjust their internal turgor pressure, but with only limited capability. For example, a higher turgor pressure in seedlings with induced PME was seen, but the cells were still struggling to enlarge. Hence turgor pressure is not likely to be the primary factor that a plant regulates to directly control cell growth, as it is difficult to change the turgor pressure

substantially within a short time. Turgor can only be changed by changing the osmotic potential inside a cell, and a suitable value is essential to maintain a healthy cell. It is slow and inefficient if plants control the cellular growth rate by adjusting the internal turgor pressure. Over a long time, the turgor drops. I hypothesise that the dropping turgor is more likely due to the enlarged cell size, but not a way for plants to precisely control the growth rate.

In contrast, cell wall modifications can happen quickly, by changing the cell wall thickness, bond energy within the wall (wall composition), or wall structure (hence bond energy distribution). The mechanical properties of the cell wall can be dramatically changed in relatively shorter time. For example, a 90-degree reorientation of the cellulose microfibril totally changes the anisotropy, and the cell wall stiffness can be increased significantly when the wall is thickened (Fig. 2.9), potentially as much as 6-fold[113] in the outer epidermal wall, or when pectin methylation changes[7]. The model seemed to be very sensitive to the wall thickness as a strong effect in growth rate was seen with a 6.5% change in the thickness parameter. There are two hypotheses to explain this: 1) In plant cell walls the bond energy distribution may not be constant across time, whereas in the model the total bond energy has a linear relationship with the wall thickness, i.e. twice thicker means twice stiffer in the model. 2) Plant cells are permanently attached to one another and the growth of a single cell is limited by its surrounding cells, so the growth of epidermal cells may not truly reflect their observed individual cell wall thickness.

The wall promotes the growth by softening. But it is also possible that there is another process of wall re-stiffening towards the end of the growth, which slows the elongation down and stops the growth (red line in Fig. 2.3B). Stiffness is an important property of the cell wall. The stiffness of the wall can be interpreted in many ways such as Young's modulus, which measures the elasticity of the wall, or yield stress, representing how much stress a bond in the wall can load before deforming in shape. These interpretations are all related but also different from each other[10][102]. The elasticity is proportional to the stiffness by definition, and elasticity measurements based on AFM (apparent Young's Modulus) have been reported to correlate well with growth phenotypes observed[122][123][79][5]. It was also found that the pectin chemistry and the amount of calcium crosslinks could control growth rate of *Chara* cells[96]. All of this evidence implies strong relationships among cell wall properties, elasticity (stiffness), plastic deformation and growth.

Although a strong correlation appears to exist between the turgor pressure and the cell wall mechanical properties, the two are not likely to be directly controlled by each other. In fact, the isoxaben-treated seedlings have reduced cell wall stiffness and burst cells (Fig. S1.3, S1.4). So the

turgor is not capable of changing accordingly to prevent the cell from bursting, and hence it is not likely to be directly responsive to modifications of the cell wall.

Insights from the model: The physical properties of the cell wall and the role played by the bond energy distribution

The model was constructed to simulate the growth of a single cell, and it provided a new way to understand the relationships among different factors controlling the cellular growth. Simulations suggest that chemical modifications of the cell wall can be more effective than physical ones in terms of regulating cell growth.

Initially, when the cell wall was only modelled by the number of bonds in the wall, the model was very sensitive to any change in the total bond energy. In reality, the cell wall should have a mechanism to adjust itself and be resistant to any minor change in the total bond energy.

The bond energy distribution was then introduced to the model inspired by the observed random microtubule orientations in the cell wall (Chapter 1), which led to the assumption that not all the bonds in the cell were bearing the same load. It was then found that a bond distribution with a high peak was more resistant to change in the bond energy. This is because when the wall yield, bonds with stresses higher than a threshold would break, which are located at the high energy tail of the bond energy distribution. When the bond energy is changed, the energy distribution with a sharp peak has larger area under the curve to compensate for the change in bond energy, with less change in that breakage threshold, and hence less change in the yield stress.

The results suggested that a higher bond energy would limit the growth, and a lower proportion of bond energy for the pressure to overcome would promote the growth. In reality, the yield stress falls into a certain range. A stress distribution with a sharper peak covering this range is likely to be favoured by non-growing cells, due to its resistance against wall property changes. The predictions of the model suggested that the cell wall stiffness must depend on both the cell wall bond energy and the bond energy distribution, and the sensitivity analysis implied that in order to achieve a faster growth rate, changing both is more effective than changing only one of them. During the simulations of artificially stiffening the wall by changing H2, it was found that if only the H2 was changed without a corresponding change in the bond energy distribution, the reduction in growth rate and cell size was not significant, possibly due to the resistance of the bond energy distribution. Whereas if the energy distribution was adjusted to match initial yield stress, a significant reduced growth rate was seen.

Although it is hard to deduce the real bond energy distribution, the modelling results suggest that instead of adding/removing more bonds to the system, a slight modification of the bond energy distribution can be a more efficient way to control the growth. The bond energy distribution is less likely to be changed by the physical parameters, as the network formed by pectin, MF and xyloglucan is less likely to experience dramatic changes. Rather, it is more likely that certain protein activities affect the pectin chemistry (e.g. PME) or network structure (e.g. XTH, which cuts/re-join xyloglucans), which then modify the bond energy distribution and achieve a more efficient control during the growth.

The model uncovered part of the very complex cell wall structure and provided a new way of understanding the mechanism of cell growth; it suggested that the physical factors of pressure and stiffness had limited power to explain cell growth fully. In particular, the chemical signal 'S', as the trigger and terminator of growth, was only addressed superficially. A more quantitative study on this chemical signal is done in later chapters, and I believe a better understanding on this chemical signal could cover some of the limitations which the current model is unable to address, such as the non-perfect match between the simulations and experimental data, or why some cells grow for longer/shorter periods.

Limitations of the model

The intrinsic model was constructed based on simple physical assumptions among key variables (pressure, yield stress), together with other parameters set with default values. The model has the advantage of studying the relationships and progression of key variables, and it is not limited by the selection of measurable/unmeasurable parameters. Beyond what was tried so far, the key variables can also be studied when other parameters are altered (e.g. what happens to the growth rate when the osmoticum of the surrounding media has a sudden peak at 48 HPG?), allowing many other possible variations to be studied. However, this is also the biggest limitation to the model, the arbitrary unit of the predicted variables (pressure, yield stress, volume) means the output is comparable with the real data only in terms of the progression pattern, and calculating the difference between the output and the real data in short quantitative comparisons would be naive and meaningless here. Also, there is no validation method to evaluate the performance of the model quantitatively. Fundamentally, the growth of a plant cell is a very complex process, an intrinsic approach of modelling is unlikely to accurately reproduce the cellular growth from all perspective, due to the lack of knowledge of some parameters in the model.

Despite the unmeasurable parameters, the model adopted the simplest assumptions among variables and parameters. For example, when the environmental osmotic potential is changed, the model does not account for the plant's internal adjustment for this changed osmotic pressure, nor how this changed osmotic pressure affects the signal of growth. The model does not address the properties of MF well enough. The prediction suggests that the MF not only controls the anisotropy but also controls the growth rate, along with the growth signal, pressure and wall elasticity. However, the simulation only considered a change in the irreversible energy but not the energy distribution as it is not yet understood how the internal bond energy is affected by MF reorientations. This is controversial. The model is already complicated enough, with an excess of unmeasurable parameters. On the other hand, many of the assumptions made the model to be oversimplified. (e.g. binary chemical signal was assumed, whereas the chemical secretion rate was found to correspond well with the oscillation period of growth[124][125])

Beyond the hypocotyl epidermal cells

Not all plant cells grow like the hypocotyl epidermal cells. The studied hypocotyl epidermal cells are special because of their fast elongation rate, a short period of growth, and cylindrical, anisotropic shape. There are many other plant cells that possess different properties, but the growth of most plant cells depends on the same key factors, namely the growth signal, the turgor pressure, and the cell wall mechanical properties. Hence, this model can be adapted to other plant cell systems, by changing the parameters including the growth signal length/period, cell wall thickness, bond strength, initial turgor pressure, initial size and the osmotic pressure of the surroundings. Because the model is heavily based on the relationship between volume and turgor pressure, and the cell diameters were used as an input, the size predictions are limited to volume rather than length or perimeter with complex cell shapes.

CHAPTER 3: AN EMPERICAL MODEL OF THE WAVE OF GROWTH OF THE HYPOCOTYL EPIDERMAL CELLS

All work contained here was performed by Yuanjie Chen.

SUMMARY

The growth of dark-grown hypocotyl epidermal cells is characterised in Chapter 1. However, no cellular level data is available beyond 72 HPG due to technical measurement difficulties. The elongation of dark-grown hypocotyls lasts for around 8 days (192 HPG) and it is not known how epidermal cells behave after 72 HPG, especially for the upper hypocotyl cells where their fast elongation period starts later than 72 HPG. In this chapter, an empirical model of the cellular wave of growth was built based on the dataset of cell sizes up to 72 HPG. Three sigmoidal functions were used to fit the data; parameters of the functions were identified and extrapolated to predict the growth of cells beyond 72 HPG. The extrapolation was found by identifying linear/polynomial trends of the parameters over cell indices. Out of the three sigmoidal functions, the Probit function produced a very close match between predicted cell length (predicted hypocotyl length) with the measured hypocotyl length. The empirical model provided estimates of growth rates for the upper hypocotyl epidermal cells, and it successfully recapitulated the growth pattern at the organ level based on the growth at the cellular level. A better quantification and understanding of the hypocotyl cellular wave of growth and their correlation with the organ level elongation was gained in this study.

INTRODUCTION

In the previous chapter, an intrinsic model of a single cell was built. The model investigates the relationships among physical factors affecting the growth and provides insights into the ways in which cellular expansion is achieved. In contrast to intrinsic modelling, an empirical model is based on experimental data rather than on a detailed description of the system which can be mathematically described[126]. In this chapter, an empirical model was built, based on the epidermal cell growth characterised in Chapter 1. Instead of studying the expansion mechanism of a single plant cell, the entire 17 non-dividing hypocotyl epidermal cells were modelled. In the dark, hypocotyl cell elongation follows an acropetal wave[1]; and the position and magnitude of the wave were studied in Chapter 1. Because plant cells are permanently attached to the adjacent cells by the middle lamella[127], the

wave indicates local organ expansion, which can be studied using the epidermis.

Modelling the entirety of hypocotyl elongation was of interest in this chapter. However, the experiment in Chapter 1 was only conducted in the first 72 hours-post-germination (HPG); beyond 72 HPG, the measurement of the epidermal cell size became difficult due to a long length of the cell, twisting of the hypocotyl and dimmed signal intensity. Epidermal cells with indices larger than 11 had not reached their fastest elongation period by 72 HPG and hence it was not possible to determine the growth rates and final lengths for these cells.

In this chapter, the cellular length data from 0-72 HPG were fitted with three distinct known sigmoidal functions, and then progressive patterns of the parameters in the three functions were explored. Using that, the modelling efforts aimed to predict the growth characteristics of the dark-grown hypocotyl epidermal cells with indices larger than 11, resulting in a full empirical model of hypocotyl elongation. The predicted cellular growth rates were integrated and compared with the organ level growth rates for validation.

The Three Sigmoidal Functions

Plant tissue/cell/organ growth often exhibits an approximately sigmoidal pattern[19] (Chapter 1, Chapter 2) Three most-standard sigmoidal functions were chosen to fit the data of cellular growth: Logistic, Log-log and Probit, which are described by a small number of parameters. The Logistic function was firstly published by Pierre Verhulst (1845, 1847) as a tool of population growth modelling, with an assumption of the rate of changing population ($\frac{dy}{dt}$) proportional to the current population (y) and the difference between the current population and the maximum population (k, carrying capacity), i.e. $\frac{dy}{dt} = \frac{ay(k-y)}{k}$. It produces a continuous sigmoidal curve, which is symmetric with respect to its middle point (the inflexion point). The Log-log function is a variation of the Logistic, it has a sigmoidal pattern but is not symmetric with respect to any point. The Probit function is a quantile function of the normal distribution and is also symmetric with respect to its middle point. Compared to the Logistic curve, its tails are less flat[128]. (Supplementary Fig S3.1)

METHODS

The dataset used in this chapter is identical to the one used in Chapter 1, containing the length of cells with indices 1 to 17, and time points from 0 HPG till 72 HPG, with 6-hour intervals. The data of the first

11 cells are used as a training set, to predict the growth patterns of cells with indices 12-17.

Three sigmoidal functions are used for fitting, where y is the cell length in micrometres and t is time in HPG. The Logistic, with the general equation:

$$y(t) = \frac{a \cdot e^{b(t-c)}}{1 + e^{b(t-c)}} + d$$

Where a, b, c, and d are the four parameters to be fitted.

The Loglog, with general equation:

$$y(t) = a \cdot (1 - e^{-e^{b(t-c)}}) + d$$

Where a, b, c, and d are the four parameters to be fitted.

The Probit, with general equation:

$$y(t) = \int_{-\infty}^{bt} a \cdot e^{-(x-c)^2}\, dx + d$$

Where a, b, c, and d are the four parameters to be fitted. These three sigmoidal functions are widely used as models for biological population growth[129].

The Four Parameters (coefficients)

There are four parameters in each of the three sigmoidal functions: a, b, c, and d. Together they control the size and position of the sigmoidal curve in Cartesian Coordinates (x,y). The parameter a controls the size in direction of y-axis; a large value of a causes the sigmoidal curve to be steeper and higher. b controls the size in direction of x-axis; a large value of b makes the sigmoidal curve to be steeper and thinner. c controls the position in x-axis; a large value of c shifts the curve to the right. d controls the position in y-axis; a large value of d shifts the curve upwards.

Fitting the sigmoidal function

Given a sigmoidal function, the growth pattern of any cell can be described by the function with a good selection of parameters. Parameters for hypocotyl epidermal cells with indices 1-11 were found precisely, by fitting the function with experimental data in a least-squares manner (lsqcurvefit, Matlab2017b). However, the parameters for the upper cells (indices 12-17) could not be determined due to a lack of experimental data at later times when the upper cells grow. Those parameters were determined by fitting data with extra constraints, which was gained by parameter extrapolation.

Parameter extrapolation

The key assumption for parameter extrapolation is that every dark-grown non-dividing hypocotyl epidermal cell (with index i) behaves similarly to its neighbouring cells (with index $i+1$ or $i-1$). This was supported by the early observation in Chapter 1 that the acropetal wave was progressive along cell indices. As such, the set of parameters defining the growth of each cell should not differ dramatically between neighbouring cells. However, there existed large difference between cells with small indices (grow early, shorter final length) and cells with larger indices (grow later, longer final length). Therefore, if a trend of the parameters over cell indices is identified, this trend can be used to constrain the parameters for cells with large indices (>12). Linear extrapolation and parabola extrapolation was attempted and compared (polyfit, Matlab2017b)

Prediction validation

As no cellular level data was available beyond 72 HPG, the predicted cell length was summed together to get a hypothetical organ length, and that length (referred as predicted hypocotyl length) was compared with the measured dark-grown hypocotyl length over an 8 day (192 HPG) period. (Hypocotyl length measurement: n=20, Mann-Whitney test, p-value<3.34e-6)

The absolute error between the predicted and measured length was calculated as the sum of absolute difference between the prediction and measurement, at 8 time points: (24, 48, 72, 96, 120, 144, 168, 192 HPG).

RESULTS

The data of cellular growth (Chapter 1) were firstly fitted with the Logistic function, followed by parameter extrapolation to get the growth prediction of cells that grow later. The same processes were conducted with the Log-log and the Probit function, and their outputs were compared.

The initial fitting of the lower hypocotyl cells re-demonstrated the cellular wave of growth

The 0-72 HPG data for 17 epidermal cells were fitted with the Logistic function minimising the mean squared error, and a sigmoidal pattern was well captured (Fig. 3.1). The wave of growth could be clearly seen for cells with indices 1-10 (Fig 3.2): the larger the index, the later the cell started to elongate, and the faster it grew. However, for cells with indices 11-15, the fitted curve showed dramatically reduced cell sizes, and for cells with indices 16-17, the first turn-ups (when cells start to elongate fast) in fitted sigmoidal curves were delayed. Predictions of growth curves for those cells could be improved by adjusting parameters.

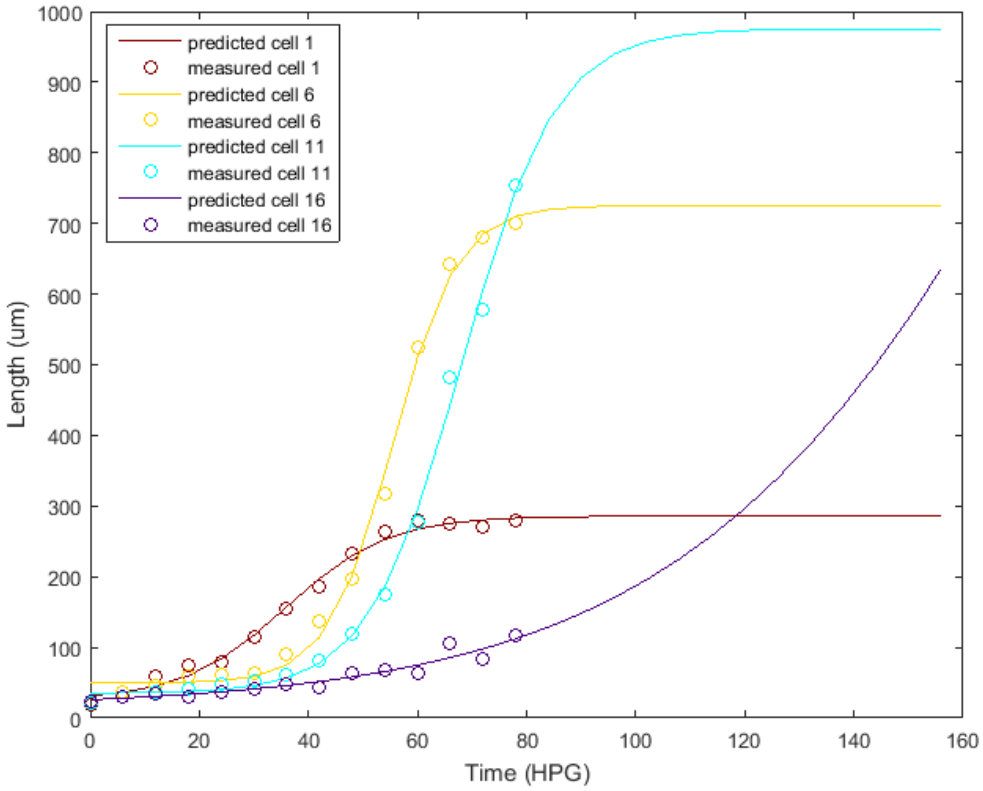

Figure 3.1 Logistic fitting predicts vs measured cell length as illustrated by selected cell indices: 1, 6, 11 and 16

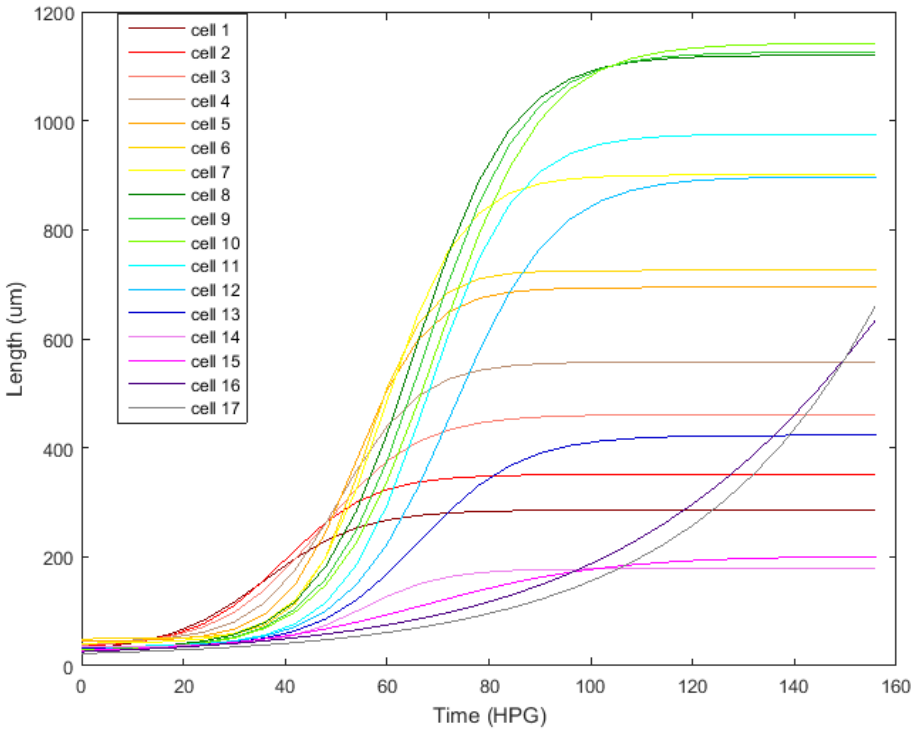

Figure 3.2 The fitting of the cellular data with the Logistic function without constraint. The cellular wave of growth can be seen for cells with indices<11

In order to test how well the function fitting recapitulated cell behaviours from indices>11, cell lengths were summed over time. The predicted hypocotyl size was gained by summing the 17 non-dividing epidermal cells. The predicted length had an absolute error of 2.22×10^4 µm when compared to measured length. The predicted size was shorter and lost the sigmoidal pattern in later time points (Fig. 3.3). This deviation was likely due to the predicted growth curve for cell 16 and cell 17, which had delayed fast elongation periods, slower growth rates, and longer elongation periods. (Fig. 3.2). The predicted growth curve for cell 12-15 were also not trustworthy, as the data at 72 HPG did not suggest when their growth would slow down.

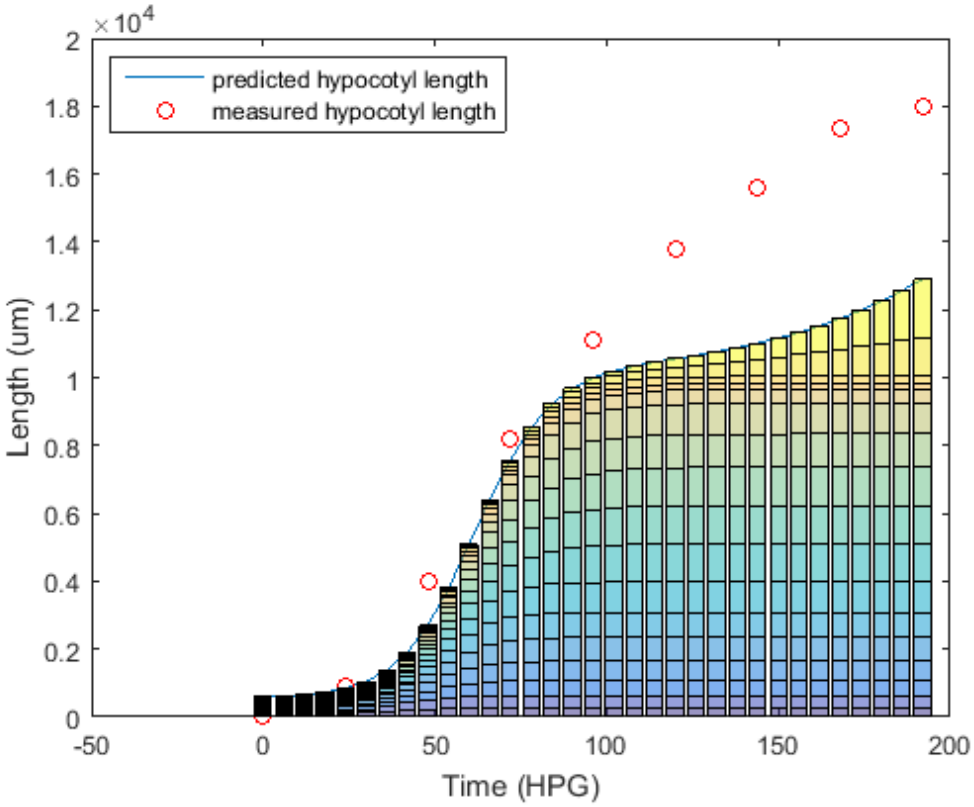

Figure 3.3 The predicted hypocotyl length deviates from the actual measurement at later times. The absolute difference between the prediction and measurement is 2.22 x10^4 µm. Bars indicate the fitted (and predicted) cell sizes. Circles represent measured hypocotyl length over time.

Value of the parameters were stable for cells with indices<11

Growth patterns for the first 10 cells were nicely fitted and captured by the Logistic function (Fig. 3.1, 3.2) and parameters associated with those cells were plotted over cell index (Fig. 3.4). Parameters of cell index>12 seemed to deviate from previous trends. Focusing on cell with indices<12, a clear linear trend was seen for parameter *c* (Fig. 3.4C), which represented the shift or delay of the growth in time. So this parameter was chosen first to extrapolate where its values for cells with indices >12 were constrained not to deviate from the linear trend line more than 3 units away.

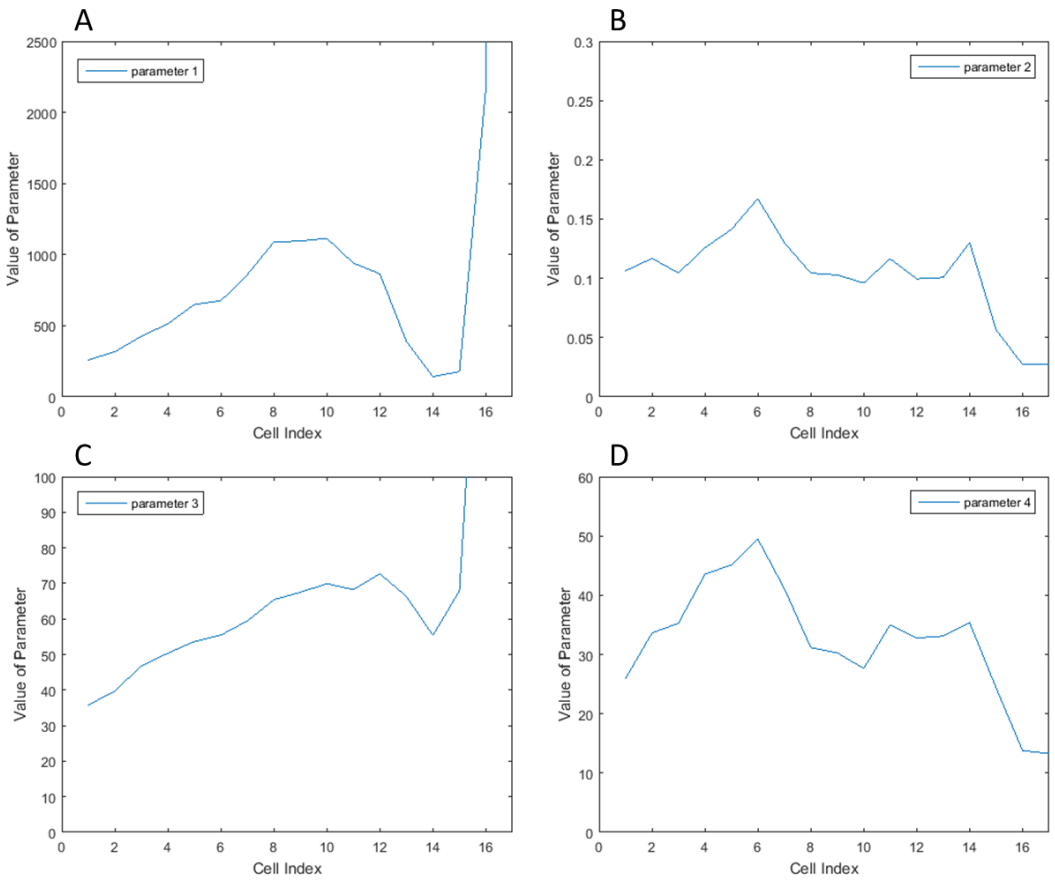

Figure 3.4 Values of four parameters of Logistic function over cell index, fitted with cellular data without constraint. (parameter 1,2,3,4 correspond to a, b, c and d)

Constraining parameter c, a sigmoidal growth curve for the hypocotyl was predicted

Parameter c was well fitted with a linear function (Fig. 3.5). After constraining parameter c to the linear trend, the position of the cellular wave of growth was better visualised (Fig. 3.6); the predicted hypocotyl length had a sigmoidal growth pattern, yet the predicted length was still shorter than the measured length (Fig. 3.7). Cells with small indices stopped their elongation early and they would not contribute more to the organ length once their growth were finished. This shortage in predicted organ length was therefore due to underestimation of predicted lengths for cells with larger indices.

Parameter a and b were chosen to extrapolate afterwards for two reasons: 1) Apart from the position of the wave which is controlled by parameter c, the magnitude of the wave and cellular growth rates are also important, and they are controlled by parameter a and b, respectively. 2) In contrast, parameter d only changes the position of the sigmoidal curve in y-axis, and its variation (±30 µm) is very small relative to the cell size (<10%). Hence it does not have significant effects on the cell size and

growth pattern, especially for cells with larger indices.

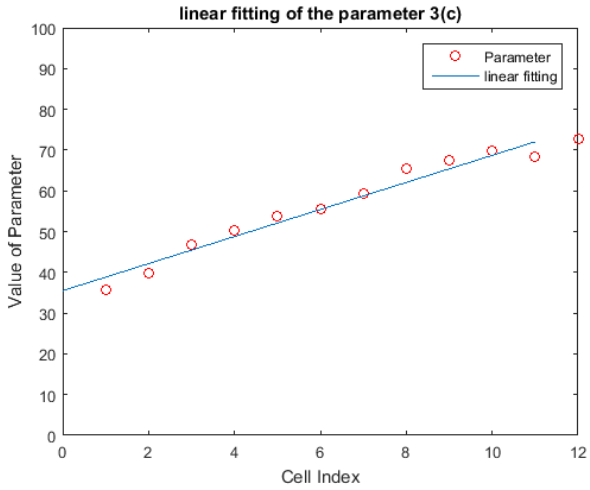

Figure 3.5 Parameter c over cell index can be well fitted with a linear line

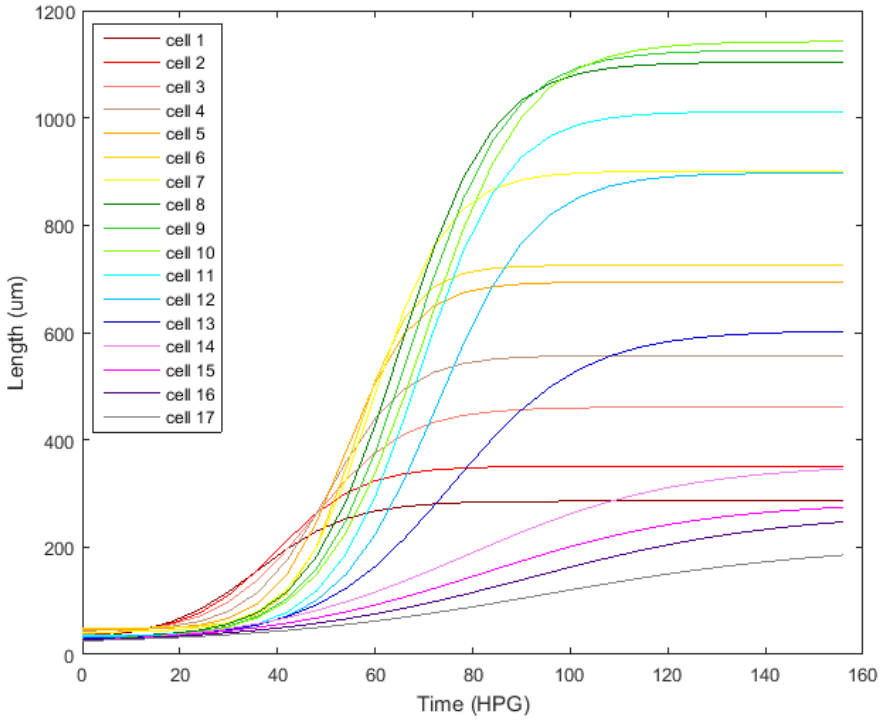

Figure 3.6 The prediction of cellular growth, fitted with the Logistic function after parameter extrapolation (c)

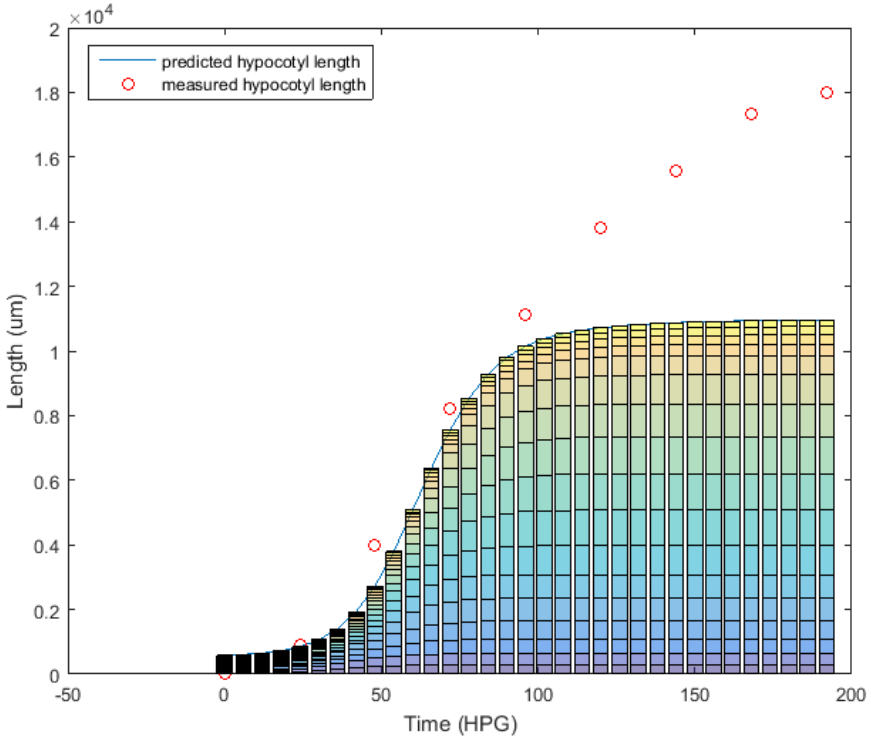

Figure 3.7 The predicted hypocotyl growth was sigmoidal, but the predicted length was shorter than the measured length. The absolute difference between the prediction and measurement is 2.47 x10^4 µm. Bars indicate the fitted (and predicted) cell sizes.

A linear extrapolation was more appropriate than a polynomial extrapolation for parameter a and b

After the 0-72 HPG cell data was refitted with the constraint on parameter c, trends for the other parameters were examined. The trends for parameter a and b were not as clear as the trend for parameter c (Fig. 3.8A, B, Fig. 3.4C). It could be fitted with a linear line but it could also be fitted with a second-order polynomial (parabola).

Both fittings were attempted; the parabola did not give a better fitting compared to the linear-line (Fig. 3.9). With parameter a and b fitted with a parabola, predicted cellular length had a maximum at cell 10, and cells with indices>10 grew later and smaller (Fig. 3.10B). The predicted growth curve for cell 17 appeared abnormal as it did not have a sigmoidal pattern. In contrast, linear fitted parameters produced a clear cellular wave of growth (Fig. 3.10A). Cells with larger indices grew at later times, had faster growth rates and larger final lengths. Based on experimental data showing that cells with larger indices would grow larger[1], predicted cellular growth was more reasonable when parameter a and

b were linearly fitted. In addition, avoiding polynomial fittings would reduce the risk of overfitting.

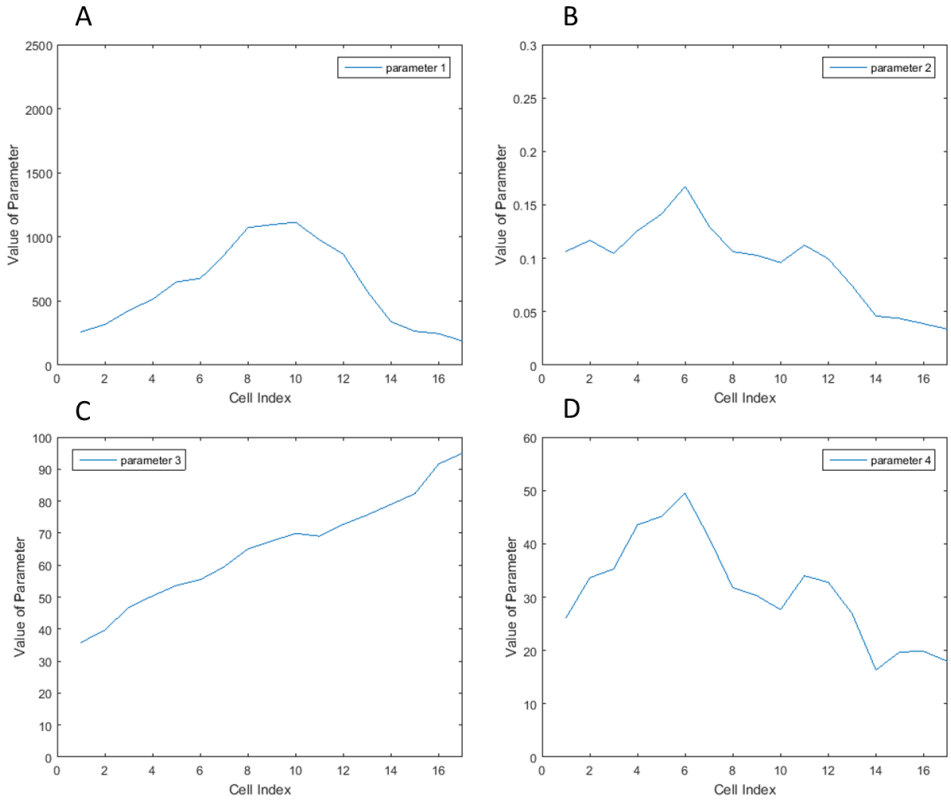

Figure 3.8 Values of four parameters of Logistic function over cell index, fitted with cellular data with linear constraint on parameter c (parameter 1,2,3,4 correspond to a, b, c and d)

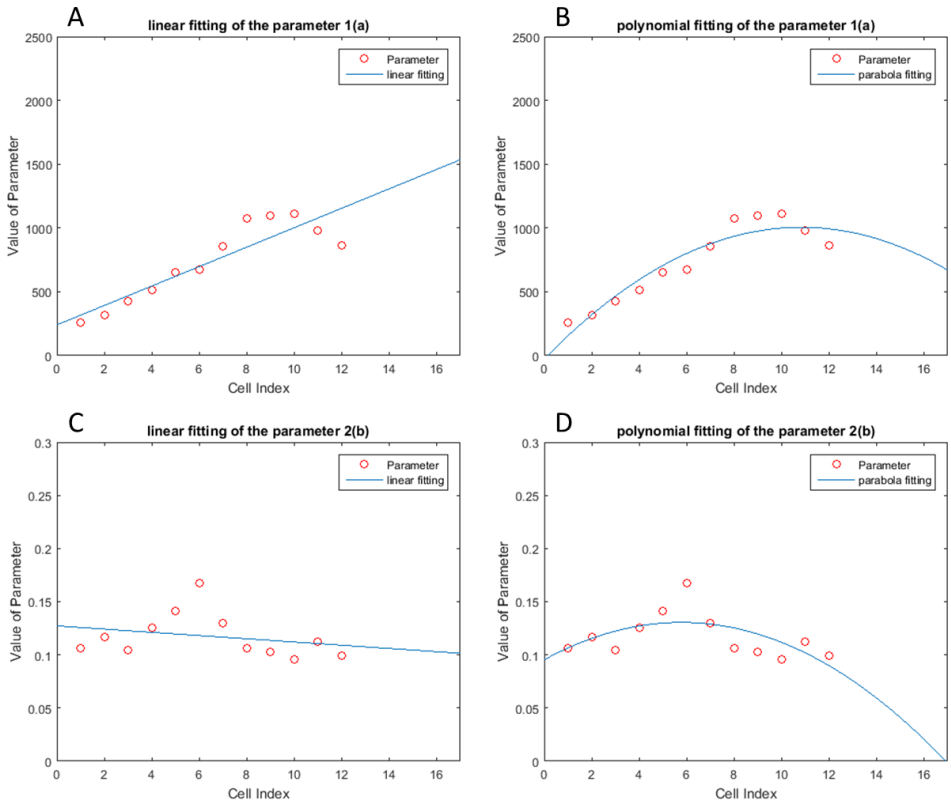

Figure 3.9 Finding trends to parameters. Parameter a and b fitted with linear line (A,C). Parameter a and b fitted with parabola (B,D).

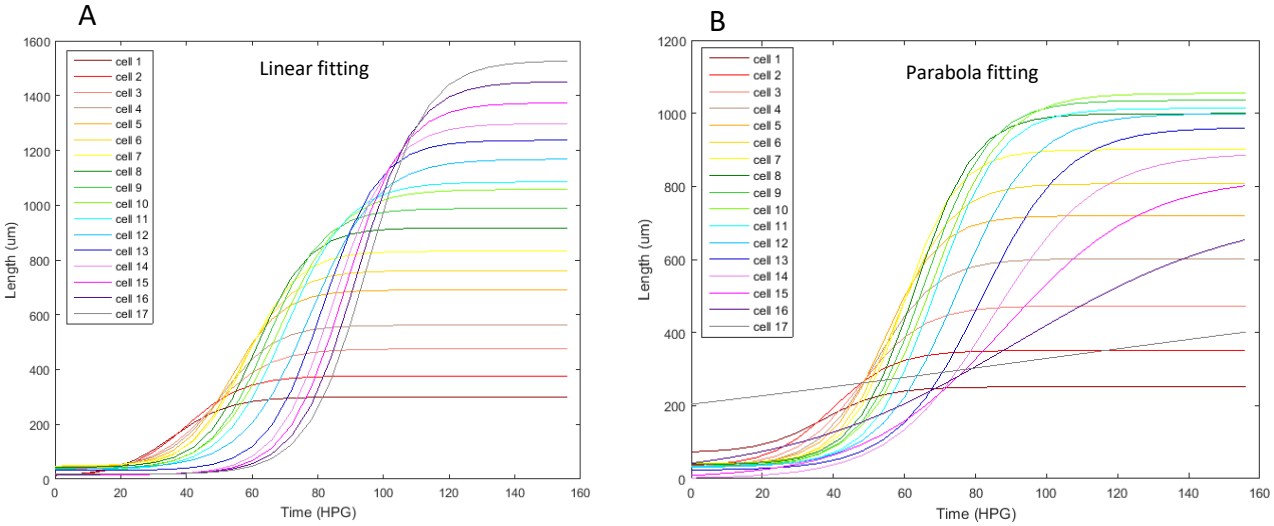

Figure 3.10 The predicted cellular growth for the hypocotyl epidermal cells, **A**: parameter a and b were fitted with a linear line. **B**: parameter a and b were fitted with a parabola.

The Logistic function and its parameter extrapolation did not attain a good prediction of hypocotyl growth

Using the Logistic function to fit the data of cellular growth and extrapolate the parameter linearly to predict the cellular growth beyond 72 HPG, growth patterns of the dark-grown hypocotyl epidermal cells were obtained, with an expected prediction of the cellular wave of growth (Fig. 3.10A). To verify this, the prediction of hypocotyl size (summation of the cellular size) was compared with the measured hypocotyl size from 0 to 192 HPG (Fig. 3.11A). The predicted hypocotyl size using parabola fitting of parameters was also plotted for comparison (Fig. 3.11B). Neither of the two predictions were close to the actual hypocotyl growth curve. The parabola fitted prediction matched the measured data closely until 96 HPG; after that, the predicted growth slowed down whereas the hypocotyl kept elongating in reality, resulting in an underestimated final size. It has an absolute error of 1.56x10^4 µm; it only improved by 30% compared to the original fitting without constraint and parameter extrapolation. The linear fitted prediction had a steeper slope compared to the measured data; the absolute error was 1.01 x10^4µm, which gave a better 55% improvement on the original fitting. The final predicted length (~16000µm) was closer to the actual final length(~18000 µm) but the absolute error between the prediction and measured length was still large.

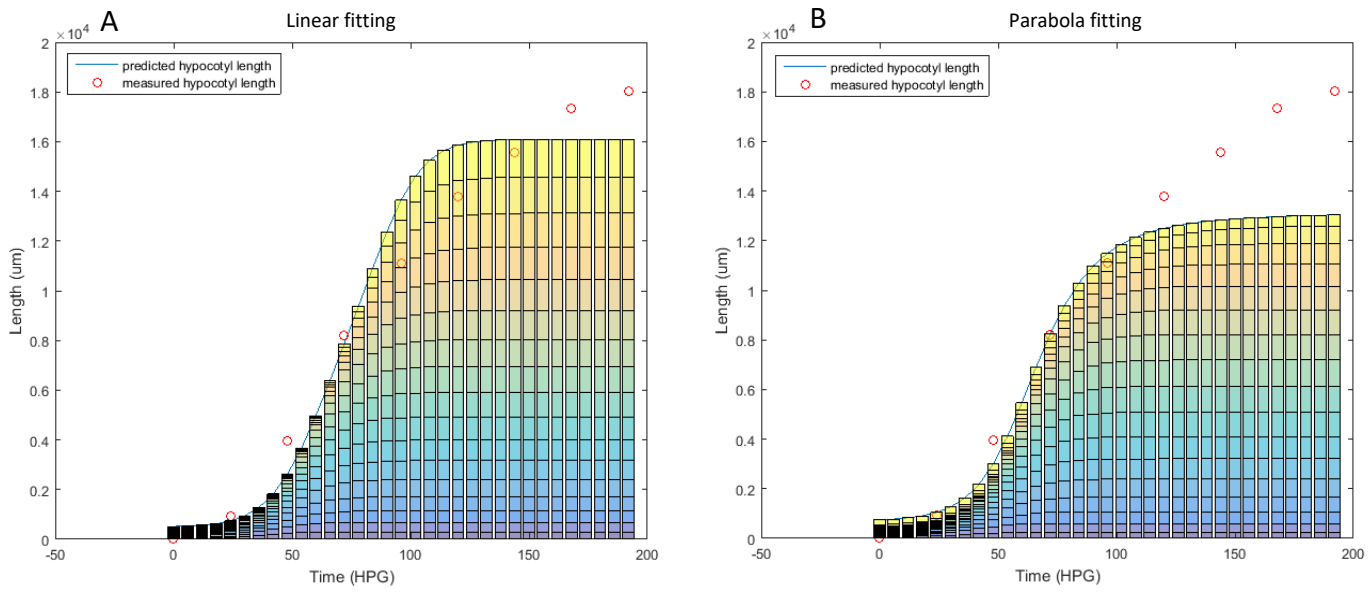

Figure 3.11 The predicted hypocotyl growth vs the measured length. **A**: parameter a and b were fitted with a linear line. The absolute difference between the prediction and measurement is 1.01 x10^4 µm. **B**: parameter a and b were fitted with a parabola. The absolute difference between the prediction and measurement is 1.56 x10^4 µm. Bars indicate the fitted (and predicted) cell sizes

The Loglog function was unable to outperform the Logistic function

A variation of the Logistic function, Loglog, was used in replacement of the Logistic function. The same dataset was fitted with the Loglog function, followed by the same procedure of parameter extrapolations (Fig. S3.2). Similarly as before, linear fittings in the parameter extrapolation was better than polynomial fittings. However, the Loglog function performed worse than the Logistic function. Its predicted cellular growth curves were not as smooth (Fig. 3.12 A). The initial fitting had a larger absolute error of 3.22 x10^4 µm. (Fig 3.12 B, cf. 2.24 x10^4 for Logistic, Fig 3.3), and it was reduced by 46% after parameter extrapolation, leaving an absolute error of 1.74 x10^4 µm. This was a worse prediction of the cellular and hypocotyl size, compared to the Logistic function.

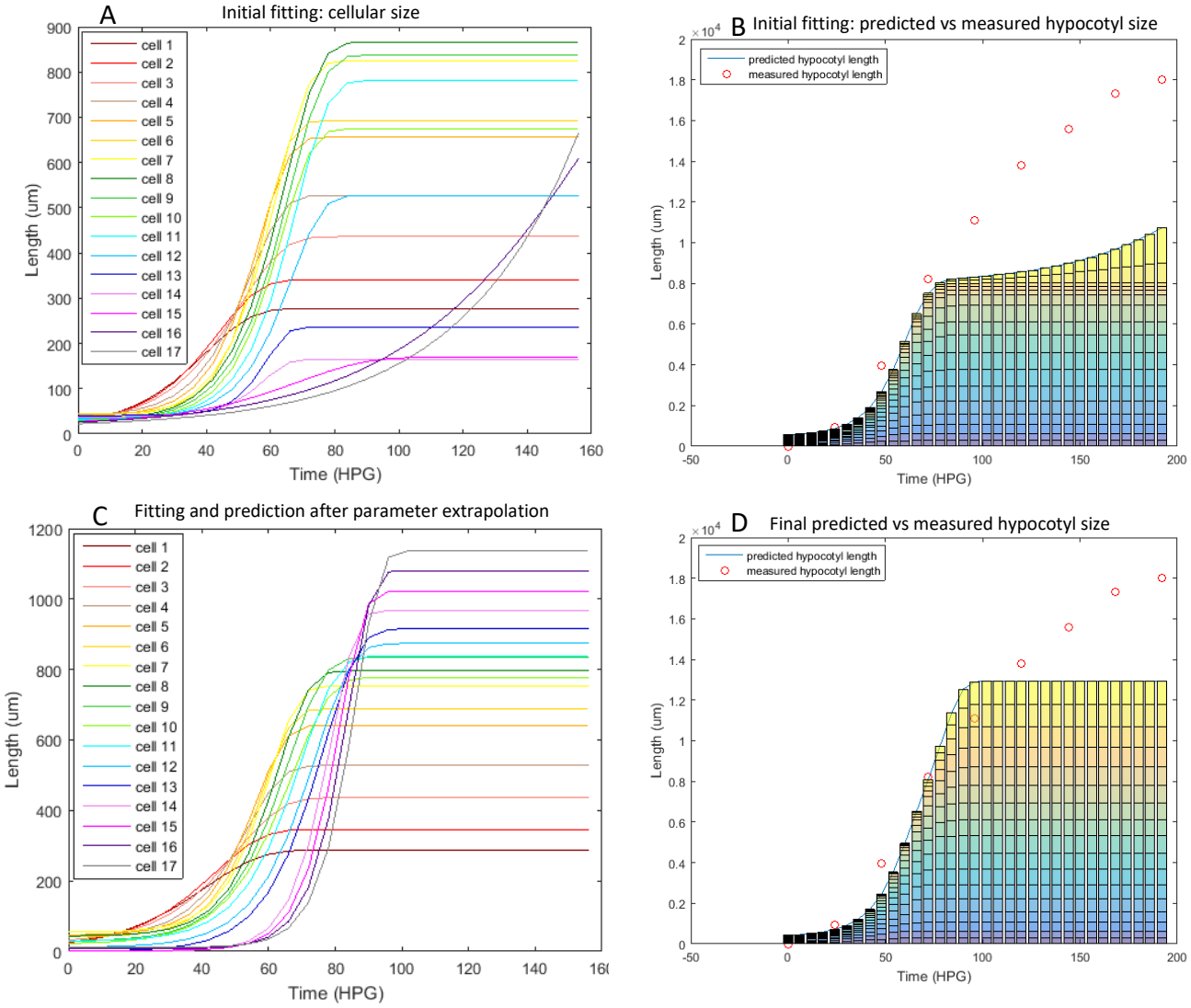

Figure 3.12 The predicted cellular and hypocotyl size with the Loglog function. **A**: The initial fitted cellular growth, no constraint. **B**: The initial predicted hypocotyl growth curve vs the measured hypocotyl length. The absolute difference between the prediction and measurement is 3.22 x10^4 µm. **C**: The prediction of cellular growth, fitted with the Loglog function after parameter extrapolation. A wave of growth can be seen. **D**: The final predicted hypocotyl growth curve vs the measured hypocotyl length after parameter extrapolation. The absolute difference between the prediction and measurement is 1.71 x10^4 µm.

The Probit outperformed the other two sigmoidal functions

Mathematically, the Probit function is a cumulative distribution function of a normal distribution. It was considered here due to its symmetric sigmoidal nature, with a sharper inflection point compared to the Logistic. Similarly as before, parameter c was linearly extrapolated, followed by the extrapolation of parameter a and b (Fig. S.3.3). Polynomial fittings of parameter a and b over time were not found to be significantly better than linear fittings; for the purpose of avoiding over-fitting, linear extrapolations for parameter a and b were used. The final prediction of cellular growths demonstrated a wave of growth, where cells with larger indices grew later and larger. Compared to the growth waves predicted by the Logistic and Loglog fittings, the cellular growths predicted by the Probit fitting lasted longer (Fig. 3.14, cf Fig. 3.10B, Fig. 3.12C). The initial prediction of hypocotyl growth had an absolute error of 2.2 x10^4 µm (Fig. 3.13B), and after parameter extrapolation, the error reduced to 3.75 x10^3 µm, with an 83% improvement. The predicted hypocotyl growth matched well with the measured data (Fig. 3.15)

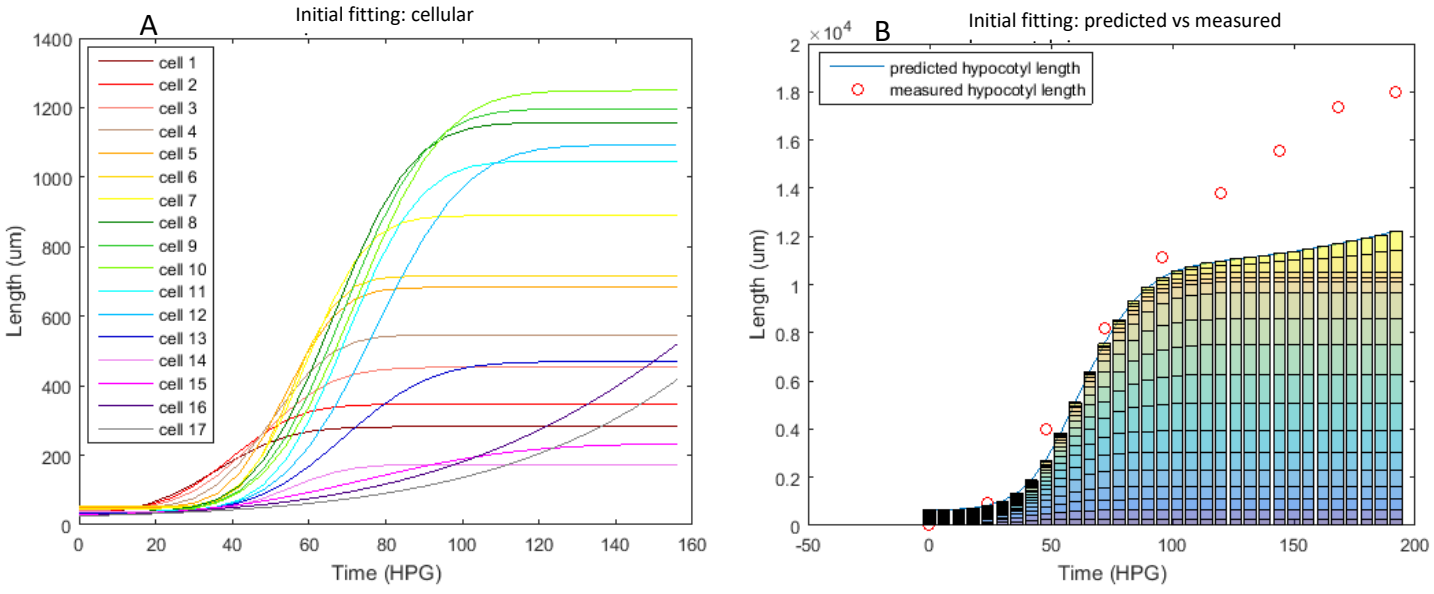

Figure 3.13 Initial fittings and predicted cellular/hypocotyl sizes with Probit function without constraint. **A**: The initial fitted cellular growth with the Probit function. **B**: The initial predicted hypocotyl growth curve vs the measured hypocotyl length. The absolute difference between the prediction and measurement is 2.20 x10^4 µm.

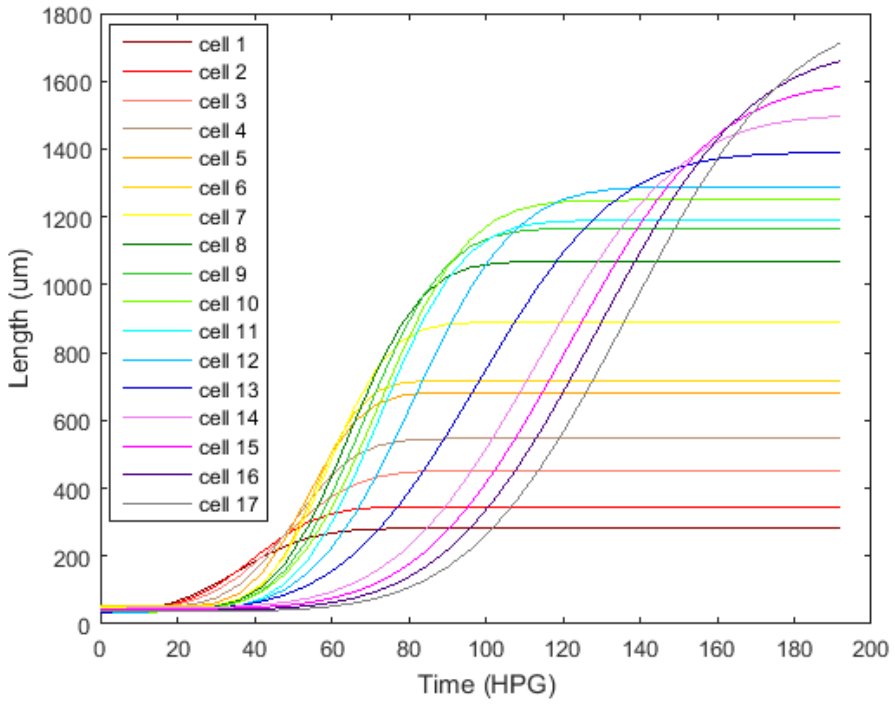

Figure 3.14 Prediction of cellular growth, fitted with the Probit function after parameter extrapolation

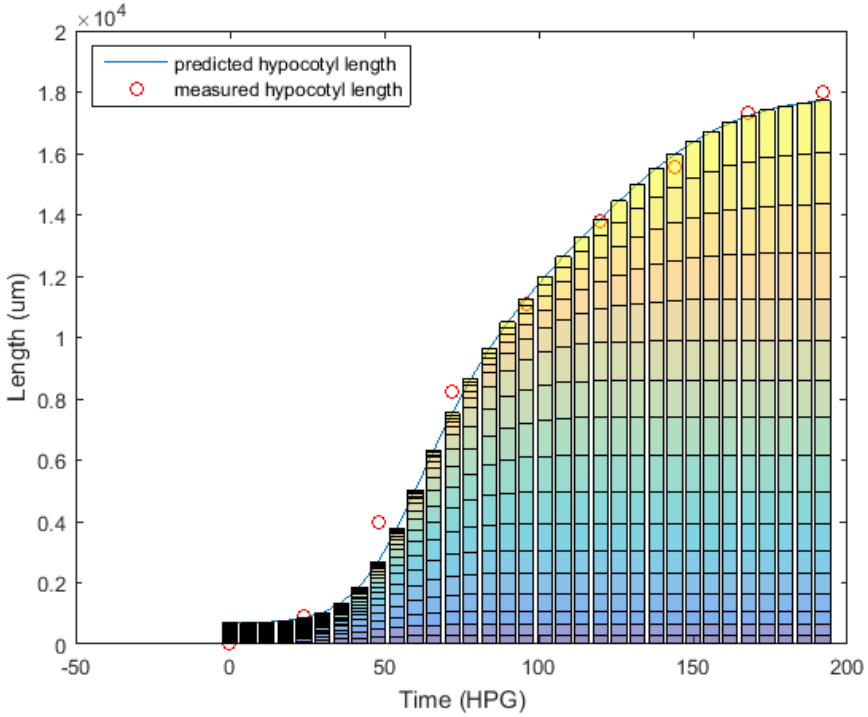

Figure 3.15 Prediction of hypocotyl growth, fitted with the Probit function after parameter extrapolation. The absolute difference between the prediction and measurement is 3.75 x10^3 µm. Bars indicate the fitted (and predicted) cell sizes

Fitting Function/ Absolute Error	Initial Prediction(µm)	Final Prediction(µm)	%Difference	Final Accuracy
Logistic	2.22x10^4	1.01x10^4	55%	88%
Loglog	3.22x10^4	1.71x10^4	46%	81%
Probit	2.20x10^4	3.75x10^3	83%	96%

Table 3.1 Summarising the performance of predictions. Final Accuracy was calculated as:

$$1 - \frac{\text{Absolute Error (Final Prediction)}}{\text{Total Measured Hypocotyl Length}}.$$

The Probit model can be further improved by reducing extrapolated parameters

A further test was conducted aimed to improve the model by simplifying parameter fittings. In the Probit model parameter c is no longer a delaying parameter and in fact it does not have a clear linear trend like that in the previous two functions (Fig. S3.3). Note that a substitution of $\tau = x - c$ will make the Probit function into $y(t) = \int_{-\infty}^{b(t-\frac{c}{b})} a \cdot e^{-\tau^2}\, d\tau + d$, which is a form where $\frac{c}{b}$ would

represent the delaying parameter comparable to that in the Logistic and Probit function. Rather than a linear fitting of c, a constant fitting of c reduces the complexity of the model while only increases the total error by 0.03% (Absolute Error of Final Prediction=3.76x103μm, Final Accuracy=96%). Since parameter d only has less than 0.5% effect on the predicted final length, the Probit model followed by extrapolation of two parameters, a and b, is capable of providing descent results on growth prediction of hypocotyl and hypocotyl epidermal cells.

DISCUSSION

The Probit-fitted data of cellular growth predicts a hypocotyl growth closely matched with the measured data.

The predicted hypocotyl length matches well with the measured length when data of cellular growth was fitted with the Probit function followed by parameter extrapolation (Fig. 3.15), and hence providing a likely model describing the wave of growth. The other two sigmoidal functions used did not provide a satisfactory prediction of the hypocotyl length over time, despite the procedures of parameter extrapolations being performed exactly the same. Among the three, the initial absolute error between predicted and measured hypocotyl size was the smallest when the data were fitted with Probit function without constraint, and this error was reduced the most in the Probit-fitting model (Table 3.1). Predictions of the other two functions showed early stopping of cell growth (Fig. 3.10A, Fig 3.12C), which was their main issue. Using the Probit, the predicted cell growth stopped at the right time; the cellular growth rate and growth period, controlled by parameter b, was not well extrapolated using the Logistic and Log-log function.

Results of fittings and parameter extrapolations imply that the Probit function may be a better fitting to growth of the dark-grown hypocotyl epidermal cells. The Probit has a less flat tail compared to the other two (Supplementary Fig S3.1), which means the starting and ending of cell growth happen more rapidly rather than gradually. That also implies the existence of a global controller of cellular growth/termination, and likely to be some chemical signals such as the hormone gibberellin (Chapter 2, Chapter 5)

For all three sigmoidal functions attempted, linear parameter extrapolations were better than polynomial extrapolations. From the modelling side, using linear extrapolations minimises issues of overfitting. Biologically, a very well-fitted linear behaviour of parameter a and b means the position of the cellular growth wave travels linearly upwards, and the final length of cells also linearly increases over cell indices.

The prediction was only based on the data up to 72 HPG but the prediction was quite accurate until the end of hypocotyl elongation (192 HPG). So there was no issue of overfitting in Fig. 3.15 because the measured hypocotyl length was not used at all for fitting purpose, just plotted for comparison.

The pattern of cell-level growth may not imply the same pattern for the organ growth

Epidermal cell growth was found to fit best with a Probit function, which is symmetric with respect to

its middle point. However, that does not imply the hypocotyl growth follows the same Probit function, as the predicted hypocotyl growth is not symmetric (Fig. 3.15). So there is not necessarily a correlation between patterns of cellular growth and organ growth, due to the differential growth of the hypocotyl cells.

But how can this happen? Is it due to the heterogeneous growth period, growth rate, or starting point for the 17 epidermal cells? If all cells have the same growth rate and growth period (hence the same final length) but have shifted starting point, then the organ growth would still be symmetric. If all cells start to grow at the same time grow for the same period of time, but with different growth rates, then the organ growth would still be symmetric. On the other hand, if all cells grow at the same time, with the same growth rate, but with different growth period, then the organ growth symmetry would be broken. Hence the non-symmetric growth pattern of the hypocotyl is likely to be caused by heterogeneous regional growth period, but not heterogeneous regional growth rate or starting time.

The hypocotyl cellular acropetal wave of growth increases in magnitude

It was established by Gendreau et al[1], and expanded by our work[7] (Chapter 1) that epidermal cells in the dark-grown hypocotyl grow in a wave of elongation, and such wave was not observed in the light-grown seedlings[1]. This wave of growth is modelled in this chapter, and the modelling results suggested that cells with larger indices grow later, and larger, from the beginning of the hypocotyl elongation till the end (~8 days post germination). This is consistent with early observations[1] and the hypothesis based on cellular level data up to 72 HPG (Chapter 1). Since precise descriptions of the growth of upper hypocotyl cells are not available due to technical difficulties, the model provides a good reference to the growth rate and size of those cells.

Unfortunately, the prediction could not be validated at the cellular level, but rather, on the organ level. This means that even though the predicted hypocotyl length has a good match to the measured organ length, the contribution from each cell may be different in reality. Three potential problems of the cellular level prediction exist: (1): Final sizes of the cells may not increase with cell indices, rather, maximum cell size may occur at the middle part of the hypocotyl. (2): Cells with small indices behave differently from the model's prediction. (3) The pattern found for cells with small indices do not imply the pattern for cells with larger indices. To address problem (1), Gendreau showed that cells in the upper region indeed grew longer and later than the basal cells using hypocotyls labelled with paint marks[1], which was consistent with the model's prediction. Our data of cellular and hypocotyl length do not match perfectly with Gendreau's data, possibly due to the addition of sucrose in our

experiments or different growth conditions. Problem (2) is of the least concern among the three, since the models were built based on data, in which the sizes of the epidermal cells were precisely measured until 72 HPG, and they do not elongate further once stopped[1][3]. Problem (3) is also unlikely, since the growth curves for the basal and middle cells (elongation started before 72 HPG) were used for fitting, and the predicted hypocotyl size matched well with the measurement, leaving not much room for variation. Further, good linear trends were seen in the parameters for cells with indices 1-12; only parameters for cells with 13-17 were largely based on parameter extrapolation, and it is unlikely that these five cells behave significantly different from others.

Cell growth interval by index is not linear in time

Compared to Logistic and Log-log model, Probit model achieved better results not only in cell-by-cell size, but also in the growth time: predicted hypocotyl and epidermal cell growth terminated at the correct time. A key reason was that the parameter representing shift in growth starting time, was no longer extrapolated linearly but rather in a inverse function manner ($t - c$ in Logistic and Log-log, but $t - \frac{c}{b}$ in Probit). The successful prediction provided by the Probit model also suggested that the starting growth time of the epidermal cells may not be linear, instead, cells with larger indices would wait longer before they could grow. i.e. the difference in growth starting time between cell 1 and cell 2, t_1, is shorter than the difference in growth starting time between cell 2 and cell 3, t_2. Probit model accidentally modelled the progression of this time interval with a negative inverse function, and resulted in good performance.

This is biologically reasonable: even if the 'growth signal' has a fixed-size window and moves upwards with a constant speed, the fact that upper cells are larger would cost the growth signal more time to travel through them, resulting in their delayed starting time. While initially, when all cells are relatively small, this effect could be very subtle.

Why is there a wave of growth?

The empirically modelled wave of growth shows that the basal hypocotyl cells are a lot smaller in size, compared to the very top epidermal cells. The growth of epidermal cells is a good indicator of regional hypocotyl growth, as cells are permanently attached to another. So why do hypocotyls in the dark follow an acropetal wave of growth from the basal cells? This question can be divided into two sub-questions: (1) Why is there a non-simultaneous growth of hypocotyl cells? And (2): Why is the wave

travels from the basal region to the top region of the hypocotyl?

If we take three assumptions:

A. It takes more energy for a hypocotyl to expand longer
B. The plant wants to minimise the energy spent to reach the light
C. Some cells can grow longer than others

Then the first sub-question can be answered: Hypocotyls want to elongate to just right size to break out from the soil. Because the distance between the seedling and the surface of the soil is unknown for the plant, the most efficient way is to grow small cells first, then gradually, larger ones until the shoot tip is out of the soil. If larger cells grew first, energy might be wasted when the seedling was originally very close to the surface of the soil.

According to the prediction, the upper cells not only grow faster but also grow for a longer period. This, together with the acropetal direction of the wave, may be explained if we establish the relationships between plant hormone and cellular growth. Many hormones, such as the auxin, are synthesised at the meristem. So compared to cells located at the basal hypocotyl region, upper cells have more exposure to newly synthesised hormones, possibly both in time and concentration. The level and exposure time to hormones might cause the differential growth of cells at different hypocotyl regions.

The exact causal and mechanisms of the wave of growth are still not well understood. The cellular wave of growth is modelled empirically in this Chapter and the model predicts the growth of the hypocotyl epidermal cells from germination until the end of organ elongation. Results from model suggest that growth of hypocotyl cells are more likely to follow a Probit function, where cells grow heterogeneously with a noticeable trend, and the prediction matched well with the organ growth measurement.

CHAPTER 4: A STUDY OF DARK-GROWN HYPOCOTYL GROWTH AT THE TRANSCRIPTOME LEVEL

All work contained here was performed by Yuanjie Chen unless otherwise indicated.

SUMMARY

In this chapter, transcriptome data from fast and slowly-elongating hypocotyl regions was examined for links to regulation of the acropetal wave. Dark-grown hypocotyls were dissected into the top (slow-growing) and the bottom (fast-growing) regions when sampled at 24, 36, and 48 HPG, giving altogether 6 samples. Firstly, all expressed genes were categorised based on their expression pattern. Several hormone-related genes and cell wall modification genes were studied in detail. In particular, our transcriptome dataset suggested that the wave of cell growth may be correlated with the level of gibberellic acid (GA), auxin, and the expression of the xyloglucan endotransferase/hydrolase family of wall modifiers. The categorisation also provided a method of grouping genes with similar expression pattern and gene ontology analysis was performed. It was found that many of the biological processes involved in hormone response and cell wall modification were over-represented in categories with higher expression in fast-growing regions.

INTRODUCTION

As detailed in Chapter 1 and 3, hypocotyl elongation begins slowly, transitions to a rapid but steady elongation, and eventually slows. This sigmoidal behaviour is the result of a wave of cell elongation that begins at the base of the hypocotyl and extends upwards with little change in cell width[1]. At 24 HPG, the rapid elongation phase of growth is about to begin; the hypocotyl's basal cells have a large relative growth rate and that of top cells remains small and slow growing. At 36 HPG, the basal cells are elongating rapidly while the top cells have very small growth rate. At 48 HPG, elongation of the very basal hypocotyl cells slows, the middle hypocotyl cells exhibit a fast elongation rate and the top cells are about to grow. Therefore, at early stages the bottom part of the hypocotyl is rapidly growing and the top part of the hypocotyl is slowly growing. This wave of growth is commonly accepted but it is not clear whether there are characteristic signatures at the transcriptome level, and how genes with different functionality correspond to this wave.

Previously, gene expression levels in dark-grown hypocotyls were studied using microarray analysis, after removal of cotyledons and roots[22]. In that study, seedlings were harvested at 45, 48, 52 and 55 hours post incubation (corresponding roughly to 23, 26, 30, and 33 HPG in our system) and differentially regulated genes and their functionality were examined. Among genes that were down-regulated over time, over-representation of the functional categories related to the ribosome and cytoplasm synthesis and peroxidase activity were indicated. This suggested that cytoplasm synthesis had slowed down in a large subpopulation of cells very early after the growth acceleration, at a time when the hypocotyl length had barely exceeded 2mm. Among genes that were up-regulated over time, over-represented ontology classes including chloroplast biogenesis and photosynthesis, auxin signalling, cold and water stress and cell wall-related processes were indicated. Several cell wall modification genes such as XYLOGLUCAN ENDOTRANSFERASE HYDROLASEs (XTHs) and PECTIN METHYLESTERASE INHIBITORs (PMEIs) were also identified as up-regulated. The study provided key information about how the hypocotyl 'growth acceleration' was correlated to gene expression at the transcriptome level at these early stages; however, since they only focused on early time points from 23 HPG to 33 HPG, and used whole hypocotyls, it is difficult to tell how these changes relate to the wave of growth, which exists for a longer period of time and has spatial context.

Within this chapter, I focus on the transcriptional changes occurring with the rapid elongation wave with an eye towards understanding its molecular-level regulation. In order to address this question, dark-grown hypocotyls were isolated from roots and cotyledons and then cut into the 'fast' and the 'slow' regions at 24 HPG, 36 HPG and 48 HPG. These samples, in biological triplicate, were used to generate RNAseq libraries for illumina sequencing. Transcriptomic analysis was used to identify genes that were differentially expressed across different regions of the hypocotyl, and over different times. Because of the wave of growth, the 'fast' and 'slow' regions have different expansion rate at the three time points, the two regions will be referred to as the 'top' and 'bottom' regions for simplicity. For the three time points studied, the 'top' was the slow growing region and the 'bottom' was the faster growing region. This will be discussed in more detail later.

Two categorisation approaches were used to study the pattern of gene expressions. Approach 1 studied genes differentially expressed over time. Approach 2 studied genes that were differentially expressed between the top and bottom regions of the hypocotyl. The combination of the two approaches provided a unique and powerful way to study specific genes, and family/groups of genes, allowing us to study the role of genes during hypocotyl growth, and their dynamics over time. In addition, in order to study genes that are closely related to elongation which may correlate with the physical parameters modelled in Chapter 2 and 3, I focused on the gene groups that were more likely

to be growth causals. These categories include cell wall synthesis and modification and hormone biosynthesis, transport, response, metabolism, and catabolism.

METHODS:

Sample harvesting and RNAseq preparation (Experiment done by S. Braybrook, F. Bou Daher J.Landymore and Y.Chen)

At three distinct time points (24HPG, 36 HPG and 48 HPG) seedlings in biological triplicate were cut into slow-growing and fast-growing parts (Fig. 4.1). 100mgs of tissue (250 seedlings per replicate) were collected and frozen in liquid nitrogen (Braybrook, Bou Daher, Landymore). RNA was extracted from the 18 samples (3 time points, 3 replicates, 2 sections) using the QIAGEN RNeasy mini prep kit (Landymore). 50µl of RLT buffer(lysis buffer+ β-Me) was added to each of the samples on ice and a tungsten bead was added in a fume hood. The samples were then ground using a Tissue Lyser II (QIAGEN) as follows: 25Hz for 1min, repeated 4-5 times with the samples being mixed and placed on ice after each round. The samples on ice were then put back in the fume hood and the remaining lysis buffer solution was added – 400 µl. The samples were vortexed and the lysate was then transferred to a QIAshredder spin column (QIAGEN). The protocol was followed from that point on with the optional drying step performed. The samples were eluted in 35 µl RNase free water and subsequently DNase treated using the Ambion TURBO DNA-free™ Kit (Cat. No AM1907). The RNA quantity was checked using a Qubit® 2.0 Fluorometer (Invitrogen Cat. No Q32866) and the Qubit High Sensitivity (Cat. No Q32852) reagents. This was to determine how much would be required for 1ug needed for RNAseq library preparation.

The RNAseq library was prepared following the low sample protocol by Illumina (Braybrook and Landymore). The individual samples/ libraries were normalized and then pooled at a concentration of 20nM. The pooled library was then quantified using qPCR with the KAPA Library Quantification Kit (KAPA Biosystems Cat. No KR0405) and diluted to 1nM and re-tested. The 1nM pooled library was then used for sequencing and run on the sequencer following the sequence protocol for the given library (Landymore). 1 µl of PhiX was added to act as a control.

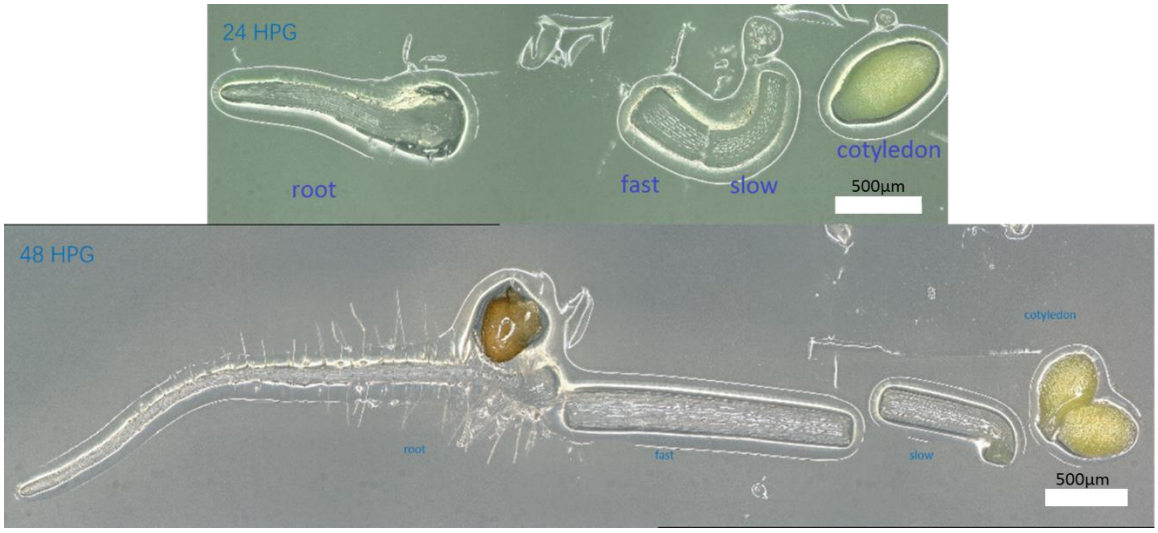

Figure 4.1 Dissected hypocotyls at 24 HPG and 48 HPG(from left to right): root, fast growing (bottom) region, slow growing (top) region, cotyledon. Scale bar=500μm

With two samples (top and bottom) at each time point and three time points, this gave RNA sequence for 6 samples: [24 top, 24 bottom, 36 top, 36 bottom, 48 top, 48 bottom], and each sample was in triplicate. The RNA sequence data produced short reads of 35-76 in sequence length. Each one of the triplicates had 4 fastq files. Sequencing files were merged using cat function in shell[130]. Trimmomatic3.2[131] was used for trimming the Illumina data the data, including cutting adapter, threshold cutting and crop. Quality assessment was performed in fastQC[132]. Mapping was performed using Tophat[133] and Bowtie2[134], with reference genome for the *Arabidopsis thaliana* downloaded from the TAIR 10 website[135]. The downloaded .GFF file needed to be converted to .GTF file before called by Tophat using Cufflinks software suite[136]. A .bam file was produced and the differential gene expression analysis was performed in R, which generated a Count Matrix with the raw number of counts of all the genes. DESeq2[137] package was used for comparing samples and generate differentially expressed genes, using a built-in normalisation method (Relative Log Expression, RLE), which measures the Euclidean distance for clustering. Two approaches were used to study the differentially expressed genes, approach 1 compared samples over time and approach 2 compared samples across regions.

Following the analysis using the DEseq2 package, two outputs were generated: the file 'countdata' was a matrix with each row being a different gene, and each column being the number of raw counts in each triplicate of samples. The normalised counts were generated using the RLE method and genes that were not active had very low number in counts; the file 'resSig' used the normalised counts and compare gene expression between two different samples. It was a data frame with all the genes in

'countdata' and their up/down regulation patterns. For example, the gene 'AT1G01010' had total raw count number of '2697' in the bottom region at 48 HPG, a total raw count number of '987' in the top region at 48 HPG, and therefore was found to be down regulated in the top region with a Log2 Fold Change=-2.27 after normalisation.

Sample similarity verification

Three biological replicates at two regions and three time points yield 18 samples. However four of them were suspected to be swapped during experiment library preparation or sequencing. (Fig. S4.1a) To avoid this potential issue, they were removed from the analysis, together with two samples randomly chosen to even out the sample numbers. Therefore the analysis was based on 12 samples, with a duplicate at each region & time combination. The Euclidean distance among samples were assed to confirm their similarity. All samples are neighbouring with their duplicates and there was a clear difference between samples of top (T) and bottom (B). (Fig. S4.1b)

Counts normalisation verification

To verify the normalisation, normalised counts of housekeeping genes were plotted. (Fig. S4.2) Previously 22 housekeeping genes were identified in *Arabidopsis* by Czechowski[138], 12 of them with average count>500 were presented. Their similar normalised counts verified the normalisation method (c.f. Fig. S4.3, raw counts for those housekeeping genes).

Agrigo and GO analysis

List of genes were pasted in the webpage of Agrigo and GO and overrepresented biological processes were automatically identified. GO provided detailed expected number of genes and p-values, where Agrigo provided better visualisations

Categorisation approach 1: RNA levels across three time points

With a selected cut-off of the log2 fold change value, the regulation of each gene can be categorised as being up, down, or flat between two samples. Four lists of differentially expressed genes were generated with DESeq2. List 1: differentially expressed genes between 24 HPG and 36 HPG at the top region, List 2: differentially expressed genes between 36 HPG and 48 HPG at the top region, List 3: differentially expressed genes between 24 HPG and 36 HPG at the bottom region, and List 4: differentially expressed genes between 36 HPG and 48 HPG at the bottom region. Different values of log2 fold changes were used to see how it affected the resulting number of genes. Later, a cut-off of log2 fold change=1 was used throughout the analysis, which pulled out genes that had at least doubled/halved their expression level for up/down regulations. Using the four lists, each gene was categorised into one of the 81 categories (see table 4.1) using the following algorithm: Set n=0, n=27 and n=54 for up, flat and down regulations in List 1, respectively. Set m=0, m=9 and m=18 for up, flat and down regulations in List 2, respectively. Set l=0, l=3 and l=6 for up, flat and down regulations in List 3, respectively. Set k=1, k=2 and k=3 for up, flat and down regulations in list 4, respectively. Then the category index for each gene is given by category index=n+m+l+k. Note that this is a well-defined one-to-one mapping, its inverse function can work backwards from the index number to the expression pattern over time.

For each gene in each area, across the three time points (24HPG, 36HPG and 48HPG), there are 9 possible patterns over time: {up,up}, {up, flat}, {up,down}, {flat, up}, {flat, flat}, {flat, down}, {down, up}, {down, flat}, {down, down}. Since we had samples in top region of hypocotyls (less growing) and bottom region of hypocotyls (more growing), giving a total 81 possible combinations.

A table was created to identify each gene in one of those 81 categories as follows.

Category Index	Top region		Bottom region	
approach 1 (a)	24-36HPG	36-48HPG	24-36HPG	36-48HPG
a1	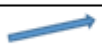			
a2	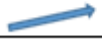	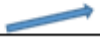	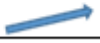	
a3				

a4		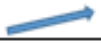		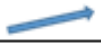
a5				
a6	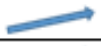			
a7	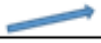	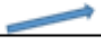		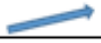
a8	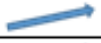	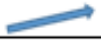	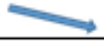	
a9				
a10				
a11				
a12				
a13	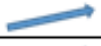			
a14				
a15				
a16				
a17				
a18				
a19				
a20				
a21				
a22				
a23				
a24				
a25				
a26				
a27				
a28				
a29				
a30				
a31				
a32				
a33				
a34				
a35				
a36				
a37				
a38				
a39				
a40				
a41				
a42				
a43				
a44				
a45				
a46				
a47				

a48				
a49				
a50				
a51				
a52				
a53				
a54				
a55				
a56				
a57				
a58				
a59				
a60				
a61				
a62				
a63				
a64				
a65				
a66				
a67				
a68				
a69				
a70				
a71				
a72				
a73				
a74				
a75				
a76				
a77				
a78				
a79				
a80				
a81				

Table 4.1. The expression pattern (over time) of genes in each category, categorised using approach 1

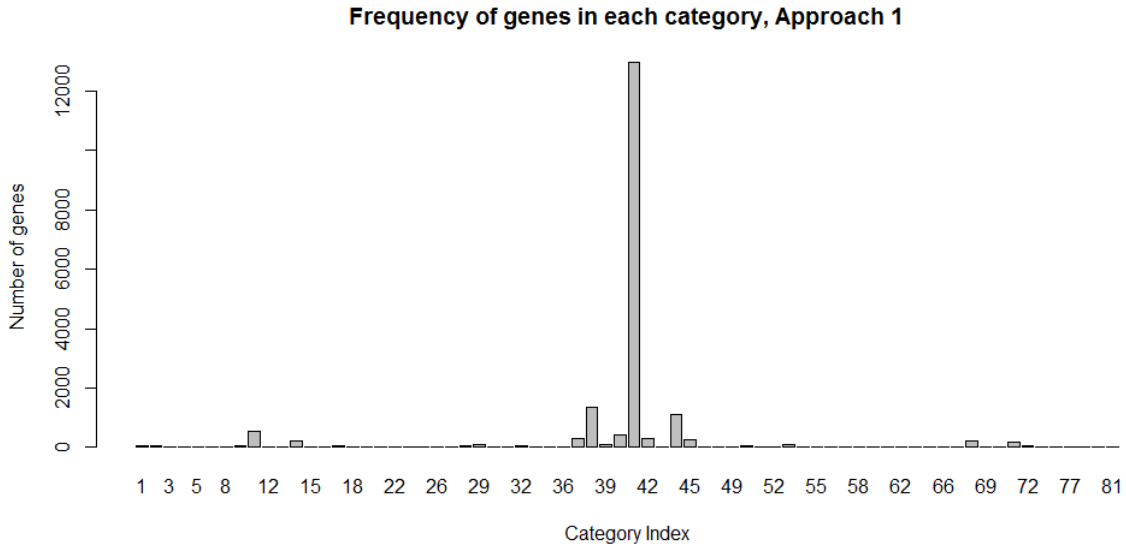

Figure 4.2 Distribution of number of genes belong to different categories. Category 41 is an outstanding peak in the plot with 68% of the data

Note that 68% of genes were categorised with index 'a41', which was {flat, flat} at the bottom region and the top region. i.e. No change in gene expression pattern over time in any region.

After removing the genes with no difference in expression pattern, genes with total raw counts (top+bottom) less than 500 in the RNA-seq experiment were also removed. Out of a total number of 33604 genes, 19053 of them, that have a total count number >500, were kept. The value of log2FC was selected to be 1, meaning the expression of any gene was at least doubled to be considered up-regulated, and more than halved to be considered down-regulated. Depending on the cut-off value of log2FC, different genes could end up with different categories. E.g. gene 'AT1G01200' had category index 11 (up-flat at the bottom region, up-flat at the top region) when log2FC was 0.2 and had category index 38 (up-flat at the bottom region, flat-flat at the top region) when log2FC was raised to 0.5. In order to make sure the selection of log2FC value did not change the categorisation of the majority of the genes, a paired Wilcoxon-test was used to study the change in ordering when different values of log2FC were used (0.2, 0.5 and 1). The result suggested a non-significant difference between distributions with log2FC 0.2 and 0.5, and 0.5 and 1(p-value=0.2648, 0.834 respectively). I concluded that the value of log2FC did not affect the distribution of gene category in terms of their percentile ranking.

Categorisation approach 2: Study across the two regions, top and bottom

The previous work studied how genes were up/down-regulated over time, but differentially expressed genes across the two regions (top and bottom) were not revealed in the 81 categories. Here genes that were differentially expressed in the top/bottom hypocotyl regions were studied.

Similar to approach 1 but now comparing top and bottom regions of the hypocotyl at the same time point, the regulation of each gene can be categorised as being up, down, or flat between two samples. Three lists of differentially genes were generated with DESeq2. List 1: differentially expressed genes between top and bottom region of the hypocotyl at 24 HPG, List 2: differentially expressed genes between top and bottom region of the hypocotyl at 36 HPG, and List 3: differentially expressed genes between top and bottom region of the hypocotyl at 48 HPG. As before, different values of log2 fold change were used to see how they affect the result number of genes, and the value was selected to be ±1 later for further analysis. Using the three lists, each gene was categorised into one of the 27 categories (table 4.3) using the following algorithm: Set n=0, n=9 and n=18 for up, flat and down regulations in List 1, respectively. Set m=0, m=3 and m=6 for up, flat and down regulations in List 2, respectively. Set l=1, l=2 and l=3 for up, flat and down regulations in List 3, respectively. Then the category index for each gene is given by category index=n+m+l. Like before, this is a well-defined one-to-one mapping, a formula was also provided to work backwards from the index number to the expression pattern across region.

For each gene in each of the three time points (24HPG, 36HPG and 48HPG), it can be in one of the three groups: {up-regulated at the bottom region}, {down regulated at the bottom region}, and {not differentially expressed across the two regions}. Since we had samples in three different time points, giving a total 27 possible combinations. A table was created to identify each gene in one of those 27 categories as follows.

Category Index	Non-growing vs growing		
approach 2 (b)	24HPG	36HPG	48HPG
b1			
b2			
b3			
b4			
b5			
b6			
b7			
b8			
b9			
b10			
b11			
b12			
b13			
b14			
b15			
b16			
b17			
b18			
b19			
b20			
b21			
b22			
b23			
b24			
b25			
b26			
b27			

Table 4.3. The expression pattern (over time) of genes in each category, categorised using approach 2

In approach 1, category a41, the category of genes not differentially expressed over time, had the most number of genes (68%). Similar results were seen in this approach, where most of the genes fell into category ‘b14’, with 48% in total, which represented genes that were not being differentially changed between the top and bottom regions at all times. Like before, genes which showed no difference in expression pattern were removed, as well as genes with low count number (total raw counts<500). Then the distribution of number of genes in each category was plotted with values of different log 2 fold change.

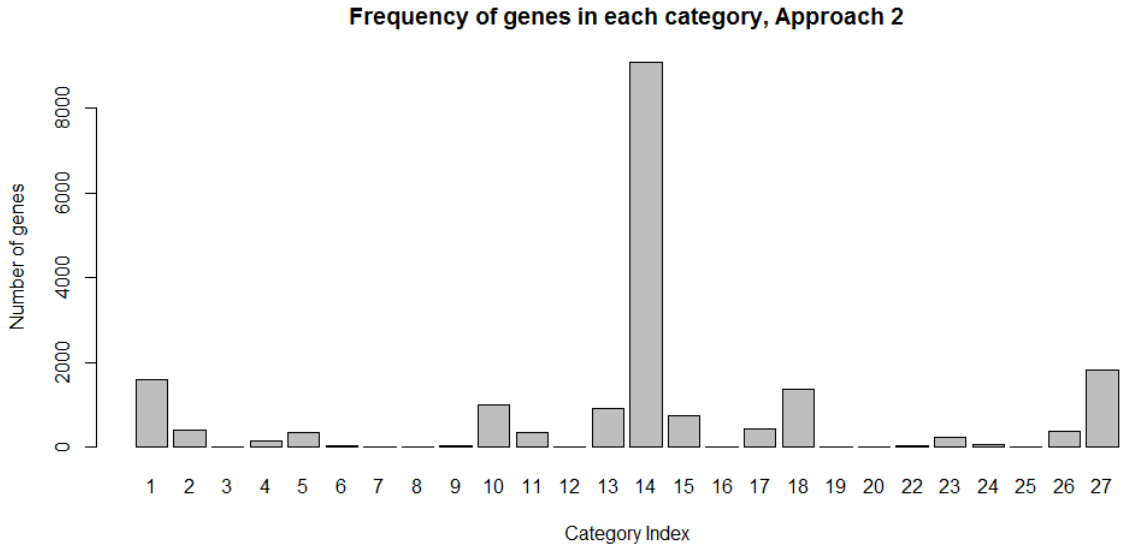

Figure 4.3 Distribution of number of genes belong to different categories, with log2 fold change equals to 1. Category 14 contains the most number of genes with 48% in total

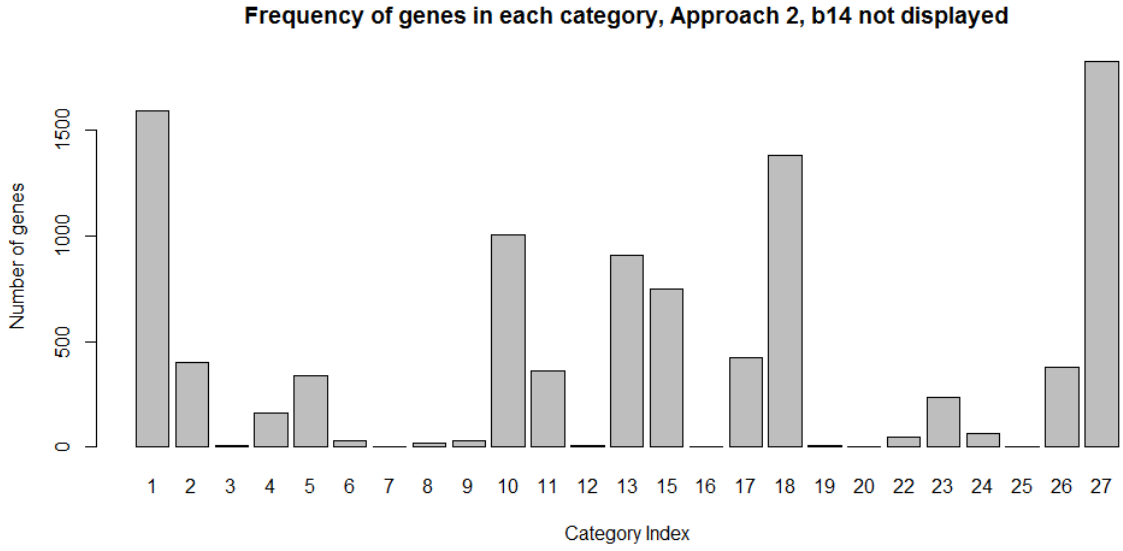

Figure 4.3(b) Replot of Fig 4.3, with category b14 not displayed

Like before, the log2FC was selected to be 1 throughout the analysis. To make sure a different value of the log2FC did not affect the overall distribution, a paired-Wilcoxon test was run and the p-value for difference in percentile ranking among the four different log2FC values (1,0.5,0.2,0.01), which yielded p-values 0.9403, 0.5317, and 0.7454, suggesting the distribution of categories of genes were not different with a changing cut-off. Ignoring category with index 14 (b14), the two peaks at the two ends (category b1 and b27) represented genes that were constantly down-regulated at the bottom

region and constantly up-regulated at the bottom region. These two peaks had roughly the same height, indicating overall there was no bias toward the top or the bottom region in terms of gene expression.

The other two less outstanding peaks were category b10 and b18, which represented genes that were down and up-regulated at the bottom region at 36 HPG and 48 HPG but not differentially expressed at 24HPG, respectively.

FAMILIES OF GENES RELATED TO GROWTH

Groups of genes with known ontology were studied: Hormone-related genes (GA, Auxin), and cell wall modification genes (*PME,PMEI, CESA, XTH* families). Through this study, a better understanding of the role of the different family of genes possibly linked to growth behaviour, such as initiating, regulating or inhibiting growth, was gained.

GA genes

Introduction

The GAs (gibberellic acid) were originally found to be metabolites of the phytopathogenic fungus *Gibberella fujikuroi*[139][140]. Being a large class of tetracyclic diterpenoid carboxylic acids[139], GA is present in flowering plants, lower plants, fungi and bacteria, and it controls seed germination, elongation and flowering[141][142], and other important aspects of growth. In higher plants, GA promotes organ growth and induces certain developmental switches[143][144]. The current view is that GA binds to a soluble GID1 receptor[145], which interacts with the DELLA repressor protein and induces DELLA protein degradation[146][147][148][149], where the DELLA protein act as a growth repressor[150]. Mutants with deficient DELLA grow taller and flower earlier than the wide types[151][152][153][154] and overexpression of DELLA causes plants to flower late or become dwarfed[155][156]. Light[157], temperature[158], and stress[159], as well as auxin[160], abscisic acid[161] and DELLA signalling[162], regulate GA biosynthesis, metabolism and concentration. GAs are synthesised predominantly in young, growing organs in shoots[139]. Usually GA concentration is higher in growing organs compared to the mature ones[24], and the mature organ has a reduced activity in GA biosynthesis and higher rates of GA deactivation[163].

The main biological active GAs in higher plants are GA_1 and GA_4, and their biological activities results in tissue growth through enhanced cell expansion and/or cell division[164]. GA_{12} and GA_{53} are formed from *ent*-kaurene, where *ent*-kaurene oxidase (KO) converts *ent*-kaurene through *ent*-kaurenol and *ent*-kaurenal to *ent*-kaurenoic acid[165]. The *ent*-kaurenoic acid is converted by *ent*-kaurenoic acid oxidase (KAO) to GA_{12} and GA_{53}[165]. GA_{12} and GA_{53} lie at a branch point in the biosynthetic pathway, and convert in parallel to GA_1 and GA_4 respectively, being the active end-products of the pathway[166]. The conversion reactions are catalysed by GA 20-oxidase (GA20ox) and GA 3-oxidase (GA3ox), where the GA20ox convert GA_{12} and GA_{53} to GA_9 and GA_{20}, respectively[167], and hence to GA_4 and GA_1 by GA3ox[165][168][169].

To allow precise regulation of GA concentration in plant tissues, turnover of GAs is an essential process. The most common deactivation mechanism is 2β-hydroxylation, being ubiquitous in higher plants. 2β-hydroxy group reduces interaction with the GA receptor by promoting steric interference within GA-binding pocket[164] and the GA 2β-hydroxylases (GA2ox) can also form the GA catabolites[170]. GA2*ox* is particularly important in the deactivation mechanism, which ensures the tissues are not accumulating GAs in excess[170]. GA2*ox* was reported to be more active in late-developing seeds, and more active during flowering[171].

In many species, auxin signalling was shown to stimulate GA biosynthesis in stems and this may represent a major mechanism for auxin-induced elongation growth[160], where *GA2ox* and/or *GA3ox* are up-regulated, and *GA2ox* is down-regulated. It was also shown in *Arabidopsis* that genes encoding auxin carrier proteins were up-regulated by exogenous GA_4 during seed germination[23]. However, the role of auxin in seed germination or cell expansion is still unclear.

The movement of GAs in plants can occur over both short and long distances, although the biological properties of this transport are not yet understood[172][173][174]. It was shown that the GA_{12}, one of the GA precursors, was the major mobile GA signal over long distances and it moved through the plant vascular system[166]. The existence of long-range transport endogenous GA_{12} implies a possible way of controlling the developmental phase transitions in plants.

Previously genes that were involved in GA biosynthesis and signalling, together with the GA responsive genes were studied in a mixture of organs studied including seeds, shoots, flower buds, using microarray experiments[175][146][176][177][178][23][179]. In this study, I took genes that were identified to be related to the GA, from the 11 different[175][146][176][177][178][23][179] microarray experiments. Combining these lists of genes gave 3812 genes that were related to GA. 232 of them were considered to be strongly related to GA where in more than 3 out of 11 microarray

experiments, their transcript changed in relation to altered GA/GA signalling. Then the GA biosynthesis (18 in total), GA receptors (5 in total) and GA catabolism genes (8 in total) were studied specifically.

Results

The GA related genes tend to be more expressed over time

In a total number of 3812 GA-related genes, 232 of them were considered to be strongly related to GA. Only genes with a significant number of hits in the RNA-seq experiment were considered, and that left with 2974 GA-related genes, where 205 of them were strongly related to GA.

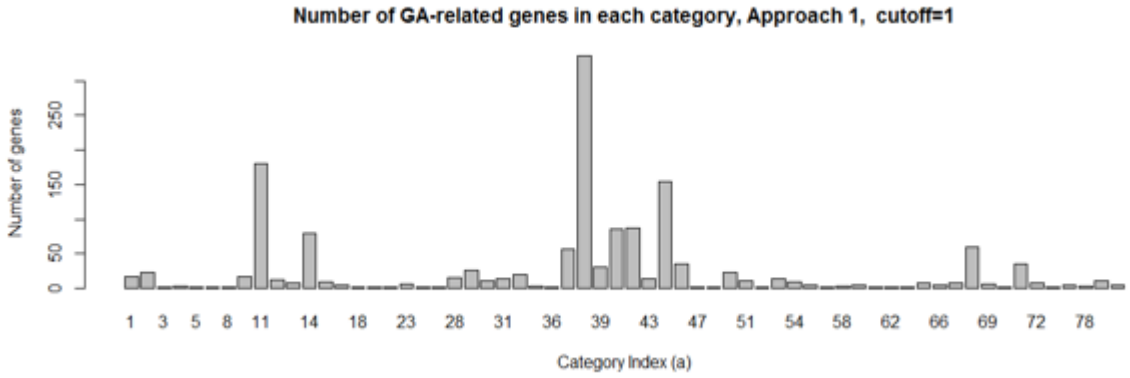

Figure 4.4 Number of GA-related genes in each category, categorised with approach one. Each gene is categorised into 1 out of 81 categories depending on their expression pattern over time. Category 41 was not shown the graph. This was the category with the most number of genes, representing genes not differentially expressed over time.

Fig. 4.4 is the distribution of the categories of all GA-related genes, categorised using approach 1. The behaviour of GA related genes over time is studied here. Several peaks can be identified, such as category a11, a38, and a44. Then the distribution was compared by plotting alongside with all the genes normalised. The difference in distribution between the GA-related genes and all the genes indicates which categories were the GA-related genes more likely to be in.

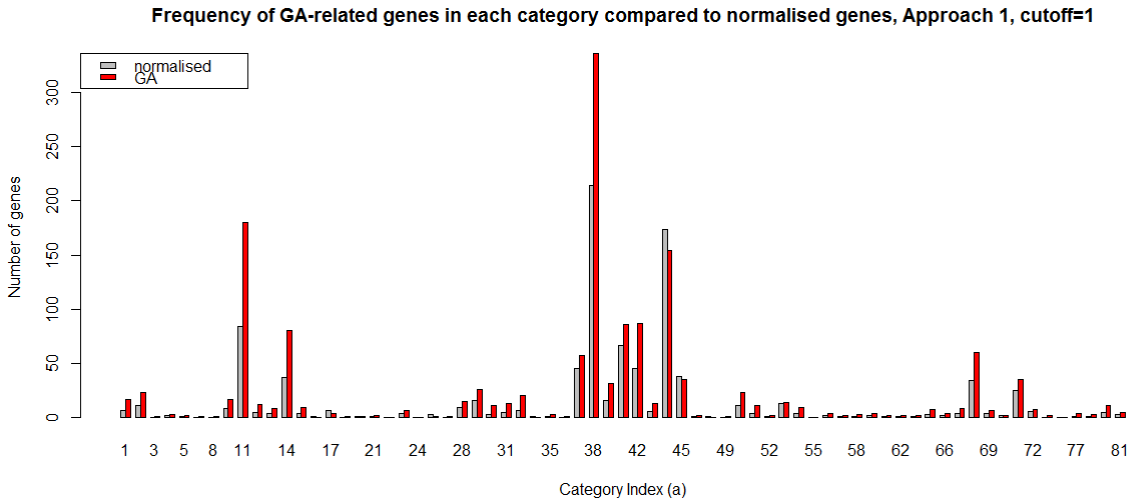

Figure 4.5 The distribution of GA-related genes categorised using approach 1, compared with the same distribution for all the genes after normalisation (RLE normalisation, Category a41 removed).

The percentile of each category was computed by the formula $\frac{genes\ fell\ into\ this\ category}{total\ number\ of\ genes}$, and only genes with differential expression were included. This gave a measure of how likely a gene was in this category given a group of genes. When compared to all the genes after normalisation, the difference in this percentile indicated a tendency towards a certain category where the GA-related genes (or any other groups of genes) were more likely to fall in. The percentile of GA-related genes and the percentile of all genes have very similar values in most of the categories. Yet I was interested in categories that were more favoured by the GA-related genes. 10 such categories were identified, with indices {a1,a2,a10,a11,a12,a14,a28,a38,a39,a68}. In these categories, the number of GA genes (red bar, Fig. 4.5) was much higher than the expected number (grey bar, Fig. 4.5). The percentile for both GA-related genes and all genes after normalisation was calculated and the top ten categories with the largest difference in percentile are presented in Table 4.5. Genes in category a41 (non-changing expression over time) were removed before computing the percentile, which would otherwise make the percentile too small for visualisation and comparison.

Category Index (a)	Non-growing region		Growing region		percentile	percentile
	24-36HPG	36-48HPG	24-36HPG	36-48HPG	GA-related	All genes normalised
a1	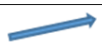	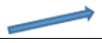		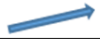	1.14%	0.66%
a2	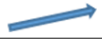	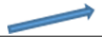			1.54%	1.10%
a10	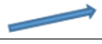				1.14%	0.85%
a11	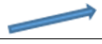				12.06%	8.80%
a12	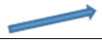			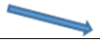	0.80%	0.47%
a14					5.36%	3.8%
a28		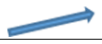		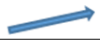	1.00%	0.99%
a38					22.51%	22.5%
a39					2.10%	1.68%
a68					4.02%	3.63%

Table 4.5. The top ten categories that favoured by the GA-related genes, with their expression pattern over time, and the percentile of genes.

Table 4.5 contains the top categories favoured by the GA genes. There are 18 up-pointing arrows, 17 flat, and 3 down-pointing arrows over time, from 24 HPG to 48 HPG. This suggested that in general, the GA-related genes tended to be more up-regulated over time when compared to other genes. More specifically, the three highest peaks at category a11, a14 and a38 represented genes that were more up-regulated in early time. The strong affinity of GA-related genes with these three categories indicated that those genes may have potential correlations with growth signalling and growth initiation.

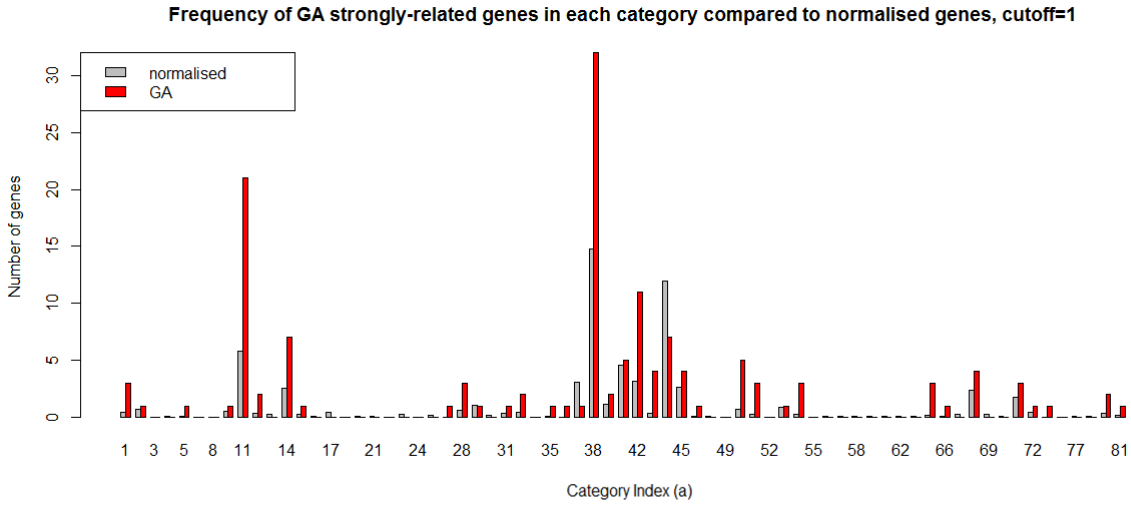

Figure 4.6 The distribution of GA strongly-related genes categorised using approach 1, compared with the same distribution for all the genes after normalisation.

Similar to the GA-related genes (red bar, Fig. 4.6), the distribution of categories was plotted for all the genes after normalisation (grey bar, Fig 4.6). As before, the top 10 categories favoured by these genes were identified with indices: {1,11,12,14,28,38,42,50,51,54}. Rather than the comparing the percentile, this time number of genes in each category vs expected number of genes from normalised data was computed, due to the small number of genes. The results are shown in the Table 4.6.

Category Index	Non-growing region		Growing region		GA strongly related genes	expected number of genes
	24-36HPG	36-48HPG	24-36HPG	36-48HPG		
a1	↗	↗	↗	↗	3	0.43
a11	↗	→	↗	→	21	5.77
a12	↗	→	↗	↘	2	0.31
a14	↗	→	→	→	7	2.53
a28	→	↗	↗	↗	3	0.64
a38	→	→	↗	→	32	14.75
a42	→	→	→	↘	11	3.12
a50	→	↘	→	→	5	0.74
a51	→	↘	→	↘	3	0.28
a54	→	↘	↘	↘	3	0.22

Table 4.6. The top ten categories that favoured by the GA-related genes, with their expression pattern over time, and the number of genes compared to the expected number for each category.

As before, the GA strongly-related genes exhibited similar expression pattern and favour similar categories which were mostly more expressed over time. Compared to the GA-related genes, the GA strongly-related genes showed a higher affinity to category a11 and a38, which represented genes that were more expressed at early times. The exceptions were category a50, a51 and a54, with a total number of 11 genes, which showed less expression over time. A shorter peak of category a44 (red bar) compared to other genes (grey bar) was also observed. Giving the fact that category a44 represented genes that were down-regulate at the early time, opposite to those of potential 'growth initiation' genes. This also indicated that the GA strongly-related genes tended to be more up-regulated at the early time, and hence some were possibly involved in growth initiation.

The GA related genes tend to be more expressed in the fast-growing region of the hypocotyl

Fig. 4.7 is the distribution of categories of all GA related genes, categorised using approach 2. The behaviour of GA related genes in different regions of the hypocotyl was studied. The highest two peaks appeared at category b18 and b27, both represented a higher expression level at the bottom region. The overall distribution did not appear to be very similar to that in Fig. 4.3(b), suggesting this group of genes had different characteristics with all other genes combined. Like before, this graph was plotted alongside the distribution of all genes after normalisation, and the difference indicated categories favoured/not favoured by the GA related genes.

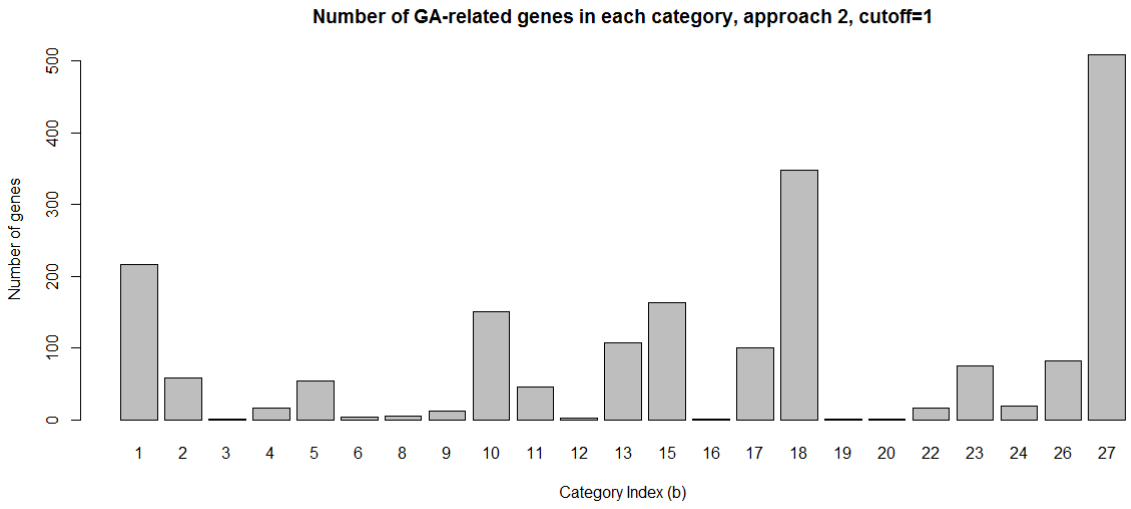

Figure 4.7 Number of GA-related genes in each category, categorised with approach two. Each gene is categorised into 1 out of 27 categories depending on their expression pattern across hypocotyl regions. Category 14 was removed from the graph. This is the category consists the most number of genes, which represents genes not being differentially expressed.

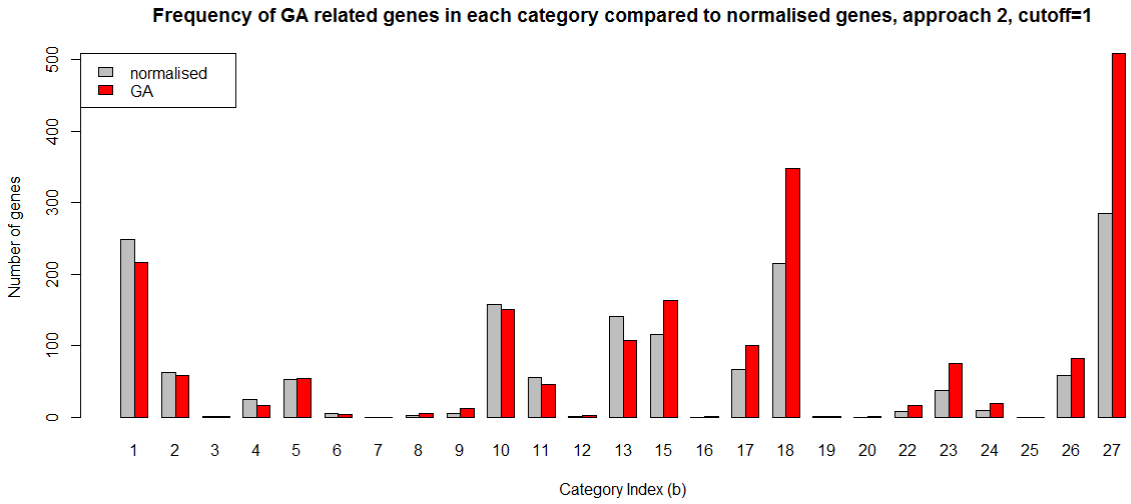

Figure 4.8 The distribution of GA related genes categorised using approach 2, compared with the same distribution for all the genes after normalisation.

Three key observations were drawn from Fig. 4.8.

1) Overall the red bars representing the GA related genes were taller than the grey bars. This was counterintuitive because the normalisation was done with respect to the number of GA genes, so overall there shall be no net height difference. The reason for of this was the absence of category b14, which contained a smaller proportion of GA related genes and a larger proportion of all the other genes. Recall that category b14, which contains the majority of genes (see Fig. 4.3), was omitted because it represented genes with no differential expression

2) Category b27 represented genes being more expressed at the bottom region at all time, and category b1 represented genes being more expressed at the top region at all time. Category b27 was the conjugate (reverse) category to category 1, and overall these two categories were similar in height for all genes (grey bar). But for the GA related genes, there was a clear tendency toward b27 over b1, and similarly, a tendency toward b18 over b10. Since b18 and b27 represented genes being more expressed at the bottom region, I concluded that the GA related genes favour the bottom region rather than the top region.

3) In general, the red bars representing GA-related genes were taller on the right-hand side of the graph, and the grey bars were taller on the left-hand side of the graph. Looking at Table 4.3 with all the expression patterns, it appears that the category with larger index number tended to be more up-regulated at the bottom region at 24 HPG. Therefore this suggested that overall at 24 HPG the GA-related genes tended to be more expressed in the bottom region of the hypocotyl.

All the evidence suggests that overall the GA related genes were more likely to be more expressed in the bottom region compared to the top region. Since the bottom region was the fast-growing region, and at 24 HPG the rapid hypocotyl elongation was about to start, the GA related genes were inferred to have strong correlations with growth regulations and growth initiations.

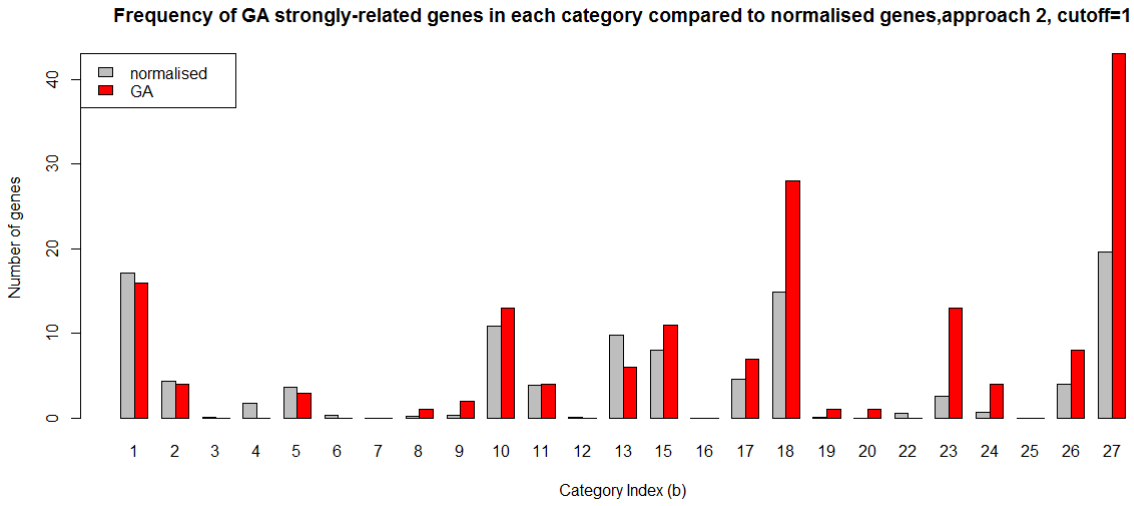

Figure 4.9 The distribution of GA strongly-related genes categorised using approach 2, compared with the same distribution for all the genes after normalisation.

A similar graph was plotted for the 232 genes that were considered to be strongly related to GA. Compared with the previously 3812 GA related genes, the same observation was seen and the same conclusion could be applied to this list of GA strongly-related genes. In addition, there were greater relative differences between the red and grey bars at category b27 and b18. A bigger relative difference was also seen for category b23 and b26, which represented genes with expression pattern a step before and a step behind the growth wave, respectively.

In order to gain a more detailed understanding of the GA biological processes in the transcriptome level, the group of GA biosynthesis genes, GA receptors and GA catabolism genes were studied.

GA biosynthesis genes expressed slightly before the cell growth wave

The GA biosynthesis genes are involved in the process of GA synthesis, including making GA_9 from GA_{12}, or promoting the conversion from GA_9 to GA_4, or other upstream biosynthesis processes related to KAO. Since the GA genes were hypothesised to regulate cellular growth, the GA biosynthesis genes

were expected to express before the rapid cellular growth, and their expression patterns were expected to be a step ahead of the growth wave.

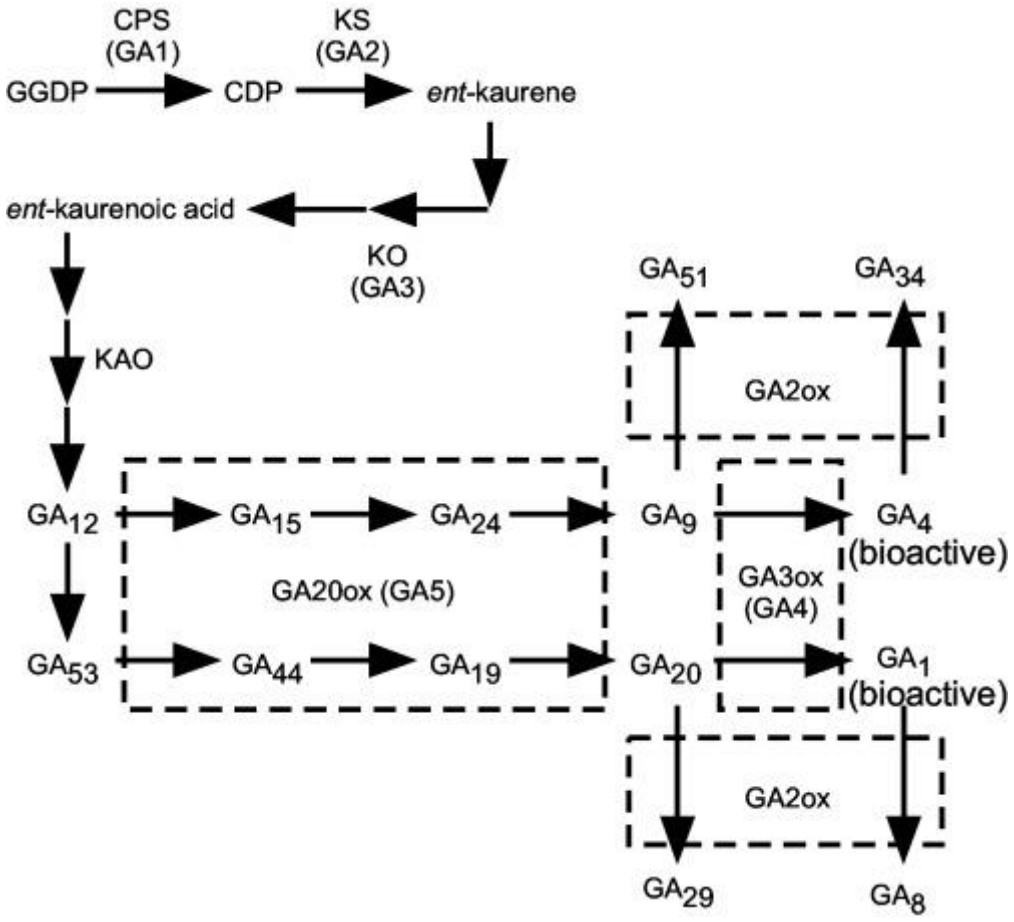

Figure 4.10 Pathways of GA synthesis and degradation in *Arabidopsis*. Geranylgeranyl diphosphate (GGDP), ent-copalyl diphosphate (CDP), ent-copalyl diphosphate synthase (CPS), ent-kaurene synthase (KS), ent-kaurene oxidase (KO), ent-kaurenoic acid oxidase (KAO), GA 20-oxidase (GA20ox), GA 3-oxidase (GA3ox), GA 2-oxidase (GA2ox)[165].

14 genes were identified as GA biosynthesis genes[165]. Nine of them had >500 counts, and 7 of them were differentially expressed over time and/or across region, as shown in Table 4.7, together with their normalised total counts (Fig. 4.11).

GA biosynthesis		Category Index(a)	Category Index(b)
AT4G02780	GA1, CPS: Catalyzes the conversion of geranylgeranyl pyrophosphate (GGPP) to copalyl pyrophosphate (CPP) of gibberellin biosynthesis	41	1
AT1G79460	GA2, KS, KS1: Encodes for a protein with ent-kaurene synthase B activity which catalyzes the second step in the cyclization of GGPP to ent-kaurene in the gibberellins biosynthetic pathway.	41	14

AT5G25900	GA3: Encodes a member of the CYP701A cytochrome p450 family that is involved in later steps of the gibberellin biosynthetic pathway.	41	14
AT1G05160	KAO1:brassinosteroid biosynthetic process, brassinosteroid homeostasis, gibberellin biosynthetic process	41	10
AT2G32440	KAO2: brassinosteroid biosynthetic process, brassinosteroid homeostasis, gibberellin biosynthetic process	45	10
AT4G25420	gibberellin 20 oxidase 1	45	10
AT5G51810	gibberellin 20 oxidase 2	15	23
AT5G07200	gibberellin 20 oxidase 3	N/A	N/A
AT1G60980	gibberellin 20 oxidase 4	N/A	N/A
AT1G44090	gibberellin 20 oxidase 5	N/A	N/A
AT1G15550	gibberellin 3-oxidase 1	14	23
AT1G80340	gibberellin 3-oxidase 2	71	2
AT4G21690	gibberellin 3-oxidase 3	N/A	N/A
AT1G80330	gibberellin 3-oxidase 4	N/A	N/A

Table 4.7. The differentially expressed GA biosynthesis genes with sufficient counts, categorised using both approaches[180]. Category Index (a) and (b) represents the two approaches, respectively. N/A means the gene was not expressed in our experiment.

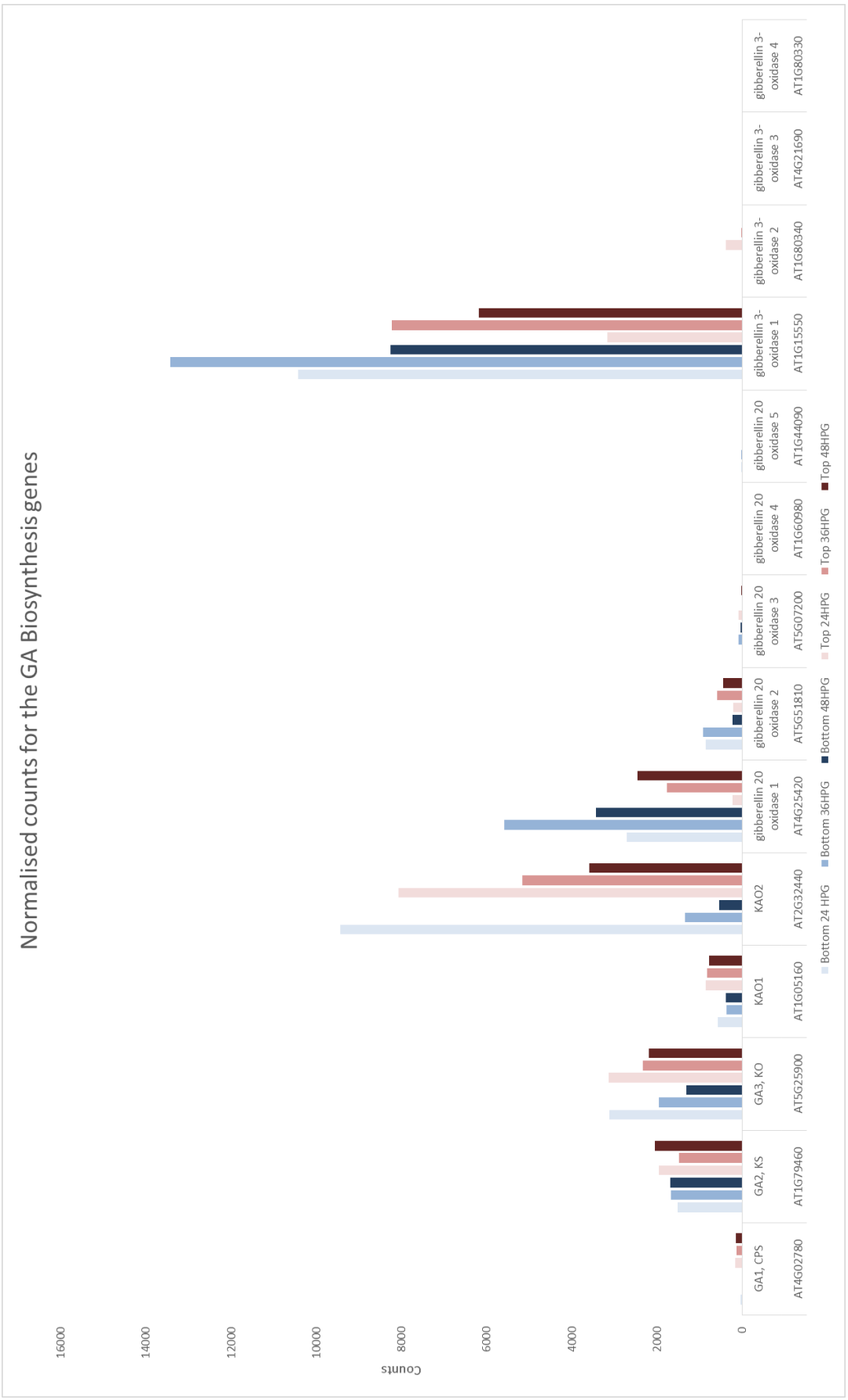

Figure 4.11 The normalised counts for the GA biosynthesis genes

The GA biosynthesis genes showed different expression level and pattern from 24 HPG to 48 HPG. In general, the GA biosynthesis genes expressed a step ahead of the growth wave, and this step was larger for more upstream GA biosynthesis genes (*CPS, KO, KAOs*).

For the genes involved in very upstream GA biosynthesis processes, GA1(*CPS*), GA2(*KS*) and GA3(*KO*) did not have different expression level over time, and only GA1 was more expressed at the top region of the hypocotyl, where the rest two had no difference in expression level across the region. *Arabidopsis* Ent-Kaurenoic Acid Hydroxylase 2 (*KAO2*), was categorised into a45 and b10, which suggested an inversed expression pattern responding to the growth wave. It was not initially differentially expressed across the two regions of the hypocotyl, but less expressed at the bottom region at 36 HPG and 48 HPG. At the bottom region, it was also down-regulated over time, from 24 HPG to 36 HPG, and again from 36 HPG to 48 HPG. *Arabidopsis* Ent-Kaurenoic Acid Hydroxylase 1 (*KAO1*), was categorised into a41 and b1. It behaved very similar to *KAO2* but with a much lower count number at all three times, and it was not differentially expressed over time at any of the two regions.

The *gibberellin 20 oxidase 1* (*GA20ox1*), one of the main GA 20 oxidase family, was categorised into a11 and b26, both suggest an expression pattern a step ahead of the hypothetical growth wave. The *GA20ox1* was more expressed at the bottom region of the hypocotyl compared to the top region at 24 HPG and 36 HPG, and then not differentially expressed between the two regions at 48 HPG. It was up regulated from 24 HPG to 36 HPG in both top and bottom regions, and was not differentially expressed between 36 HPG and 48 HPG. The *gibberellin 20 oxidase 2* (*GA20ox2*), another gene of the main *GA20* oxidase family, was categorised into a15 and b23, indicating it expressed before the growth wave, even earlier than the *GA20ox1,* although with lower count numbers. The *GA20ox2* was initially more expressed at the bottom region of the hypocotyl, and then showed no differential expression across the two regions later on. Its expression level increased from 24 HPG to 36 HPG at the top region and decreased from 36 HPG to 48 HPG at the bottom region. The gibberellin 3 oxidase 1 (*GA3ox1*), one of the main GA 3 oxidase family, was categorised into a14 and b23, both indicating it expressed before the hypothetical growth wave. It behaved very similar to *GA20ox2*, with very high count numbers, and not differentially expressed from 36 HPG to 48 HPG at the bottom region. The gibberellin 3 oxidase 2 (*GA3ox2*), in the same family but found to be the antagonist of *GA3ox1* in expression[169], was not highly active and categorised into a71 and b2, which was opposite to the expression pattern of *GA3ox1*. The rest of the *GA20ox* and *GA3ox* did not produce a significant number of counts during our experiment.

GA receptors are expressed slightly behind the growth wave

GA receptors sense the GA after they are made, and so the GA receptor genes are likely to be expressed later than the GA biosynthesis genes. They should be good indicators of the current GA level, and their expression patterns are expected to be closely related to the wave of growth of the hypocotyl.

Three genes were identified as the GA receptors. All three had >500 counts, and 2 were differentially expressed over time and/or across the two regions, as shown in Table 4.8, together with their normalised count numbers (Fig. 4.12).

GA receptors		Index(a)	Index(b)
AT3G05120	ATGID1A, GA INSENSITIVE DWARF1A, GID1A:Encodes a gibberellin (GA) receptor ortholog of the rice GA receptor gene (OsGID1). Has GA-binding activity, showing higher affinity to GA4. Interacts with DELLA proteins in vivo in the presence of GA4. The DELLA region alone can interact with GID1A in GA-dependent manner in a Y2H assay.	41	14
AT3G63010	ATGID1B	38	18
AT5G27320	ATGID1C	41	15

Table 4.8. The differentially expressed GA receptor with sufficient counts, categorised using both approaches[180]. Category Index (a) and (b) represents the two approaches, respectively.

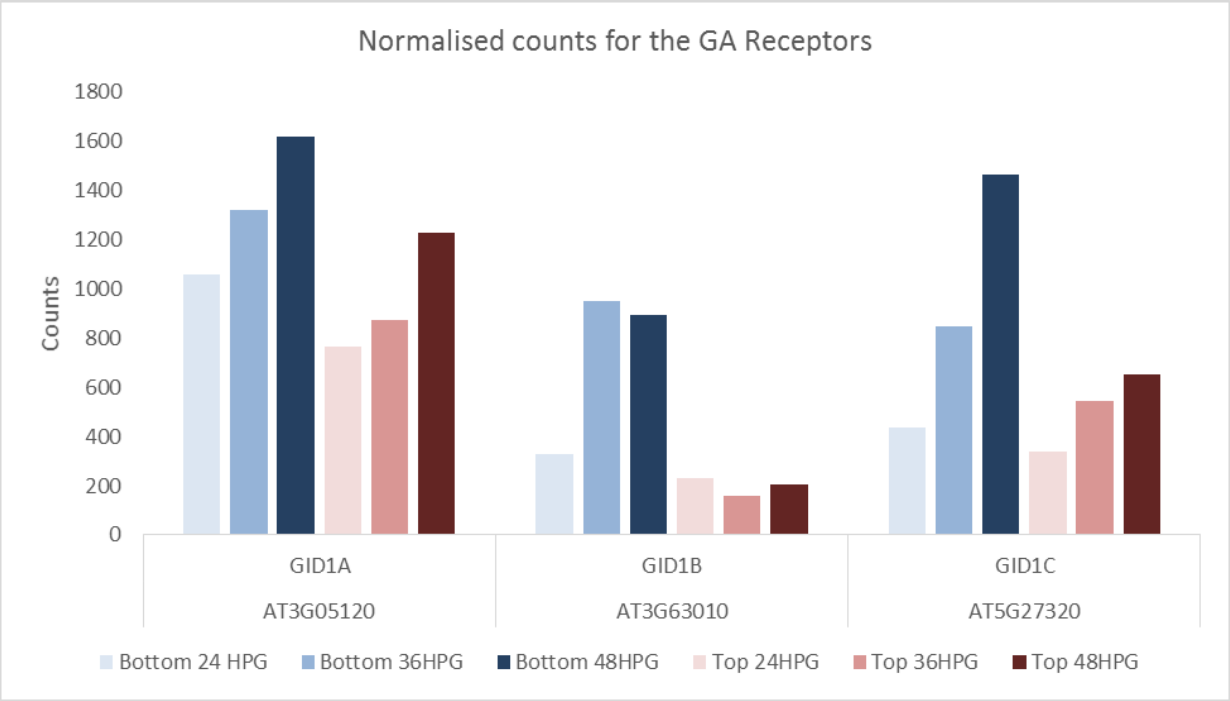

Figure 4.12 Normalised counts for the GA receptors. Bottom time series in blue, top time series in red

All three GA receptors were active during our experiment. The three GA receptors increased in their expression levels according to their normalised count number, but this was not revealed by their category index because the increase in expression level was not significant (log2Fold Change<1), except for *GID1B* from 24 HPG to 36 HPG at the bottom region. *GID1A* was highly active but did not show any difference between the two regions, *GID1B* had higher expression levels at the bottom region, from 36 HPG to 48 HPG, and *GID1C* had a high expression level at the bottom region only at 48 HPG. As a whole, the three GA receptors had increased expression level over time. *GID1A* was not differentially expressed across the two regions, where the other two had expression patterns a step behind the hypothetical wave.

GA catabolism genes are not highly active during the early hypocotyl elongation phase

The GA catabolism genes are responsible for GA destructive metabolic processes, and degrade GA when it is not required, or when it is in excess. They are expected to be active after the rapid hypocotyl elongation as GA is thought to be closely related to the wave of growth.

12 genes were identified as the GA catabolism genes (Jones Group, SLCU). 4 of them had >500 counts, and 3 of them were differentially expressed over time and/or across region, as shown in Table 4.9, together with the normalised counts (Fig. 4.13).

GA Catabolism		Index(a)	Index(b)
AT1G78440	gibberellin 2-oxidase 1, Other names: ARABIDOPSIS THALIANA GIBBERELLIN 2-OXIDASE 1, ATGA2OX1, GA2OX1, GIBBERELLIN 2-OXIDASE 1 Encodes a gibberellin 2-oxidase that acts on C19 gibberellin	N/A	N/A
AT1G30040	gibberellin 2-oxidase 2	39	13
AT2G34555	gibberellin 2-oxidase 3	N/A	N/A
AT1G47990	gibberellin 2-oxidase 4	N/A	N/A
AT3G17203	gibberellin 2-oxidase 5	N/A	N/A
AT1G02400	gibberellin 2-oxidase 6	41	14
AT1G50960	gibberellin 2-oxidase 7	N/A	N/A
AT4G21200	gibberellin 2-oxidase 8	41	27
AT4G26420	GAMT1	N/A	N/A
AT5G56300	GAMT2	N/A	N/A
AT5G24910	ELA1	28	27
AT5G24900	ELA2	N/A	N/A

Table 4.9. The differentially expressed GA catabolism genes with sufficient counts, categorised using both approaches[180]. Category Index (a) and (b) represents the two approaches, respectively.

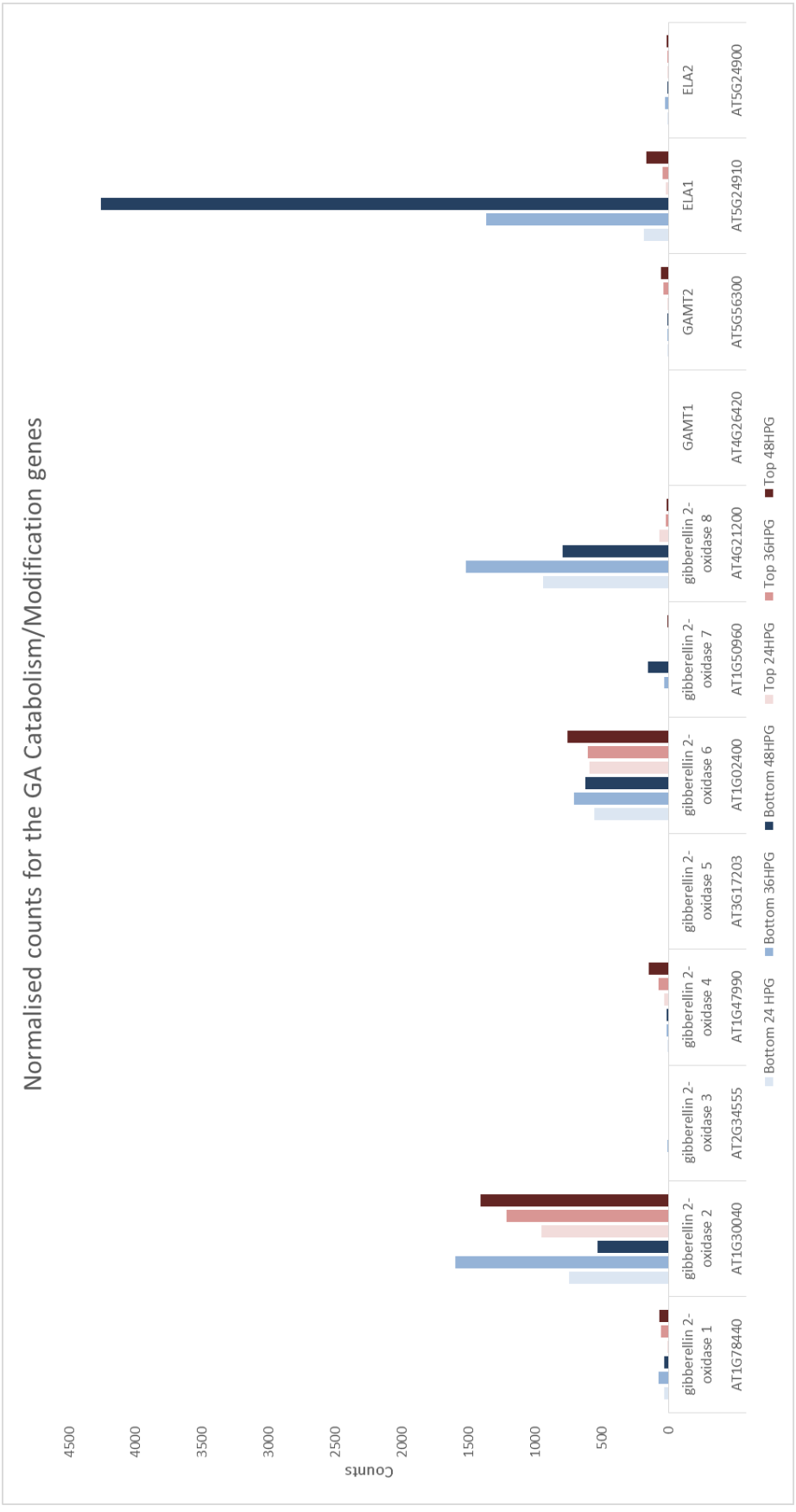

Figure 4.13 The normalised counts for the GA Catabolism genes

Only four out of twelve GA catabolism genes had more than 500 counts, suggesting most of the GA catabolism genes were not active during the three time points of our study. *GA2ox6* was not differentially expressed between the two regions and it was not differentially expressed over time. *GA2ox2* was categorised into a39 and b13, which meant a change in the expression level over time at the bottom region. At the bottom region, it was up-regulated from 24 HPG to 36 HPG and down-regulated from 36 HPG to 48 HPG. *GA2ox8* also had the same expression pattern at the bottom region, but a lot less active at the top region. *ELA1* was categorised into a28 and b27, so it was more expressed over time at the bottom region from 24 HPG to 48 HPG, and also more expressed over time at the top region from 36 HPG to 48 HPG. The expression level for *ELA1* was always higher at the bottom region in comparison to the top.

The four catabolism genes did not appear to have a common pattern, and the other catabolism genes were not active during the experiment (counts<500).

Discussion

The expression level of GA-related genes were studied, and transcriptome level evidence of GA biosynthesis, transport and catabolism genes suggests that GA might have a close role with regional hypocotyl growth rates. The gibberellins are thought to be closely related to higher plant development and promote organ growth[141][143]. In our RNA sequence experiment, it was found that the overall expression pattern of the group of genes related/strongly related to GA stood out from other genes, reflecting a pattern that corresponded well with the hypocotyl wave of growth. More specifically, these genes were more active in the fast-growing region of the hypocotyl and also became more active over time, as the hypocotyl elongation became faster. A greater percentile of genes in the category representing growth initiation also supported the idea that GA genes might be involved in early shoot development signalling and cellular growth initiation[142][144].

A previous study by Ogawa[23] has shown that GA stimulated the seed germination by cross-talking with other hormones and regulating GA-responsive genes, which then alter activities including abscisic acid, and XTHs. The GA (strongly) related genes with certain expression patterns were more active compared to other genes (Fig. 4.8, Fig. 4.9). The number of GA-related genes occurred much more than expected in categories indicating higher expression level in the fast-growing region, as well as categories with gene expression a step ahead of/a step behind the growth wave. These evidences supported the theory that GA was synthesised in young, growing organs and was functional in growth regulation[141][23].

More specific studies were conducted on the GA biosynthesis, receptors and catabolism genes. The genes involved in very upstream biosynthesis processes were almost invariant over time and across the two regions, with the exception of *GA1 (CPS)*, which were more expressed at the top region of the hypocotyl at all three times. This implied that the expression level of *KS* and *KO* remained high during the fast hypocotyl cellular elongation, although their expression may start a lot earlier than other GA biosynthesis processes such as *GA20ox* and *GA3ox*. By contrast, *GA1 (CPS)*, involved in the most upstream GA biosynthesis process here, seemed not to be required during the rapid cellular elongation and started to be active in the top region. Hence the expression level and pattern of *CPS*, *KS* and *KO* could be used as the very early indicator of the GA level and hence organ growth.

KAO1 and *KAO2* had similar expression pattern as *KO*, but with a more exaggerated difference in expression level between the top and bottom region. A previous study found that during seed germination, *KO* had the highest mRNA level among the three, followed by *KAO1* and then *KAO2*[23], and the expression level of all three decreased over time. In our experiment, the *KO* and the two *KAOs* had decreased expression level over time as expected, and the two *KAOs* had higher expressions at the top region of the hypocotyl at later times, where the expression at the bottom region decreased significantly. This implied the *KAOs* rapidly make GA_{12} up to 36 HPG, and then become less active in the hypocotyl, especially at the bottom region where cells are rapidly elongating. Their expression pattern suggested that they were involved in upstream GA biosynthesis processes, supporting their functionality found earlier[139][165].

KAO1 and *KAO2* produce GA_{12}, which is a substrate of *GA20ox*[139]. GA20ox would be active after the production of GA_{12} by the *KAO*, and therefore an opposite expression pattern of *KAO* to *GA20ox* was expected and observed. *GA20ox1* and *GA20ox2* had high expression levels and were differentially regulated in our experiment. They were shown to be important in growth and fertility[181][182][152], and were closely related to each other, together with GA20OX3 and GA20OX4, which were functionally redundant to *GA20ox1* and *GA20ox2*[167]. They catalyse partial conversion of GA_{12} to GA_9, and the loss of those genes blocks germination and causes dwarfism[167]. Compared to *GA20ox2*, *GA20ox1* has higher expression in tissues and its expression last for a longer period[167][165]. These characteristics were well captured in our experiment as both *GA20ox1* and *GA20ox2* were activated at 24 HPG, expressed higher at the bottom region initially, and their expression travelled upwards. While the *GA20ox2* behaved more like a growth initiator, the *GA20ox1* was more expressed at the bottom region for a longer period of time with an expression pattern that was a little step ahead of the hypothetical growth wave. Since GA_{12} has a long-distance transport mechanisms[166], the tissue level growth may be regulated by GA_{12} together with the expression level of the *GA20ox* genes. *GA20ox3*, *GA20ox4* and *GA20ox5* did not have a high expression levels during our experiment. This

was consistent with the previous finding that *GA20ox3* was shown to have almost entirely redundant function with *GA20ox1* and *GA20ox2*, and *GA20ox4* and *GA20ox5* had very minor roles in developmental stages in comparison with *GA20ox1* and *GA20ox2*.[167]

In contrast, the GA3OX catalyses the final step in the synthesis of bioactive gibberellins, from GA_9 to GA_4, and it was often regarded as the most important in all the physiological process directed by GA[168]. It was reported that *GA3ox1* were up-regulated during seed germination and downregulated at later time points[23]. In our experiment, *GA3ox1* behaved like a growth initiator, and remained highly expressed in both regions of the hypocotyl, indicating it played a crucial role during early cell development stage. *GA3ox2* was only active at the top region of the hypocotyl at 24 HPG, opposite to the behaviour of *GA3ox1*. Earlier studies found that *GA3ox2* was the antagonist of *GA3ox1* in expression, expressed in opposite way as *GA3ox1* despite their similar functions[168][169]. *GA3ox3* and *GA3ox4*, the other two members of *GA3OX* were not active in the hypocotyl in our experiment. They were thought to be more involved in anther development[168], and less likely to be an essential gene for the shoot development.

All three GA receptors were highly active in our experiment, implying a high-level GA activity in the hypocotyl from 24 HPG to 48 HPG. It was expected that the GA receptors should have expression patterns similar to the GA20ox or the GA3ox. In contrast, the GA receptors were up-regulated over time and had expression pattern a step behind the growth wave, and hence a step behind the GA biosynthesis genes, by approximately 12-24 hours. There are two possible explanations: 1) the GA biosynthesis gene expression indicated the GA level, which correspond well with the growth wave, while the GA receptors can stay active for longer period of time, even with diminishing GA. 2) the GA biosynthesis gene expression does not imply the GA level in the hypocotyl because GA level can still remain high in the cells when the GA biosynthesis is stopped. The GAs can stay in cells for much longer and the actual GA level is indicated by the GA receptors. From the analysis of nGPS1 in Chapter 2, the latter would be more likely.

The GA catabolism genes reduce the GA activity in tissues. Their expression levels were expected to be high in the region that cellular elongation was slowing down, low in the region that cellular elongation was fast, and they should not be seen in the region without GA. In our experiment, we chose time points corresponded to early hypocotyl development stage. Most of the GA catabolism genes (eight out of twelve) were not active as expected, and only three were active and differentially expressed between the two hypocotyl regions: *GA2ox2*, *GA2ox8* and *ELA1*. The three genes had different expression patterns, suggesting they might mediate GA catabolism via different substrates. *GA2ox8* catabolises GA_{12}[135], which is the precursor of GA_4, and also the only GA that is able to move

through hypocotyl in long distance[163][166]. *GA2ox8* was more expressed at the bottom region of the hypocotyl at all times. *GA2ox8* was highly likely to behave like a negative regulator, balancing the production and overall quantity of GA_4 through GA_{12}. On the other hand *GA2ox2* catabolises GA_9, which is the direct precursor of GA_4. It was expected to be low at the fast-growing region because the GA biosynthesis needs the substrate, and our result suggested an up-down expression pattern over time at the bottom region. It was likely to act also as a negative regulator to balance the amount of GA_4, together with *GA2ox8*. *GA2ox2* also had an increasing expression at the top region of the hypocotyl, which was unexpected, implying the GA_9 could already exist at the top region a long time before the wave of rapid elongation arrived. At the bottom region, both GA20x2 and GA2ox8 had higher expression level at 36 HPG compared to 48 HPG, indicating the level of their substrate (GA_9 and GA_{12}) might decrease from 36 HPG to 48 HPG. Although the GA2ox was identified as the main mechanism to inactivate GAs, recently *ELA1* and *ELA2* were considered to act early in GA biosynthetic pathway and mediate GA catabolism[183] through catabolising the bioactive GA such as GA_4[184]. Similar to *GA2ox8*, It was more expressed at the bottom region at all times, but its expression level increased significantly over time, indicating the level of GA_4 might increase from 24 HPG to 48 HPG. Since the hypocotyl was rapidly growing at 48 HPG, I propose that the high expression of *ELA1* was to control and balance the amount of GA_4, just like how GA_9 and GA_{12} were controlled by GA20ox2 and GA20ox8.

The Auxin-related genes

Introduction

Auxin plays a key role in plant development and cellular growth, and it regulates cell division, elongation, differentiation, lateral root formation and flowering[185]. Indole-3-acetic acid (IAA) is a major auxin and the name IAA has often been used interchangeably with auxin for more than 70 years[186]. In this section, I studied four types of auxin-related genes: 1) genes related to auxin biosynthesis, 2) genes involved in auxin regulator and receptors, 3) genes identified to be up-regulated in response to auxin, and 4) genes encoding the auxin transporters.

Although auxin plays an important role in plant development, the IAA biosynthesis is not well understood, and it is not clear how auxin is synthesized in plants. Recently it was shown that tryptophan is the main precursor for IAA in plants[187], and several pathways of IAA biosynthesis was proposed. The insole-3-pyruvic acid (IPA) pathway and the YUCCA(YUC) pathway, two of the main biosynthesis IAA pathways, were studied in detail by Mashiguchi[186] and he demonstrated that the

YUC was involved in conversion IPA to IAA in *Arabidopsis*. It was proposed that the TRYPTOPHAN AMINOTRANSFERASE OF ARABIDOPSIS1(TAA1) mediates the first step of the conversion from Trp to IPA[188][189]. Mutants of those genes had significant reductions in IAA and showed severe growth defects[189]. *Arabidopsis* has 4 TAA1-like genes, termed TRYPTOPHAN AMINOTRANSFERASE RELATED (TAR), and their expression was also studied in this section.

Arabidopsis has 11 YUC genes[190][191]. The YUC proteins act as a rate-limiting factor in IAA biosynthesis[192]and the *yuc1D* mutants show increased IAA level and high-auxin phenotypes[192].

It was proposed that IPA was converted to IAA via IPA DECARBOXYLASE (IPD) and ALDEHYDE OXIDASE (AO)[193][187], which was independent to the YUC pathway. Four *AO* genes were found in *Arabidopsis* and no *IPD* genes have yet been found in plants[194]. Their expression is studied in this section.

One of the most studied auxin receptors is TRANSPORT INHIBITOR RESISTANT1 (TIR1)[195][196], together with five homologues of TIR1, AFB1-AFB5, which bind auxin but with different affinities[197]. The binding between auxin and the F-box protein TIR1/AFB promotes the interaction with AUXIN/INDOLE ACETIC ACID (Aux/IAA) and then triggers the ubiquitination of Aux/IAA proteins[198]. Altogether 29 *Aux/IAA* genes[199] were found in *Arabidopsis*. Aux/IAA inhibits the transcription factor to AUXIN RESPONSE FACTOR (ARF) and hence with the presence of auxin, the degradation of Aux/IAA leads to the release of the ARF transcription factors, giving transcriptional responses[195][199]. There are 23 genes in *Arabidopsis* encoding the ARF[135]. They regulate auxin-mediated transcriptional activation and repression, however, the biological functions of most of the ARF are not well understood[200]. Some of the ARF mutants showed an auxin-related phenotype and most of them were proposed to be highly redundant to each other[200]. AUXIN-BINDING PROTEIN1(ABP1) is another auxin receptor[201]. Much of its nature and role is still unclear, but ABP1 is one of the best sensors for auxin concentrations[202]. In this section, the 29 *Aux/IAA* genes and 23 *ARF* genes[135] were studied together with the *ABP* and *TIR1/AFB* genes, representing auxin regulator and receptors.

The genes that are differentially expressed in response to auxin exposure are good indicators of auxin level. Paponov[203] studied multiple transcriptome datasets based on auxin response in *Arabidopsis* and a good number of genes were identified to respond to different auxin treatments. Here, I took the list of most regulated genes (up-regulated to at least 5 conditions of auxin treatment, including different concentration and treatment time of IAA, on different tissues) and studied their expression pattern in our transcriptome dataset.

In addition to the auxin biosynthesis, the auxin transport from one cell to another builds up the auxin gradients, which are crucial to plant growth and development[204][205][206]. Auxin moves in plant

cells via two mechanisms: carrier-mediated transport and diffusion[207]. The PIN-FORMED (PIN) proteins were thought to transport auxin and direct the auxin flow within tissues through their polar subcellular localisations[208], and hence control the development mediated by auxin distribution, including cellular growth[209]. Manipulation of PIN polarity led to predicted changes in auxin distribution[208][210]. There are 8 PIN proteins in *Arabidopsis*, many found in different locations (Table 4).

Protein	Location
PIN1	vascular tissues of embryos, leaves, roots, shoot apices epidermis
PIN2	lateral root cap, root epidermis
PIN3	Inner side of shoot endodermis cells
PIN4	Central root meristem
PIN7	Embryonic suspensor
PIN5, PIN8	Endoplasmic reticulum

Table 4.10. The location of PIN proteins found in *Arabidopsis*[211].

PIN-LIKES(PILS) is another family of auxin transporters, which are evolutionarily distinct from the PINs[212]. The PILSs were proposed to reduce the local auxin level in cells by moving auxin from the cytoplasm to the endoplasmic reticulum[213][214]. The expression pattern of seven *PILS*s found in *Arabidopsis* were studied together with that of the *PINs*

Results:

The TAA1 became less expressed at the bottom region over time, and all the TARs were less expressed

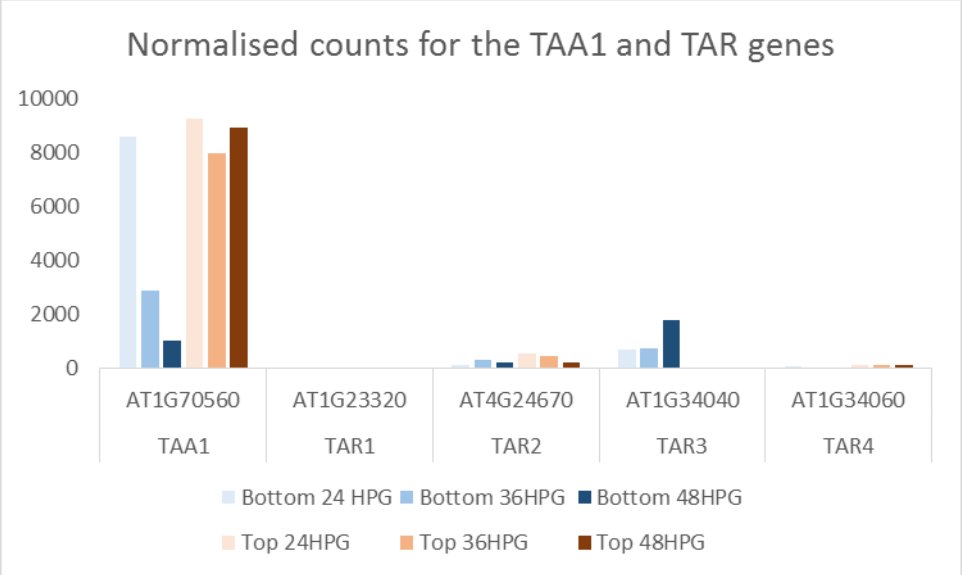

Figure 4.14 The normalised counts for the TAA1 and TAR genes

TAA1 was an upstream enzyme in auxin biosynthesis, converting Trp to IPA[188][189]. Its normalised count number was studied with our transcriptome data. At 24 HPG, the *TAA1* expression level was about the same at the top and the bottom regions. The expression level decreased over time at the bottom region, with the count number dropped from 8623 to 1024, whereas at the top region, the expression level remained high over time. The *TAR* genes encode proteins with similar functions of TAA1, but they have much less count number than *TAA1* in our experiment. In which, the *TAR1* showed no expression in our experiment; the *TAR2* was more expressed at the top region at 24 HPG and then was not differentially expressed between the two regions; the *TAR3* showed opposite behaviour as *TAA1*, where the expression level at the bottom region was higher than the top and went up over time; the *TAR4* had similar expression pattern as *TAA1* but had very low counts.

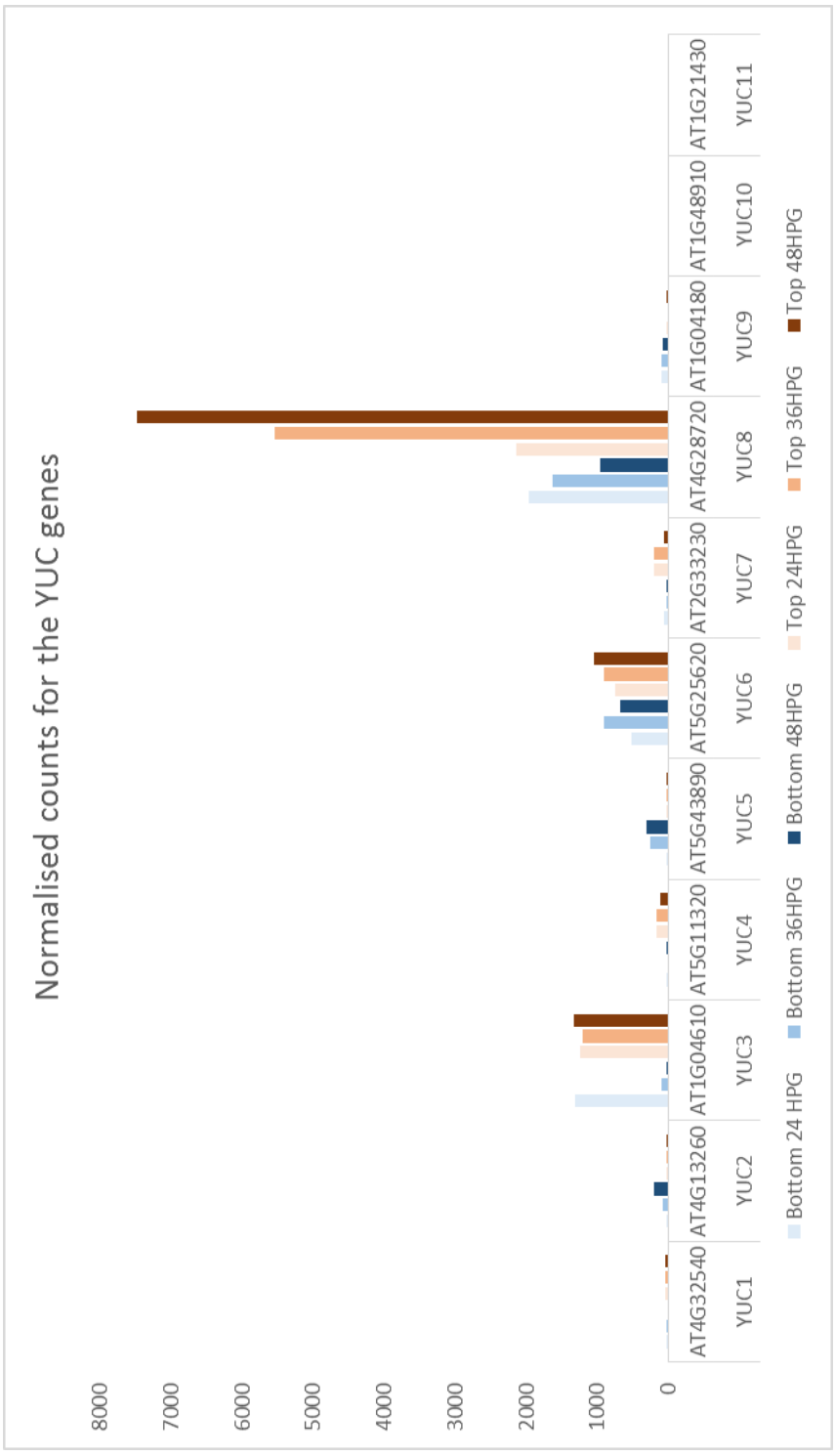

Figure 4.15 The normalised counts for the YUC genes

Most of the YUC genes were more expressed at the top region of the hypocotyl

The YUC was involved in conversion from IPA to IAA and acted as rate limiting factors[186][192]. According to their normalised counts in our experiment, 6 out of 11 *YUC* genes had total count

number >500 (*YUC3, YUC4, YUC5, YUC6, YUC7, YUC8*); 4 of which were significantly more expressed at the top region at one or more time points (*YUC3, YUC4, YUC7, YUC8*), *YUC6* was not differentially expressed between the two regions, and *YUC5* was the only exception, being more expressed at the bottom region at 36 HPG and 48 HPG. *YUC8* had the highest number of counts among all *YUC* genes, and it behaved very similarly to the *TAA1*, but with an increasing expression at the top region over time. This suggested that the TAA1 expression level was independent of the cell sizes whereas the expression of YUC8 might be proportional to the cell sizes.

The *AO* showed different expression pattern with the *TAA1* and *YUC* genes

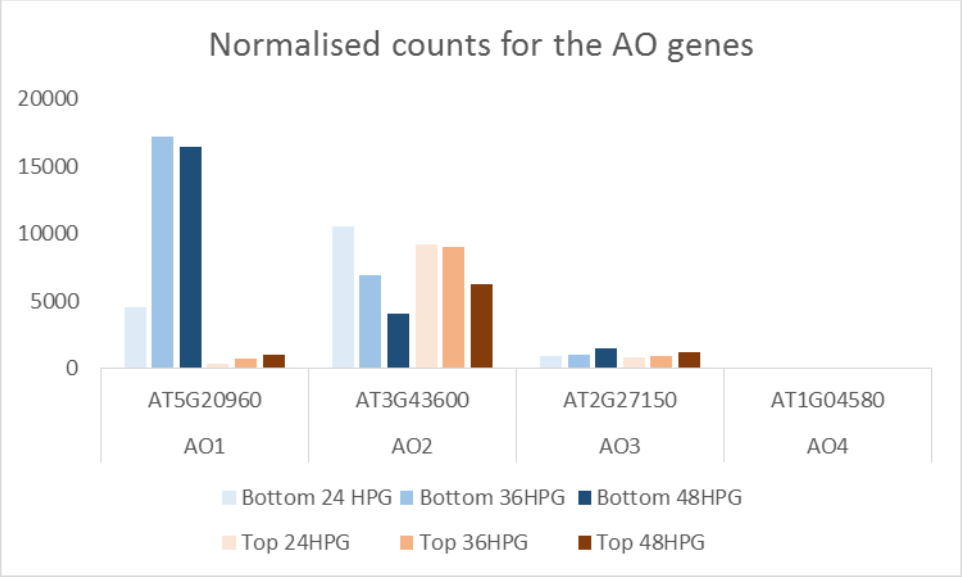

Figure 4.16 The normalised counts for the AO genes

The four *AO* genes were involved in the pathway converting IPA to IAA, and their normalised counts were studied. Unlike the majority of *YUC* and *TAA1*, *AO1* was more expressed at the bottom region at all times, and the counts were higher at 36 HPG and 48 HPG. *AO2* was not differentially expressed across the two regions, but at the bottom region, its expression level decreased over time. *AO3* was low in expression level and was not differentially expressed among all samples, and *AO4* was not expressed in our experiment.

The TIR1/AFB and ABP1 genes were not differentially expressed between the two regions in general

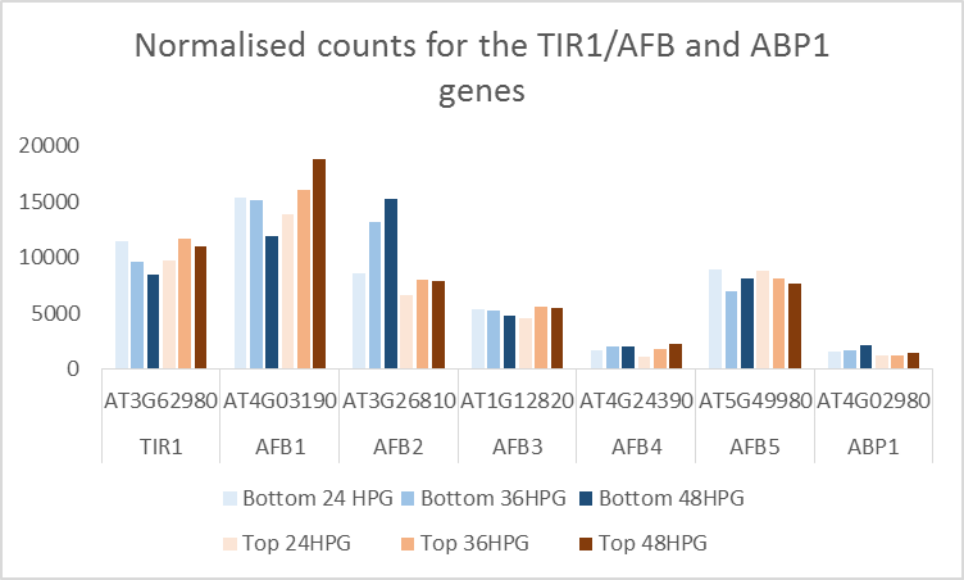

Figure 4.17 The normalised counts for the TIR1/AFB and ABP1 genes

The TIR1/AFB were identified as auxin receptors, and most of the *TIR1/AFB* genes were not differentially expressed among the six different samples in our experiments. *AFB2* was the only exception, with an insignificant increasing expression level over time at the bottom region (log2FC<1). The ABP1 was also an auxin receptor and was also not differentially expressed among samples. The expression of those genes was likely not a reflection of the corresponding protein level, and hence no significant conclusion can be drawn from this result.

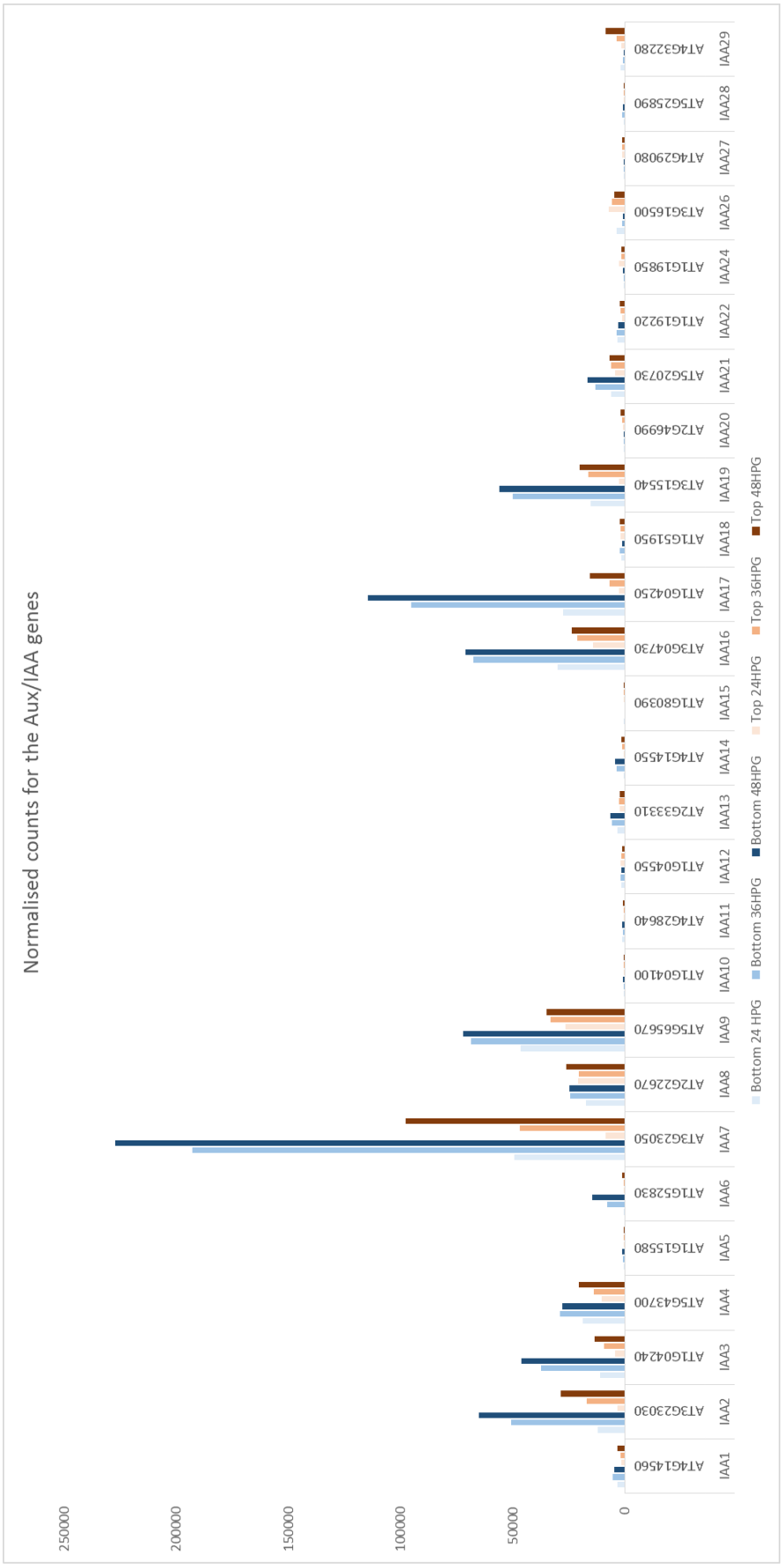

Figure 4.18 The normalised counts for the Aux/IAA genes

Most of the Aux/IAA genes were more expressed at the bottom region, and increased in expression level over time

The Aux/IAA were suppressors of auxin response and the *Aux/IAA* genes were studied with our transcriptome dataset. Note that *Aux/IAA21*, *Aux/IAA23* and *Aux/IAA25* had the same nomenclature code (AT5G2073), only *Aux/IAA21* was plotted. The *Aux/IAA* genes gave a very consistent pattern in general: higher expression at the bottom region than the top region, and the expression level went up over time. Out of 10 *Aux/IAA* genes with relatively high number of counts (*IAA2, IAA3, IAA4, IAA7, IAA8, IAA9, IAA16, IAA17, IAA19, IAA21*), 8 possessed such pattern. The two exceptions were *IAA4*, which had a very similar pattern but with a slight decrease in expression level from 36 HPG to 48 HPG at the bottom region, and *IAA8*, which showed no difference in expression level among samples.

Most of the ARF genes were more expressed at the top region, and their expression at the bottom region decreased over time

The ARFs were auxin receptors, and their transcription factors were released by the activity of Aux/IAA[195][199]. The expression patterns of the *ARF* genes were not as consistent as those of the *Aux/IAA* genes. 8 of the 23 *ARF* genes had little counts. Among the *ARF* with high counts, the expression level was high at the top region, without much difference over time; the expression levels at the bottom region were lower and tended to decrease over time. *ARF7* and *ARF10* were two obvious exceptions, where they behaved more like those *Aux/IAA* genes, being more expressed at the bottom region and the expression level increased over time.

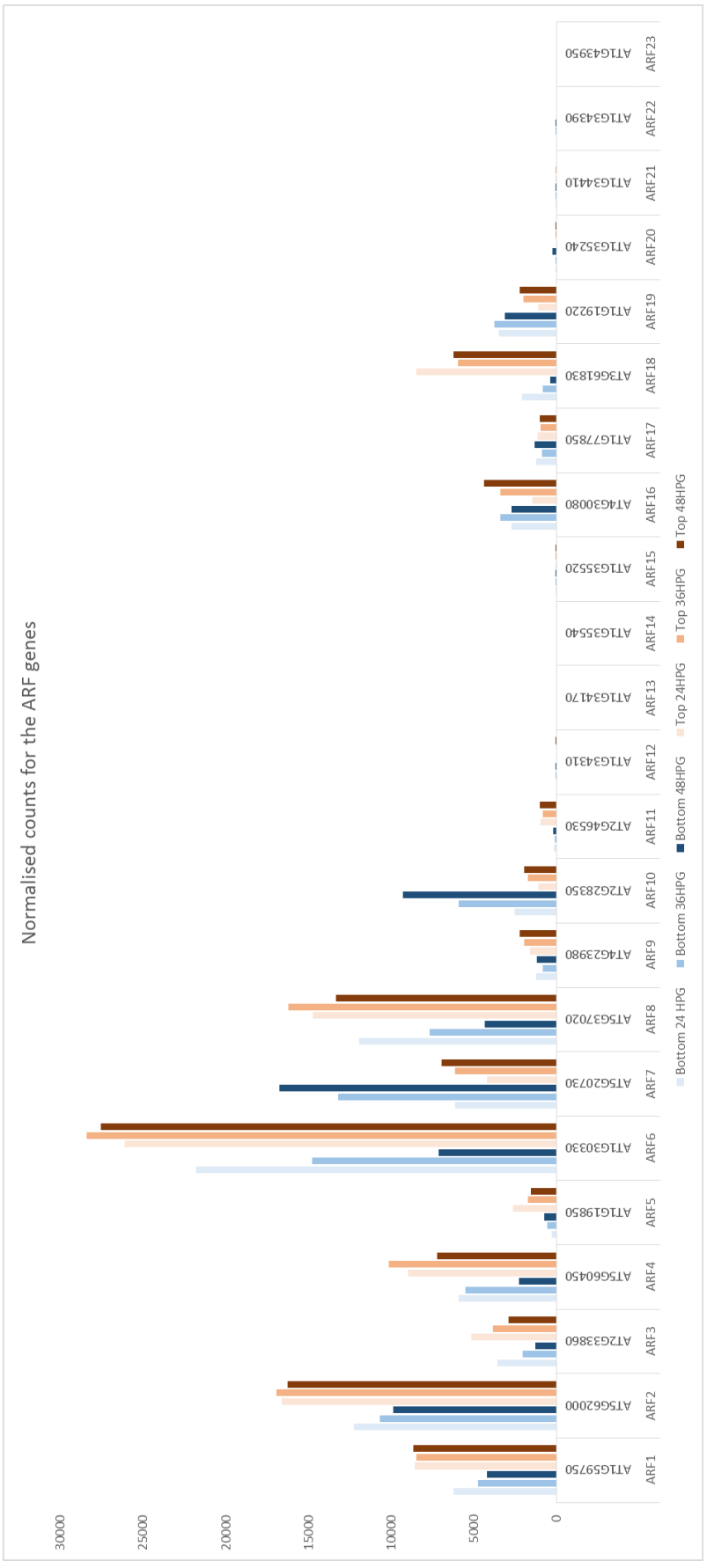

Figure 4.19 The normalised counts for the Aux/IAA genes

The auxin up-regulated genes were more active at the bottom region of the hypocotyl

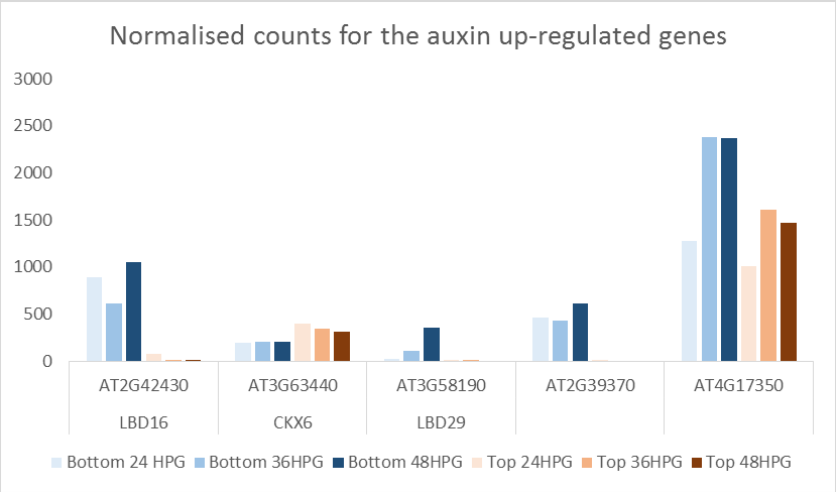

Figure 4.20 The normalised counts for the auxin up-regulated genes

After studying a number of published transcriptome datasets, Paponov[203] identified 9 genes that were up-regulated in at least 5 conditions of auxin treatments. Four of them were the *IAA* genes (*IAA5, IAA13, IAA19,* and *IAA29*), and the normalised counts for the remaining five were plotted. Most of those genes were more active at the bottom region of the hypocotyl at all times, including the four *IAA* genes, but no conclusive pattern was seen for their expression level over time. The two LBDs were known to be involved in lateral root formation, and therefore the difference in expression level between the two regions seen here might not be due to the auxin level in the hypocotyl. *CKX6* was an exception with higher expression level in the top region. It encoded a protein that catalysed the degradation of cytokinins[135]. It was not clear why the *CKX6* behaved differently to other auxin up-regulated genes in our experiment. Because the dataset studied by Paponov[203] contained both short-time and long-time auxin treatment and those genes pulled out here were up-regulated in both conditions, the responding time should no longer be an issue and these genes were expected to provide a good indicator of the auxin level in the hypocotyl.

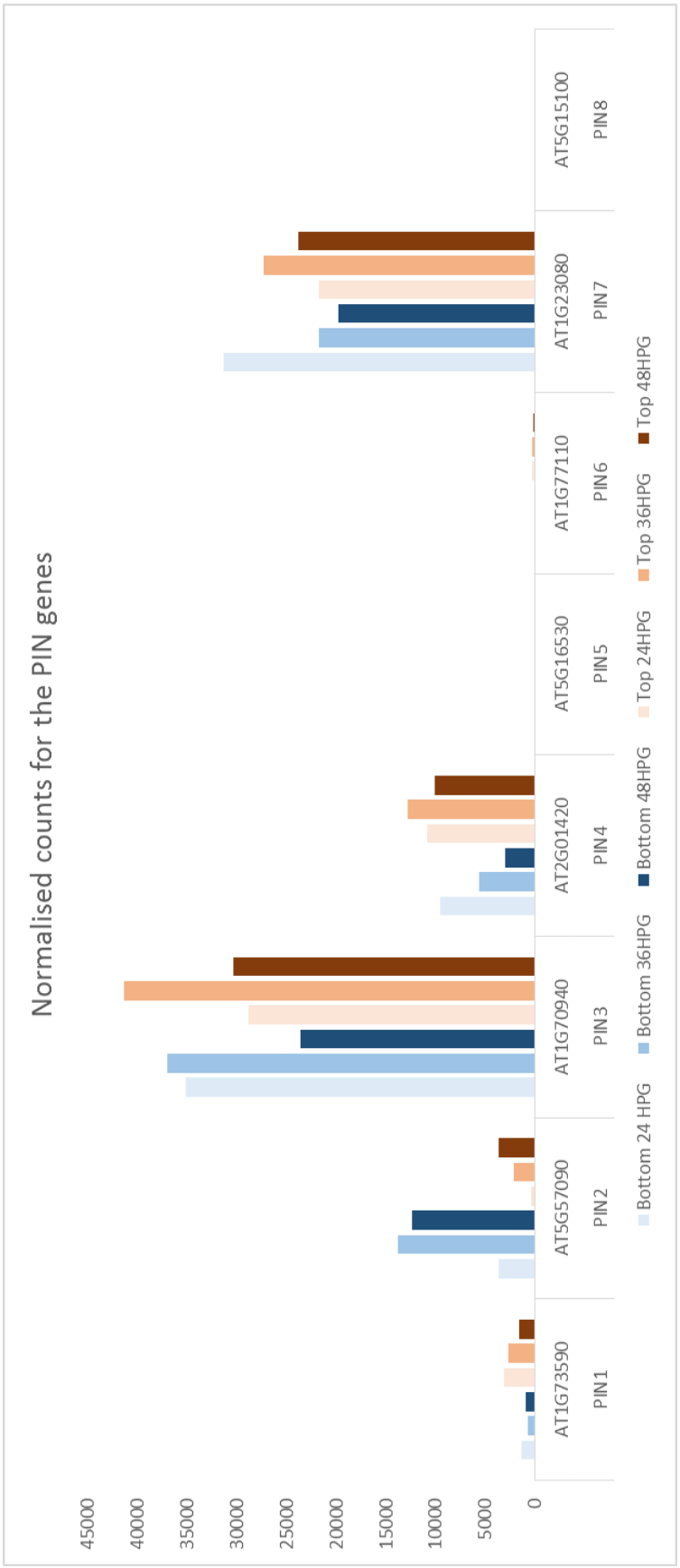

Figure 4.21 The normalised counts for the auxin PIN genes

No consistent expression pattern was seen for the *PIN* genes

The PIN protein was responsible for auxin polar transport between cells[208], and the expression of *PIN*s in our dataset was plotted and studied. Among the 5 PINs with counts>500, PIN2 and PIN4 were identified to be in the root meristem, lateral root cap and root epidermis[211]. This could be the reason why PIN2 and PIN4 were more expressed in the bottom part of the hypocotyl, as the bottom part were closer to the roots and some of the root-hypocotyl junction cells possessed certain root cell properties. The other three *PIN* genes had more similar expression level among samples, and a consistent expression pattern was not seen.

The PILS genes were more expressed at the bottom region, and increased in expression level over time

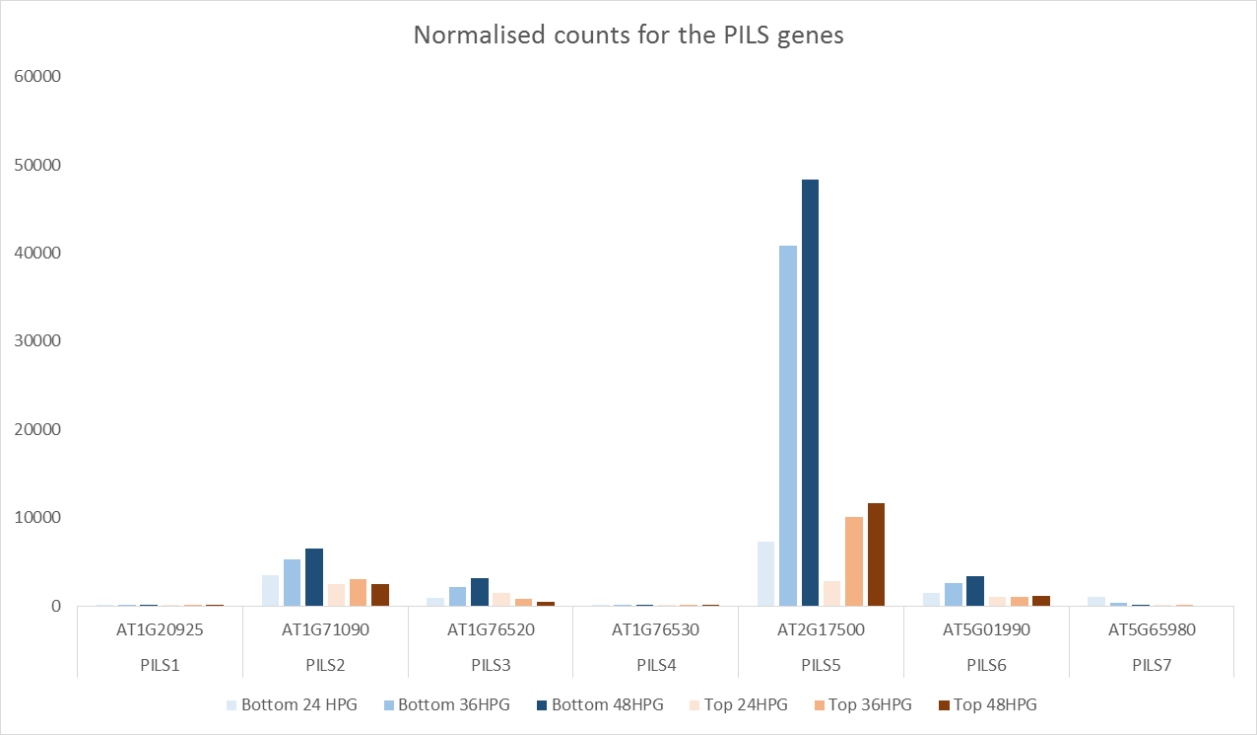

Figure 4.22 The normalised counts for the PILS genes

Unlike the *PIN* genes, the *PILS* genes possessed very consistent pattern in our experiment, and they behaved similarly to the *Aux/IAA* genes: more expressed at the bottom region and the expression level increased over time. Out of the 7 *PILS*, all 4 with counts>500 had such expression pattern. Unlike the PINs in the hypocotyl, which were involved in the shoot-root auxin transport[205], the PILS suppressed

local auxin signal by removing auxin from cytoplasm[213]. Therefore the expression of *PILS* served as a better indication of auxin level compared to that of *PIN*s.

Discussion

The role auxin plays in hypocotyl growth is still unclear, and different possibilities are discussed here based on our evidence at transcriptome level. Auxin biosynthesis and auxin gradient are important to plants growth and development, yet it is still unclear how they impact the cellular growth rate. It was proposed that the dependence of hypocotyl elongation on auxin transport was different between seedlings grown in the light and those grown in the dark.[215] Here I discuss the possibility of how auxin level and auxin transport are potentially correlated to the growth rate of the dark-grown hypocotyl, based on the transcriptome study.

Overall, expression of the auxin biosynthesis genes in the fast-growing region decreased over time but remained active in the region where the fast growth had not yet arrived. At the first sight, the auxin up-regulated genes seemed to suggest a higher level of auxin at the bottom region. However, out of the 5 auxin up-regulated genes excluding the *IAA*, two of which were mainly involved in lateral root formation, so their high expression at the bottom region might not reflect the auxin level. Out of the remaining three, only one was more expressed at the bottom region. The *TIR/AFB* expressed everywhere in the hypocotyl, so there was not any region blind to auxin, as TIR binds Aux/IAA and triggers auxin sensing pathway.

Inhibition of YUC leads to less growth[216], so auxin is generally thought to be required in growth. We would like to know the auxin level, auxin gradient and transport along the dark-grown hypocotyl, which can then be correlated to regional hypocotyl growth. There are three potential ways on how the level of auxin can regulate growth.

I: Auxin level depends on the auxin transporters. The auxin biosynthesis genes were more expressed in the top region. So auxin may be synthesised in the top region (including meristem and cotyledon) and then get transported downwards by the PINs in the vasculature, and outwards to the epidermis by PIN3 and PIN7 (unpublished data, Braybrook lab). The downward auxin transport was also observed in *Lupinus* hypocotyl[217]. So the regional auxin level depends on activities of different PINs, and their might be auxin differences along the hypocotyl as well as between different tissues.

II: Local auxin biosynthesis is preceding growth. Although many of the auxin biosynthesis genes were more expressed at the top region of the hypocotyl, *TAA1* and *YUC8*, the two highly active auxin biosynthesis genes, were not differentially expressed between the two regions at 24 HPG and their

expression level decreased at the bottom region over time. This implied that the auxin biosynthesis at the bottom region might start before 24 HPG and by the time of our experiment, the synthesis of auxin at the bottom region had reached an end. Hence an auxin gradient was likely to exist during the time of our experiment across the hypocotyl and there was likely a correlation between the cellular growth rate and the auxin gradient. However from the transcriptome data, it was impossible to tell how fast the process of auxin biosynthesis or auxin degradation was happening, and hence the direction of the auxin gradient was still not clear. The repressor of auxin response, *Aux/IAA*, increased in expression over time at the bottom region, which would lower the activity of transcription factor of ARF, and hence reduce the expression level of ARF. My results of the expression level of ARF were found to be consistent with this. Further, the PILS, which reduced the auxin signal by removing it from the cytoplasm, showed an increased level in its gene expression over time at the bottom region. Together, these results of the auxin biosynthesis, receptors and transports, the evidence suggested that there might be a negative correlation between the elongation of dark-grown hypocotyl and the current auxin level.

III: Auxin level might be evenly distributed along the hypocotyl. Our auxin sensors did not show any difference in signal intensity along the dark-grown hypocotyl (unpublished data, Braybrook lab), which implied that there might not be an auxin gradient. In this case, the cell growth rates may be regulated by the combination of *Aux/IAA* and *ARF* differential expressions. Aux/IAA and ARF form a negative feedback loop on their own, so the sensitivity of auxin sensing may be changed by the activities of them. A recent publication showed that double mutants of deficient in ARFs had shortened length of the dark-grown hypocotyl[218], suggesting a positive relationship between the existence of ARF and cell growth.

Following the analysis of auxin-related processes in the growing hypocotyl at the transcriptome level, it was still not clear whether the absolute auxin level was higher at the fast-growing region or the slow-growing region. The transcriptome data suggests that the local auxin level may decrease along with the growth, or before the growth. The auxin biosynthesis was likely to be finished by 24 HPG at the bottom region, and we do not know how much auxin was in the hypocotyl at that time. Therefore it was unable to determine whether auxin level was higher or lower in the fast-growing region, despite it being highly likely to be reduced over time. Based on the transcriptome analyses I was unable to find a certain correlation between the auxin and local hypocotyl growth rate. The expression of *AO*, *PIN,* and the auxin up-regulated genes underlined a possibility of evenly distributed auxin across the dark-grown hypocotyl, and it was also possible that there does not exist a correlation between local auxin level and hypocotyl growth rate. Giving that the auxin transport impacts the hypocotyl

elongation differently between light- and dark-grown seedlings[215], the relationship between auxin and cell elongation remained mysterious.

The *PECTIN METHYLESTERASE* Genes

Introduction:

Pectin is a type of heteropolysaccharide, which is mostly found in the primary cell wall of land plants[219]. Pectin gels are capable of changing the behaviour of cells and tissues by altering its hydration and stiffness[220]. Increasing the stiffness of cell wall's pectin gel may result in decreased growth and vice versa softening of a gel may lead to increase in growth[220]. In dicot plants, PME is involved in important developmental processes including cellular adhesion and stem elongation[84]. It was found that the elasticity measured for cell walls was strongly influenced by the pectin matrix, which has a huge impact on organ formation[5]. Homogalacturonan (HG) is a major plant cell wall polysaccharide in *Arabidopsis*[221]. PECTIN METHYLESTERASE(PME) catalyses the demethoxylation of homogalacturonan pectin by removing its methyl group[92]. PME can change the number and distribution of methyl-esters on the pectin backbone, and hence regulate the enzymatic conversion reactions and gel formation of pectin[92]. Removing the methyl group leads to a free carboxyl group and the release of a proton and methanol[222]. The de-esterification leads to a readily cross-links of HG by free calcium ions, Ca^{2+}. The cross-links alter the mechanical properties of the wall material and leading to a stiffer cell wall[71][221][5][9]. In *Arabidopsis*, knocking out the ubiquitously expressed *PME3* leads to an increase in length in dark-grown hypocotyls[223]. We have seen similar results in our overexpression lines, where over-expression of PME/PMEI led to shorter/longer hypocotyls length in the dark (Chapter 1). The PME is also important as its activity changes the outcome of the plant-pathogen interactions, by making pectin more susceptible to the action of the enzymes produced by those pathogens[220]. These evidence suggest that the PME plays an important role in controlling the growth, development, and ensuring a healthy establishment of the plants.

PMEs are classified into two groups by their primary structures with the distinguishing feature being the presence or absence of an N-terminal PRO region[224][225][226]. The type I PMEs three long PRO domains[71][93]. The type II PMEs have no N-terminal PRO region, or only a short one[71][93]. The PRO region is found to be involved in maintaining unprocessed PME in the Golgi[227]. Being highly similar in structure to some of the PMEI domains, the PRO region was also inferred to play a role in auto-inhibition of mature PME proteins. Some evidence suggests that the PRO region is cleaved off

during protein maturation before the PMEs are secreted into the cell wall[228][223]. Out of the 67 putative PMEs found in *Arabidopsis*, 45 fall into type I, and 22 into type II[229].

PME activity can be counteracted by the activity of another family of cell wall proteins, PECTIN METHYLESTERASE INHIBITORS (PMEI). There are almost as many *PMEI* genes as *PME* genes in *Arabidopsis.* (69 for *PMEI* and 67 for *PME*) It is still unclear how PMEI acts, but several studies shown that individual PMEIs can interact in a 1:1 ratio with a number of PMEs in a pH-dependent manner, even across species[230][231].

A network analysis of the *Arabidopsis* PME and PMEI families shown that the genes were mainly involved in the molecular function of transferase activity, ion binding and hydrolase activity[79]. Many of the interactions were directly related to cell wall formation[232][233].

Results

PME and PMEI genes tend to be more expressed in the growing region

The process of cell wall modification takes place during the cell elongation, and hence the *PME* and *PMEI* genes were expected to be more active in the growing region. Approach 2 was used to analyse the gene expression between the top and bottom regions of the hypocotyl for the two families of genes and the number of genes in each category were plotted.

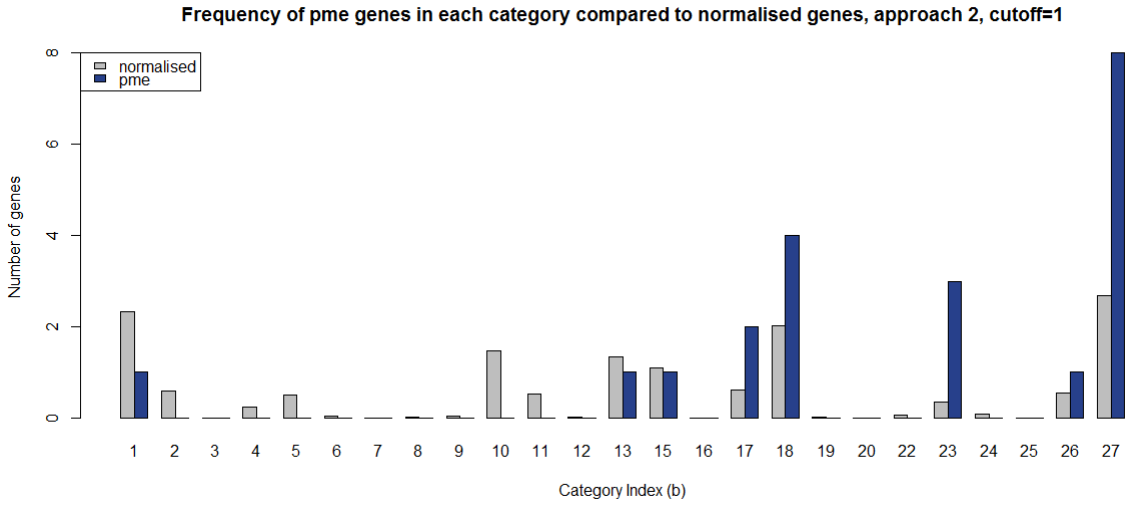

Figure 4.23 The number of all genes in PME family, categorised using approach 2

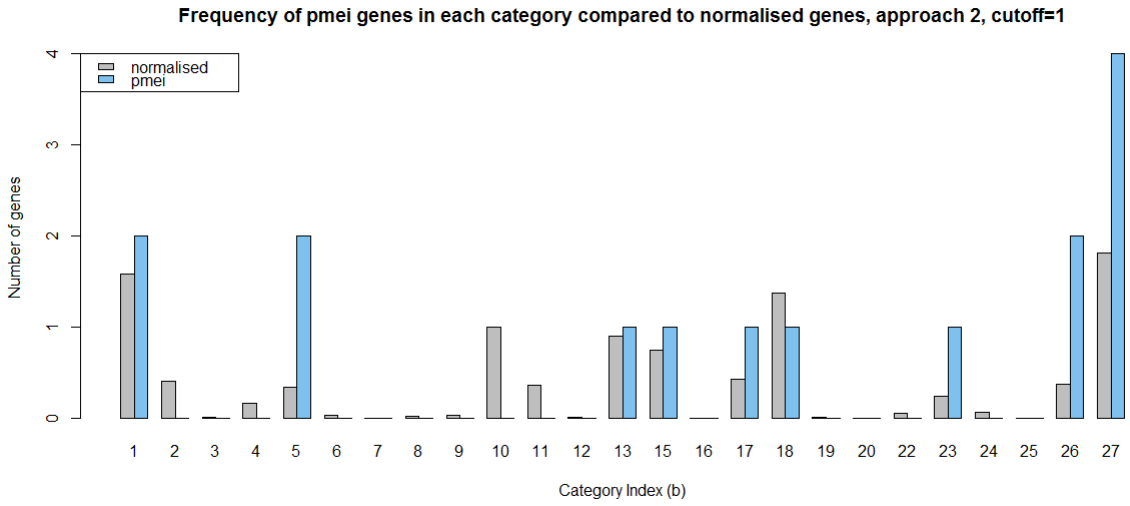

Figure 4.24 The number of all genes in PMEI family, categorised using approach 2

In both Fig. 4.23 and Fig. 4.24, the blue bars were at least two times taller than the grey bars in category 27, suggesting both PME and PMEI genes were more likely to be more expressed at the bottom region than by chance. In particular, the PME genes also tended to favour category b17, b18 and b23 but not b1 or b10, where the number of genes was lower than that by chance. Refer to table 3, category b17, b18 and b23 corresponded to 'more expression at the bottom region' and category b1 and b10 corresponded to 'more expression at the top region'. Similar to the PME genes, the PMEI genes also favoured category b17, b23, and b26 in addition to b27, which corresponded to 'more expression at the bottom region'. But the PMEI genes did not show a drawback in category b1, and the two PMEI genes were categorised into b5, corresponding to genes that were more expressed at the top region at 24 HPG.

The PME and PMEI genes had similar distributions in expression level in general when categorised using approach 2. The difference occurred in category b1, b5, b18 and b26, but was not statistically significant due to the small number of genes. Hence I conclude that at the transcriptome level, both *PME* and *PMEI* genes were expressed in similar patterns in the hypocotyl, despite the fact that PME and PMEI might have opposite effects on the cell wall. Note that the exact functions of PME and PMEI proteins are to be determined.

Genes encoding type I PME had higher expression in the dark-grown hypocotyl during our experiment compared to those encoding type II PME

Genes encoding the two types of PMEs were studied differently. Type I PMEs had a region which might play a role in auto-inhibition due to its structure similar to some of the PMEI domains[225]. The normalised counts for genes encoding the two types of PMEs were generated using the RLE method in DEseq2 and genes with total raw counts>500 were plotted.

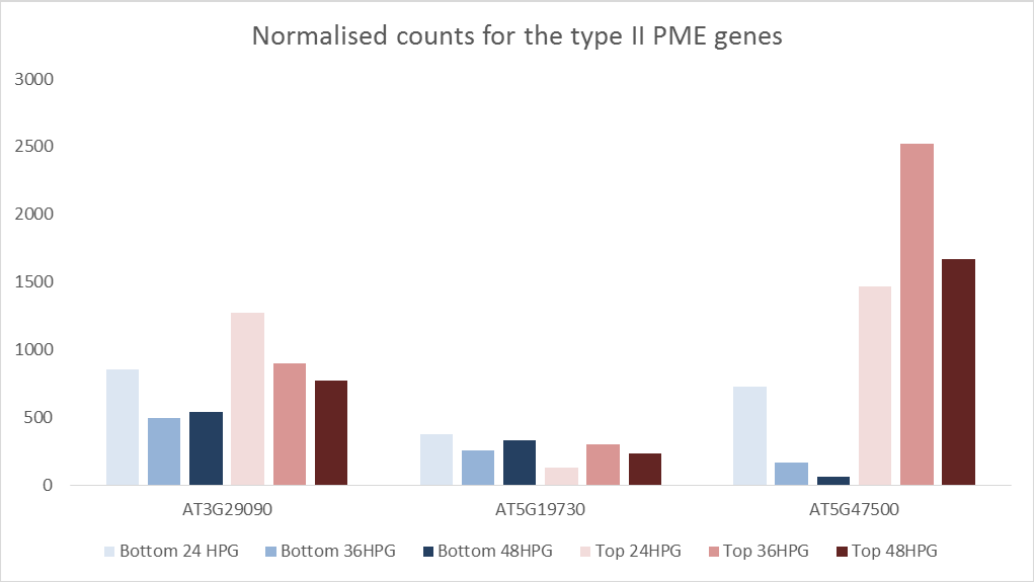

Figure 4.25 The normalised counts for the genes encoding type II PMEs

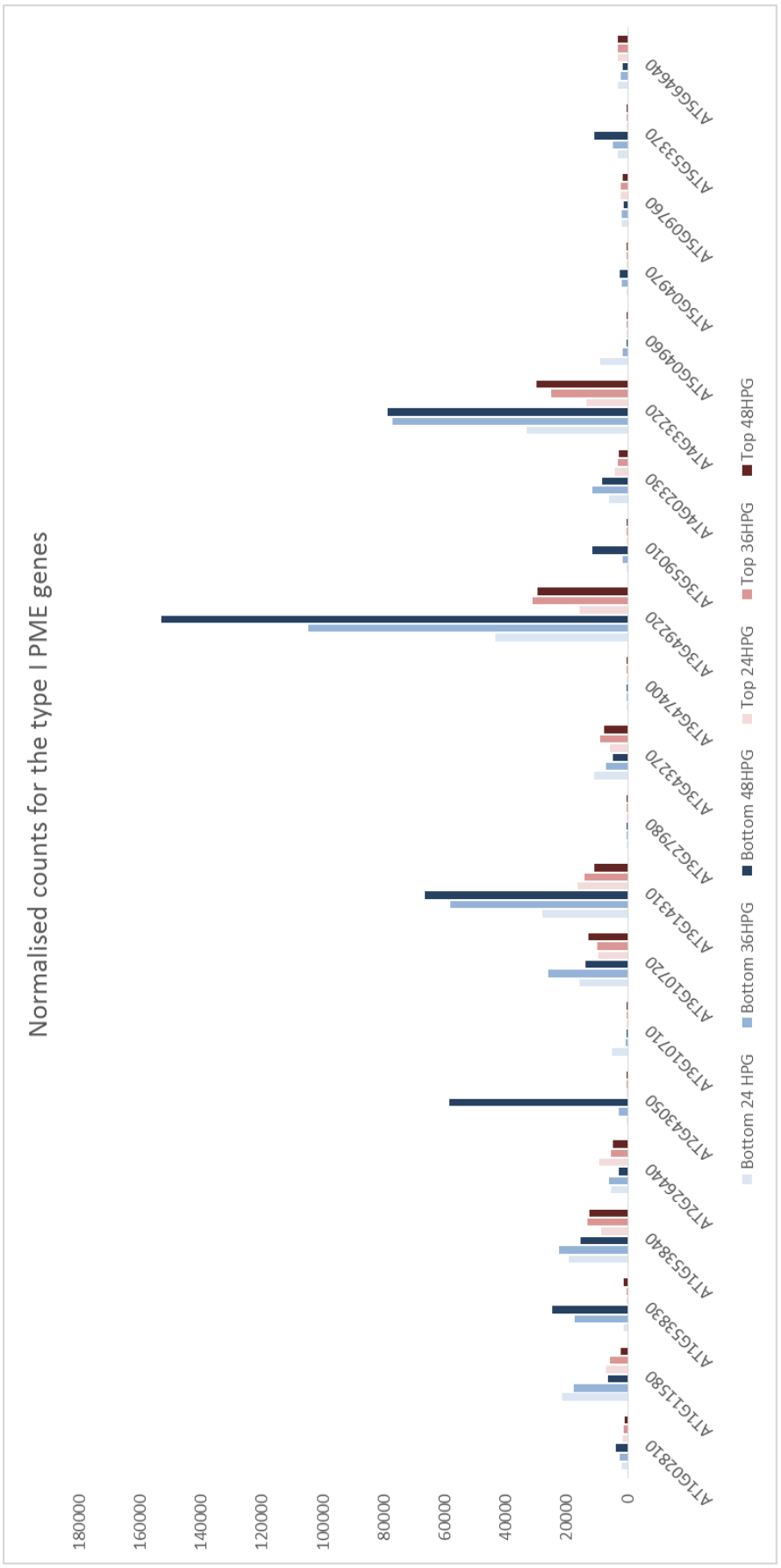

Figure 4.26 The normalised counts for the genes encoding type I PMEs

As seen in Fig. 4.25 and Fig. 4.26 above, 21 out of 45 genes encoding type I PMEs had total raw counts >500 and only 3 out of 22 genes encoding type II PMEs had counts >500. So the genes encoding type I PMEs were more active in the hypocotyl at the three time points. In particular, AT3G49220 and AT4G33220 had normalised counts >100000 in the bottom region at 36 and 48 HPG, whereas none of the genes encoding type II PMEs had normalised counts >3000 at any time or region of the hypocotyl.

The expression pattern of genes encoding the two types of PMEs were also different. Out of the three genes encoding type II PMEs, two were more expressed at the top region at all three time points, and the other showed no difference in expression level between the two regions. In contrast, with only a few exceptions, most of the genes encoding type I PMEs were more expressed at the bottom region, especially at late times (36 HPG and 48 HPG). In fact, 10 out of the 21 genes encoding type I PMEs plotted above were more expressed at the bottom region at 36 HPG and/or 48 HPG, with a log2FC>1

Discussion

My results have shown that, in general, genes encoding PMEs and PMEIs tended to be more expressed at the bottom region at all three time points, providing a verification of the cell wall modification during growth at the transcriptome level. The similar categorical result of the PME family and the PMEI family implied they work together spatially and temporally. From earlier studies (Chapter 1, chapter intrinsic model) we know that the *PME* genes stiffens the cell wall through pectin de-esterification and inhibits the growth, where the PMEI inhibits the PME activity and promotes the growth. However, the correlation between growth and the expression level of *PMEI* genes were not seen at the transcriptome level. Comparing the two families, a stronger correlation between the PME genes and the non-growing region, or a stronger correlation between the *PMEI* genes and the fast-growing region, was not observed. I postulate six possible explanations: 1) The PME activity may not depend on the expression level between *PME* genes and *PMEI* genes, but rather, depends on the expression level of genes encoding type II PMEs. Since the type I PMEs have their own PMEI domain, the expression of type I *PME* genes may be a false indicator of the actual PME level. 2) The PME and PMEI protein level was not reflected by the number of genes expressed at the transcriptome level. The PMEI efficiently inhibits the PME at the bottom region and results in a less active PME and hence a softer wall during the growth. 3) The wall is indeed stiffer at the growing region. Compared with the non-growing region, the process of cell wall material synthesis is active and rapid at the growing region, which can result in a stiffer wall compared to the non-growing region of the hypocotyl. Yet the growth rate depends on the presence of chemical signals (e.g. GA intensity) and the magnitude of turgor pressure, and so a cell with high turgor rapidly grows when the signal arrives, despite having a

relatively stiffer cell wall compared to cells in other regions of the hypocotyl. 4) The high expression level of *PME* and *PMEI* only indicate a fast process of cell wall modification, rather than the mechanical properties of the cell wall. Cell wall properties are rapidly changed during the fast elongation phase, and the wall stiffness is changed by not only the pectin but also by cell wall materials such as the cellulose microfibril. Activities of PME and PMEI may hence only indicate the process of wall modification, but there might not be a certain correlation between the wall stiffness and the level of PME/PMEIs. 5) The function of each *PME* gene is not fully understood. Depends how the PMEs act on HG (can be randomly or linearly blockwise) de-methylation can lead to calcium cross linking or breaking down the pectin[220], which means the PMEs can strengthen the wall as well as loosen the wall. Interestingly, the PME5 (third gene, Fig. 4.25), which was used as the inducible over-expressor in the previous chapters, was the only PME gene being more expressed in the top region. Its expression pattern was consistent with our expectations, but whether it was just a coincidence or PME5 actually acted differently with other PMEs in hypocotyl was not clear. 6) While RNA levels may change, the protein activity may be regulated by other factors[220].

The genes encoding PMEIs and type I PMEs had similar expression patterns, and were more expressed at the bottom region of the hypocotyl, especially at the later time points when cells at the bottom region were elongating more rapidly. One might hence propose that both PME and PMEI genes appeared to correlate well with the cell growth. However, a different picture arose when genes encoding the type I and type II PMEs were considered separately. Unlike the genes encoding type I PMEs, the genes encoding type II PMEs behaved oppositely to those encoding the PMEIs. They were less active in the hypocotyl at the three time points, and they tended to be more expressed at the top region of the hypocotyl. It was known that the elongating cells have softer cell walls and the non-growing cells have stiffer cell walls (Chapter 2), and the expression level of genes encoding type II PMEs were more consistent with this result, as the PMEs were thought to make the cell wall stiffer.

The transcriptome analyses of the genes encoding PMEs and PMEIs suggested that the two types of the PMEs should be considered differently, where the genes encoding type II PMEs were more likely to regulate the stiffening of the cell wall, as they were more expressed in the slow-growing parts of the hypocotyl with stiff cell walls. In contrast, genes encoding PMEIs were more active in the growing region as expected. Genes encoding the type I PMEs were highly active and expressed similarly with the PMEI genes, possibly due to the existence of the extra PMEI domain. From the transcriptome analyses, it was unclear how type I PME level was distributed in the hypocotyl, but it is more likely to be involved in cell wall modification in the growing cells together with the PMEIs, and less likely to behave like a type II PME, due to the opposite expression pattern.

The *CELLULOSE SYNTHASE* genes

Introduction:

Cellulose microfibril has a crystallised and strong structure, and it is a major component of the cell wall, embedded in a matrix of complex polysaccharides[36]. Cellulose is synthesised by plasma membrane complexes[234], and altogether 10 CELLULOSE SYNTHASE (CESA) proteins were identified[40]. The 10 *CESA* express in different tissues and in different types of cells, and there has been much evidence that normally three different *CESA* genes work cooperatively to make functional cellulose synthesising complexes[235][236][237]. The expression level of *CESA1, CESA3, and CESA6* are required for deposition of cellulose in the primary wall, which form during cell expansion[236], and a mutant in any of the three results in reduced cellulose level[236][238]. On the other hand, CESA4, CESA7, and CESA8 are required for deposition of cellulose in the secondary wall, which form after cell expansion finishes[239][235]. By studying the hypocotyl length and isoxaben-treatment response, CESA2, and CESA5 were showed to be partially redundant to CESA6[238]. CESA9 is also functionally related to CESA6 but the gene only express during embryogenesis[238]. In *Arabidopsis, CESA1, CESA3,* and *CESA6* are highly expressed in all tissues[240], *CESA4, CESA7*, and *CESA8* are only strongly expressed in stems[240], and CESA10 is expressed only at the base of rosette leaves[240].

Results

The CESAs involved in cellulose biosynthesis in the primary cell wall possess consistent expression pattern

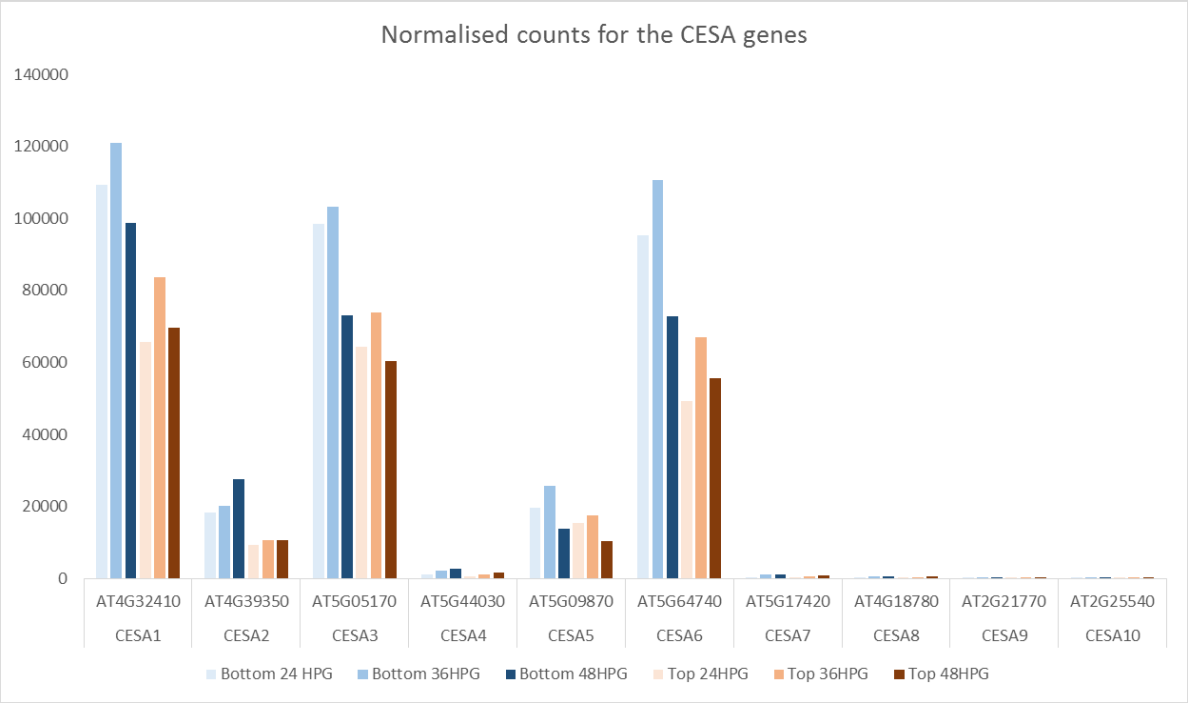

Figure 4.27 The normalised counts for the CESA genes

The three *CESA* genes with the highest counts were *CESA1*, *CESA3,* and *CESA6*, and they were previously identified to be involved in cellulose biosynthesis in the primary cell wall. All three of them had very similar expression patterns: Overall, there was no difference between six samples more than 1 fold change, but the three genes were all more expressed at the bottom region, at all time points. Further, at both the top and the bottom regions, all three genes were up-regulated from 24 HPG to 36 HPG, and then downregulated from 36 HPG to 48 HPG. This periodic, or possibly circadian pattern was not commonly seen in the previous genes analysed since the seedlings were grown in the dark.

CESA2 and CESA5 were considered to be partially redundant to CESA6, and the *CESA2* and *CESA5* had much lower counts in our experiment. *CESA5* also had the same expression pattern with CESA6, and *CESA2* had very similar expression pattern but was slightly up-regulated from 36 HPG to 48 HPG, rather than being downregulated.

Other genes, including the three previously identified to be involved in cellulose biosynthesis in the secondary cell wall (*CESA4*, *CESA7,* and *CESA8*), were not strongly expressed during our experiment. *CESA4*, *CESA7,* and *CESA8* tended to be slightly up-regulated over time.

Discussion

Our results supported the argument that three of the CESA work cooperatively on cellulose biosynthesis, proposed earlier[235][236], since *CESA1*, *CESA3* and *CESA6* all had the same expression pattern. It also indicated a positive correlation between the *CESA* expression in the primary cell wall and hypocotyl elongation, as the *CESA*s are always more active in the fast-growing region. When comparing the expression pattern with the actual cellular growth wave defined in Chapter 1, the expression of the three *CESA*s also seemed to have a pattern of a wave (up-down over time), but earlier than the growth wave in time. By the time of 48 HPG, the counts ratio between the two regions reached a minimum, for the three genes involved in primary wall cellulose biosynthesis. This was expected, as the cellulose should be already synthesised before the rapid cell expansion starts. Previous findings suggested that slowly growing hypocotyl cells had thicker walls and fast growing hypocotyl cells had thinner walls and it was concluded that cell wall synthesis was not coupled to the cell elongation rate[117]. The transcriptome data provides an alternative explanation; biosynthesis of cellulose and other cell wall components are essential for plant growth and correlated with growth rate, but with a shifted time: cells need to acquire enough wall materials before their fast elongation, and it is the elongation which makes the wall thinner, but not opposite.

During our experiment, the hypocotyl was growing rapidly, and therefore the majority of the cell wall was the primary cell wall. From 24 HPG to 48 HPG, some of the basal hypocotyl cells expansion slowed down over time and possibly some secondary cell wall was formed. Therefore the expression of the three genes involved in secondary wall cellulose biosynthesis had low counts but their expression level increased over time.

It was not possible to tell the level of cellulose microfibril in the hypocotyl based only on the expression pattern of the *CESA* genes, and the alignment and orientation of cellulose microfibril were also important to the cellular growth rate. In addition, microtubules and CESA tracks showed independent alignment at the inner and outer wall of *Arabidopsis* hypocotyl epidermal cells[2], so a direct linear correlation between the *CESA* level and cellular growth rate was unlikely to exist. In general, the expression level of *CESA* genes might act as a precursor to the growth.

The *XYLOGLUCAN ENDOTRANSGLUCOSYLASE/HYDROLASE(XTH)* Genes

Introduction

Detailed functions of the XTHs were introduced in Chapter 1. In *Arabidopsis*, there are altogether 33 *XTH* genes[241][60]. They are expressed at distinct locations, at different developmental stages, and have different response stimulus, and the function loss of a single *XTH* gene can cause alterations in plant development[63]. The 33 genes were divided into three groups, depending on their evolutionary origin as well as their structure and organisations[241], with *XTH1-11* in Group 1, *XTH12-26* in Group 2 and *XTH27-33* in Group 3.

In addition to the 33 *XTH* genes, the five genes encoding the XYLOGLUCAN XYLOSYLTRANSFERASE (XXT) are also studied in this section. *XXT1* and *XXT2* encode xylosyltransferases, which is essential for xyloglucan biosynthesis. A reduced xyloglucan content was found in the double mutant of *xxt1 xx2*[242], and similarly, XXT5 was also shown to be a xyloglucan xylosyltransferase functioned in xyloglucan biosynthesis[243]. Later, *XXT3* and *XXT4* were also shown to have similar expression and might be redundant to the other *XXT*s[244].

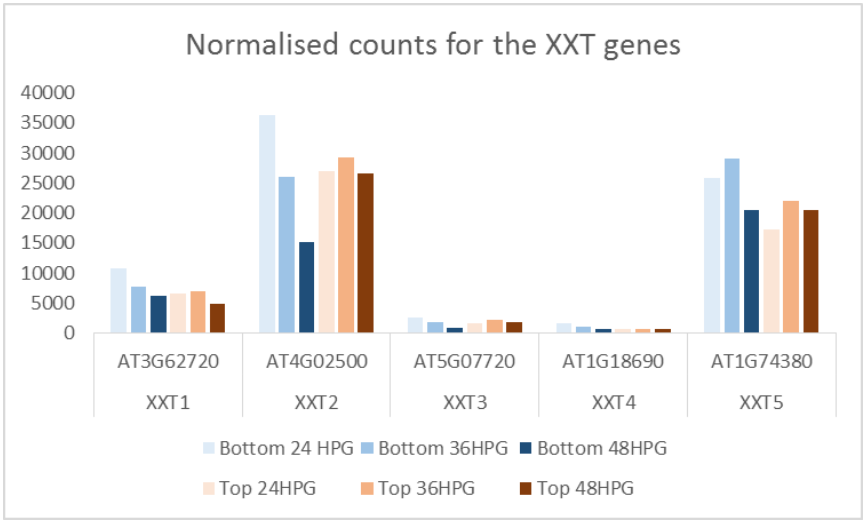

Figure 4.28 The normalised counts for the XXT genes

Results

The *XXT* genes were downregulated over time at the bottom region but not at the top region

Being the genes involved in of xyloglucan biosynthesis, the five XXTs did not possess a consistent pattern. At the top region, the expression pattern only changed slightly over time, being slightly more up-regulated from 24 HPG to 36 HPG, and slightly downregulated from 36 HPG to 48 HPG. This pattern was the same with the *CESA* genes discussed in the previous section, but most likely just a coincidence, since none of the expression levels changed significantly. At the bottom region, four *XXT* genes decreased in expression level, with three (*XXT2, XXT3, XXT4*) decreased more than 1 fold from 24 HPG to 48 HPG. So there was possibly a reduction in the xyloglucan biosynthesis at the fast-growing region of the hypocotyl, but not in the region that rapid growth had not reached.

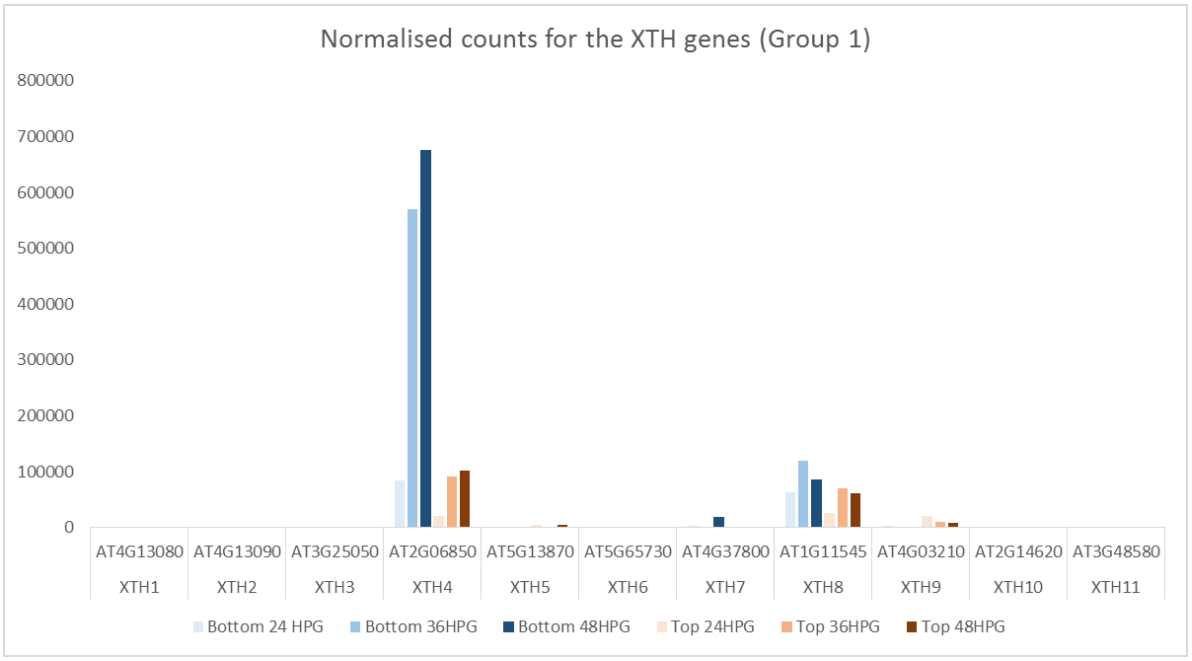

Figure 4.29(a) The normalised counts for the XTH genes (Group 1)

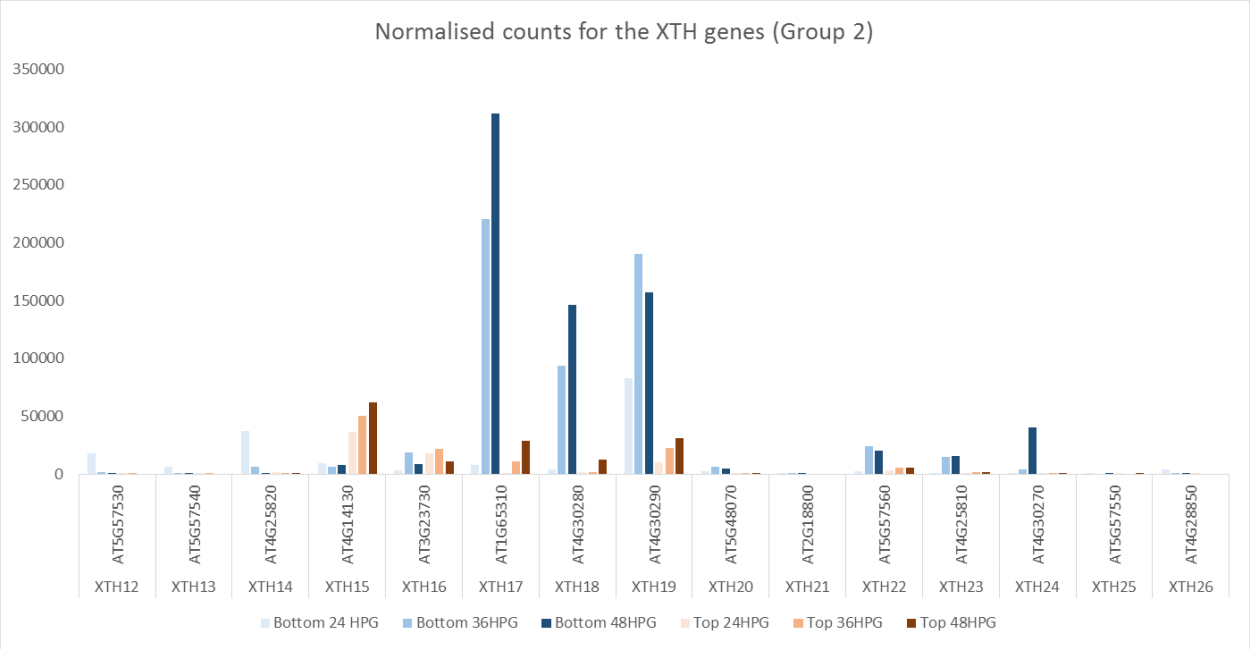

Figure 4.29(b) The normalised counts for the XTH genes (Group 2)

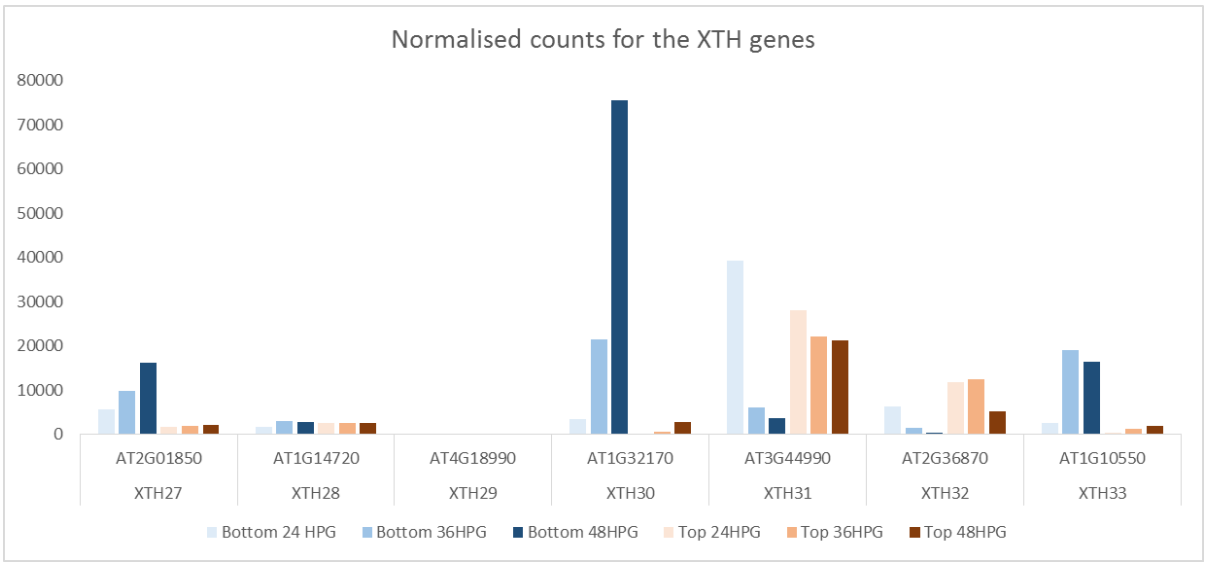

Figure 4.29(c) The normalised counts for the XTH genes (Group 3)

Most of the highly active XTH genes were more expressed at the bottom region, and highly expressed during the rapid elongation period

The three groups of XTH genes did not appear to have a difference in expression pattern, and so the functions of *XTH* genes were unlikely to be categorised based on their structure and organisations.

The genes with very high activities in each of the three groups, were *XTH14*, *XTH17*, *XTH18*, *XTH19*, and *XTH30*, and all of them were highly expressed at the bottom region at 36 HPG and 48 HPG, but not at the top region, nor at any region at 24 HPG. *XTH19* was an exception, where it was also relatively active at 24 HPG at the bottom region. Apart from *XTH19*, other four highly active *XTH* genes were up-regulated over time in both regions.

Among the other less active genes, some were more expressed at the top region (*XTH9, XTH15, XTH31, XTH32*) but the majority had the same pattern with the highly active *XTH*s, being more expressed at the bottom region.

Discussion

The transcriptome data of the xyloglucan biosynthesis genes and xyloglucan endotransglucosylase/hydrolases genes provided expression patterns fitting our general understanding of hypocotyl growth and cellular elongation. The biosynthesis of xyloglucan mainly happened before the rapid cell elongation, possibly around the same time with cellulose biosynthesis, and then the activity of xyloglucan biosynthesis was slightly reduced over time during the rapid cell elongation, suggesting less newly made xyloglucan was required during the rapid elongation phase. In the meantime, the top region had not started to grow rapidly from 24 HPG to 48 HPG, and the biosynthesis activity was high.

The fast cellular elongation at the bottom region started around 36 HPG and most of the cells at the bottom region were still growing rapidly at 48 HPG. This fitted well with the expression level of the *XTH* genes, where outstanding expression was observed at 36 HPG and 48 HPG at the bottom region but not earlier. The XTHs were known to be involved in wall modification[59][60]. During the rapid elongation the cells enlarge in volume, causing dramatic changes in their wall property, and hence a lot of action of the cell wall modification is required. XTHs cut and re-join the xyloglucans, and our results indicate that the XTHs are more likely to promote growth rather than restrict growth, consistent with the previous finding that the growth of hypocotyl was stimulated by overexpression of *XTH18*, *XTH19,* and *XTH20*[85].

XTH15 and *XTH31* behaved differently to other *XTH*s according to our transcriptome data. Their aluminium-repressed protein products have been known to be different from other members of the *Arabidopsis* XTH family[245] in many ways, including their activity and pH optimum[245].

In general, the *XTH* expression level is highly correlated with the rapid cellular growth, where the process of rapid wall modification takes place. Unlike the genes involved in the biosynthesis of

xyloglucan, which are more likely to be precursors to the growth, the *XTH*s levels are good indications of the current level of activity of the cell wall modification.

GENE ONTOLOGY ANALYSIS

In comparison to analysing families of genes, gene ontology analysis is able to study a larger number of genes and find overrepresented/underrepresented biological processes. It provides broader but less detailed biological information. Gene ontology enrichment analysis was run with GO and Agrigo[246] for the genes in different categories (see below) , with a log2 fold change >1 or <-1. This unbiased approach would provide an idea on which biological processes changed over time with statistical power, allowing a better understanding of the time evolvement of growth process at the transcriptome level to be gained. Interesting categories from approach 1 was identified and studied first, followed by categories from approach 2.

Categorisation approach 1: Identifying interesting categories

Several categories of genes have interesting patterns, which can be associated with growth. The 'bottom region', which grows fast from 24 HPG to 48 HPG but at 48 HPG some very basal cells in this region have already stopped their elongation. The 'top region' on the other hand grows slowly from 24 HPG to 48 HPG, and at 48 HPG some cells in this region have just started their fast growth. This allowed me to pick out categories and suggest potential functionality of genes in those categories based on their expression pattern, and check the functionality through the gene ontology analysis.

Some categories that reveal certain behaviour of genes over time were chosen to study. Category 1 (and 10&28 being very similar) represents genes that are more expressed over time, in both regions of the hypocotyl. Category 81 (and 54&72 being very similar) represents genes that are less expressed over time, in both regions of the hypocotyl. Genes with oscillation expression behaviour over time may have less correlation with the growth but genes related to circadian are likely to be in those categories (category 21,61,39,48, 12, 43, 34, 70, etc.). Since the rapid elongation of hypocotyl starts between 36 HPG and 48 HPG, category 40 (and categories 28&31 being very similar) represents genes that only more expressed during the fast elongation period

There are also genes in several categories which correspond to a 'growth trigger'. For example, genes with patterns {flat, up}, {up, flat} or {up, down} at the bottom region have a dropping trend over time, so the genes involved in growth initiations can potentially possess these expression patterns.

Description	Index
Gene expressed more over time	a1, (a10,a28)
Gene expressed less over time	a81, (a54,a72)
Gene expression changed over time (up down)	a21, (a39, a48,a12)
Gene expression changed over time (down up)	a61, (a43, a34,a70)
Genes act as a growth trigger	a29, a38, a32,a33,a39
Genes only associate with rapid growth	a40, (a28,a31)

Table 4.2 Description of the categories of interest. In the brackets are category with very similar expression pattern

Genes up-regulated over time

Genes that were up-regulated over time were likely to be in category a1, a10 or a28. Since there was a tremendous boost of the absolute growth rate of the hypocotyl from 24 HPG to 48 HPG, a number of genes that were up-regulated during this period were likely to be involved in the cellular growth process. The enrichment analysis was run on PANTHER and results shown as following.

Summary table:

Category	Number of genes	Over-represented biological process	Under-represented biological process
a1,a10,a28	147	1	No statistically significant result

Category a1, a10 and a28 consisted of a total number of 147 genes, which was a relatively small number in order to give statistical significant functional over-representations. The only over-represented biological process was water transport. Vacuole expansion was mostly by water, and as the hypocotyl rapidly increased in size in the period of 24 HPG to 48 HPG, water transport was an important process. Previously it was found that ribosome and cytoplasm synthesis was downregulated over time[22] so the hypocotyl cells grew by taking water, not synthesising cytoplasm.

Genes downregulated over time

Genes that were less expressed over time were likely to be in category a54, a72 and a81. In oppose to genes that were up-regulated during the period of study, those genes were unlikely to promote the cellular growth. Instead, they might be inhibitors or precursors of cell growth. The enrichment analysis was run on PANTHER and results shown as following.

Summary table:

Category	Number of genes	Over-represented biological process	Under-represented biological process
a54,a72,a81	74	3	No statistically significant result

Similar to the group of up-regulated genes over time, not many significant ontologies were found for the group of downregulated genes. The only over-represented biological processes were (cellular) glucan metabolic process and polysaccharide metabolic process, suggesting a possible decrease in the polysaccharide metabolic activity in the hypocotyl over time. Downregulation of cytoplasm synthesis was over-represented in Pelletier's data[22] but not here, possibly due to the different time points studied. It was shown to be downregulated very soon after the growth acceleration[22] so at later times (36-48 HPG) they were not downregulated further.

Genes with changing expression pattern over time

Some genes changed their expression over time, e.g. up-regulated from 24 HPG to 36 HPG and down-regulated from 36 HPG to 48 HPG, or vice versa. This expression pattern is difficult to be mapped to the hypocotyl growth, as there was no such 'reversed' change observed in the organ or cellular growth rate. Hence these genes are unlikely to be directly associated with growth, they might be some positive/negative regulators to balance hormone level, or relate to the circadian rhythm. I studied genes in category a21, a39, a48, a12 (up-regulated->downregulated), and a61, a43, a34, a70 (downregulated->up-regulated) together, and the enrichment analysis was run on PANTHER and Agrigo[246].

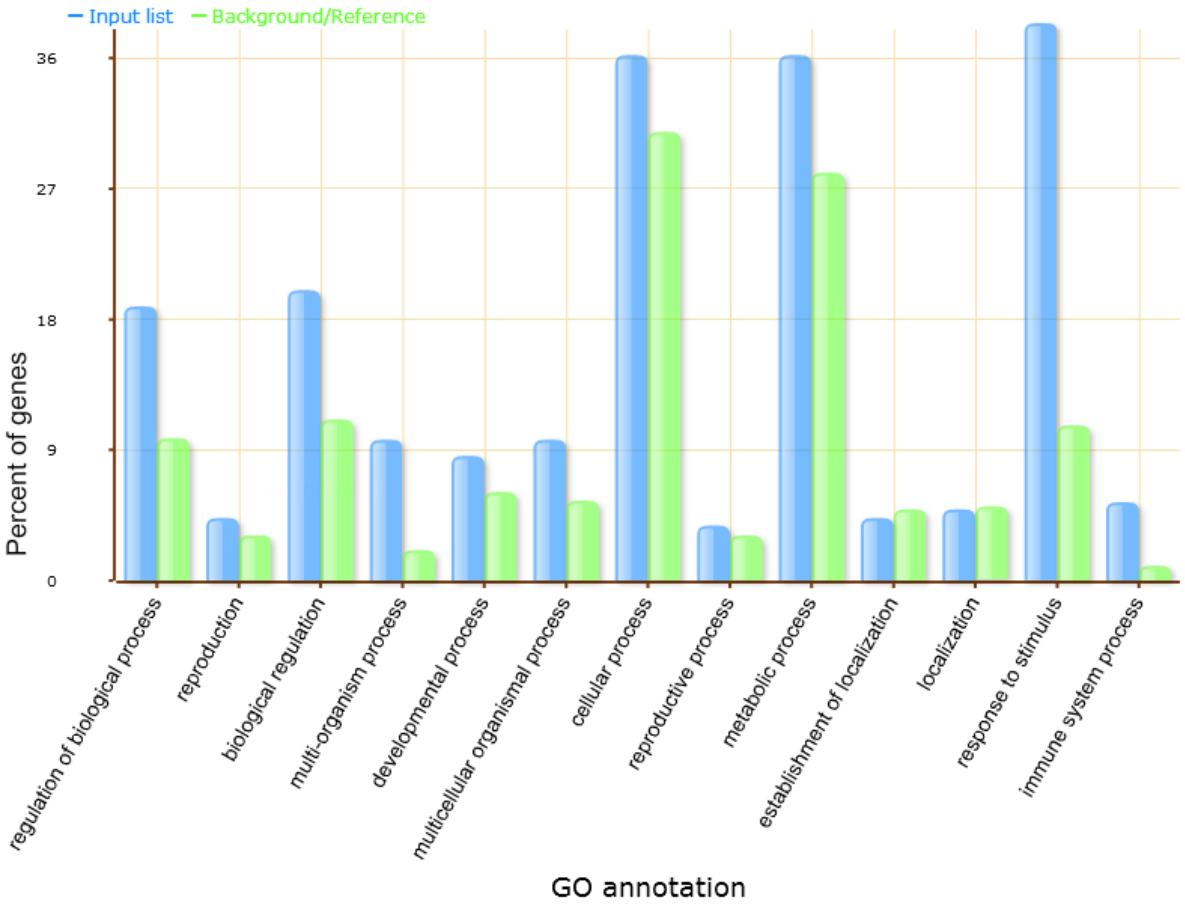

Figure 4.30 The GO annotation of genes that changed expression pattern over time, image generated with Agrigo[246].

Summary table:

Category	Number of genes	Over-represented biological process	Under-represented biological process
a21,a39,a48,a12, a61,a43,a34,a70	189	65	No statistically significant result

Compared to the previous two groups, the group of genes with changing expression pattern over time had many over-represented biological processes, despite the number of genes being relatively small. This meant that many genes with similar functionality were expressed in these patterns that changed over time. The full list of enrichment analysis can be found in Table S4.1. The top over-represented biological process was 'response to stimulus' (p-value=3.5e-56) and 'regulation of biological process' (p-value=8.9e-21), which included regulation of circadian rhythm, response to chitin, rhythmic process, organic cyclic compound biosynthetic process, hormone biosynthetic process etc. Many of the genes

were involved in circadian/rhythmic/cyclic processes, which was expected to match the varying expression pattern.

Genes act as a growth trigger

Understanding genes that initiate growth was an important part of the study of early seedling development. However, the growth initiation was a complex biological process, and biosynthesis of different hormones/protein/cell wall components started at different times and took various durations. This made it difficult to pull out these genes by only their expression pattern over the three time points. Here I studied genes that expressed in patterns like a growth trigger: genes that were only up-regulated in regions that were about to grow, and the enrichment analysis was run on PANTHER and Agrigo[246].

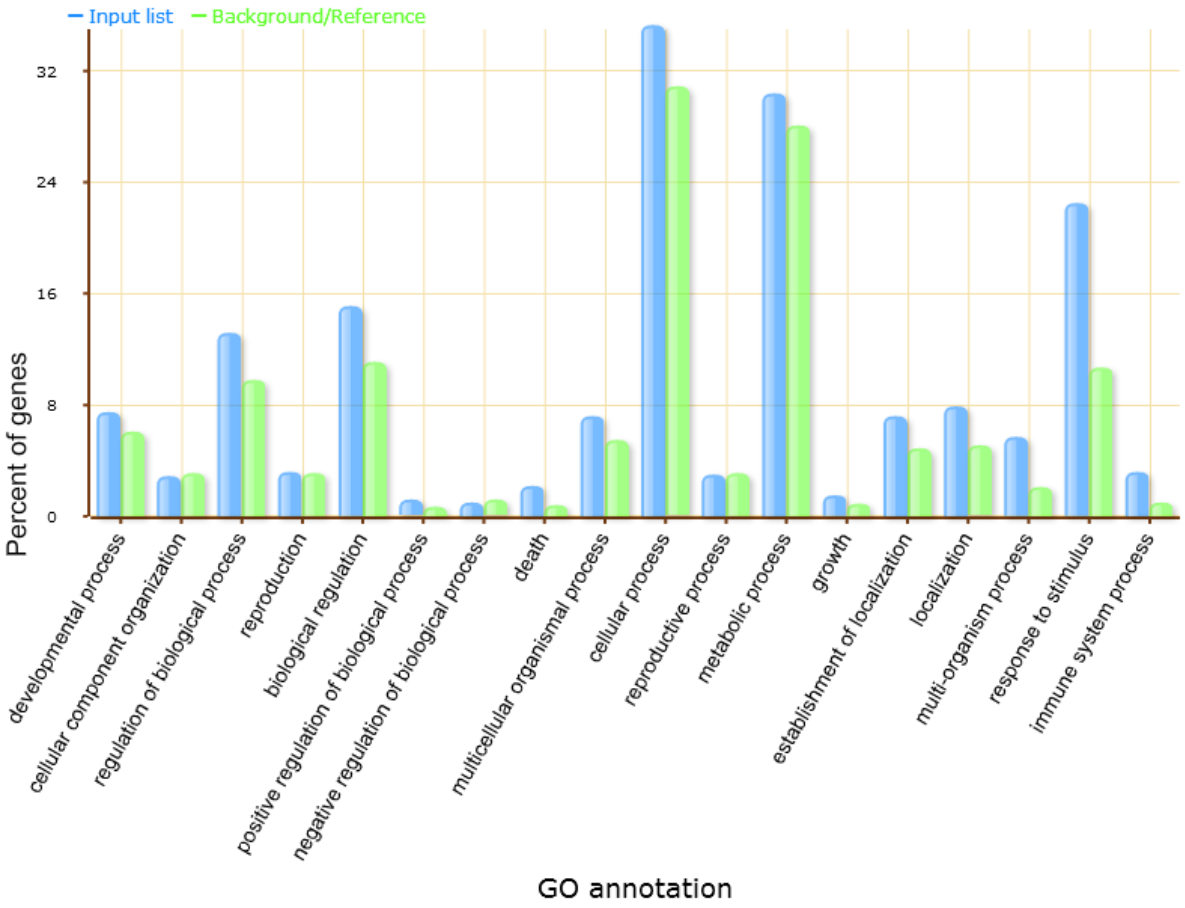

Figure 4.31 The GO annotation of genes that expressed like a growth trigger, image generated with Agrigo[246].

Summary table:

Category	Number of genes	Over-represented biological process	Under-represented biological process
a29,a38,a32,a33,a39	1578	165	22

1578 genes were acted like potential growth triggers. 187 significant ontologies were identified, with 165 over-represented and 22 under-represented biological processes, respectively. The full list of enrichment analysis can be found in Table S4.2. The top over-represented ones included cell wall thickening, cellular metabolic process, response to stimulus, hormone biosynthesis process, phytoalexin biosynthesis process, suberin biosynthesis process, wax biosynthetic process, tryptophan biosynthetic process, glucosinolate biosynthetic process, etc. The under-represented ones include RNA processing, chromosome organisation and photosynthesis. This ontology has shown that during the initial growth, the cells respond to different kinds of stimulus including the hormone, and then facilitated a lot of biosynthesis processes, which might contribute to some aspects of the growth. There were also many other over-represented biological processes in these categories representing growth triggering (Table S4.2), so the process of 'growth triggering' might be a lot more complex than just biosynthesis, cell wall thickening, and stimulus responsiveness.

Genes with expression pattern correspond to the rapid acceleration phase

Similar to the previous section, I also studied genes that were only up-regulated during the fast cellular elongation period, depending on the organ level growth rate (Chapter 1). Since there were only 3 time points, relatively early in time, it was difficult to identify categories precisely correspond to this criterion. Category a40, a28 and a31 were chosen as a representation, and the enrichment analysis was run on PANTHER and Agrigo[246].

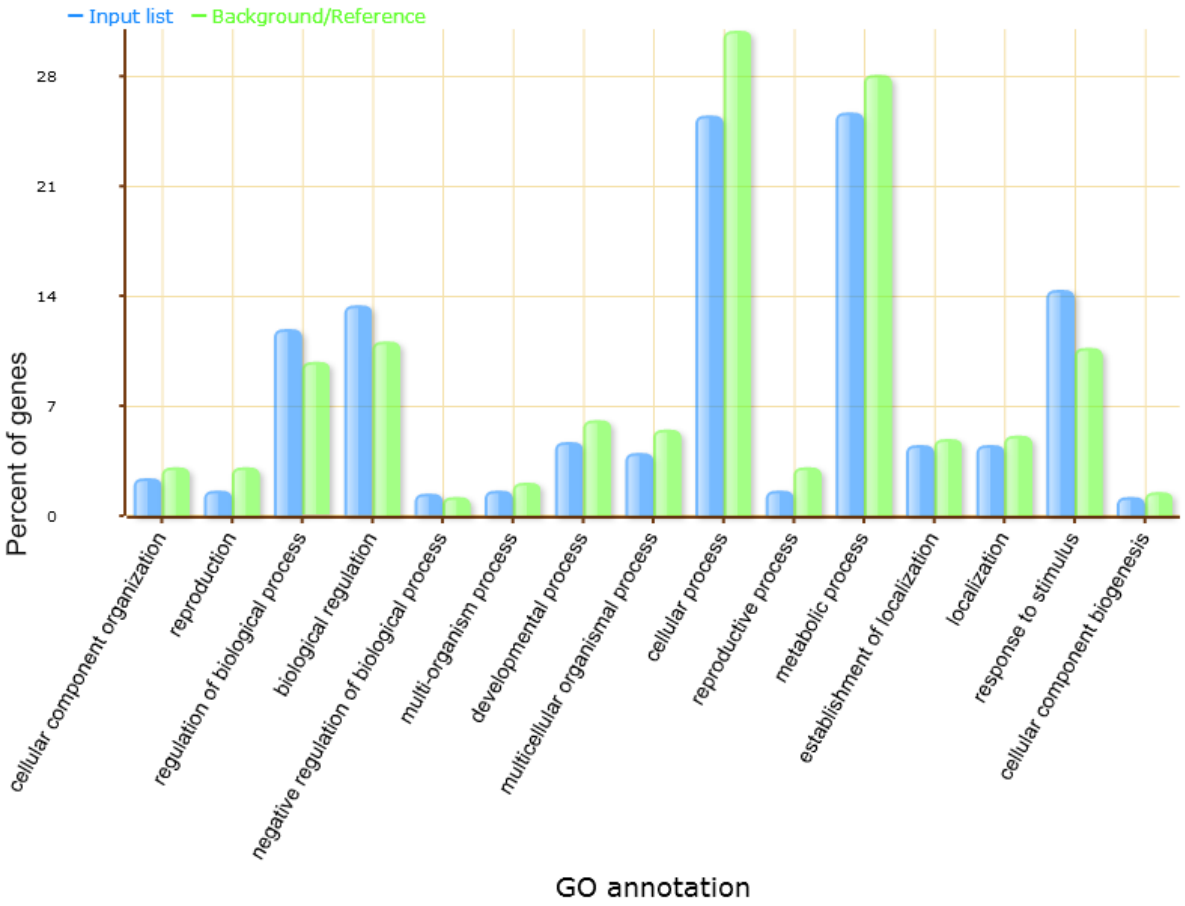

Figure 4.32 The GO annotation of genes that expressed with patterns correspond to the rapid acceleration phase, image generated with Agrigo[246].

Summary table:

Category	Number of genes	Over-represented biological process	Under-represented biological process
a40,a28,a31	497	No statistically significant result	No statistically significant result

Surprisingly, despite a relatively large number of genes, no statistically significant over-represented biological process or under-represented biological process was found. This could also be seen in Fig. 4.32, where no biological process had a significant difference between input list and the background reference. The three categories (a40, a28 and a31) were chosen such that all of them were more expressed over time in either or both regions, which were expected to be growing. What was found here should not be a result of an insufficient number of genes, since 65 over-representations were found with only 189 genes in the earlier section and here the three categories gave a combination of 487 genes. It was also not likely to be caused by the diversity of the three categories, as the three

categories had similar patterns. In fact, none of them gave any over- or under-represented biological process when separate GO analysis was run.

This result suggested that there did not exist large groups of genes in the three categories that were functionally correlated. The three categories selected here might not be a true representation of how genes would express during the phase of rapid growth. Alternatively, the GO categories are too broad to identify associated genes of interest.

Discussion

The two groups of genes that were 'up-regulated over time' and 'downregulated over time' did not give many functional over-representations due to a small number of genes, and therefore some the early hypotheses made for those groups of genes could not be tested. There are a couple of ways to address this issue: 1) Include more categories in each criterion, so more genes will be included. For example, rather than use a1, a10 and a20 as a representation of genes that were up-regulated over time, a2 and a4 could also be included since they behave very similarly to a1. However, as more categories were included, the restriction would become less robust and those genes would less closely fit the criterion 'up-regulated over time'. 2) Reduce the statistical power of the ontology enrichment analysis. This would give in more over/under-represented biological processes, but the result would be less statistically significant and so potentially less reliable for future hypotheses generation. 3) Do nothing. The result provided a simple conclusion that few genes behaved as the criterion suggested (e.g. up-regulated over time). These groups of interesting categories, although not statistically significant in the unbiased ontology analysis, were still informative when the families of genes or individual genes were studied. The results were, however, similar to the earlier findings by Pelletier[22] that few over- or under-represented biological processes were found for genes that were up/down-regulated over time in the dark-grown hypocotyl. Pelletier[22] found that the only up-regulated genes over time during the elongation of dark-grown hypocotyl were chloroplast biogenesis and photosynthesis, auxin signalling, cold and water stress and cell wall-related processes, and only downregulated genes over time were related to the ribosome and cytoplasm synthesis, and peroxidase activity. The auxin signalling, water stress, and cell wall related processes were also seen in our results. The process of chloroplast biogenesis and photosynthesis were not found to be over-represented in our results of genes up-regulated over time. Those processes were mainly due to the presence of the cotyledon, which was included in their samples but not included in our experimental setup.

The group of genes with changing expression pattern (up down, or down up) over time had a large number of functional overrepresentations, including many related to the circadian or other cyclic rhythms. This indicated that some cyclic properties of plants could be revealed at the transcriptome level, and possibly regulated by the gene expressions directly, such as the circadian oscillators[247][248]. Since the hypocotyls were grown in the dark, the oscillations of circadian genes indicated that light may not be the essential trigger for some of the circadian rhythms of plants.

The group of genes which displayed a pattern that mimicked a potential growth trigger consisted of 1578 genes and gave 165 functional overrepresentations. It should be noted that not all of them were the actual growth initiation genes as only three discrete time point was studied, and by only looking at the expression over time it was not possible to tell how those genes behaved in the specific regions. Nevertheless, the real growth initiation genes (if they exist) were likely to be in this group. Within the 165 functional representations, many were biosynthesis and biosynthetic processes, which would be expected during the growth initiation. Others included cell wall thickening, which was seen in hypocotyl epidermis cells[113] before elongation began. Photosynthesis was an under-represented process, implying the expression pattern of the photosynthesis genes were different from that of the growth initiation genes. They were more likely to be up-regulated over time in the upper part of the hypocotyl, as the seedling aged. Yet there were a lot of other over-represented biological processes which did not seem to be obviously related to growth initiation (Table S4.2). They could be studied further, to understand whether they were involved in the growth and processes of growth triggering, or they just possess the expression pattern by coincidence.

I also tried to identify categories that could underline genes with patterns that reflect the phase of fast elongation of hypocotyl growth, but genes from those categories were not functionally clustered, suggesting the selected categories were not good representations. This gave rise to some issues associated with studying the ontologies using this analysis approach: 1) The resolution of the experiment was low. Only three time points were studied, and the hypocotyls were cut into only two regions. When the expression pattern was tried to be matched with hypocotyl regional growth, the experimental resolution became a limiting factor and accurate conclusion could not be drawn. 2) During the analysis, the log2FC was selected to be >1 or <-1. Many of the genes were up/down-regulated but not significant in the level of fold change to meet the criteria. In fact, this log2FC value caused 68% of the genes categorised as ‘no change in expression over any time, at any region’, and it was likely that some interesting genes were missed such way. However, by lowering the log2FC value we would face a risk of decreasing statistical power and including too many unimportant genes. Some genes could need a 10-fold change to show functional difference, other may need only a 20% increase. 3) The temporal analysis performed here allowed gene expression pattern over time to be studied,

yet different regions of the hypocotyl grew differently according to the wave of growth (Chapter 1), and this analysis approach did not address the difference between the two regions of the hypocotyl. To study how genes were differentially expressed between fast- and slow-growing regions of the hypocotyl, another analysis approach should be developed.

Categorisation approach 2: Identifying interesting categories

Several categories of genes behaved in interesting patterns, which could be associated with growth. The 'bottom region', which grows fast from 24 HPG to 48 HPG but at 48 HPG some of the very basal cells in this region have already stopped their elongation. The 'top region', which grows slowly from 24 HPG to 48 HPG, and at 48 HPG some of the cells in this region have just started their growth. This allowed us to pick out categories and suggest potential functionality of genes in those categories based on the pattern, and check the functionality via gene ontology analysis.

Cellular growth travels upward in hypocotyl as a wave. As described and quantified in detail in Chapter 1, the position of the wave at a given time was defined as the index of any cell such that it was experiencing the sharpest increase in absolute growth rate in the past 6 hours. The wave starts at cell index 1 at 24 HPG, and the speed of the wave travels approximately $\frac{3}{8}$ cell per hour. Yet it is still unclear whether this wave would be reflected at the transcriptome level. Here, 6 categories that showed different responses to the 'wave' were chosen to study in addition to category b27 and b1 which corresponded to genes that were constantly more/less expressed at the bottom region of the hypocotyl. Category b22 corresponds to a 'signal' travelling early in time from bottom to up, starts before 24 HPG and travels faster than the actual growth wave. Genes in this category are more expressed at the bottom region of the hypocotyl at 24 HPG, not differentially expressed across the two regions at 36HPG, and more expressed at the top region at 48 HPG. This describes a wave of signal starting at the bottom region of the hypocotyl before 24 HPG, travels rapidly and reaches the top region at 48 HPG.

Category b26 corresponds to genes with an expression pattern a step ahead of the growth wave. Genes in this category are more expressed at the bottom region of the hypocotyl at 24 HPG and 36 HPG, but not differentially expressed at 48 HPG. This describes a signal starting at the bottom region of the hypocotyl, travels upwards and just reaches the top region at 48 HPG.

Category b18 corresponds to genes with an expression pattern that go just a step behind the growth wave. Genes in this category show no difference in expression level at 24 HPG but are more expressed

at the bottom region at 36 HPG and 48 HPG. This describes a signal only starts between 24 HPG and 36 HPG, and still remains at the bottom region at 48 HPG.

Category b6, b2 and b10 are the conjugate of category b22, b26 and b18, respectively, with the 'inverse' behaviour. Another interesting category is b23; Genes in this category are only more expressed at the bottom region of the hypocotyl at 24 HPG, and then show no difference in expression level at later times. This is the expected expression pattern of genes corresponding to growth initiation, and it is expected that some genes related to growth initiation may be found by looking at the ontology of genes in b23. Note that these could also be related to germination.

The study of these categories can provide a support of the 'wave of growth' at the transcriptome level, and pull out groups of genes that are associated with growth and growth inhibition. In addition, these lists of categories can be used together with the categories identified previously in Approach 1. Genes with desired behaviour across region and pattern over time can be gained by taking intersection between genes of two categories, one from each of the approaches.

Description	Category Index
Genes expressed more at the bottom only at early time	b23
Gene expression correspond to a wave travelling early and fast	b22
Gene with expression pattern a step ahead of the growth wave	b26 (b25)
Gene with expression pattern a step behind of the growth wave	b18
Inversed expression pattern with b22	b6
Inversed expression pattern with b26 (b25)	b2 (b3)
Inversed expression pattern with b18	b10
Gene expressed more at the bottom region (coincident with the wave of growth)	b27
Gene expressed more at the top region	b1

Table 4.4. Descriptions of categories of interest. Category with very similar patterns worth considering had their index in brackets.

Genes expressed more at bottom only at early time (category b23)

Genes in category b23 were more expressed at the bottom region of the hypocotyl at 24 HPG but not differentially expressed between the bottom and the top region at later times. Since the rapid

elongation of hypocotyl started between 24 HPG and 36 HPG, this category was likely to consist of genes that were related to the initiation of cellular growth. The enrichment analysis was run on PANTHER and Agrigo[246].

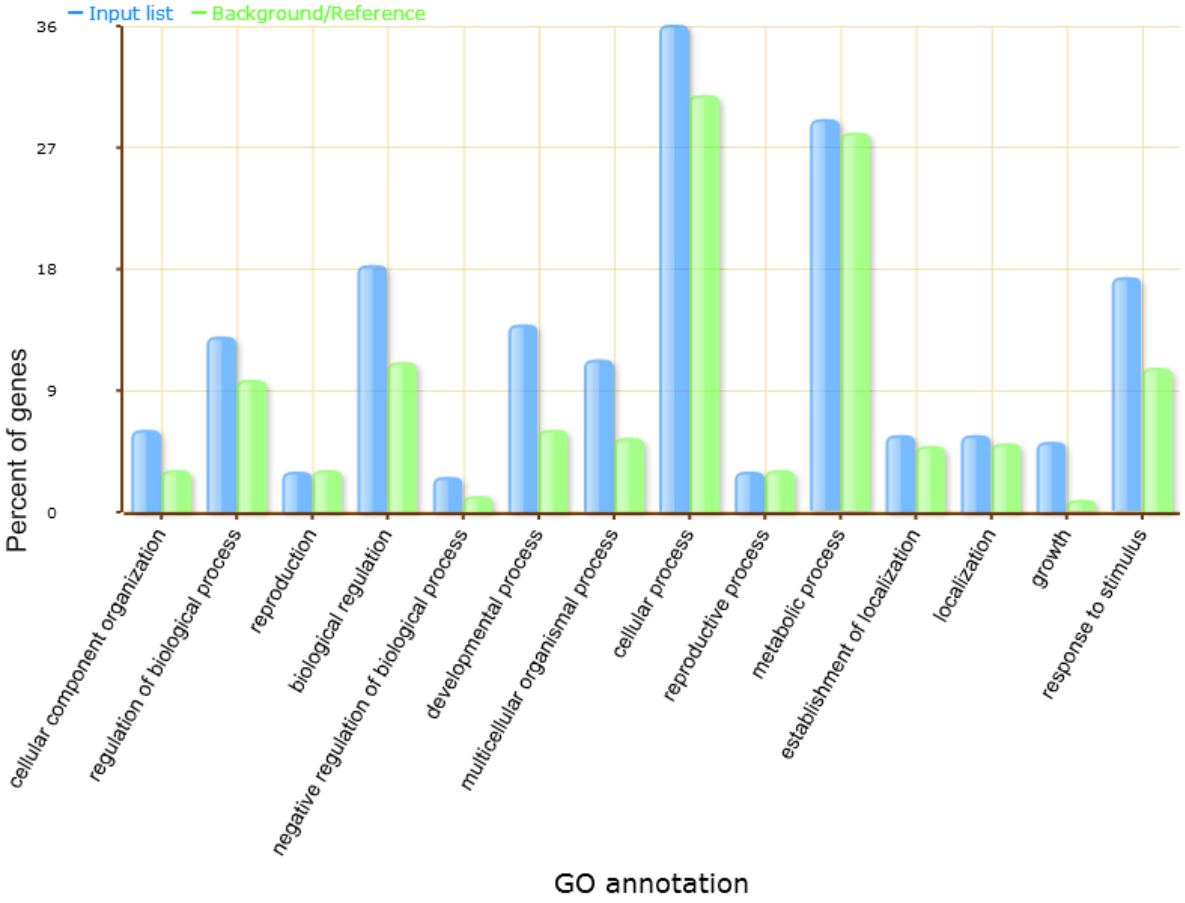

Figure 4.33 The GO annotation of genes in category b23, image generated with Agrigo[246].

Summary table:

Category	Number of genes	Over-represented biological process	Under-represented biological process
b23	232	12	No statistically significant result

The full list of enrichment in biological processes is in Table S4.3. 12 over-represented biological processes were found in this category, including response to gibberellin, unidimensional cell growth, cell growth, cell morphogenesis, response to red or far-red light, cell wall organisation or biogenesis, etc. As in Fig. 4.33, 'growth', 'response to stimulus' and 'developmental process' had the most difference in gene number between the input list and the background reference, suggesting certain

types of genes that response to stimulus and that related to growth were only more expressed at the bottom region of the hypocotyl in the beginning but not later on.

Discussion

The rapid elongation of the hypocotyl started between 24 HPG and 36 HPG. Genes in category b23 were more expressed in the bottom part of the hypocotyl only at 24 HPG. At 36 HPG and 48 HPG, they do not show a difference in expression level between the two parts. Genes in this category were either expressed strongly at 24 HPG and then became less important and were expressed less at later times, or, their expression level was raised in the upper part of the hypocotyl at the later times, so no differential expression was seen. Either way, genes in this category were active at the start or just before the cellular wave of growth, and hence possibly involved in growth initiation.

Only 232 genes were categorised into b23, with 12 over-represented biological processes and no under-represented ones. The most enriched over-representation was 'response to gibberellin', with Fold Enrichment equals to 6.36. Other over-represented biological processes included unidimensional cell growth, development growth involved in morphogenesis, cellular developmental process and cell wall organisation or biogenesis. This was consistent with the widely accepted idea that gibberellin initiated the growth, and the cell wall modification started before the rapid hypocotyl growth. This result also indicated that not all gibberellin response genes were constantly needed during the growth, instead, some of them act as a growth trigger. In addition, this result implied that the cell wall modification might also not be a constant process, but rather behave like a wave travelling upwards.

This result also suggested that in the category discussed above, some genes were only more expressed in the bottom at 24 HPG but not at 36 and 48 HPG. Either those genes were only active at the beginning of growth, or their expression at the top region caught up at later time points. The former was the true growth initiation genes, and they could be distinguished by looking at their counts.

Some potential genes responsible for growth initiation were identified in category b23, however, their exact role in growth was not revealed by this analysis. A more detailed look into the family of those genes (e.g. gibberellin, cell wall modification) would provide a better insight in terms of growth initiation at the transcriptome level. The germination GA list from Ogawa[23] were analysed together with this list in Chapter 5.

Gene expression corresponding to a wave travelling early and fast (category b22)

Genes in this category expressed were more expressed at the bottom region at 24 HPG, and gradually, became more expressed at the top region at 48 HPG. This expression pattern would be consistent with to a signal travelling upwards along hypocotyl early in time. The enrichment analysis was run on PANTHER and results shown as following.

Summary table:

Category	Number of genes	Over-represented	Under-represented
b22	49	No statistically significant result	No statistically significant result

Only 49 genes were found in this category, and no statistically enrichment was found. This suggested that not many genes behaved such way as described by category 22, and hence it was very unlikely that any biological process in the hypocotyl was highly active at the bottom region at 24 HPG and became highly active at the top region.

Inversed expression pattern with b22 (category b6)

Category b6 is the conjugate of b22, and genes in category 6 had expression pattern with opposite behaviour to those in b22. The enrichment analysis was run on PANTHER and results shown as following.

Summary table:

Category	Number of genes	Over-represented biological process	Under-represented biological process
b6	30	No statistically significant results	No statistically significant results

Similar to category b22, not many genes belong to category b6 and their biological process did not seem to be closely related to cell growth. No statistical enrichment was found.

Gene with expression pattern a step ahead of the growth wave (category b26 and b25)

Genes in category b26 were more expressed at the bottom region at 24 HPG and 36 HPG; this difference in expression gradually disappeared and no longer seen at 48 HPG. They expressed in a pattern consistent with a wave a step ahead of the growth wave defined in Chapter 1.Genes in

category b25 have a similar pattern but contains only 3 genes. The three were added to genes in category b26 and enrichment analysis was run on PANTHER and Agrigo[246].

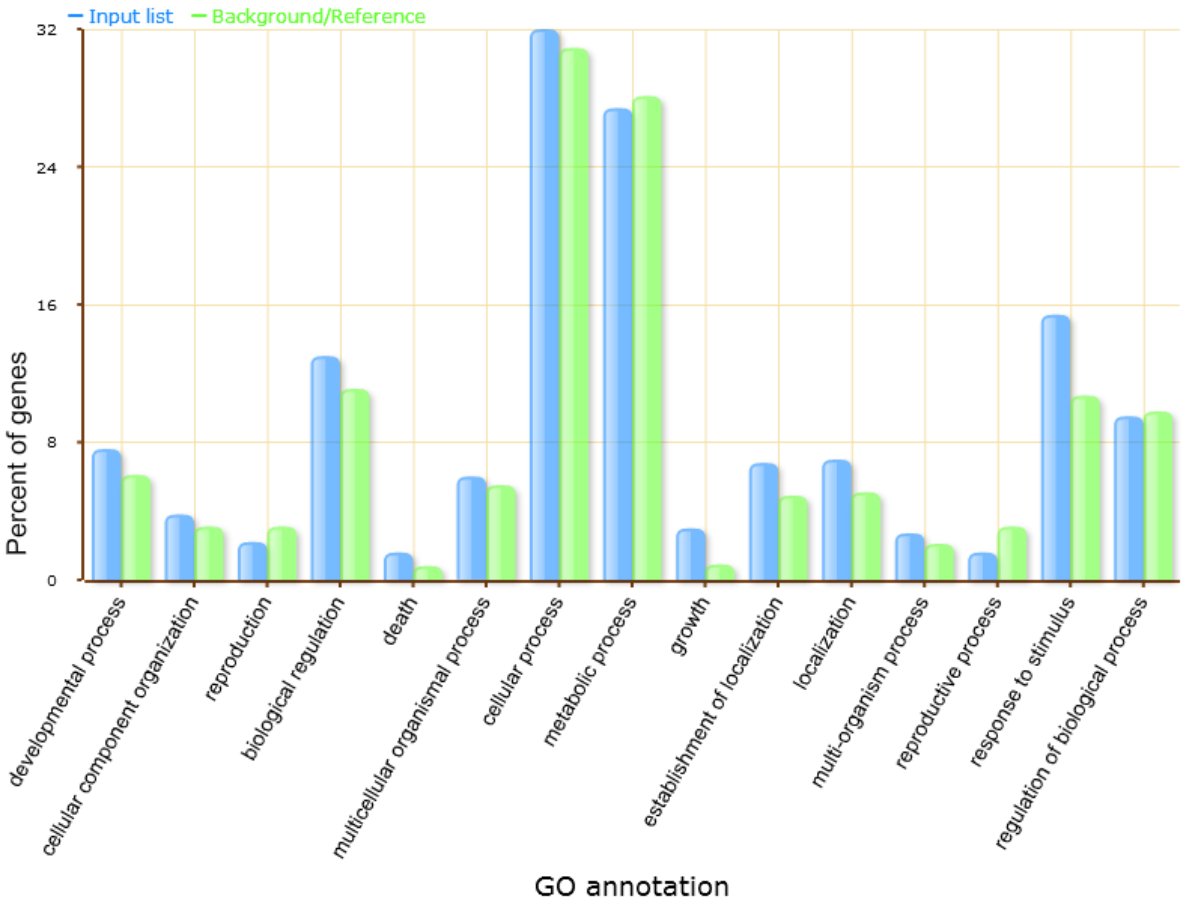

Figure 4.34 The GO annotation of genes in category b26 (and 3 genes from b25), image generated with Agrigo[246].

Summary table:

Category	Number of genes	Over-represented biological process	Under-represented biological process
b26 (and b25)	369	32	1

The full list of enrichment in biological processes is in Table S4.4. The top over-represented biological processes were 'response to stimulus' (p-value=4.69e-8) and 'protein autophosphorylation' (p-value=8.66e-8). Since over-representations in category 26 described biological processes happened a step before the growth wave, this suggested that cell growth may be triggered by some signal and that a certain level of protein kinases (many regulated by autophosphorylation[249]) existed before the wave of growth reached a cell.

Fig. 4.34 suggested that 'growth' was an over-represented biological process. The gene ontology analysis also identified a number of over-represented biological processes, that were well-understood and growth-related, including 'plant epidermal cell differentiation', 'plant-type cell wall loosening', 'plant-type cell wall organization or biogenesis', 'unidimensional cell growth', etc. Out of all the over-represented biological processes, 10 out of 32 are related to cell growth and cell wall. There are also a large number of genes related to root hair initiation, differentiation and root development in this category.

Inversed expression pattern with b26, b25 (category b2, b3)

Category b2 is the conjugate to category b26. Genes in this category had opposite behaviour in their expression pattern to those in category b26. Genes in category b3 had a similar pattern but contained only six genes. The six genes were added to genes in category b2 and enrichment analysis was run on PANTHER and Agrigo[246].

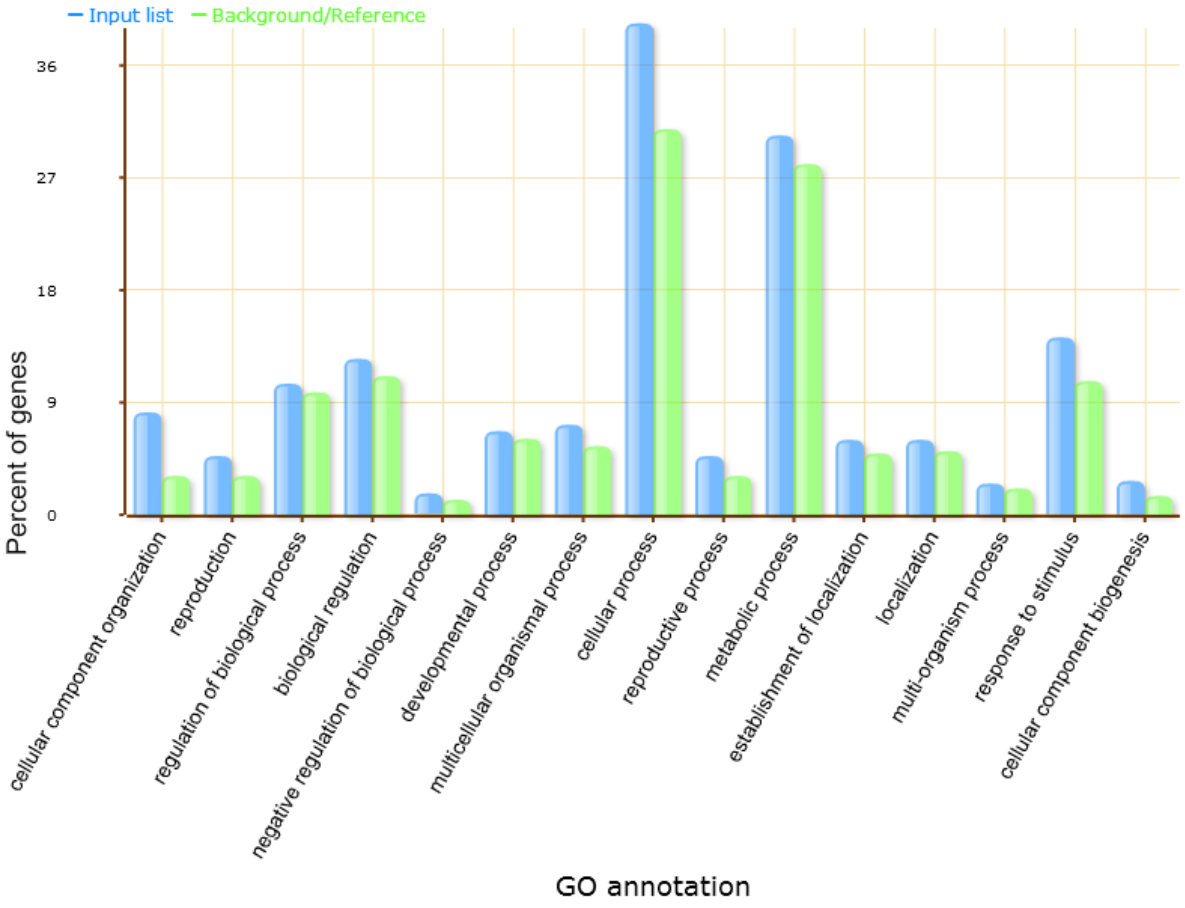

Figure 4.35 The GO annotation of genes in category b2 (together with 6 genes in b3), image generated with Agrigo[246].

Summary table:

Category	Number of genes	Over-represented biological process	Under-represented biological process
b2(+b3)	401	63	0

The full list of enrichment in biological process is in Table S4.5. 63 over-represented biological processes were found in this category, and no under-represented biological process was found. The most over-represented biological process was 'cellular component organization', and other functional enrichment included histone phosphorylation, regulation of cytokinesis, negative regulation of mitotic cell cycle transition, mitotic spindle organisation, protein import into chloroplast stroma, regulation of tetrapyrrole biosynthetic process, microtubule-based movement, etc. Overall the over-represented biological processes in category b2 were very different from those found in b26 or b18; the processes involved here seemed to be more involved in early development phases and many well-understood biological processes closely related to growth, such as cell wall modification or hormone synthesis, were however not found.

Gene with expression pattern a step behind the growth wave (category b18)

Genes in category b18 were not differentially expressed at 24 HPG, and gradually became more expressed at later times. They were expressed in a pattern consistent with a wave a step behind the growth wave defined in Chapter 1. Among all categories, genes in category b18 had an expression pattern with the closest match to the absolute rate (Chapter 1). Since the rapid growth did not start at 24 HPG, but at the two later times, cells at the bottom region had much higher absolute growth rates.

The enrichment analysis was run on PANTHER Agrigo[246].

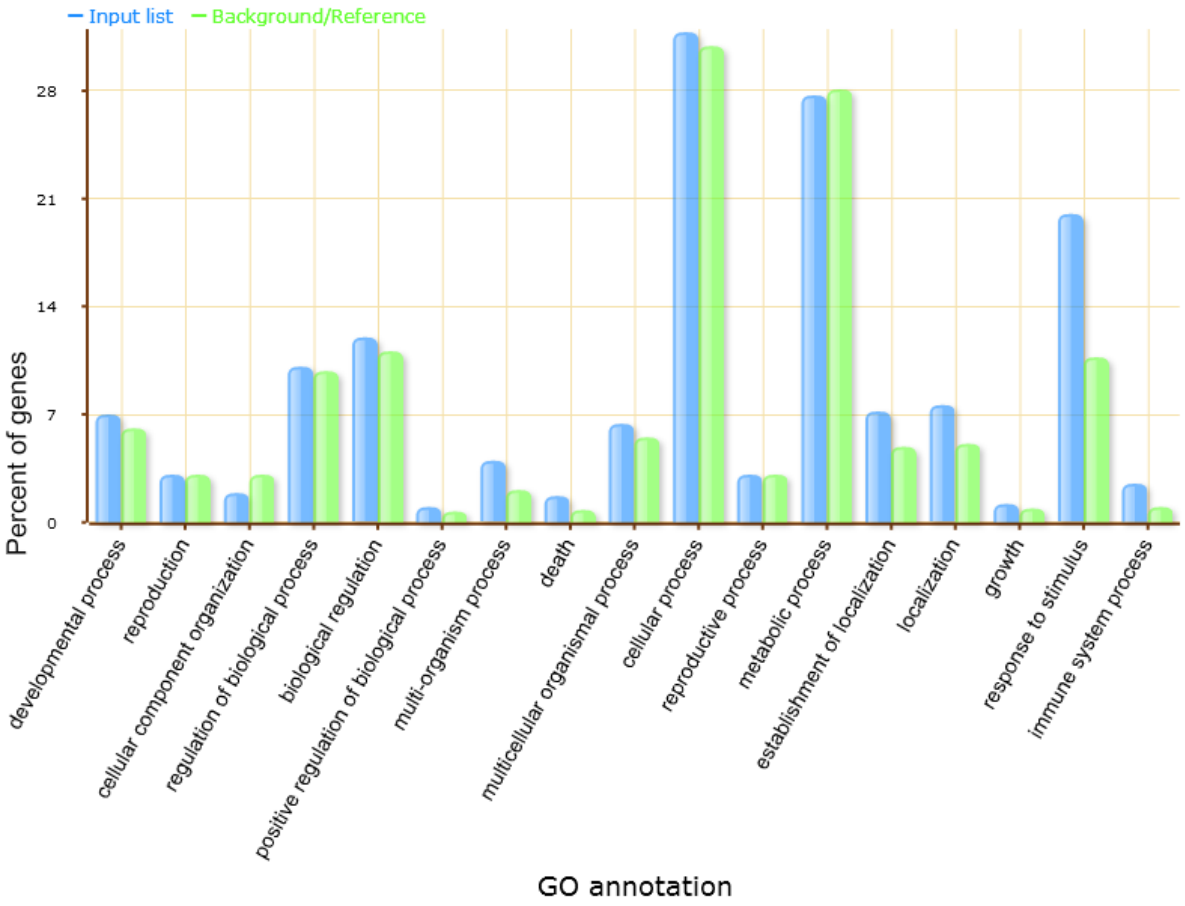

Figure 4.36 The GO annotation of genes in category b18, image generated with Agrigo[246].

Summary table:

Category	Number of genes	Over-represented biological process	Under-represented biological process
b18	1337	107	26

Category 18 consisted of the 3rd largest number of genes among all categories, with 1337 genes in total. The full list of enrichment in biological processes is in Table S4.6. The top over-represented biological processes were 'response to stimulus' (p-value=1.27e-19), 'cell communication' (p-value=6.25e-14) and 'response to organic substance' (p-value=9.81e-14). Genes in this category were also enriched in catalytic, binding, transporter and receptor activities, including indole glucosinolate biosynthetic process, defence response, auxin metabolic process, response to brassinosteroid, response to chitin, response to wounding, response to starvation, etc. Genes in this category tended to act as passive responders, ensuring a healthy establishment of the plant. Compared to genes in category b26, genes in category b18 were not as enriched in biological processes that involved in

primary growth or growth initiation of plants cells. Rather, there was a relatively big difference between the input list and background reference in 'death'. This result was not counterintuitive, as category b18 was expected to be more correlated with later cellular development process such as immune system process (Fig. 4.36), whereas category b26 would be expected to be more correlated with pre-growth processes.

Inversed expression pattern with b18 (category b10)

Category b10 was the conjugate to category b18. Genes in this category had opposite behaviour in their expression pattern to those in category b18. The enrichment analysis was run on PANTHER and Agrigo[246].

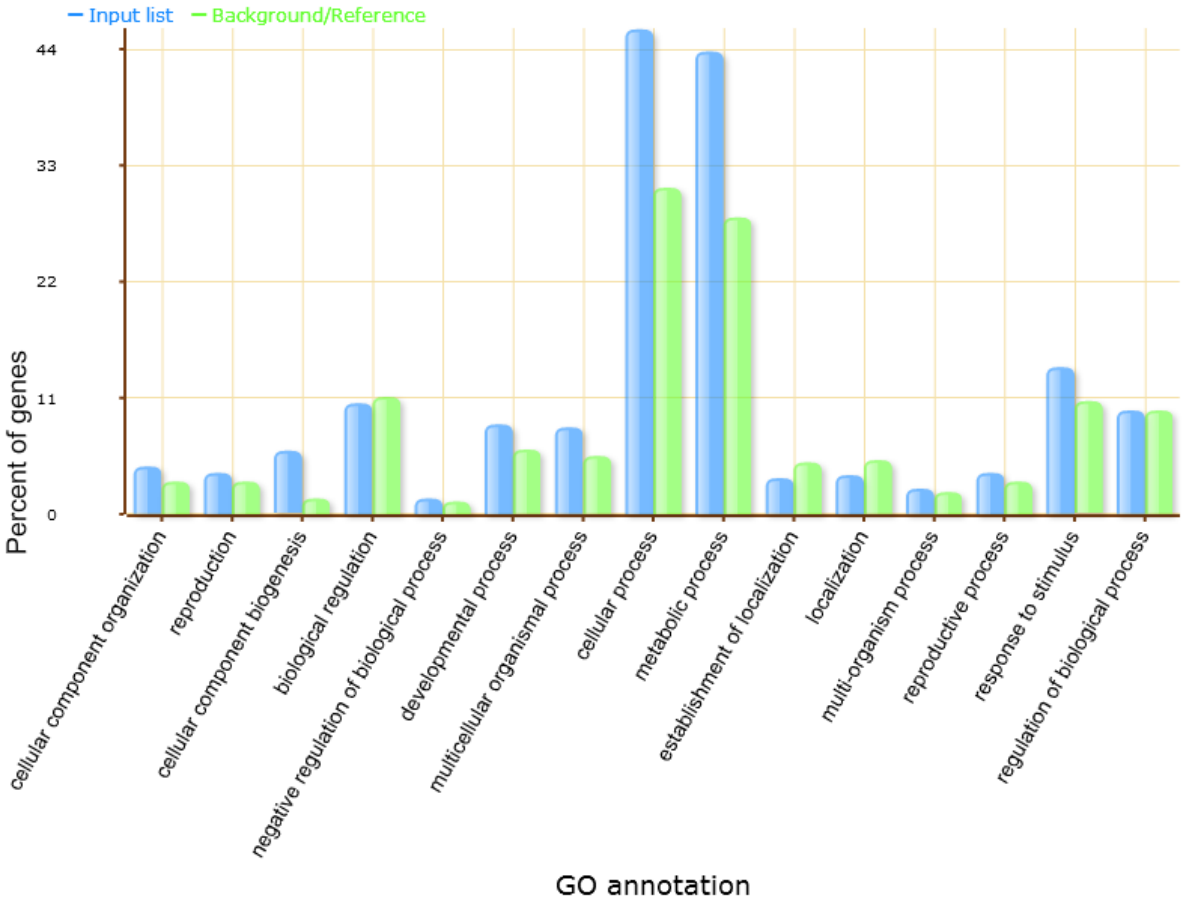

Figure 4.37 The GO annotation of genes in category b10, image generated with Agrigo[246].

Summary table:

Category	Number of genes	Over-represented biological process	Under-represented biological process
b10	971	101	3

Category b10 consisted of 971 genes in total, and 101 over-represented biological processes were found in this category, together with 3 under-represented ones. The full list of enrichment in biological process is in Table S4.7. The over-represented biological processes included mitotic DNA replication, isoleucine biosynthesthic process, glycogen metabolic process, starch biosynthetic process, nucleosome assembly, etc. Similar to b2, many well-understood processes related to growth were not found in the over-represented biological processes in b10.

The three under-represented biological processes were cell growth, growth and vesicle-mediated transport. It was shown earlier that cellular growth was mainly water uptake and transport, and all three under-represented biological processes were closely related to cellular growth. Statistically speaking, underrepresentation required a larger number of input genes, and hence they were less common but had more statistical power. This result implied that b18, being the category 'opposite' of b10, had the highest probability of correlating well with the growth.

Discussion

Following the gene ontology of each of the selected category, the enriched biological processes were studied and compared.

Each enrichment analysis of a selected category gave a list of over-represented biological processes and a list of under-represented biological processes. The former gave a good implication of the functionality of genes with a specific expression pattern, and the latter gave an indication of repressed biological activities. The enrichment analysis on PANTHER took a list of genes as input and statistically enriched biological processes as output. For every functionality, firstly the total number of the *Arabidopsis* genes with that functionality was identified and hence the number of genes seen by chance with that functionality. Then this number was compared with the number of genes in input with such functionality, and over-representation/under-representation was identified using the fold change value. However, the number of under-represented biological processes was typically small, as with a relatively small number of genes (<1000), the under-representation was not likely to be significant.

The 'wave of growth' starts at bottom of the hypocotyl and travels upwards. The three categories representing three waves at the transcriptome level (category b22 for early, b26 for intermediate and b18 for late) had very different biological processes. Category b22 had only 49 genes and no significant enriched biological processes. Category b26 had 366 genes, 32 over-represented and 1 under-represented biological processes. Many of them were closely related to growth such as cell wall

organisation and unidimensional cell growth. This was a good implication that the wave of growth in the hypocotyl happened at the time described by category 26, or slightly later due to the time took to respond to the transcriptome. Most of the others over-represented biological processes were related to root development, such as root morphogenesis, root system development and root hair initiation. The biological processes in root development might be a result of the development of collet at the very bottom part of the hypocotyl. This suggested that root hair initiation and development of the root hair near hypocotyl happened at 24 HPG and 36 HPG. At 48 HPG, the root hair initiation and development at the collet had finished and hence those genes fell in the category b26. Category b18 had 1337 genes, with 107 over-represented and 26 under-represented biological processes. Several over-represented biological processes were related to signalling, response to hormone and hormone metabolic processes but no biological process related to cell wall or cellular growth was found. DNA metabolic process, RNA metabolic process, mRNA metabolic process RNA processing, mRNA processing were under-represented biological processes, suggesting the early developmental biological processes were less active in this category of 'wave travelling late in time'. Looking at the three categories of wave together, the small amount of genes with no significant biological process in b22 suggested that no wave in any form travelled that early in time at the transcriptome level. The primary growth-related genes expressed in the pattern represented by category b26, where the Expansin activities were high and cells elongated. b18 represented a wave travelling late, after the rapid elongation, in which a lot of hormone responses and metabolic processes were found. This analysis showed that the wave at the transcriptome level correspond well with the actual cellular growth wave. A number of genes promoted cellular elongation and genes for growth initiation expressed before 24 HPG at the bottom region of the hypocotyl, and reached the top region at 48 HPG. However, the enrichment analysis of b18 showed that many genes for hormone response and metabolism do not follow the same wave but travel late in time. They were not likely to be the necessary genes for growth initiation. After the cellular growth had started and cell wall had modified to a softer state for growth, those genes turned on for hormone regulation. They might be involved in controlling the cellular growth rate, division, or acted as growth termination catalyser.

The reversed wave was studied to analyse biological processes that were under-represented. The under-representation in reverse waves could potentially be a good indicator of growth. Yet no significant under-represented biological process was found in category b2 and b6 due to the low number of genes. Three were found in category b10, which strongly correlated to growth. This reinforced the concept that the wave of growth also exists at the transcriptome level.

Genes expressed more at the bottom region (category b27)

b27 is one of the two categories with most number of genes. Genes in category b27 are more expressed at the bottom region of the hypocotyl at all times. The enrichment analysis was run on PANTHER and Agrigo[246].

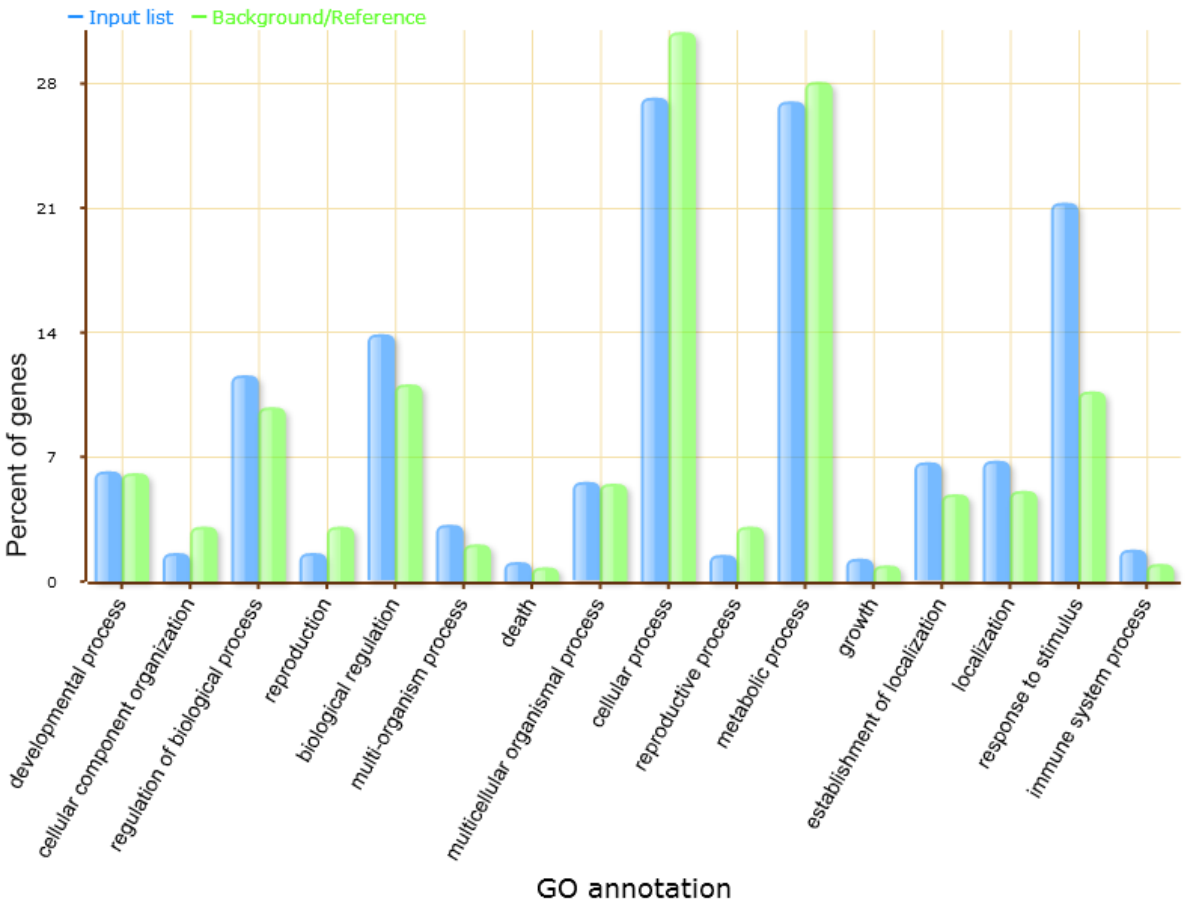

Figure 4.38 The GO annotation of genes in category b27, image generated with Agrigo[246].

Summary table:

Category	Number of genes	Over-represented	Under-represented
b27	1790	173	83

The full table is give in the Table S4.8. Category b27 contains 1790 genes, giving 173 over-represented biological processes and 83 under-represented biological processes. Compared with b18 and b26, b27 had more over-represented biological processes, due to a large number of genes it contained.

The over-represented biological processes in b27 were similar to those in b18 and b26, since all three of them underlined the genes that were more expressed in the fast-growing region. Many of the over-represented biological processes were related to cellular growth, the top ones include cell-cell

junction assembly, regulation of organ growth, brassinosteroid homeostasis, water transport, xyloglucan metabolic process, cell wall polysaccharide metabolic process, auxin transport, hormone transport, cell wall polysaccharide biosynthetic process, cell wall organisation, cell wall modification, cellular response to auxin stimulus, response to auxin, root development, response to gibberellin, cell growth, developmental growth involved in morphogenesis, etc.

Category b27 had the similar GO annotation with b18 and b26, with a peak in 'response to stimulus', suggesting the growth state of the hypocotyl cells were constantly monitored and regulated by those genes responding to different stimulus.

The under-represented biological processes of b27 gave rise to processes that were not happening in the fast-growing region of the hypocotyl, include cell killing, embryo development, photosynthesis, protein transport, cellular protein localisation, gene silencing(all p-value<6.85e-4), etc.

Genes expressed more at the top region (category 1)

b1 is the other category with the most number of genes. Genes in b1 are more expressed at the top region of the hypocotyl at all times. The enrichment analysis was run on PANTHER and Agrigo[246].

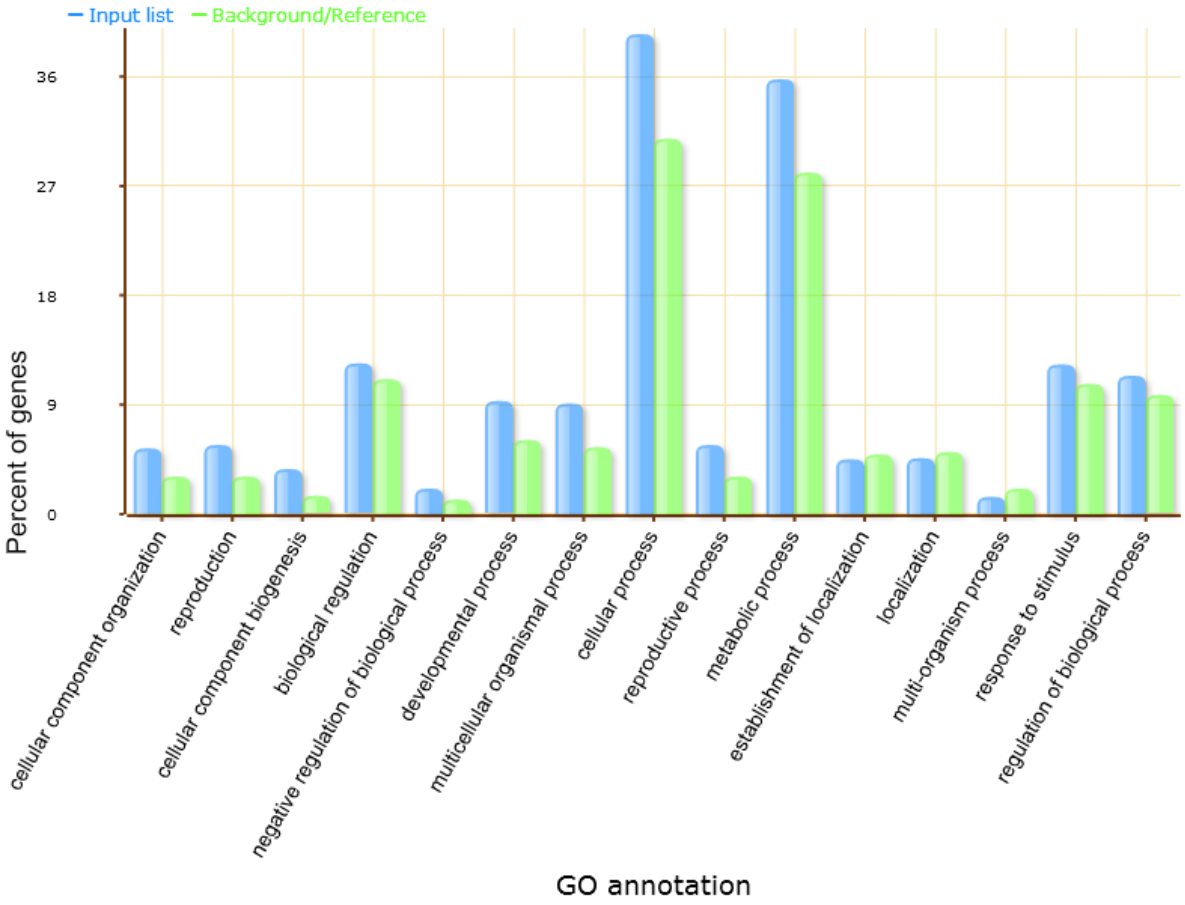

Figure 4.39 The GO annotation of genes in category b1, image generated with Agrigo[246].

Summary table:

Category	Number of genes	Over-represented	Under-represented
b27	1563	217	26

The full table is given in Table S4.9. Category b1 contains 1563 genes, giving 217 over-represented biological processes and 26 under-represented biological processes. Category b1 contains genes with opposite expression pattern to those in b27, and b1 also had very different percentage of genes in GO annotation when compared with b27. Unlike category b18, b26 and b27, b1 underline genes that were more expressed in the slower growing region, and it no longer had a significant difference in the proportion of genes with function 'response to stimulus' between the input list and the background reference. This again confirmed the important roles of those genes responding to different stimulus in hypocotyl growth regulatory. The genes in b1 also had a higher percentage in 'reproduction', 'cellular process' and 'metabolic process', when compared to the background reference, and opposite was true in b27. The most significant difference occurred in 'reproduction', in which many genes were functional in 'post embryonic development'. This suggested the slow growing (top) region of the hypocotyl was not simply a less active region than the fast-growing regions, but rather, it was likely to be in an intermediate developmental phase before the fast elongation.

The over-represented biological processes in category b1 suggested that the top region of the hypocotyl was involved in some processes, that the bottom region had never experienced. The top over-representations (all with p-value<1.2e-4) include plastid transcription and translation, photosynthesis, light harvesting, chloroplast rRNA processing, chloroplast RNA processing, chloroplast RNA modification, photosynthesis, light harvesting in photosystem II, photosystem I assembly, photosystem II assembly, regulation of shoot apical meristem development, photoinhibition, gynoecium development, etc.

Because the top region was likely to be involved in other developmental processes rather than cellular elongation during 24-48 HPG, and category b1 captured genes that were highly active at the top region at all times, under-represented biological processes of b1 gave less information about cellular growth. They included: response to fungus, response to nitrogen compound, vesicle –mediated transport, cell killing, etc.

Discussion

Due to the three relatively early time points we choose as well as the way hypocotyls were cut into the 'top' and 'bottom' regions, there was more absolute growth at the bottom region at all three time points. Therefore category b27 was the best representation of 'growing' versus 'non-growing'. 1790 genes were categorised into b27, giving a total of 173 over-represented and 83 under-represented biological processes. Many essential cellular growth processes were found to be over-represented, such as the metabolism and organisation of polysaccharide, synthesis and metabolism of xyloglucan, auxin transport and response, brassinosteroid biosynthetic process and cell wall modification. These confirmed our hypothesis that the fast growth at the organ level can be reflected by gene expression at the transcriptome level. Category b27 also identified active biological processes in the growing region, which correlated to growth, but remained unclear whether they were necessarily direct causals of growth. E.g. response to salt stress, response to bacterium, hydrogen peroxide catabolic process, lignin biosynthetic process, coumarin metabolic process and peptidyl-threonine modification. This provided some potential targets to be studied in the future that were closely related to growth.

The under-represented biological processes indicated activities that were not happening during the rapid hypocotyl growth, and hence not correlate to the hypocotyl growth, such as embryo development, photosynthesis, cellular protein localisation, DNA repair, RNA modification, gene silencing, ATP metabolic process, mRNA processing, DNA recombination, etc. These could be concluded as 'unnecessary activities of cellular growth'. These processes might either happen before/after the hypocotyl's growth, or might not be active in the hypocotyl. Category b27 also had a huge under-representation in pectin catabolic process, as pectin was one of the most important components of the cell wall, and it was unlikely to get catabolised during the fast growth phase of the hypocotyl.

Under-represented biological processes in category b27 were due to either 1) genes expressed less at the bottom region compared to the top region of the hypocotyl, such as those functionalised in photosynthesis or light responses, or, 2) low number of genes in the functional group with sufficient counts, such as those functionalised in pectin catabolic processes. The way to distinguish between 1) and 2) was to look at the over-represented biological processes in the conjugate category; in this case category b1. Yet, due to the low number of under-represented biological processes in general, it was not always easy to tell one from another.

Unexpectedly, some of the biological functions that were closely related to growth, identified earlier, were not found to be over-represented in category b27, such as cellulose synthase activities and pectin methylesterase activities. Three potential reasons were proposed: 1) Those genes did not

express during the growth but expressed earlier before the growth started, or belong to other categories. 2) There was a large number of genes with such function, but only a small proportion of them expressed in the hypocotyl, so the enrichment analysis was statistically insignificant. 3) There was only a small number of genes with such function, so the enrichment analysis was statistically insignificant. To address this, the family of *PME* and *PMEI* genes were studied further in later part of this chapter.

The over-represented biological processes in category b1 represented active biological processes in the top part of the hypocotyl. They were either precursor of growth, such as DNA metabolic process, mRNA processing, shoot system development, protein import into chloroplast stroma, cell cycle process, nuclear division, plastid transcription and translation, etc. Or, they might not related to growth at all, such as photosynthesis, chloroplast RNA processing, photosystem I assembly, photoinhibition, response to low light intensity stimulus, etc. The cotyledon and meristem located closely to the hypocotyl, and the top hypocotyl cells adapted some of the functionality of the cotyledon/meristem cells. Therefore the over-represented biological processes in category b1 identified genes that were functionalised in photosynthesis activities. Category b1 also identified a number of biological processes that appeared not to be related to growth. It remained unclear whether those processes were precursors and necessary steps of growth, or not related to growth at all.

Genes in category b27 had very similar functionality when compared with those in category b18, b26, as all three of them pulled out genes with high expression level at the fast-growing region, at slightly different time points. 'Response to stimulus' always had the most significant difference between the input list and the background reference according to the GO annotation, and so those genes played important roles in regulating cellular growth. In the previous model I made, the 'growth signal' was modelled as a simple binary function with two states: on/off. These result of transcriptome analyses suggested that it was oversimplified. Genes respond to the 'growth signal' were highly active throughout the growth period, and it was a very complicated process when all the stimulus were considered, including abscisic acid, auxin, GA, stress, and other hormones, etc.

The ontology analysis of b27 and b1 provided information of functional enrichments for the growing and non-growing regions of the hypocotyl, but also some further questions were raised. Another more detailed approach of studying the behaviour of each family of growth-related genes would answer some of these questions and provide a better understanding in specific to those families of genes.

FINAL DISCUSSION ON TRANSCRIPTOME ANALYSES

In this chapter, I studied the expression of the *Arabidopsis thaliana* genes, based on our RNA-seq experiment where dark-grown hypocotyl was cut into the bottom and the top regions and sampled at three different time points. Based on our previous quantified knowledge on hypocotyl growth (Chapter 1), the bottom and the top regions were thought to be the fast-growing and slow-growing regions, respectively. Especially at 36 HPG and 48 HPG, the bottom region grew a lot faster than the top region, but at 24 HPG, the difference in the actual growth rate between the two regions was not as remarkable. By studying this transcriptome data, I aimed to find correlations between the expression pattern of certain genes and the hypocotyl/cellular growth, and connect back to different growth factors which were studied earlier, including the 'growth signal' and properties of the cell wall.

Two different ways were used to study the transcriptome dataset, which contained 33604 genes and 6 samples. In the first way, each gene was assigned with to a category, either based on their changing expression pattern over time (Approach 1), or based on their difference in expression level between the two regions (Approach 2). This way allowed me to study a large number of genes, and determine statistically how the overall expression pattern of a list of genes was different from the theoretical non-biased expectation. It also allowed an unbiased gene ontology analysis to be performed on each category. However, it was tricky to choose the cut-off value for the log2 fold change, which determined whether a gene was up or down or flatly regulated. The value was selected to be 1 throughout the analysis, meaning only doubling/halved expression levels were considered being just significant. Using this approach, two genes were considered having the same pattern, even if one was up-regulated by 1 fold and the other up-regulated by 10 folds. Some other interesting genes can be missed, for example, if a gene was up-regulated at the bottom region from 24 HPG to 48 HPG by 1 fold but not from 24 HPG to 36 HPG, or from 36 HPG to 48 HPG, then it would be considered not to be up-regulated at all at the bottom region. The number of counts was also an issue, as the level of up/down regulation was represented by the log2 fold change but the absolute counts were not revealed. I manually removed genes with total counts<500, but genes with total counts>100,000 and genes with total counts>1,000 were not considered differently. The first way (categorisation based on approach 1 and approach 2) was not applicable to a list with few genes, as the analysis was less likely to be significant. Therefore, I studied different families of genes using a second way, which was plotting their normalised counts directly. This, in fact, addressed all the problems of the first way as no information was lost, but once the number of genes became large (>30), the plot became difficult to interpret visually and the overall patterns became less obvious. Another compromising way was to

plot the log-graph of the normalised counts, this would help to visualise the change in gene expression in log fold, but the difference in absolute counts among different genes would be less obvious.

The unbiased ontology analysis identified many biological processes related to growth with Approach 2 but not with Approach 1, suggesting genes that related to growth were more likely to be differentially expressed between the fast-growing and the slow-growing region, but less likely to change significantly in expression level over time. Many of the genes related to growth were categorised into b18, b26 and b27, whose expression pattern has been discussed previously. Response to the stimulus was the top over-represented biological process in all b18, b26 and b27, therefore chemical signal was an important process of controlling growth, supporting my earlier conjecture.

The group of genes studied in the second way were hormone related, including GA and auxin, and cell wall modification genes, including the *PME/PMEI* family and the *XXT*, *XTH* family. In general, the biosynthesis genes of GA and auxin behaved like precursors to the cellular growth. According to the data at transcriptome level, the GA level seemed to have a potential positive correlation with the growth. However for the auxin, the growth was seemed to be correlated with the reduction of local auxin level, and it was still not clear whether the absolute auxin level or the auxin transport was the more important growth regulator. The wall modification genes (*PME, PMEI, XTH*), on the other hand, were all more expressed in the fast-growing region, especially for the XTHs, which were highly active at the bottom region during its rapid elongation. The few genes encoding type II PME were expressed oppositely and they were thought to be active to stiffen the cell wall at the slow-growing region. Due to the resolution of our data, I was unable to conclude a complete pattern of the expression of these genes. However if only the expression pattern based on the three time points was considered, the hormone biosynthesis genes seemed to express a large step ahead of the growth wave (defined in Chapter 1), the cellulose and xyloglucan biosynthesis genes seemed to express a small step ahead of the growth wave, and the hormone receptor/cell wall modification genes seemed to express together with the growth wave.

A few improvements can be done to address some of the issues I encountered. Firstly, a finer experimental resolution would allow me to correlate the gene expressions to the cellular growth rate (Chapter 1); taking shorter time interval (6 hours rather than 12 hours) and longer time points (extend the experiment up to 72 HPG) would allow much more powerful conclusions to be drawn. Cutting hypocotyl into more regions would be ideal but technically difficult, single-cell RNA-seq analysis might be another solution, which would also address the issue of different cellular behaviour among dividing epidermal/non-dividing epidermal/cortical cells. Secondly, the hypocotyl could be cut not only without the apical hook region and the root region, but further, without the hypocotyl-hook and

hypocotyl-root conjunction region, to achieve a cleaner result. Thirdly, all the conclusion was drawn only based on the transcriptome data, hence investigation on the corresponding protein level is essential to prove the correlation between those genes and the growth. The protein products of genes with outstanding expression behaviour can be focused to study in the future.

CHAPTER 5: THE GIBBERELLIN IN THE DARK GROWN HYPOCOTYL

All work contained here was performed by Yuanjie Chen.

SUMMARY

Following the intrinsic cellular model in Chapter 2 and the empirical model in Chapter 3, a possible identity of the 'chemical signal' in the models is explored and discussed. Inspired by the previous studies[23][24][164], the GA level was studied using the nlsGPS1 sensor in the dark-grown hypocotyl at three time points: 24 hours post germination (HPG), 48 HPG, and 72 HPG. A correlation was found between nlsGPS1 emission ratio and growth rate (Chapter 1) in non-dividing hypocotyl epidermal cells. Further, by a comparative analysis at the transcriptome level, it was found that GA up-regulated genes tended to be relatively higher expressed in the fast growing regions of the hypocotyl, within the acropetal wave. These pieces of evidence suggested that GA was a good growth indicator, and may be a strong candidate for the 'chemical signal' stimulating growth in models presented in this thesis.

INTRODUCTION

The model in Chapter 2 describes the dynamic growth of a plant cell. Despite the complexity of the model, the simulated cell length over time is not a close-enough match to the observed data (Fig. 2.4B, Fig 2.2A). This means that cell growth characteristics are unlikely to be completely explained and perfectly modelled if only physical properties are concerned. The sensitivity analysis (Fig. 2.8) implies that cellular growth rates may be more efficiently modified by changing the cell wall's biochemical properties (bond energy distribution). Hence there may exist dynamic chemical signals in growing cells, with direct modification of cell wall properties and control cellular growth rates. In Chapter 2 this chemical signal was modelled with two states: 'on' and 'off'. In this chapter, the possible characteristic of this chemical signal is explored and discussed.

The goal of this chapter was to identify a phytohormone candidate for the 'chemical signal' stimulating hypocotyl cell elongation. The hypocotyl exhibits a wave of growth (Chapter 1, Chapter 3), so there should also be a gradient of the chemical signal, matching the wave of growth. Hormones naturally occur in plants and they influence many physiological processes such as growth and differentiation developments[250] , so hormones are strong candidates for the chemical signal. As discussed in Chapter 4, gibberellin regulates many of the plant developmental stages[141], and a positive

correlation between GA level and cell area was observed for dark-grown hypocotyls 3 days post sowing[24]. At the transcriptome level, GA biosynthesis genes were expressed slightly before the wave of growth and GA-related genes were highly expressed in fast growing regions of the hypocotyl (Chapter 4). These data make GA a strong candidate for the chemical signal controlling the cellular growth.

Previously it was shown that the level of GA affected the elongation of dark-grown hypocotyls significantly[251]: exogenous GA increased the hypocotyl growth rate and final length, in dark and light grown seedlings, and a GA deficient mutant or treatment with a GA biosynthesis inhibitor reduced hypocotyl length. In order to gain a better understanding of how GA level is correlated to cellular growth in the dark-grown hypocotyl, GA level was quantified in dark-grown hypocotyls using the nlsGPS1 GA sensor at three time points: 24 HPG, 48 HPG and 72 HPG and compared with the cellular growth rates quantified in Chapter 1. Further, a microarray dataset of GA up/down-regulated genes during seed germination[23] was studied compared with our RNA-seq dataset (Chapter 4), to identify genes up-regulated by GA as well as expressed more in fast-growing hypocotyl regions. Such genes support a GA-regulated growth mechanism in the hypocotyl and their ontology could provide an indication of how this regulatory process was achieved.

METHODS

Seedling preparation:

Seedlings of the transgenic line nlsGPS1[24], with a segregating membrane marker td-Tomato (Jones Lab, SLCU)were utilized. Seeds were sterilised as described in Chapter 1. Seedlings were grown vertically on 1/2 MS agar medium (1/2MS salts, 0.8% Agar, 0.05% MES pH5.7). Plates were stratified for 2 days at 4℃ in the dark, and then transferred to a long-day growth chamber (16h light/8h dark cycling, temperature cycling 22℃ day/18℃night, 70% RH) for 24 hours to induce germination. Seedlings were then transferred to 1/2 MS agar medium with sucrose (1/2MS salts, 0.8% Agar, 0.05% MES pH5.7, 1.5% sucrose), wrapped with foil and placed vertically in the same chamber for 24 hours, 48 hours and 72 hours before imaging.

Imaging with fluorescence microscopy

Seedlings prepared for imaging were placed on glass slides with 50 µL water and a rectangle cover slip.

Confocal images were acquired on a Zeiss LSM780 using a 20x dry objective. The laser and detector settings for the CFP and YFP were identical to Rizza[24], with the addition of 554nm laser to excite the membrane-tdTomato and additional detector set to 565 to 600 to detect it.

Image processing and analysis:

Confocal images were processed in IMARIS8.3.1, with the same setting and steps as used as before[24]. The nlsGPS1 emission ratio was calculated by dividing the mean value across the 530-535 range by that across the 480-485 nm range[24]. With the aid of the membrane marker, cellular indices were noted. The emission ratio was then grouped by location on the apical-basal axis of the hypocotyl and defined by dividing and non-dividing file (See Chapter 1).Hypocotyl cells from non-dividing files were divided into four regions (six regions for seedlings at 48 HPG and 72 HPG), defined by location (bottom region: cell with indices 1-4, lower middle region: cell with indices 5-9, upper middle region: cell with indices 10-13, and the top region: cell with indices 14-17). The emission ratio was plotted as bar charts in Excel against cell index for cells at the same time. An ANOVA test was conducted to show statistical significance of the nlsGPS1 emission ratio at different locations.

Comparing nlsGPS1 emission ratio with growth rate

The nlsGPS1 emission ratio was plotted against the cell index, in batches of 4-5 cells for 24 HPG (four regions in total, described in the previous paragraph), and a batch of 2-3 cells for 48 HPG (six regions in total, defined by location of non-dividing epidermal cells with indices 1-3, 4-6, 7-9, 10-11, 12-14 and 15-17, respectively). Then the average absolute/relative growth rates of the correspondent batches of cells was calculated using the data in Chapter 1, and plotted together on a secondary axis.

Extraction and ontology of genes supporting how GA regulate growth

Extract list of genes: The GA up-regulated genes from Ogawa[23] were used to intersect with genes that were more expressed in the bottom/top region (with a log2Fold Change>1) at 24 HPG, 36 HPG and 48 HPG respectively, resulting in 3 list of genes: List 1: genes that were up-regulated by GA at germination and more expressed in the bottom region at 24 HPG. List 2: genes that were up-regulated by GA at germination and more expressed in the bottom region at 36 HPG. List 3: genes that were up-regulated by GA at germination and more expressed in the bottom region at 48 HPG.

Ontology analysis: The ontology analysis of the three lists of genes were performed in Agrigo[246] as described in Chapter 4.

RESULTS

The patterns of GA-level over time show spatial patterns along the hypocotyl

The nlsGPS1 emission ratio, indicating the level of bioactive GAs, was studied at three time points: 24 HPG, 48 HPG, and 72 HPG. In order to distinguish the bioactive GA level for cells at different growth stages, the average nlsGPS1 emission ratio was quantified at four regions of the hypocotyl: 1) the basal region, defined by the region of non-dividing epidermal cells with index 1-4, 2) the lower middle region, defined by the region of non-dividing epidermal cells with index 5-9, 3) the upper middle region, defined by the region of non-dividing epidermal cells with index 10-13, and finally 4) the top region, defined by the region of non-dividing epidermal cells with index 14-17. (Fig. 5.1)

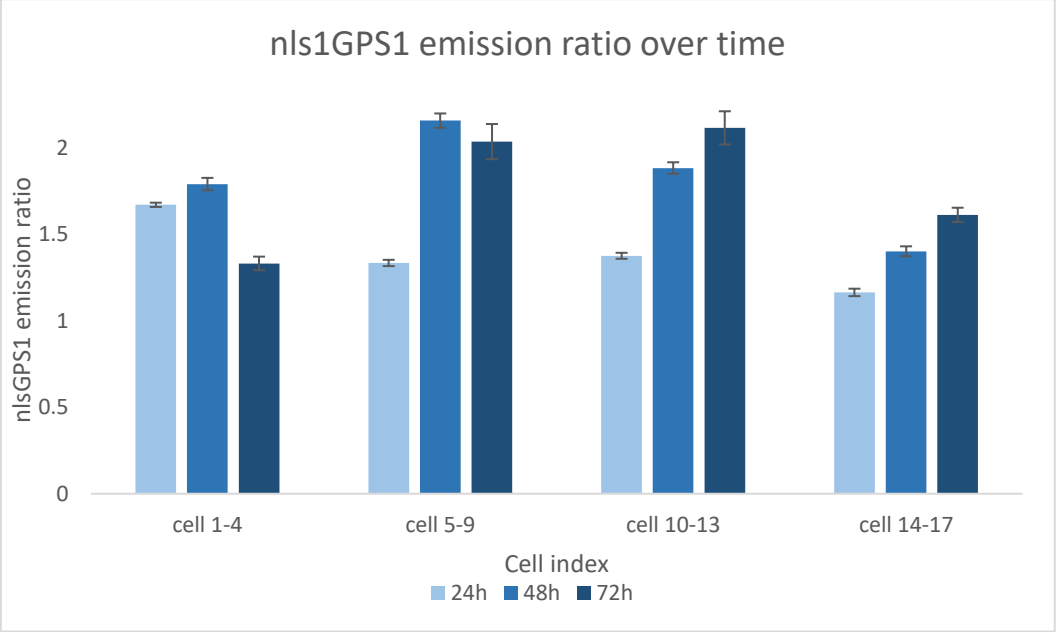

Figure 5.1 The GA emission ratio over time, for the hypocotyl region defined by the non-dividing file of basal (index1-4), lower middle (index 5-9), upper middle (index10-13) and top (index14-17) epidermal cells. The expression pattern of those cells changed over time, and the patterns were different depending on the hypocotyl region. (n>40 cells sampled, ANOVA test with F-statistic=55.44, p-value=5.21E-23 for the basal cells, F- statistic =186.94, p-value=3.34E-61 for the lower middle cells,

F- statistic =103.27, p-value=2.72E-38 for the upper middle cells, and F- statistic =47.71, p-value=1.35E-19 for the top cells)

The pattern of nlsGPS1 emission ratio over time was different in the four regions. In the basal cells and lower middle cells, the GA level went up at 48 HPG and down at 72 HPG, whereas in the upper middle and top cells it constantly went up over time (Fig 5.1). This pattern matched well with the cellular growth stage and the wave of growth (Chapter 1). The basal cells started to elongate before 24 HPG, and accelerated during 36 HPG and 48 HPG. By 72 HPG, their growth has stopped. The lower middle cells started their elongation after 24 HPG, rapidly expanded at 48 HPG and at 72 HPG, their growth was slowing down. The upper middle cells were growing very slowly in the beginning and did not expand rapidly until 72 HPG. The top cells grew very slowly in the beginning, and gradually speeded up in the first 72 HPG, but not yet reached their fast elongation stage by 72 HPG.

The average nlsGPS1 emission ratio for any region ranged between 1.16 and 2.15 (Fig. 5.1), which corresponded, respectively, to 'not expanding' (24 HPG, top cells) and 'rapidly expanding' (48 HPG, lower middle cells). Although the emission ratio was not linearly proportional to the amount of GA, a higher number implied a higher GA level[24]. These data indicate that bioactive GA was present in all cells, including the slow-growing upper cells, but relatively higher levels in rapidly-expanding cells. Among samples, small variation in nlsGPS1 emission ratio was observed, resulting in small standard errors (Fig. 5.1). Together with previous findings[24], these results suggested that the npsGPS1 emission ratio was a good indicator of GA level in the hypocotyl cells, and it was comparable among different hypocotyl regions, among different seedlings, and among different time points. These results also indicated a strong correlation between the bioactive GA level and the cellular growth state.

The GA level across the hypocotyl corresponds well with the local cellular growth rate

The pattern of nlsGPS1 emission ratio seemed to correlate with the acropetal growth wave position. To study precisely how bioactive GA level corresponded to the cellular growth, nls GPS1 emission ratio were compared with cellular growth rates described in Chapter 1. Three questions were addressed by comparing these datasets: 1) Does the GA level at distinct hypocotyl regions correspond well with the non-dividing epidermal cellular growth rate? 2) How long does it take before an effect in the growth rate was seen after the GA level changed? And 3) Does the GA level correspond to the relative growth rate or the absolute growth rate of the non-dividing hypocotyl epidermal cells?

Absolute and relative epidermal cell growth rates were plotted together with nlsGPS1 emission ratios, grouped by cell position index (Fig. 5.2, Fig. 5.3). At 24 HPG the hypocotyl cells were relatively small, and so the hypocotyls were divided into four regions (basal, lower middle, upper middle, and top) as before. At 48 HPG the hypocotyl cells were larger the hypocotyl could be divided into six regions, so a finer data resolution was gained. The nlsGPS1 emission ratio at 72 HPG was not plotted together with the growth rates, due to a lack of data of cellular size beyond 72 HPG.

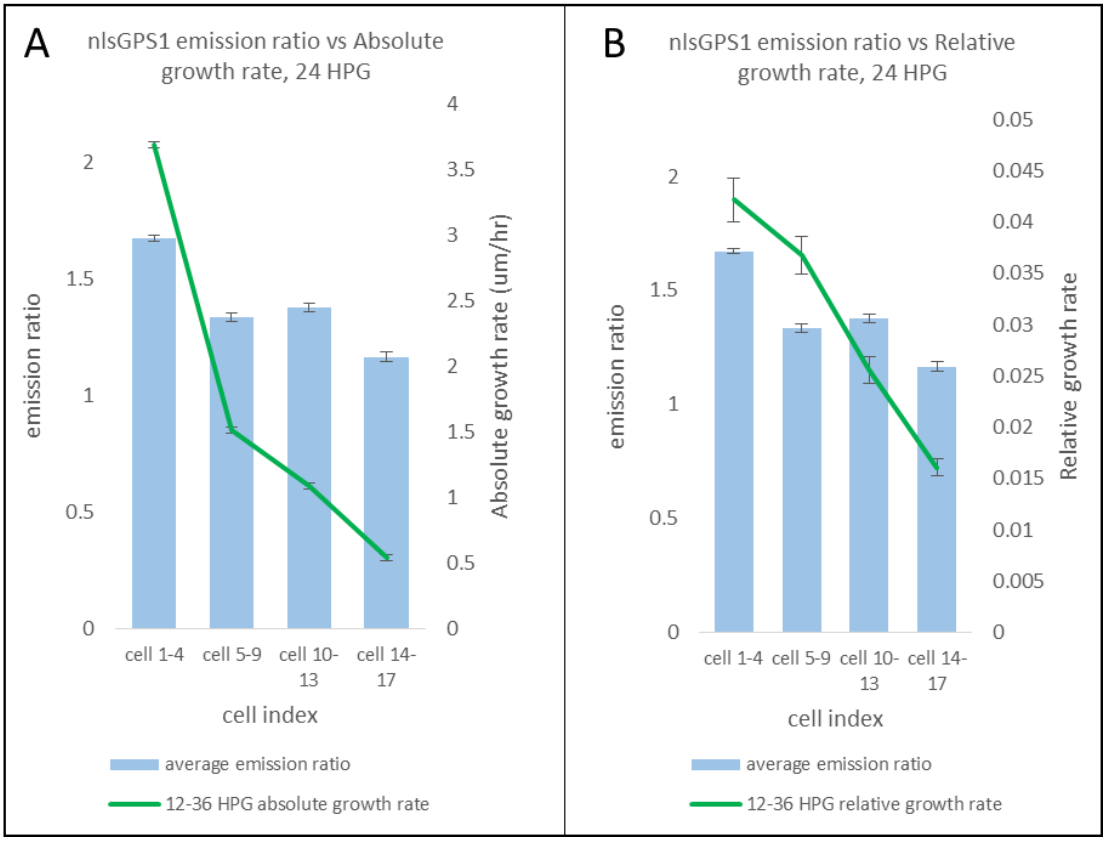

Figure 5.2 The nlsGPS1 emission ratio at 24 HPG, compared with the absolute cellular growth rates (A) and relative cellular growth rates (B), taken a 24 hour interval (12-36 HPG). The growth rate data (green line) calculated from the dataset used in Fig 1.10 (n>20 hypocotyls, n>34 cells per hypocotyl), and nlsGPS1 statistics is detailed in Fig. 5.1.

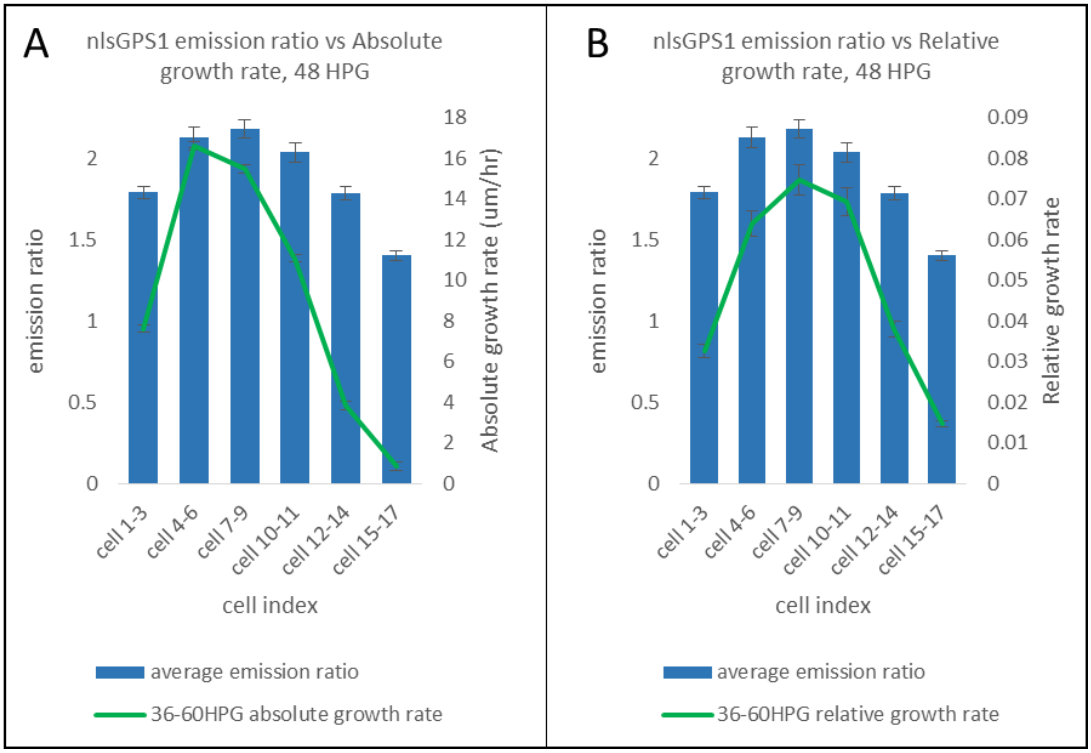

Figure 5.3 The nlsGPS1 emission ratio at 48 HPG, compared with the absolute cellular growth rates (A) and relative cellular growth rates (B), taken a 24 hour interval (36-60 HPG). The growth rate data (green line) calculated from the dataset used in Fig 1.10(n>20 hypocotyls, n>34 cells per hypocotyl), and nlsGPS1 statistics is detailed in Fig. 5.1.

The absolute growth rate and the relative growth rate were calculated from the same cell-level dataset described previously (Chapter 1) and hence the two are 100% correlated. In this context, both the absolute growth rate and the relative growth rate qualitatively correlated well with the nlsGPS1 emission ratio. At 24 HPG, the emission ratio was high at the basal cells (around 1.67±0.012), lower at the middle cells (around 1.35±0.018), and was very low at the top cells (around 1.16±0.022). From the lower middle cells to the upper middle cells, a decrease in the emission ratio was not seen (Fig. 5.2, Fig. 5.3, green lines). This matched well with the absolute growth rate: At 24 HPG, the basal cells were expanding fast, the middle cells were slowly growing, and the top cells were growing the slowest (Fig 5.2, blue bars). At 48 HPG, a wave-shaped nlsGPS1 emission ratio could be seen over cell index (Fig 5.3, blue bars), suggesting a distribution of the GA level peaked at the hypocotyl region with epidermal cells 7-9. This distribution did not correlate to the cellular sizes reported earlier[24] (See supplementary Fig S5.1), but rather, correlated well with the absolute and relative growth rates. Both the absolute and relative growth rates had a pattern matched well with the nlsGPS1 emission ratio, with the relative growth rate's pattern matched slightly better at cells with smaller indices (Fig. 5.3).

These data suggested that the GA level and the cellular growth rates were closely related, and both absolute and relative growth rate matched reasonably well with the pattern of GA level over hypocotyl. The relative growth rate was chosen to be used throughout the rest of this chapter, but it could be replaced with the absolute growth rate, without causing different conclusions.

GA appears to act as a precursor to growth, correlates with growth rates within 12 hour windows and correlation decays by 24 hours

In the previous section, GA level was shown to be closely qualitatively correlated to growth rates, yet it was still unclear whether this correlation suggested GA be the 'precursor' or the 'successor' to a change in the growth rate.

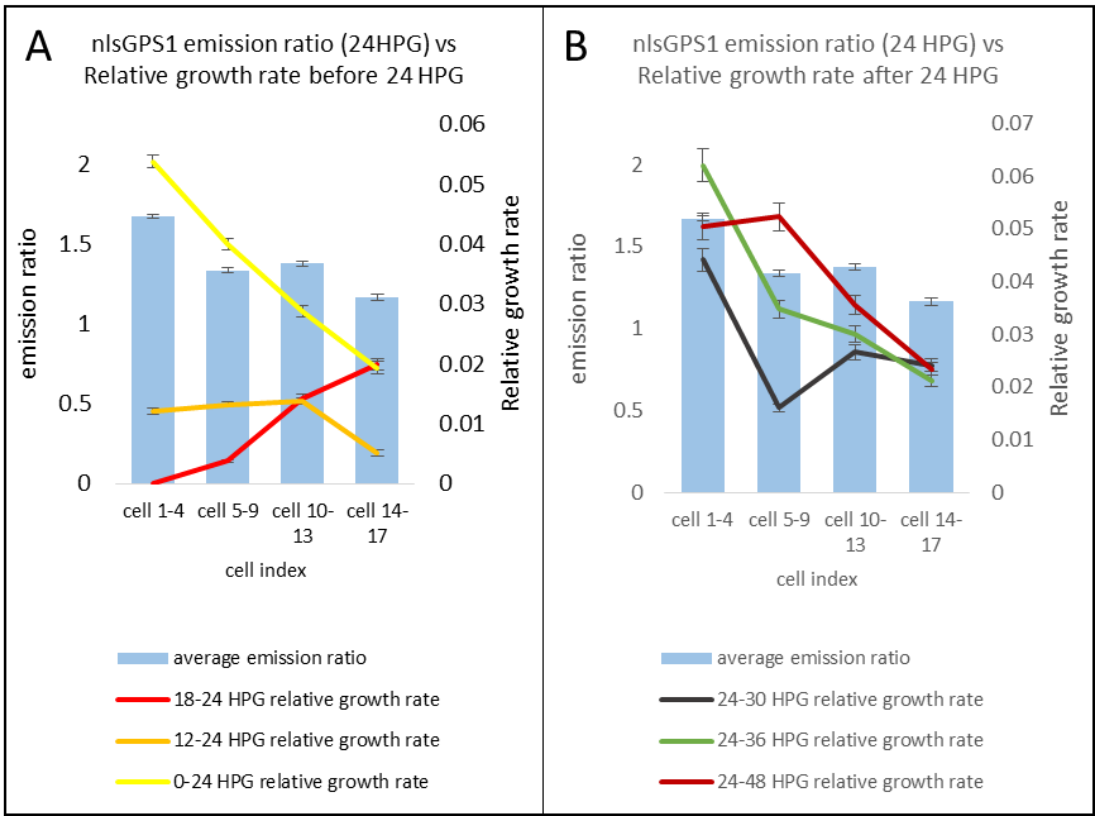

Figure 5.4 The nlsGPS1 emission ratio at 24 HPG, compared with the relative cellular growth rates before (A) and after (B) 24 HPG. (n>20 hypocotyls, n>34 cells per hypocotyl), and nlsGPS1 statistics is detailed in Fig. 5.1.

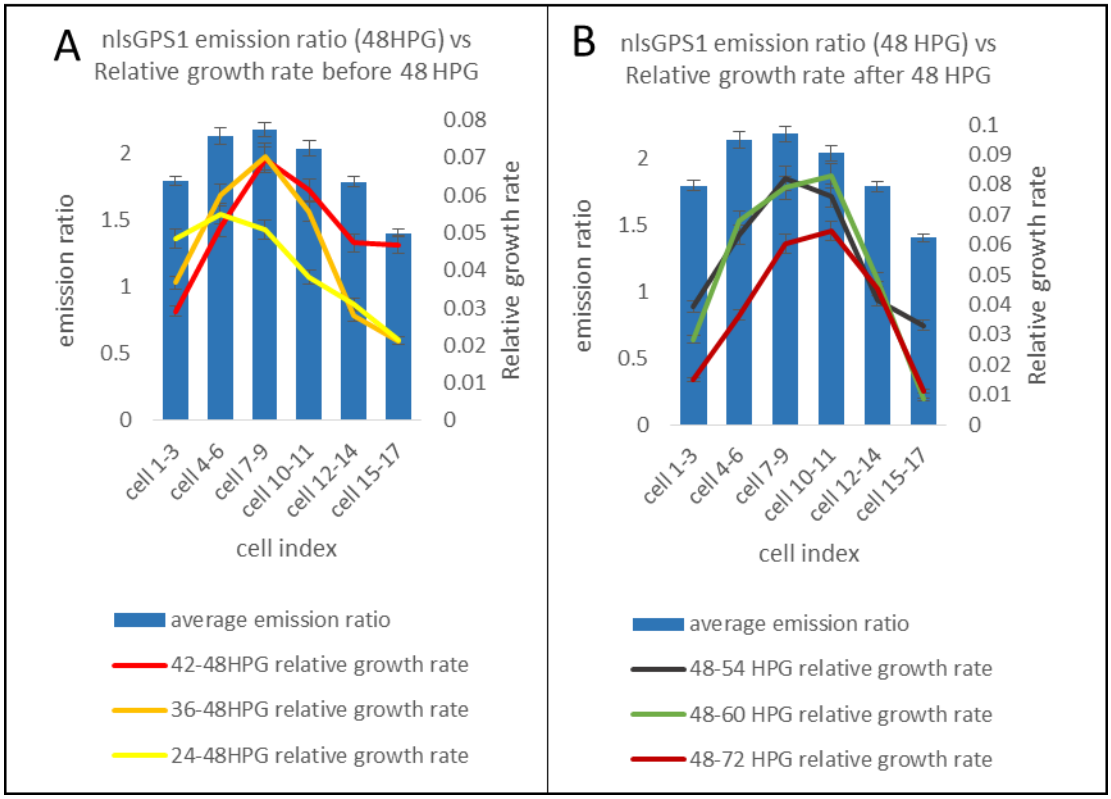

Figure 5.5 The nlsGPS1 emission ratio at 48 HPG, compared with the relative cellular growth rates before (A) and after (B) 48 HPG. (n>20 hypocotyls, n>34 cells per hypocotyl), and nlsGPS1 statistics is detailed in Fig. 5.1.

Fig. 5.4 and Fig. 5.5 compared the relative growth rate before and after the time when the nlsGPS1 emission ratio was measured, taken time interval of 6 hours, 12 hours and 24 hours. At 24 HPG, the cellular growth rate of 18-24 HPG and 12-24 HPG did not correlate well with the pattern of emission ratio, the cellular growth rate over the 24 hours period before (0-24 HPG) had a better-matched pattern, but that was more likely to be a coincidence due to the elongation of the basal or collet cells before 12 HPG. In contrast, the relative growth rate from 24 to 30 HPG and that from 24 to 36 HPG matched well with the pattern of the nlsGPS1 emission ratio. The relative growth rate from 24 to 48 HPG was not correlated with the pattern of the nlsGPS1 emission ratio (Fig. 5.4).

At 48 HPG, the cellular growth rate for windows starting 6 hours before and 12 hours before correlated well with the pattern of the nlsGPS1 emission ratio, as well as the cellular growth rate from 48-54 HPG (6 hours post). The relative growth rates at other time intervals did not matched as closely (Fig. 5.5).

The data from 24 HPG suggested that GA increase was unlikely to follow a growth rate increase yet the data from both 24 HPG and 48 HPG suggested that a change in growth rate might follow an increase in GA. The relative growth rate from the time point when the emission ratio was measured

until 6 hours after (24-30 HPG, and 48-54 HPG) had the best match with the pattern of the emission ratio overall.

It is not yet known how fast the nlsGPS1 sensor degrade, yet experience indicated that it is stable for at least 8 hours (A. Rizza, Jones lab, personal communication). Due to the resolution of the data, it was not possible to tell whether the measured nlsGPS1 emission ratio represented the GA level at the three time points (24, 48, 72 HPG), or since sometime earlier than the three time points (e.g. the emission ratio measured at 48 HPG reflected the GA level at 48 HPG, but might also be the GA level as early as 30 HPG). The 24-30 HPG and 48-54 HPG relative growth rates suggested that the time needed for a GA increase to affect growth rate could be as short as 6 hours; the relative growth rate at 36-48 HPG also matched well with the emission ratio, indicating that the maximum time took for the GA to affect the growth rate was 12 hours (assuming the extreme, the measured emission ratio at 48 HPG reflected the GA level at 24 HPG), but most likely a lot shorter than that. The effect of current GA level on cellular growth rate appeared to last less than 24 hours, as none of the emission ratios correlated well with the growth rate 24 hours away from when it was measured.

The GA level had the closest match with the cellular relative growth rate in the interval from 6 hours before to 6 hours after its measurement

It was shown that the nlsGPS1 had similar patterns with the local epidermal cell growth rates. The GA rapidly affected the cellular growth rates (around 6-12 hours) and its effect lasted less than 24 hours. Based on this, the emission ratio was plotted again, with the epidermal cellular growth rates on the secondary axis to find the time interval which the cellular relative growth rates had the closest match with the GA levels across the hypocotyl.

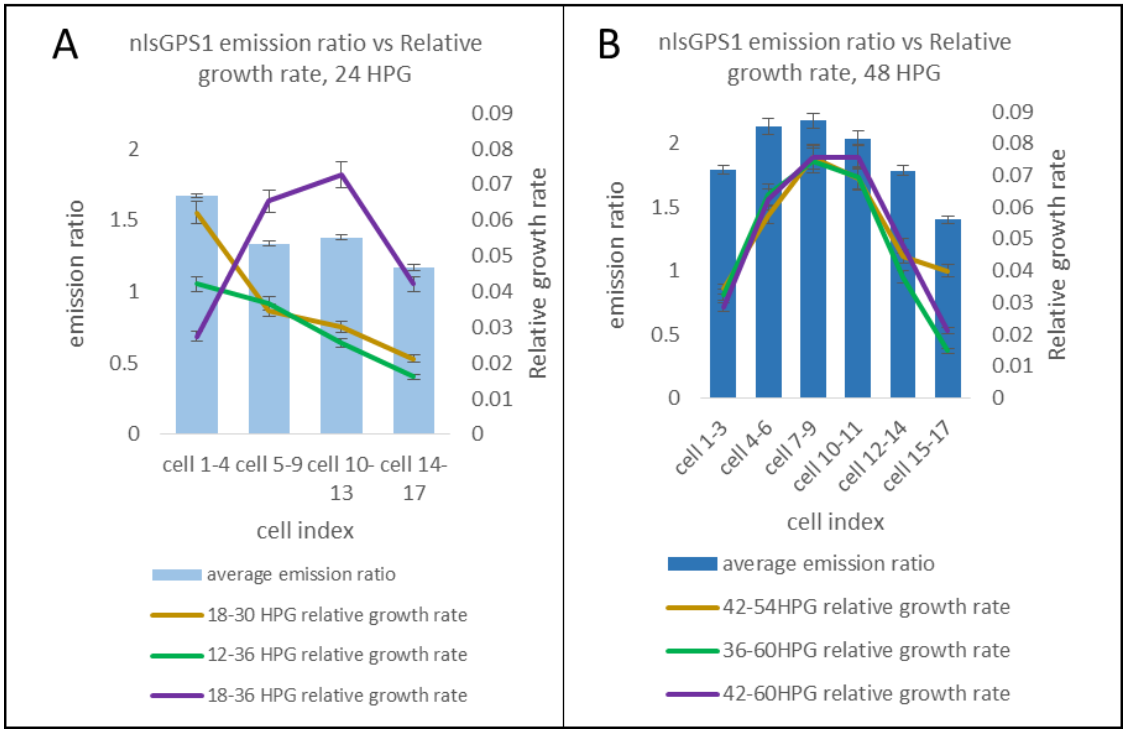

Figure 5.6 The nlsGPS1 emission ratio at 24 and 48 HPG, compared with the relative cellular growth rates in the interval of 12 hours, 24 hours and 18 hours around the time when nlsGPS1 was measured.

At 24 HPG, the relative growth rates at 18-30 HPG and 12-36 HPG both had patterns which correlated well with the nlsGPS1 emission ratio. The 18-36 HPG had a very different pattern, suggesting that during 30-36 HPG, the pattern of epidermal cellular relative growth rate across the hypocotyl was very different from the pattern of GA level acquired at 24 HPG. (n>20 hypocotyls, n>34 cells per hypocotyl), and nlsGPS1 statistics is detailed in Fig. 5.1.

At 48 HPG, all three relative growth rates at different intervals had a well-matched pattern with the GA level. However, the 42-60 HPG relative growth rate seemed to have a mismatch at cell 10-11; it was similar with the growth rate of cell 7-9 but the nlsGPS1 emission ratios of those cells were lower than that of cells 7-9.

The GA level at 48 HPG in cells 7-9 and 10-11 gave an interesting story when studied together with the relative growth rate taken from the three intervals. Cells 7-9 had higher relative growth rate if the interval 42-54 HPG was considered (Fig. 5.6B, brown line). However, cells with indices 7-9 had about the same relative growth rate with cells 10-11 if the interval 42-60 HPG was considered (Fig. 5.6B purple line). Because fast elongation of cells 10-11 started around 54 HPG, the 42-60 HPG window included that period and resulted in a larger relative growth rate. Yet if 36-60 HPG was considered the increased growth rate was no longer observed. That does not mean the relative growth rate during 36-60 HPG gave a better representation of the GA level at 48 HPG, but rather because those cells were

growing too slowly between 36-42 HPG, the effect of their fast elongation during 54-60 HPG on the overall relative growth rate was balanced out.

Taking all these together, these result suggested that 6 hours after the measurement of the nlsGPS1 emission ratio, the cellular relative growth rate no longer correlated with the measured GA level. Hence to correlate the GA level with the growth rate, a time interval of no more than 12 hours for the growth rate should be selected. For these data, the resolution was taken at a time interval of 6 hours, and relative cellular growth rate 6 hours before and after the measurement of nlsGPS1 emission ratio had the closest match with the pattern of nlsGPS1 emission ratio. It was concluded that cell-level growth rate responded within a 12 hour window to increased GA level.

Fast growing regions of dark-grown hypocotyls share common gene expression profiles with seeds at germination

Germination and hypocotyl elongation are both plant developmental processes that happen early in time, when growth of organ (increase in size) happens fast. 230 genes were considered to be up-regulated after treatment of the GA biosynthesis mutant *ga1-3* with GA_4 at germination and 127 genes were considered to be down-regulated[23]. In order to examine the genes shared by hypocotyl elongation and germination, these genes were compared to our dataset (Chapter 4). Below is a table with the number of common genes with the dataset we acquired. The number of genes in List 1, List 2 and List 3(List 1=More expressed in the bottom at 24 HPG, List 2=More expressed in the bottom at 36 HPG and List 3=More expressed in the bottom at 48 HPG) were coloured in orange.

Number of common genes	Up-regulated by GA	Down regulated by GA
24 HPG higher at bottom	60	22
36 HPG higher at bottom	93	32
48 HPG higher at bottom	86	39
24 HPG higher at top	33	11
36 HPG higher at top	48	8
48 HPG higher at top	55	11

Table 5.1 Number of common genes between different groups. Each row represents a list of genes from the RNA-seq experiment in Chapter 2, intersects with GA up/down regulated genes from Ogawa[23]. The list of genes to be studied further were coloured in orange.

Not surprisingly, the genes that were more expressed at the bottom region had the highest number of common genes when intersecting with genes that were up-regulated by GA (Table 5.1, number coloured in orange). This result supported the conclusion that GA, as well as the genes that were up-regulated by GA, was more active in the fast-growing region of the hypocotyl. Of the three lists, List 2 had 93, which was the most number of common genes with the list of GA-up-regulated genes at germination[23], followed by List 3, which had 86, and then List 1, which had 60. From this it could be concluded that the genes expressed at the bottom region at 36 HPG and 48 HPG were more similar to those genes up-regulated by GA during germination, and those at 24 HPG were not as similar, although the time was closer to the time of germination. To investigate further the biological processes of those genes, the ontology of those genes (union of the three lists) was examined using Agrigo[246].

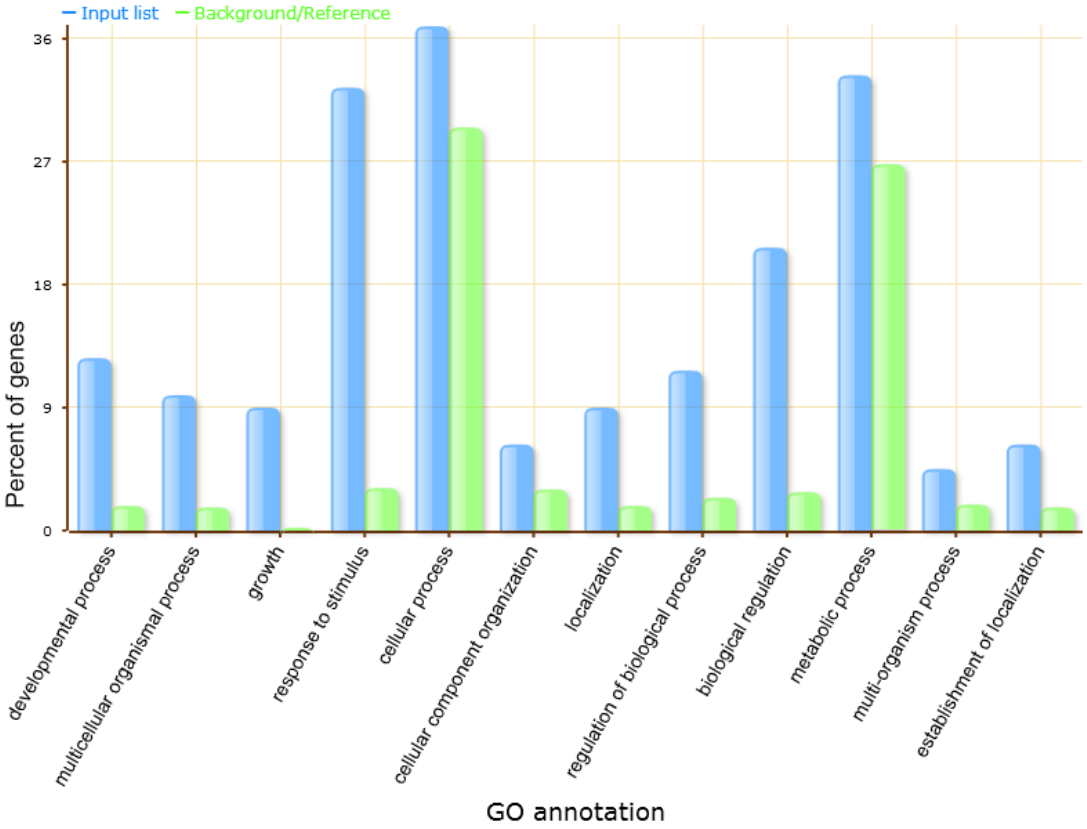

Figure 5.7 The biological processes of union of List 1, List 2 and List 3, representing genes that were both more expressed in the bottom region and up-regulated by GA, against the expected number.

Several biological processes of genes were enriched in the list of genes that were both more expressed in the hypocotyl bottom regions and up-regulated by GA treatment during germination[23]: Developmental process, growth, cellular process and cellular component organization were over-represented, and these processes might be involved in promoting the cellular growth. There was also

a very significant overrepresentation in 'response to stimulus', which might be expected since all those genes were up-regulated by the treatment of GA, a stimulus. Many of the biological processes were related to response to stimulus, such as hormone, water, and lipid. The rest of the biological processes could be good indicators of how GA was impacting growth at the transcriptome level. These include: defence response, cell wall modifications, wall thickening, wall loosening, indoleacetic acid biosynthetic and metabolic processes, glucosinolate biosynthetic and metabolic processes, tryptophan metabolic process, toxin metabolic process and pectin metabolic process.

DISCUSSION

The level of GA is a good indicator of cellular growth rates

This chapter aimed to find a 'chemical signal' controlling hypocotyl cell growth, and evidence suggests that GA is a good candidate. The results of nlsGPS1 emission ratio suggested a close relationship between the hypocotyl non-dividing epidermal cellular growth rate and the bioactive GA level in the region defined by those cells. The effect of dividing cells and cortical cells may not be subversive since they sit in the same region and they would have about the same net absolute growth rates with those epidermal cells. The nlsGPS1 is a powerful tool for studying the level of GA, having a positive (although non-linear) relation with the cellular/organ GA level. The value of the emission ratio is comparable among cells at different positions as well as seedlings/cells at different times. Despite the fact that the degradation time of the sensor is unknown, a more accurate answer to the question: 'how fast the cellular growth rate response to a change in the GA level' can be gained by increasing the experimental resolution.

The experimental data was subject to some limitations. In the experiment, the GA level at each hypocotyl region was represented by the average nlsGPS1 emission ratio for all the cells in the defined region of the hypocotyl. So it included signals from the non-dividing epidermal cells, the dividing epidermal cells, as well as some of the cortical cells. Ideally, only the nlsGPS1 emission ratio for the epidermal cells should be used, and a finer experimental resolution should be used, to match the epidermal cell growth data (Chapter 1, Fig. 1.10, Fig. 1.13, Chapter 5, Fig. 5.2-5.5). Previously it was found that the nlsGPS1 emission ratio had a positive correlation with the cellular size at 3 days post incubation (cold treatment)[24] implying the non-dividing cells have a higher GA level than the dividing cells (See supplementary Fig S5.2). I believe if only the data for non-dividing epidermal cells were used, the difference of the nlsGPS1 emission ratio between fast-growing and slow-growing cells would be exaggerated.

The level of GA is found to be closely related to the local absolute/relative cellular growth rate. But it is not sufficient to conclude that GA is the precursor to growth. Mechanistically, GA suppresses the activity of DELLA protein and promotes the growth[148][23][170][159]. Walia (Jones Lab, SLCU, personal communication) found that in light-grown seedlings, the level of GA was changed after 1-2 hours of treatment, and changes in cellular growth rates were observed after 5-6 hours of GA treatment. So the level of GA is more likely to be a precursor to the cellular growth rate, and its effect on the cellular growth rate happens very quickly.

In conclusion, the level of GA, given by the emission ratio of the nlsGPS1, can be used as an indicator of the cellular growth rate within a short time (within 6 hours).

Activities of GA responsive genes in the hypocotyl

In the first part of this chapter, I have shown that the cellular bioactive GA level corresponded well with the cellular growth rate, this made GA a strong candidate controlling the growth, including growth initiation, growth rate, and growth termination. This was then supported at the transcriptome level, where I studied and compared how many genes that responded to the GA treatment and resulting germination in the *ga1-3* mutant[23] (up-regulated or down-regulated) coincident with genes that were more/less expressed in the fast-growing region of the hypocotyl. The comparison was made between two very different experiments, as the up/down-regulated genes were identified after treatment of imbibed seeds with 50 µM GA, whereas the more/less expressed genes were identified using faster and slower growing regions of the hypocotyl without the GA treatment. Hence the two experiments were not directly comparable but their intersection was a good representation of genes that respond to GA and induce germination-growth as well as being highly expressed in the fast-growing region.

The analysis shows that among all the possible groups, the genes that are more expressed in the bottom region at 36 HPG and 48 HPG (but not 24HPG) are the most similar with the group of GA-up-regulated genes, which means the genes that are up-regulated by GA tend to be more expressed in the growing regions of the hypocotyl. This provides further support to the idea that the growth rate is closely associated with the GA level, as we know the dark-grown hypocotyl elongates rapidly at 36 HPG and 48 HPG, but not at 24 HPG. These pieces of evidence together, indicates that 1) The presence of GA is essential for the rapid cellular growth, 2) GA controls the growth directly or indirectly by regulating the GA-responsive genes, 3) At germination, there is not much bioactive GAs in the hypocotyl, and 4) Many of the GA responsive genes can be turned on at germination if GA is supplied.

Ontology of those GA-responsive genes provided further information about possible mechanisms on how GA is involved in the enlargement of plant cells.

Is GA the 'chemical signal' regulating the growth?

In this chapter, I have first shown that the bioactive GA level corresponded well with the cellular growth rate by quantifying the nlsGPS1 emission ratio and comparing against absolute/relative cellular growth rate. This was a strong indicator of GA might be acting as the chemical signal triggering and terminating the cellular growth. However, it was not clear through what mechanism the level of GA was transferred to the cellular growth rate. So I picked up a list of genes that were up-regulated by GA as well as being more active in the fast-growing region of the hypocotyl, and the ontology of those genes indicated biological processes related to growth that are triggered by the GA. I concluded that GA initiated the cellular growth and controlled the growth rate, through a number of different biological processes, including cell wall modification, loosening and thickening, indoleacetic acid biosynthesis and metabolic, glucosinolate biosynthetic and metabolite, and pectin metabolic processes.

Even though the GA was found to be correlated to cell growth rates, it is not sufficient to say that the level of bioactive GA is the determine factor for cell growth rates. DELLA proteins suppress plant growth[252] and GA acts as a suppressor of DELLA[253][254]. Therefore, a mutant without DELLA should have no growth response to GA levels, but such mutant still have heterogeneous hypocotyl cell sizes, indicating that GA/DELLA are not the deterministic factor of regional hypocotyl growth (Siobhan Braybrook, UCLA, personal communication, Fig. S5.3). The wave of cellular growth and the heterogeneous growth of epidermal cells may be controlled otherwise, or predetermined.

The level of GA was originally brought into attention because one of the key results of Chapter 2 suggests that a chemical signal is likely to exist, which controls the growth and correlates well with the growth rates. So is GA the ultimate piece that was missing from the cellular model in Chapter 2? The answer is yes and no. Being a very good indicator of the growth rate, a better performance of the model is expected if the level of GA is fed into the model as an input. However, this is against the original purpose of the model: an intrinsic approach with only physical parameters. Further, the dynamic change of the GA level may result in changes in the wall structure and other cell wall properties, and hence the bond energy distribution function. As discussed in Chapter 2, the simulated growth is very sensitive to changes in the bond energy distribution. Without a clear idea how the change in GA is affecting other parameters in the model such as this distribution, directly using the GA

level as an input is improper. In this chapter, I have found GA to be a potential candidate for the 'chemical signal', raised in Chapter 2. But it is still not clear whether the level of GA is definitely a precursor or can just be an indicator of growth in plant cells. In fact, the chemical signal is likely to be a combination of multiple hormones, such as auxin, brassinosteroids, etc., providing room for future investigations.

CHAPTER 6: FINAL DISCUSSIONS

The anisotropic growth of hypocotyl cells

In the dark, hypocotyl cells expand anisotropically[1]. Compared to the diameter, the length of epidermal cells increases at much faster rates. The acropetal wave of growth was only observed in epidermal cell length, but not in diameter (Chapter 1). The anisotropic growth of cells was studied in our previous paper[7], and it was shown that the anisotropic growth started at the beginning of hypocotyl elongation, with contributions from both cellulose microfibril and pectin chemistry. Anisotropic growth is an interesting feature and it has not been well addressed in this thesis. The intrinsic model focused on volumetric expansion of cells over time, with the assumptions that the modelled cells grow anisotropically (Chapter 2). The empirical model only used cell length as input and ignored the variation in cell diameter (Chapter 3). And other two chapters were not relevant to anisotropic growth.

The models did not include anisotropy for simplicity, which did not limit the main conclusions of the models to be made. In the future, if growth and deformation of cell growth is modelled in 3-dimension, anisotropy should be included. However, when the transition from cell growth to organ growth is studied, anisotropic growth needs to be addressed carefully. In this thesis, it is assumed that the combined effect of cellular wave of elongation dictates the pattern of organ elongation. This is true if only length is considered; but the relationship between cell diameter and organ diameter is not as straight forward. Unlike length, organ diameter may not be a direct reflection of cell diameter. One cannot approximate the behaviour of hypocotyl diameter based on cell diameter, without knowledge of the number of cells present in the cross-section. For example. at 48 HPG, the PMEI over-expressor has the same basal cell diameter, but more epidermal cells were found at the hypocotyl circumference, giving a thicker hypocotyl (F. Bou Daher, Braybrook Lab, UCLA, personal communication)

The sigmoidal growth curves from plant cells to plant organs

It was shown previously that both hypocotyl cell growth (Chapter 2) and organ growth (Chapter 3) possess sigmoidal growth curves. This sigmoidal growth of plant organs is normally divided into three sub phases: an early acceleration phase, a linear phase, and a saturation phase, and are modelled widely[19][77][20][21].

The sigmoidal curve of growth of hypocotyl epidermal cells has very different shape from that of the organ growth, and the mechanism behind cell and organ growth is also different, although organ growth can be quantified as the sum of cell growth. Cellular growth curves are smoother at the initial accelerating phase, and can be well captured by classic, symmetric sigmoidal functions such as the Logistic and Probit (Chapter 3). At the cellular level, growth is initiated by growth signal, wall loosening and remodelling[7]; these processes do not happen instantly, and they gradually build up the cellular growth rates. This gradual, smooth cellular growth rate acceleration was captured in the intrinsic model (Chapter 2) where only physical factors were considered. Growth termination at the cellular level is likely due to a combination of growth signals and cell wall modifications. Inner wall microtubules become longitudinally aligned when cell growth stops (Chapter 1), and the level of GA seems to be reduced when cell growth slows down.

Compared to the cellular growth curves, organ growth curves typically have a sharp accelerating phase followed by a long-period linear phase (Chapter 1, Chapter 3). The period of hypocotyl growth (typically 7-8 days) is much longer than the period of an individual epidermal cell growth(around 2-3 days, depending on cell position), which makes the growth curve seem to have a sharp start at the accelerating phase. Later, the acropetal wave means that the upper cells grow longer, with faster absolute growth rates (Chapter 1, Chapter 3), but the elongation rate of hypocotyl tends to remain quite linear until slowing down. How hypocotyls maintain a long period of linear growing phase is still unclear. Since the acropetal wave of growth with increasing magnitude over time (Chapter 1), I hypothesise that the number of growing epidermal cells decrease over time: At the beginning, when the wave sits at the basal cells, more cells grow simultaneously, but with lower absolute growth rates; later, when the wave sits at top cells, less cells grow at the same time, but their absolute growth rates are much higher. Together, they achieve a relatively stable (linear) growth rate at the organ level. One possibility of this might be the constraint on each cell's relative growth rate. Upper cells have larger sizes before their fast elongation phases, and so an aimed absolute growth rate can be achieved with lower relative growth rates. Basal cells have smaller sizes when they are about to grow rapidly, and more cells are needed to achieve certain net absolute growth rate.

The sigmoidal growth curve is widely seen in plants, but the detailed mechanism, coordination and correlation of cellular sigmoidal growth and organ sigmoidal growth is complex in the hypocotyl system. Overall, the sigmoidal growth at the cellular level is controlled by a number of factors, including cell wall properties and growth signal. Whereas the linear growth rate at the organ level may be the fastest possible growth rate that can be achieved by the hypocotyl, through complex cellular coordination.

Heterogeneous growth of the epidermal cells

Why is there a heterogeneity in the growth of hypocotyl epidermal cells? The heterogeneity was seen in cell growth starting time, growth period and growth rate. The non-dividing epidermal cells represents the regional hypocotyl growth, and the heterogeneity should be considered at the organ level. Evidence (Chapter 1, position of the wave, Chapter 3, linearity of parameter *c*) suggested that if there is a moving growth signal as proposed in Chapter 5, this signal is likely to travel linearly upwards along the hypocotyl. If we make a further assumption that there is a fixed-size window of this signal in the hypocotyl, this explains the heterogeneity in the epidermal cell growth: Basal cells start the rapid growing phase early with smaller size, so more of them grow together within the window of growth signal; Upper cells start the rapid growing phase later with larger size, so they can remain in the window of growth signal for longer period of time, but less number of cells elongate simultaneously. This, as a result, causes the cellular heterogeneity we observed, as well as a relatively stable organ level growth rate over time.

Function of cell wall modification enzymes

Cell wall remodelling and modifications in pectin chemistry are crucial processes controlling the growth and anisotropy of plant cells[7]. (Chapter 1, Chapter 2). Specifically, cellulose microfibrils, hemicellulose and pectin are studied and discussed in this thesis, together with relevant genes and proteins (CESA, XXT, XTH, PME/PMEI).

Cellulose orientation controls cellular growth anisotropy[3][7]; cells with disturbance in cellulose synthesis cannot maintain their anisotropy (Fig. S1.3, S1.4). Cellulose is hence a necessary component for a healthy plant cell to grow; it may also be involved in controlling growth termination, as the inner wall microtubules (a proxy for cellulose) become longitudinally oriented when cell growth slows down (Chapter 1).

The inducible PME5 and PMEI3 over-expressors have been used for pectin chemistry modifications[92][7][9]. It was believed that the PME5 over-expressor gave a relatively stiffer cell wall, slower cellular/hypocotyl growth rates and shorter cellular/hypocotyl final length[7] (Chapter 2). However, almost all the hypocotyl expressed *PME* genes were more expressed in the faster growing region (Chapter 4), which contradicted our intuition of the *PME*'s expression pattern. Interestingly, the only *PME* gene with an opposite expression pattern with all other *PME*s happened to be the *PME5*. Is it a coincidence? In Chapter 4, it was concluded that the high expression level of *PME*s probably did not translate to active and functional PME proteins. Hence highly expressed PMEs might not lead to

stiffer cell walls, but rather fast processes of cell wall modification. Recently it was shown that the Homogalacturonan (HG) de-methylesterfication by PME activities can have stiffening (formation of calcium cross links)or softening (degradation by polygalacturonases) effects on the cell wall[220], probably depending on the pattern of de-methylation. Therefore, another possibility is that many of the PMEs in fact function in softening the cell wall and promoting growth, as supported by their expression patterns. The fact that PME can play two roles in cell wall properties means that we cannot simply link PME and PMEI to a function in cell wall stiffness, but the environmental conditions need to be considered since the activity of these proteins has also been shown to depend on the pH[34].

Xyloglucan, a major hemicellulose in the plant cell wall[255], appears to take less substantial role in growth of plant cells. The xyloglucan endotransglycosylase/hydrolase was studied and it was found that with induced XTH, no phenotype was seen on hypocotyl in the first 72 HPG, and later, longer hypocotyl was caused by two induced XTH genes at 5 and 7 days post germination. It seems that XTH activities may promote growth rate but with only limited effect. There are four possible explanations. 1) the overexpressed *XTHs* did not produce active XTHs at early time. If the proteins were not translated or the translated protein were not active, then no phenotype on hypocotyl growth would be seen. 2) XTH changes the cell wall properties but does not significantly affects the hypocotyl growth. As found by Miedes[85], overexpression of XTHs result in more extensible cell wall, whilst the hypocotyl was not significantly longer. The phenotype in length was only observed when hypocotyl became very long. 3) the XTHs are not important in the plant elongation rate. This is possible, as the double mutant *xxt1,2* was deficient in xyloglucan, but the hypocotyl growth was just slightly slower, with a reduced final length of 22%[242][47], indicating that the xyloglucan may not be playing an indispensable role in the elongation of hypocotyl cells. XTHs modifies the linkages of xyloglucan and it may be negligible in cell elongation. 4) only certain amount of XTH is needed, extra XTH is not functional. According to our transcriptome data, all *XTHs* were highly expressed in the growing region of the hypocotyl during fast elongation period. XTHs modify linkages among xyloglucan so its presence might be essential when a cell grows fast and wall remodelling happens fast. Extra XTH does not add load-bearing bonds to the cell wall and hence has limited effect on wall properties. Even if extra XTH loosens the wall further but then limiting factors of the growth rate may be others such as the hormone level or the rate of wall material deposition. So overexpressing XTH may have insignificant effect on cell growth rate. This is quite likely, as previously it was shown that a 14% reduction in the level of XTH18 mRNA by RNA interference could lead to significant growth inhibition in the *Arabidopsis* roots[256].

Can we build a perfect intrinsic model of plant cell growth?

In Chapter 2, an intrinsic model describing the growth of plant cell was built based on our knowledge of physical factors involved in cell enlargement. The model enhanced our understanding of growth mechanism of plant cells, but the two biggest limitations to the model are 1) Many parameters were introduced with physical meanings, yet unmeasurable. As a result, the model outputs arbitrary units and the mean square error (a common measurement of error between prediction and data) is no longer an appropriate method to validate the model. In other words, the model can be used to imply growth mechanisms but no quantitative evaluation can be applied on its simulation when real data is available. 2) The model does not have a quantitative 'growth signal', or 'chemical signal', which may be even a more deterministic factor in cellular growth and growth rate compared to the physical factors. Transcriptome analyses (Chapter 4) and the nlsGPS1 emission ratio (Chapter 5) supports that these chemical factors are associated with the cellular growth, and I believe that a 'perfect' growth model can never be built without including these chemical factors.

Both limitations are difficult to be addressed. If a 'perfect' model is aimed to describe growth of cells, more parameters need to be included, and accurate measurements of all these parameters are almost impossible to be achieved. Also, our current knowledge of the chemical signal and chemistry involved in cell expansion, as well as how they are related to growth rate, growth initiation and growth termination is still very shallow. Apart from the understanding of basic physical factors and chemical factors, more solid knowledge in cell wall structure and pectin biochemistry are also essential in order to build a 'perfect' model.

Although building a perfect model seems to be quite impossible at the moment, models are never aimed to be built perfectly. No perfect model exist and 'All models are wrong' (George Box). The purpose of modelling is always to help understand, to predict, but not to be accurate in all details. Different modelling techniques were tried in this thesis (intrinsic, empirical, a machine learning model, see next section); none was perfect but they all helped me to understand and picture some aspect of growth of plant/plant cells.

The chemical signal revisited

In Chapter 2, it was found that cell growth was not able to be explained fully only with physical factors. It was proposed that a more quantitative study of the chemical signal 'S' in the cell growth model would compensate some of the issues of the model. Later, the empirical modelling in Chapter 3 as well as studies in Chapter 4 and 5 all indicated that there exists a global control of the cell growth

within the hypocotyl. Hormones are likely candidates to this chemical signal. But what really is this chemical signal? In the original proposal, it controls the starting and termination of growth, and it also relates to rate of wall material synthesis/deposition, and rate where turgor pressure builds up (through depositing more dissolved ion inside the cell). However, it was shown that the wall thickening process happens before rapid growing phase of cells, and does not correlate with the cellular growth rate[117]. Simulations in Chapter 2 as well as evidence[11] suggested that the turgor might not act as the growth rate controller, instead, controlling the growth rate via modifying the cell wall might be a more effective and efficient way for plants. Therefore, there is no one thing called 'growth signal' which, on its own, controls the starting termination of cell growth, as well as wall material synthesis and ion deposition. Rather, it might be a complex chain of chemical processes. For the purpose of improving the cellular model, a hormone (e.g. GA) is a more appropriate substitution for the growth signal.

How can we 'squeeze' the most out of our current data?

'One can have data without information, but one cannot have information without data' (Daniel Keys). Data is a core element in scientific research. Progresses in many research questions often sits on progresses in data acquisition, from the function of a single protein to the theory of quantum gravity. Recently, boost in technology allowed many biological questions to be answered. High throughput genome wide screening and microarrays allowed function and expression of genes to be studied and compared[257]. Research in proteomics and metabolomics are also benefiting from latest methodologies and technologies such as the localization of organelle proteins by isotope tagging (LOPIT)[258], mass spectrometry and advanced fluorescence microscopy techniques (e.g. fluorescence localization after photobleaching, FRAP; Forster fluorescence resonance energy transfer, FRET)[259]. However, the availability of data often acts as a limiting factor in scientific researches, and squeezing more information out from the available data would often be a less expensive way to generate new information.

The empirical model in Chapter 3 is an example. Data up to 72 HPG were used to predict behaviours of cells from 72 HPG to 192 HPG, where data were unavailable due to technical issues. Previously, various population models and crop growth models were developed[19], but only used to fit data, not to predict future behaviours. This idea opens up a new way to 'extend' our current data, by extracting the hidden information of how epidermal cell length patterning over time, along the acropetal wave. This information was originally not visible and hard to quantify.

Machine learning is also a rapidly developing field, and it is capable of solving many biological problems. Microscopy images from high-content screening can be used for automatic phenotype recognition[260]. Content-aware image restoration can be used 3d surface projection restoration and denoising in fluorescence microscopy[261], which may potentially be applied on our microtubule images taken by the confocal microscope, and reduce the noise from inner epidermis wall/cortical cell wall. Convolution neural networks can be also used for detection and segmentation in microscopy images as well as 3D microscopy image stacks (presented by Microsoft Research), which can be applied in biomedical images and assist doctor's decisions (e.g. Tumour location & volume). Transfer learning can be applied when number of data are limited and synthetic data are used in supervised deep learning[262].

A small project was conducted using data acquired by G.Arsuffi (SLCU) on area prediction of *Marchantia*. Size of *Marchantia* was studied under different growth conditions (see Table 6.1, 6.2): A dataset of 2300 plants were randomly split into training set (80%) and test set (20%), and the aim of the project was to predict the area based on the inputted growth conditions. Two models were built: a simple linear regression model and a 3-layer densely connected neural network model. The linear regression was fast, with a total training time of 0.037 seconds, and a mean average error of 35.89 mm^2(Fig. 6.1A). On the other hand, the densely connected neural network took 41.8 seconds to be trained, but gave a smaller mean average error of 29.87 mm^2(Fig. 6.1B).

Plant number	Medium	B5 Vitamin	Sucrose	Photoperiod	Light Intensity
1-2300	MS or GB	Yes or No	Yes or No	Light/Dark or Light/Light	55, 75 or 150

Table 6.1 Features of the input table, where plant number is the index and the rest 5 are features

Plant number	Area (mm^2)
1-2300	Range from 25 to 280

Table 6.2 Label of the input table, Area is the label

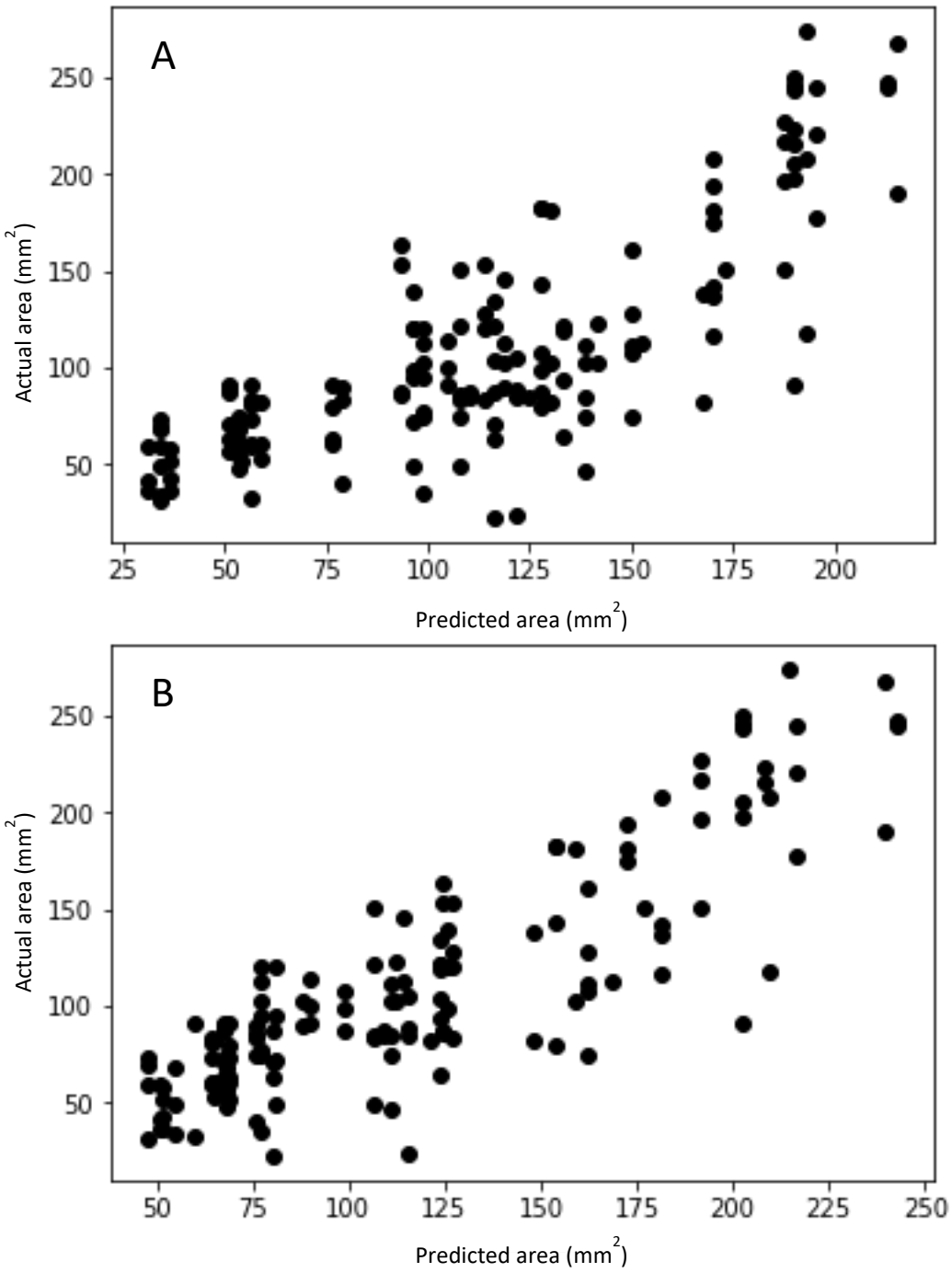

Figure 6.1 The predicted area vs actual area of *Marchantia* in different growth conditions

Application of machine learning on biological data is a fast developing area. When big data is not available, sometimes simple regression or small neural networks can be considered. Other times, transfer learning or partially reuse pre-trained neural networks may also be possible. Machine learning algorithms are sometimes a lot better than human in recognizing and extracting patterns hidden in

datasets, and I believe that benefiting from the fast-processing machines nowadays, solving biological problems can be assisted by correctly understanding, using and squeezing our datasets.

Further questions

Many aspects involved in growth mechanisms of the hypocotyl and plant cells are still not clear. For example, where is growth signal starting? Where is anisotropy coming from? These questions need to be addressed in the future.

PME and PMEI are widely used as pectin modification proteins, but how they change pectin and their environmental dependency such as pH is well classified. In the future, a more detailed study on each of the PME/PMEI family member would promote our understanding and ease our control on cell growth. At the same time, although the role of XTH in cell growth is not clear, the microtubule orientations of induced XTH lines can be investigated, at 5 days post germination; this will help finding out whether the XTH promotes the growth and growth anisotropy via modifying microtubule/microfibril.

Another unanswered question is that in the wave of growth, why do upper hypocotyl epidermal cells grow much longer than the basal ones? (Chapter 1, Chapter 3) There are three possible explanations: 1) Longer cells are exposed to more hormone. However, GA treatment or DELLA mutants do not remove the cellular level heterogeneous, suggesting that the level of GA is not a limiting factor on a cell's final length. 2) Cell sizes are predetermined, so the basal cells can never be as long as the upper cells. This is possible, since homogenous cell sizes were never observed in dark-grown hypocotyl. But can we find any genetic evidence prove/disprove this hypothesis? 3) Longer cells are exposed to hormone for longer period of time. The upper cells might receive a little growth signal and hence elongate a little bit before their fast elongation period. Therefore, when the wave reaches them, they are already a lot longer than the basal cells at germination. With a similar relative growth rate, they can reach a much larger final length. In addition, because they are very long in length, a uniform-speed wave would stay with them for longer period of time. As a result, cells in upper parts of the hypocotyl grow for longer period, with faster absolute growth rates and reach longer final length.

Turgor pressure is an important physical factors involved in growth, and its magnitude was thought to affect growth rate directly[10][103][104][12]. According to the data and modelling in Chapter 2, the turgor pressure seems to be less important than cell wall properties and chemical signals. It often changes corresponding to modifications in cell wall, and a positive correlation between pressure and growth rate is usually not seen. A recent result shows that the cellular turgor pressure depends on the

number of its neighbouring cells[263]. Yet detail mechanisms of how growing cells adjust their internal pressure is still not well understood, and the rate of turgor accumulation/releasing of growing cells is an important aspect in studies of cellular growth. In the future, if we can prove that the turgor pressure can be adjusted relatively quickly by cells, then it is less likely a limiting factor in cell growth, and more focus should be put on the cell wall.

On the modelling aspect, different approaches should be considered. The current models should not be made more complex, but different ideas of modelling can be considered, such as modelling the growth in 3D, modelling the hypocotyl cells including cortical cells, or modelling the anisotropy over time. As long as there is a clear goal, modelling approaches can be creative.

One arguable limitation in these studies is that non-epidermal cells are not reasonably considered. The hypocotyl was not modelled as a whole including cortical cells, and our transcriptome analyses did not have radial data either. Some genes might only express in hypocotyl cells other than the non-dividing epidermis, and RNA-seq at single cell level might provide finer data.

BIBLIOGRAPHY

[1] E. Gendreau, J. Traas, T. Demos, O. Grandjean, M. Caboche, and H. Hofte, "Cellular Basis of Hypocotyl Growth in Arabidopsis thaliana'," *Plant Physiol.*, vol. 114, no. 1, pp. 295–305, 1997.

[2] J. Chan, M. Eder, E. F. Crowell, J. Hampson, G. Calder, and C. Lloyd, "Microtubules and CESA tracks at the inner epidermal wall align independently of those on the outer wall of light-grown Arabidopsis hypocotyls," *J. Cell Sci.*, vol. 124, no. 7, pp. 1088–1094, 2011.

[3] J. Chan *et al.*, "The rotation of cellulose synthase trajectories is microtubule dependent and influences the texture of epidermal cell walls in Arabidopsis hypocotyls," *J. Cell Sci.*, vol. 123, no. 20, pp. 3490–3495, 2010.

[4] D. J. Cosgrove, "Re-constructing our models of cellulose and primary cell wall assembly," pp. 122–131, 2015.

[5] A. Peaucelle, S. A. Braybrook, L. Le Guillou, E. Bron, C. Kuhlemeier, and H. Höfte, "Pectin-induced changes in cell wall mechanics underlie organ initiation in Arabidopsis," *Curr. Biol.*, vol. 21, no. 20, pp. 1720–1726, 2011.

[6] D. J. Cosgrove, "Wall structure and wall loosening: A look backwards and forwards.," *Plant Physiol.*, vol. 125, no. 1, pp. 131–134, 2001.

[7] F. B. Daher, Y. Chen, B. Bozorg, J. Clough, H. Jonsson, and S. Braybrook, "Anisotropic growth is achieved through the additive mechanical effect of material anisotropy and elastic asymmetry," *Elife*, vol. 7:e38161, p. 316364, 2018.

[8] A. Peaucelle *et al.*, "Arabidopsis Phyllotaxis is Controlled by the Methyl-Esterification Status of Cell-Wall Pectins," *Curr. Biol.*, vol. 18, no. 24, pp. 1943–1948, 2008.

[9] S. A. Braybrook, H. Hofte, and A. Peaucelle, "Probing the mechanical contributions of the pectin matrix: Insights for cell growth," *Plant Signal. Behav.*, vol. 7, no. 8, 2012.

[10] J. A. Lockhart, "An analysis of irreversible plant cell elongation.," *J. Theor. Biol.*, vol. 8, no. 2, pp. 264–275, 1965.

[11] P. B. Green, "Growth Physics in Nitella: a Method for Continuous in Vivo Analysis of Extensibility Based on a Micro-manometer Technique for Turgor Pressure," *Plant Physiol.*, vol. 43, no. 8, pp. 1169–1184, 1968.

[12] B. A. Veytsman and D. J. Cosgrove, "A Model of Cell Wall Expansion Based on Thermodynamics of Polymer Networks," *Biophys. J.*, vol. 75, no. 5, pp. 2240–2250, 1998.

[13] E. L. Mccoy, "The strain energy function in axial plant growth," no. 12, pp. 575–594, 1989.

[14] M. P. Wold and R. I. Gamow, "Fiber-composite model for helical growth in the Phycomyces cell wall," *J. Theor. Biol.*, vol. 159, no. 1, pp. 39–51, 1992.

[15] D. B. Sellen, "The response of mechanically anisotropic cylindrical cells to multiaxial stress," *J. Exp. Bot.*, vol. 34, no. 6, pp. 681–687, 1983.

[16] H. I. Wu, R. D. Spence, P. J. H. Sharpe, and J. D. Goeschl, "Cell-Wall Elasticity .1. A Critique of the Bulk Elastic-Modulus Approach and an Analysis Using Polymer Elastic Principles," *Plant Cell Environ.*, vol. 8, no. 8, pp. 563–570, 1985.

[17] R. J. DYSON and O. E. JENSEN, "A fibre-reinforced fluid model of anisotropic plant cell growth," *J. Fluid Mech.*, vol. 655, pp. 472–503, 2010.

[18] J. Dumais, S. L. Shaw, C. R. Steele, S. R. Long, and P. M. Ray, "An anisotropic-viscoplastic model of plant cell morphogenesis by tip growth," *Int. J. Dev. Biol.*, vol. 50, no. 2–3, pp. 209–222, 2006.

[19] X. Yin, J. Goudriaan, E. A. Lantinga, J. Vos, and H. J. Spiertz, "A flexible sigmoid function of determinate growth," *Ann. Bot.*, vol. 91, no. 3, pp. 361–371, 2003.

[20] G. B., "On the nature of the function expressive of the law of human mortality, and on a new mode of determining the value of life contingencies.," *Philos. Trans. R. Soc.*, vol. 182 : 513-, 1825.

[21] W. Weibull, "A statistical distribution function of wide applicability," *J. Appl. Mech.*, vol. 18 : 293-2, 1951.

[22] S. Pelletier *et al.*, “A role for pectin de-methylesterification in a developmentally regulated growth acceleration in dark-grown Arabidopsis hypocotyls,” *New Phytol.*, vol. 188, no. 3, pp. 726–739, 2010.
[23] M. Ogawa and A. Hanada, “Gibberellin biosynthesis and response during Arabidopsis seed germination,” *Plant Cell …*, vol. 15, no. July, pp. 1591–1604, 2003.
[24] A. Rizza, A. Walia, V. Lanquar, W. B. Frommer, and A. M. Jones, “In vivo gibberellin gradients visualized in rapidly elongating tissues,” *Nat. Plants*, vol. 3, no. 10, pp. 803–813, 2017.
[25] L. Taiz and E. Zeiger, *Plant Physiology*. Sinauer Associates, 2002.
[26] Campbell-Reece, *Biology*. Pearson Education, 2008.
[27] N. J. M. Saibo, W. H. Vriezen, G. T. S. Beemster, and D. Van Der Straeten, “Growth and stomata development of Arabidopsis hypocotyls are controlled by gibberellins and modulated by ethylene and auxins,” *Plant J.*, vol. 33, no. 6, pp. 989–1000, 2003.
[28] E. Runkle, “Growing plants with Green Light,” vol. 2017, no. June, p. 2017, 2017.
[29] K. A. Franklin and J. R. Shinkle, “Photomorphogenesis in Natural Light Environments,” 2008.
[30] M. In, V. Extensibility, P. Cell, and D. J. Cosgrove, “The Plant Cell Wall,” vol. 715, no. 1, pp. 291–303, 2011.
[31] J. F. Thibault, C. M. G. C. Renard, M. A. V. Axelos, P. Roger, and M. J. Crépeau, “Studies of the length of homogalacturonic regions in pectins by acid hydrolysis,” *Carbohydr. Res.*, vol. 238, no. C, pp. 271–286, 1993.
[32] W. G. T. Willats *et al.*, “Modulation of the Degree and Pattern of Methyl-esterification of Pectic Homogalacturonan in Plant Cell Walls,” *J. Biol. Chem.*, vol. 276, no. 22, pp. 19404–19413, 2001.
[33] R. R. Vincent and M. A. K. Williams, “Microrheological investigations give insights into the microstructure and functionality of pectin gels,” *Carbohydr. Res.*, vol. 344, no. 14, pp. 1863–1871, 2009.
[34] J. Pelloux, C. Rustérucci, and E. J. Mellerowicz, “New insights into pectin methylesterase structure and function,” *Trends Plant Sci.*, vol. 12, no. 6, pp. 267–277, 2007.
[35] U.-N. Reide et al, *Color atlas of pathology: pathologic principles, associated diseases, sequela*. 1998.
[36] D. J. Cosgrove, “Growth of the plant cell wall,” *Nat. Rev. Mol. Cell Biol.*, vol. 6, no. 11, pp. 850–861, 2005.
[37] D. J. Cosgrove, “Expansive growth of plant cell walls,” *Plant Physiol. Biochem.*, vol. 38, no. 1–2, pp. 109–124, 2000.
[38] Y. Nishiyama, “Structure and properties of the cellulose microfibril,” *J. Wood Sci.*, vol. 55, no. 4, pp. 241–249, 2009.
[39] R. Himmelspach, R. E. Williamson, and G. O. Wasteneys, “Cellulose microfibril alignment recovers from DCB-induced disruption despite microtubule disorganization,” *Plant J.*, vol. 36, no. 4, pp. 565–575, 2003.
[40] J. R. Pear, Y. Kawagoe, W. E. Schreckengost, D. P. Delmer, and D. M. Stalker, “Higher plants contain homologs of the bacterial celA genes encoding the catalytic subunit of cellulose synthase.,” *Proc. Natl. Acad. Sci. U. S. A.*, vol. 93, no. 22, pp. 12637–42, 1996.
[41] J. Chambers and A. Elbein, “Biosynthesis Formation of Glucans in Mung Bean Seedlings and from GDP-Glucose from UDP-Glucose found that a particulate enzyme system from portion of GDP-glucose-14C into an alkali- and Gibbons (3) reported that a particulate synthesis of cellulose from,” *Arch. Biochem. Biophys.*, 1970.
[42] S. Robert, G. Mouille, and H. Höfte, “The mechanism and regulation of cellulose synthesis in primary walls: lessons from cellulose-deficient Arabidopsis mutants,” *Cellulose*, vol. 11, no. 3/4, pp. 351–364, 2004.
[43] K. Sugimoto, R. Himmelspach, R. E. Williamson, and G. O. Wasteneys, “Mutation or drug-dependent microtubule disruption causes radial swelling without altering parallel cellulose

microfibril deposition in Arabidopsis root cells.," *Plant Cell*, vol. 15, no. 6, pp. 1414–1429, 2003.
[44] A. M. C. Emons, J. Derksen, and M. M. A. Sassen, "Do microtubules orient plant cell wall microfibrils?," *Physiol. Plant.*, vol. 84, no. 3, pp. 486–493, 1992.
[45] A. M. C. Emons, H. Höfte, and B. M. Mulder, "Microtubules and cellulose microfibrils: how intimate is their relationship?," *Trends Plant Sci.*, vol. 12, no. 7, pp. 279–281, 2007.
[46] M. Fujita, R. Himmelspach, C. H. Hocart, R. E. Williamson, S. D. Mansfield, and G. O. Wasteneys, "Cortical microtubules optimize cell-wall crystallinity to drive unidirectional growth in Arabidopsis," *Plant J.*, vol. 66, no. 6, pp. 915–928, 2011.
[47] C. Xiao, T. Zhang, Y. Zheng, D. J. Cosgrove, and C. T. Anderson, "Xyloglucan Deficiency Disrupts Microtubule Stability and Cellulose Biosynthesis in Arabidopsis, Altering Cell Growth and Morphogenesis," *Plant Physiol.*, vol. 170, no. 1, pp. 234–249, 2016.
[48] T. I. Baskin, "Disorganization of Cortical Microtubules Stimulates Tangential Expansion and Reduces the Uniformity of Cellulose Microfibril Alignment among Cells in the Root of Arabidopsis," *Plant Physiol.*, vol. 135, no. 4, pp. 2279–2290, 2004.
[49] R. D. Vale, "The molecular motor toolbox for intracellular transport," *Cell*, vol. 112, no. 4, pp. 467–480, 2003.
[50] E. F. Crowell *et al.*, "Differential regulation of cellulose orientation at the inner and outer face of epidermal cells in the Arabidopsis hypocotyl.," *Plant Cell*, vol. 23, no. 7, pp. 2592–605, 2011.
[51] D. Suslov, J.-P. Verbelen, and K. Vissenberg, "Onion epidermis as a new model to study the control of growth anisotropy in higher plants.," *J Exp Bot*, vol. 60, no. 14, pp. 4175–4187, 2009.
[52] H. V. Scheller and P. Ulvskov, "Hemicelluloses," *Annu. Rev. Plant Biol.*, vol. 61, no. 1, pp. 263–289, 2010.
[53] T. Hayashi, "Xyloglucans in the Primary Cell Wall," 1972.
[54] M. Pauly, P. Albersheim, A. Darvill, and W. S. York, "Molecular domains of the cellulose/xyloglucan network in the cell walls of higher plants," *Plant J.*, vol. 20, no. 6, pp. 629–639, 1999.
[55] T. Hayashi, M. P. F. Marsden, and D. P. Delmer, "Pea Xyloglucan and Cellulose .5. Xyloglucan-Cellulose Interactions In vitro and In vivo," *Plant Physiol.*, vol. 83, no. 2, pp. 384–389, 1987.
[56] Y. B. Park and D. J. Cosgrove, "A revised architecture of primary cell walls based on biomechanical changes induced by substrate-specific endoglucanases," *New Phytol.*, vol. 171, no. 3, pp. 633–641, 2012.
[57] N. Carpita and M. McCann, *Biochemistry and molecular biology of plants*. 2000.
[58] S. C. Fry, "the Structure and Functions of the," *J. Exp. Bot.*, vol. 40, no. 1904, pp. 1–11, 1989.
[59] K. Nishitani and K. Vissenberg, "Roles of the XTH Protein Family in the Expanding Cell."
[60] J. K. C. Rose, J. Braam, S. C. Fry, and K. Nishitani, "The XTH family of enzymes involved in xyloglucan endotransglycosylation and endohyrdolosis: Current perspectives and a new unifying nomenclature," *Plant Cell Physiol.*, vol. 43, no. 12, pp. 1421–1435, 2002.
[61] K. Vissenberg, M. Oyama, Y. Osato, R. Yokoyama, J. P. Verbelen, and K. Nishitani, "Differential expression of AtXTH17, AtXTH18, AtXTH19 and AtXTH20 genes in Arabidopsis roots. Physiological roles in specification in cell wall construction," *Plant Cell Physiol.*, vol. 46, no. 1, pp. 192–200, 2005.
[62] K. Vissenberg, I. M. Martinez-Vilchez, J. P. Verbelen, J. G. Miller, and S. C. Fry, "In vivo colocalization of xyloglucan endotransglycosylase activity and its donor substrate in the elongation zone of Arabidopsis roots," *Plant Cell*, vol. 12, no. 7, pp. 1229–1237, 2000.
[63] A. Matsui *et al.*, "AtXTH27 plays an essential role in cell wall modification during the development of tracheary elements," *Plant J.*, vol. 42, no. 4, pp. 525–534, 2007.
[64] A. Maris, D. Suslov, S. C. Fry, J. P. Verbelen, and K. Vissenberg, "Enzymic characterization of two recombinant xyloglucan endotransglucosylase/hydrolase (XTH) proteins of Arabidopsis

and their effect on root growth and cell wall extension," *J. Exp. Bot.*, vol. 60, no. 13, pp. 3959–3972, 2009.
[65] J. I. Medford, J. S. Elmer, and H. J. L. B.-P. B. S. R. 260 Klee, "Molecular cloning and characterization of genes expressed in shoot apical meristems," *Plant Cell*, vol. 3, no. April, pp. 359–370, 1991.
[66] D. M. Zurek and S. D. Clouse, "Molecular Cloning and Characterization of a Brassinosteroid-Regulated Gene f rom Elongating Soybean (GIycine max 1.) Epicotyls'," *Plant Physiol*, vol. 104, pp. 161–170, 1994.
[67] K. Nishitani, "Construction and restructuring of the cellulose-xyloglucan framework in the apoplast as mediated by the xyloglucan related protein family - A hypothetical scheme," *J. Plant Res.*, vol. 111, no. 1101, pp. 159–166, 1998.
[68] J. Braam and R. W. Davis, "Rain-, wind-, and touch-induced expression of calmodulin and calmodulin-related genes in Arabidopsis," *Cell*, vol. 60, no. 3, pp. 357–364, 1990.
[69] R. J. Redgwell and S. C. Fry, "Xyloglucan Endotransglycosylase Activity Increases during Kiwifruit (Actinidia deliciosa) Ripening (Implications for Fruit Softening).," *Plant Physiol.*, vol. 103, no. 4, pp. 1399–1406, 1993.
[70] C. Fanutti, M. J. Gidley, and J. S. Reid, "Action of a pure xyloglucan endo-transglycosylase (formerly called xyloglucan-specific endo-(1-->4)-beta-D-glucanase) from the cotyledons of germinated nasturtium seeds.," *Plant J.*, vol. 3, no. 5, pp. 691–700, 1993.
[71] F. Micheli, "Pectin methylesterases: Cell wall enzymes with important roles in plant physiology," *Trends Plant Sci.*, vol. 6, no. 9, pp. 414–419, 2001.
[72] Y. Chen, "Riding the wave of growth," University of Cambridge, 2015.
[73] L. Willis *et al.*, "Cell size and growth regulation in the *Arabidopsis thaliana* apical stem cell niche," *Proc. Natl. Acad. Sci.*, vol. 113, no. 51, pp. E8238–E8246, 2016.
[74] M. Uyttewaal *et al.*, "FibrilTool , an ImageJ plug-in to quantify fibrillar structures in raw microscopy images," vol. 9, no. 2, 2014.
[75] J. Zuo, Q. W. Niu, and N. H. Chua, "An estrogen receptor-based transactivator XVE mediates highly inducible gene expression in transgenic plants," *Plant J.*, vol. 24, no. 2, pp. 265–273, 2000.
[76] A. R. Stuitje, E. C. Verbree, K. H. Van Der Linden, E. M. Mietkiewska, J.-P. Nap, and T. J. A. Kneppers, "Seed-expressed fluorescent proteins as versatile tools for easy (co)transformation and high-throughput functional genomics in Arabidopsis," *Plant Biotechnol. J.*, vol. 1, no. 4, pp. 301–309, 2003.
[77] F. J. Richards, "A Flexible Growth Function for Empirical Use," *J. Exp. Bot.*, vol. 10, no. 39, pp. 290–300, 1959.
[78] V. Lionetti *et al.*, "Overexpression of Pectin Methylesterase Inhibitors in Arabidopsis Restricts Fungal Infection by Botrytis cinerea," *Plant Physiol.*, vol. 143, no. 4, pp. 1871–1880, 2007.
[79] S. A. Braybrook and A. Peaucelle, "Mechano-Chemical Aspects of Organ Formation in Arabidopsis thaliana: The Relationship between Auxin and Pectin," *PLoS One*, vol. 8, no. 3, 2013.
[80] R. P. Jolie, T. Duvetter, A. M. Van Loey, and M. E. Hendrickx, "Pectin methylesterase and its proteinaceous inhibitor: A review," *Carbohydr. Res.*, vol. 345, no. 18, pp. 2583–2595, 2010.
[81] G. W. Tian, M. H. Chen, A. Zaltsman, and V. Citovsky, "Pollen-specific pectin methylesterase involved in pollen tube growth," *Dev. Biol.*, vol. 294, no. 1, pp. 83–91, 2006.
[82] S. Wolf and S. Greiner, "Growth control by cell wall pectins," *Protoplasma*, vol. 249, no. SUPPL.2, pp. 169–175, 2012.
[83] R. Louvet *et al.*, "Major changes in the cell wall during silique development in Arabidopsis thaliana," *Phytochemistry*, vol. 72, no. 1, pp. 59–67, 2011.
[84] F. B. Daher and S. A. Braybrook, "How to let go: pectin and plant cell adhesion," *Front. Plant Sci.*, vol. 6, no. July, pp. 1–8, 2015.

[85] E. Miedes *et al.*, “Xyloglucan endotransglucosylase/hydrolase (XTH) overexpression affects growth and cell wall mechanics in etiolated Arabidopsis hypocotyls,” *J. Exp. Bot.*, vol. 64, no. 8, pp. 2481–2497, 2013.
[86] R. Fauré, M. Saura-Valls, H. Brumer, A. Planas, S. Cottaz, and H. Driguez, “Synthesis of a Library of Xylogluco-Oligosaccharides for Active-Site Mapping of Xyloglucan *endo* -Transglycosylase,” *J. Org. Chem.*, vol. 71, no. 14, pp. 5151–5161, 2006.
[87] K. Zhang, W. Zuo, Y. Chen, D. Meng, and L. Zhang, “Beyond a Gaussian denoiser: Residual learning of deep CNN for image denoising,” *IEEE Trans. Image Process.*, vol. 26, no. 7, pp. 3142–3155, 2017.
[88] J. Pritchard, “Turgor Pressure,” *Encycl. Life Sci.*, pp. 1–3, 2001.
[89] E. Steudle and U. Zimmermann, “Effect of turgor pressure and cell size on the wall elasticity of plant cells.,” *Plant Physiol.*, vol. 59, no. 2, pp. 285–289, 1977.
[90] M. Hohl and P. Schopfer, “Water Relations of Growing Maize Coleoptiles 1,” *Plant Physiol.*, vol. 95, pp. 716–722, 1991.
[91] R. Benkert, G. Obermeyer, and F. W. Bentrup, “The turgor pressure of growing lily pollen tubes,” *Protoplasma*, no. 198, pp. 1–8, 1997.
[92] A. Peaucelle, S. Braybrook, and H. Höfte, “Cell wall mechanics and growth control in plants: the role of pectins revisited,” *Front. Plant Sci.*, vol. 3, no. June, pp. 1–6, 2012.
[93] F. Sénéchal, C. Wattier, C. Rustérucci, and J. Pelloux, “Homogalacturonan-modifying enzymes: Structure, expression, and roles in plants,” *J. Exp. Bot.*, vol. 65, no. 18, pp. 5125–5160, 2014.
[94] J. Zhang, C. R. Daubert, and E. A. Foegeding, “Fracture Analysis of Alginate Gels,” *J. Food Sci.*, vol. 70, no. 7, pp. e425–e431, 2006.
[95] A. Yoshizawa, “Statistical modelling of a transport equation for the kinetic energy dissipation rate,” *Phys. Fluids*, vol. 30, no. 3, p. 628, 1987.
[96] T. A. Bennet-Clark, A. D. Greenwood, and J. . Barker, “Calcium pectate chemistry controls growth rate of Chara corallina,” *Exp. Bot.*, vol. 57, no. 15, pp. 3989–4002, 2006.
[97] O. Ali and J. Traas, “Force-Driven Polymerization and Turgor-Induced Wall Expansion,” *Trends Plant Sci.*, vol. 21, no. 5, pp. 398–409, 2016.
[98] T. Zhang, Y. Zheng, and D. J. Cosgrove, “Spatial organization of cellulose microfibrils and matrix polysaccharides in primary plant cell walls as imaged by multichannel atomic force microscopy,” *Plant J.*, vol. 85, no. 2, pp. 179–192, 2016.
[99] S. Kerstens, W. F. Decraemer, and J. Verbelen, “Cell Walls at the Plant Surface Behave Mechanically Like Fiber-Reinforced Composite Materials 1,” 2001.
[100] P. . Green, R. . Erickson, and J. Buggy, “Physical Control of Cell Elongation Rate,” *Nature*, pp. 423–430, 1971.
[101] D. J. Cosgrove, “Analysis of the dynamic and steady-state responses of growth rate and turgor pressure to changes in cell parameters.,” *Plant Physiol.*, vol. 68, no. 6, pp. 1439–1446, 1981.
[102] D. J. Cosgrove, “Cell wall yield properties of growing tissue : evaluation by in vivo stress relaxation.,” *Plant Physiol.*, vol. 78, no. 2, pp. 347–356, 1985.
[103] J. K. Ortega, “Augmented growth equation for cell wall expansion.,” *Plant Physiol.*, vol. 79, no. 1, pp. 318–320, 1985.
[104] J. K. E. Ortega, “Governing equations for plant cell growth,” *Physiol. Plant.*, vol. 79, no. 1, pp. 116–121, 1990.
[105] J. K. E. Ortega, M. E. Smith, A. J. Erazo, M. A. Espinosa, S. A. Bell, and E. G. Zehr, “A comparison of cell-wall-yielding properties for two developmental stages of Phycomyces sporangiophores - Determination by in-vivo creep experiments,” *Planta*, vol. 183, no. 4, pp. 613–619, 1991.
[106] I. Cave, “The anisotropic elasticity of the plant cell wall,” *Wood Sci. Technol.*, vol. 2, pp. 268–278, 1968.
[107] C. N. Ahlquist, S. C. Iverson, and W. E. Jahsman, “Cell wall structure and mechanical properties of Phycomyces.,” *J Biomech*, vol. 8, no. 6, pp. 357–362, 1975.

[108] M. a. J. Chaplain, “The Strain Energy Function of an Ideal Plant Cell Wall,” *Journal of Theoretical Biology*, vol. 163. pp. 77–97, 1993.
[109] S. A. Braybrook, “Measuring the elasticity of plant cells with atomic force microscopy,” in *Methods in Cell Biology*, 2015, pp. 237–254.
[110] D. J. Cosgrove, “Plant cell wall extensibility: Connecting plant cell growth with cell wall structure, mechanics, and the action of wall-modifying enzymes,” *J. Exp. Bot.*, vol. 67, no. 2, pp. 463–476, 2016.
[111] D. J. Cosgrove, “Wall relaxation and the driving forces for cell expansive growth.,” *Plant Physiol.*, vol. 84, pp. 561–4, 1987.
[112] D. J. Cosgrove, “Re-constructing our models of cellulose and primary cell wall assembly,” *Curr. Opin. Plant Biol.*, vol. 22, pp. 122–131, 2014.
[113] P. Derbyshire, K. Findlay, M. C. McCann, and K. Roberts, “Cell elongation in Arabidopsis hypocotyls involves dynamic changes in cell wall thickness,” *J. Exp. Bot.*, vol. 58, no. 8, pp. 2079–2089, 2007.
[114] A. N. Fernandes *et al.*, “Mechanical properties of epidermal cells of whole living roots of Arabidopsis thaliana: An atomic force microscopy study,” *Phys. Rev. E - Stat. Nonlinear, Soft Matter Phys.*, vol. 85, no. 2, pp. 1–8, 2012.
[115] H. de Vries, “Eine Methode zur Analyse der Turgorkraft,” 1884, p. Jb. wiss. Bot. 14, 427–601.
[116] L. Taiz, “Regulation of cell wall mechanical properties,” *Annu. Rev. Plant Physiol.*, vol. 35, pp. 585–657, 1984.
[117] G. Refrégier, S. Pelletier, D. Jaillard, and H. Höfte, “Interaction between wall deposition and cell elongation in dark-grown hypocotyl cells in Arabidopsis.,” *Plant Physiol.*, vol. 135, no. 2, pp. 959–968, 2004.
[118] G. W. Bassel *et al.*, “Genome-wide network model capturing seed germination reveals coordinated regulation of plant cellular phase transitions,” *Proc. Natl. Acad. Sci.*, vol. 108, no. 23, pp. 9709–9714, 2011.
[119] M. C. McCann, K. Roberts, and N. C. Carpita, “Plant Cell Growth and Elongation,” *Encycl. Life Sci.*, pp. 1–8, 2001.
[120] E. C. M. Ernest, “Factors rendering the plasmolytic method inapplicable in the estimation of osmotic values of plant cells,” 1935.
[121] I. Dreyer and N. Uozumi, “Potassium channels in plant cells,” *FEBS J.*, vol. 278, no. 22, pp. 4293–4303, 2011.
[122] A. Sampathkumar *et al.*, “Subcellular and supracellular mechanical stress prescribes cytoskeleton behavior in Arabidopsis cotyledon pavement cells,” *Elife*, vol. 2014, no. 3, pp. 1–20, 2014.
[123] M. Sassi *et al.*, “An auxin-mediated shift toward growth isotropy promotes organ formation at the shoot meristem in Arabidopsis,” *Curr. Biol.*, vol. 24, no. 19, pp. 2335–2342, 2014.
[124] J. H. Kroeger, R. Zerzour, and A. Geitmann, “Regulator or driving force? the role of turgor pressure in oscillatory plant cell growth,” *PLoS One*, vol. 6, no. 4, 2011.
[125] E. R. Rojas, S. Hotton, and J. Dumais, “Chemically mediated mechanical expansion of the pollen tube cell wall,” *Biophys. J.*, vol. 101, no. 8, pp. 1844–1853, 2011.
[126] “Empirical Modelling,” *Wikipedia*. .
[127] J. E. Varner and S. Louis, “Plant Cell Wall Architecture Review,” vol. 56, pp. 231–239, 1989.
[128] Kunal, “What is the difference between logit and probit.” [Online]. Available: https://discuss.analyticsvidhya.com/t/what-is-the-difference-between-logit-and-probit-models/325/2.
[129] N. Cunniffe, “Population Models, Part IA Mathematical Biology, University of Cambridge.”
[130] Arnold Robbins, *Unix In a Nutshell*, no. May 2000. 2003.
[131] A. M. Bolger, M. Lohse, and B. Usadel, “Trimmomatic: A flexible trimmer for Illumina sequence data,” *Bioinformatics*, vol. 30, no. 15, pp. 2114–2120, 2014.
[132] S. Andrews, “FastQC A Quality Control tool for High Throughput Sequence Data.” .

[133] C. Trapnell, L. Pachter, and S. L. Salzberg, “TopHat: Discovering splice junctions with RNA-Seq,” *Bioinformatics*, vol. 25, no. 9, pp. 1105–1111, 2009.
[134] B. Langmead and S. L. Salzberg, “Fast gapped-read alignment with Bowtie 2,” *Nat. Methods*, vol. 9, no. 4, pp. 357–359, 2012.
[135] P. Lamesch *et al.*, “The Arabidopsis Information Resource (TAIR): Improved gene annotation and new tools,” *Nucleic Acids Res.*, vol. 40, no. D1, pp. 1202–1210, 2012.
[136] C. Trapnell *et al.*, “Differential gene and transcript expression analysis of RNA-seq experiments with TopHat and Cufflinks,” *Nat. Protoc.*, vol. 7, no. 3, pp. 562–578, 2012.
[137] M. I. Love, W. Huber, and S. Anders, “Moderated estimation of fold change and dispersion for RNA-seq data with DESeq2,” *Genome Biol.*, vol. 15, no. 12, pp. 1–21, 2014.
[138] T. Czechowski, “Genome-Wide Identification and Testing of Superior Reference Genes for Transcript Normalization in Arabidopsis,” *Plant Physiol.*, vol. 139, no. 1, pp. 5–17, 2005.
[139] P. Hedden, “Gibberellin Biosynthesis,” *eLS*, no. August, 2012.
[140] B. Phinney, “The history of gibberellins,” *Biochem. Physiol. Gibberellins*, pp. 19–52, 1983.
[141] D. E. Richards, K. E. King, T. Ait-ali, and N. P. Harberd, : “A Molecular Genetic Analysis of Gibberellin Signalling,” *Annu. Rev. Plant Physiol. Plant Mol. Biol.*, vol. 52, pp. 67–88, 2001.
[142] P. Hedden, “The genes of the Green Revolution,” *Trends Genet.*, vol. 19, no. 1, pp. 5–9, 2003.
[143] S. Jasinski *et al.*, “KNOX action in Arabidopsis is mediated by coordinate regulation of cytokinin and gibberellin activities,” *Curr. Biol.*, vol. 15, no. 17, pp. 1560–1565, 2005.
[144] J. MacMillan and P. J. Suter, “The occurrence of gibberellin A1 in higher plants: Isolation from the seed of runner bean (Phaseolus multiflorus),” *Naturwissenschaften*, vol. 45, no. 2, p. 46, 1958.
[145] J. Griffiths *et al.*, “Genetic Characterization and Functional Analysis of the GID1 Gibberellin Receptors in Arabidopsis,” *Plant Cell Online*, vol. 18, no. 12, pp. 3399–3414, 2006.
[146] B. C. Willige *et al.*, “The DELLA Domain of GA INSENSITIVE Mediates the Interaction with the GA INSENSITIVE DWARF1A Gibberellin Receptor of Arabidopsis,” *Plant Cell Online*, vol. 19, no. 4, pp. 1209–1220, 2007.
[147] S. Iuchi *et al.*, “Multiple loss-of-function of Arabidopsis gibberellin receptor AtGID1s completely shuts down a gibberellin signal,” *Plant J.*, vol. 50, no. 6, pp. 958–966, 2007.
[148] M. Ueguchi-Tanaka *et al.*, “GIBBERELLIN INSENSITIVE DWARF1 encodes a soluble receptor for gibberellin,” *Nature*, vol. 437, no. 7059, pp. 693–698, 2005.
[149] M. Nakajima *et al.*, “Identification and characterization of Arabidopsis gibberellin receptors,” *Plant J.*, vol. 46, no. 5, pp. 880–889, 2006.
[150] C. Peng, R. P., K. D. E., and C. K. E., “The Arabidopsis GAI gene defines a signalling pathway that negatively regulates gibberellin responses.,” *Genes Dev*, vol. 11, no. 23, pp. 3194–3205, 1997.
[151] A. Dill and T. P. Sun, “Synergistic derepression of gibberellin signalling by removing RGA and GAI function in Arabidopsis thaliana,” *Genetics*, vol. 159, no. 2, pp. 777–785, 2001.
[152] H. Cheng, “Gibberellin regulates Arabidopsis floral development via suppression of DELLA protein function,” *Development*, vol. 131, no. 5, pp. 1055–1064, 2004.
[153] L. Tyler, “DELLA Proteins and Gibberellin-Regulated Seed Germination and Floral Development in Arabidopsis,” *Plant Physiol.*, vol. 135, no. 2, pp. 1008–1019, 2004.
[154] D. Cao, A. Hussain, H. Cheng, and J. Peng, “Loss of function of four DELLA genes leads to light- and gibberellin-independent seed germination in Arabidopsis,” *Planta*, vol. 223, no. 1, pp. 105–113, 2005.
[155] J. Peng *et al.*, “‘Green revolution’ genes encode mutant gibberellins response modulators,” *Nature*, vol. 400, no. July, pp. 256–261, 1999.
[156] P. K. Boss and M. R. Thomas, “Association of dwarfism and floral induction with a grape ‘green revolution’ mutation,” *Nature*, vol. 416, no. 6883, pp. 847–850, 2002.

[157] E. Oh, S. Yamaguchi, Y. Kamiya, G. Bae, W. Il Chung, and G. Choi, “Light activates the degradation of PIL5 protein to promote seed germination through gibberellin in Arabidopsis,” *Plant J.*, vol. 47, no. 1, pp. 124–139, 2006.
[158] J. A. Stavang *et al.*, “Hormonal regulation of temperature-induced growth in Arabidopsis,” *Plant J.*, vol. 60, no. 4, pp. 589–601, 2009.
[159] H. Magome, S. Yamaguchi, A. Hanada, Y. Kamiya, and K. Oda, “The DDF1 transcriptional activator upregulates expression of a gibberellin-deactivating gene, GA2ox7, under high-salinity stress in Arabidopsis,” *Plant J.*, vol. 56, no. 4, pp. 613–626, 2008.
[160] D. P. O’Neill, “Auxin Regulation of the Gibberellin Pathway in Pea,” *Plant Physiol.*, vol. 130, no. 4, pp. 1974–1982, 2002.
[161] R. Yano, Y. Kanno, Y. Jikumaru, K. Nakabayashi, Y. Kamiya, and E. Nambara, “CHOTTO1, a Putative Double APETALA2 Repeat Transcription Factor, Is Involved in Abscisic Acid-Mediated Repression of Gibberellin Biosynthesis during Seed Germination in Arabidopsis,” *Plant Physiol.*, vol. 151, no. 2, pp. 641–654, 2009.
[162] L. Alvey and J. I. Centre, “DELLA Proteins in Signalling,” *Encycl. Life Sci.*, pp. 1–7, 2008.
[163] C. Schwechheimer, “Understanding gibberellic acid signaling-are we there yet?,” *Curr. Opin. Plant Biol.*, vol. 11, no. 1, pp. 9–15, 2008.
[164] K. Murase, Y. Hirano, T. P. Sun, and T. Hakoshima, “Gibberellin-induced DELLA recognition by the gibberellin receptor GID1,” *Nature*, vol. 456, no. 7221, pp. 459–463, 2008.
[165] H. Magome, S. Yamaguchi, A. Hanada, Y. Kamiya, and K. Oda, “Dwarf and delayed-flowering 1, a novel Arabidopsis mutant deficient in gibberellin biosynthesis because of overexpression of a putative AP2 transcription factor,” *Plant J.*, vol. 37, no. 5, pp. 720–729, 2004.
[166] Regnault., "GA12 long distance move GA4," *Nature Plants,* 2015
[167] A. R. G. Plackett *et al.*, “Analysis of the Developmental Roles of the Arabidopsis Gibberellin 20-Oxidases Demonstrates That GA20ox1, -2, and -3 Are the Dominant Paralogs,” *Plant Cell*, vol. 24, no. 3, pp. 941–960, 2012.
[168] J. Hu *et al.*, “Potential Sites of Bioactive Gibberellin Production during Reproductive Growth in Arabidopsis,” *Plant Cell Online*, vol. 20, no. 2, pp. 320–336, 2008.
[169] M. G. Mitchum *et al.*, “Distinct and overlapping roles of two gibberellin 3-oxidases in Arabidopsis development,” *Plant J.*, vol. 45, no. 5, pp. 804–818, 2006.
[170] I. Rieu *et al.*, “Genetic Analysis Reveals That C19-GA 2-Oxidation Is a Major Gibberellin Inactivation Pathway in Arabidopsis,” *Plant Cell Online*, vol. 20, no. 9, pp. 2420–2436, 2008.
[171] T. Sakamoto *et al.*, “Expression of a gibberellin 2-oxidase gene around the shoot apex is related to phase transition in rice.,” *Plant Physiol.*, vol. 125, no. 3, pp. 1508–1516, 2001.
[172] M. Katsumi, D. E. Foard, and B. O. Phinney, “Evidence for the translocation of gibberellin A3 and gibberellin-like substances in grafts between normal, dwarf1 and dwarf5 seedlings of Zea mays L,” *Plant Cell Physiol*, vol. 24, no. 3, pp. 379–388, 1983.
[173] L. Ragni, K. Nieminen, D. Pacheco-Villalobos, R. Sibout, C. Schwechheimer, and C. S. Hardtke, “Mobile Gibberellin Directly Stimulates *Arabidopsis* Hypocotyl Xylem Expansion,” *Plant Cell*, vol. 23, no. 4, pp. 1322–1336, 2011.
[174] W. M. Proebsting, P. Hedden, M. J. Lewis, S. J. Croker, and L. N. Proebsting, “Gibberellin Concentration and Transport in Genetic Lines of Pea : Effects of Grafting.,” *Plant Physiol*, vol. 100, no. 3, pp. 1354–1360, 1992.
[175] X. Hou *et al.*, “Global Identification of DELLA Target Genes during Arabidopsis Flower Development,” *Plant Physiol.*, vol. 147, no. 3, pp. 1126–1142, 2008.
[176] J. L. Nemhauser, F. Hong, and J. Chory, “Different Plant Hormones Regulate Similar Processes through Largely Nonoverlapping Transcriptional Responses,” *Cell*, vol. 126, no. 3, pp. 467–475, 2006.
[177] H. Goda *et al.*, “The AtGenExpress hormone and chemical treatment data set: Experimental design, data evaluation, model data analysis and data access,” *Plant J.*, vol. 55, no. 3, pp. 526–542, 2008.

[178] R. Zentella *et al.*, “Global Analysis of DELLA Direct Targets in Early Gibberellin Signaling in *Arabidopsis*,” *Plant Cell*, vol. 19, no. 10, pp. 3037–3057, 2007.
[179] D. Cao, H. Cheng, W. Wu, H. M. Soo, and J. Peng, “Gibberellin Mobilizes Distinct DELLA-Dependent Transcriptomes to Regulate Seed Germination and Floral Development in Arabidopsis,” *Plant Physiol.*, vol. 142, no. 2, pp. 509–525, 2006.
[180] “The Arabidopsis Information Resource.” [Online]. Available: www.arabidopsis.org/aboutarabidopsis.html, on www.arabidopsis.org, Oct 24, 2000.
[181] M. Koornneef and J. H. van der Veen, “Induction and analysis of gibberellin sensitive mutants in Arabidopsis thaliana (L.) heynh.,” *Theor. Appl. Genet.*, vol. 58, no. 6, pp. 257–263, 1980.
[182] N. Goto and R. P. Pharis, “Role of gibberellins in the development of floral organs of the gibberellin-deficient mutant, ga1-1, of *Arabidopsis thaliana*,” *Can. J. Bot.*, vol. 77, no. 7, pp. 944–954, 1999.
[183] Y. Zhang *et al.*, “Two Arabidopsis cytochrome P450 monooxygenases, CYP714A1 and CYP714A2, function redundantly in plant development through gibberellin deactivation,” *Plant J.*, vol. 67, no. 2, pp. 342–353, 2011.
[184] D. W. Nobutoshi Yamaguchi, Cara M. Winter, Miin-Feng Wu, Yuri Kanno, Ayako Yamaguchi, Mitsunori Seo, “Gibberellin Acts Positively Then Negatively to Control Onset of Flower Formation in Arabidopsis,” no. May, pp. 638–641, 2014.
[185] D. PJ, *The Plant Hormone: Their Nature, Occurrence, and Functions. (Kluwer, Dordrecht, The Netherlands).* 2004.
[186] K. Mashiguchi *et al.*, “The main auxin biosynthesis pathway in Arabidopsis,” *Pnas*, vol. 108, no. 45, pp. 18512–18517, 2011.
[187] A. W. Woodward and B. Bartel, “Auxin: Regulation, action, and interaction,” *Ann. Bot.*, vol. 95, no. 5, pp. 707–735, 2005.
[188] A. N. Stepanova *et al.*, “TAA1-Mediated Auxin Biosynthesis Is Essential for Hormone Crosstalk and Plant Development,” *Cell*, vol. 133, no. 1, pp. 177–191, 2008.
[189] K. Palme and F. Nagy, “A New Gene for Auxin Synthesis,” *Cell*, vol. 133, no. 1, pp. 31–32, 2008.
[190] Y. Cheng, X. Dai, and Y. Zhao, “Auxin biosynthesis by the YUCCA flavin monooxygenases controls the formation of floral organs and vascular tissues in Arabidopsis,” *Genes Dev.*, vol. 20, no. 13, pp. 1790–1799, 2006.
[191] Y. Cheng, X. Dai, and Y. Zhao, “Auxin Synthesized by the YUCCA Flavin Monooxygenases Is Essential for Embryogenesis and Leaf Formation in Arabidopsis,” *Plant Cell Online*, vol. 19, no. 8, pp. 2430–2439, 2007.
[192] Y. Zhao *et al.*, “A Role for Flavin Monooxygenase – Like Enzymes in Auxin Biosynthesis,” *Science (80-.).*, vol. 291, no. January, pp. 306–310, 2001.
[193] H. Sekimoto *et al.*, “Molecular cloning and characterization of aldehyde oxidases in *Arabidopsis thaliana*,” *Plant Cell Physiol.*, vol. 39, no. 4, pp. 433–442, 1998.
[194] M. Seo *et al.*, “Higher Activity of an Aldehyde Oxidase in the Auxin-Overproducing *superroot1* Mutant of *Arabidopsis thaliana*,” *Plant Physiol.*, vol. 116, no. 2, pp. 687–693, 1998.
[195] M. E. Nihal Dharmasiri, Sunethra Dharmasiri, “The F-box protein TIR1 is an auxin receptor,” *Nature*, vol. 435, no. May, pp. 8–10, 2005.
[196] S. Kepinski and O. Leyser, “The Arabidopsis F-box protein TIR1 is an auxin receptor,” *Nature*, vol. 435, no. 7041, pp. 446–451, 2005.
[197] L. I. A. Calderón Villalobos *et al.*, “A combinatorial TIR1/AFB-Aux/IAA co-receptor system for differential sensing of auxin,” *Nat. Chem. Biol.*, vol. 8, no. 5, pp. 477–485, 2012.
[198] M. Quint and W. M. Gray, “Auxin signalling,” *Curr. Opin. Plant Biol.*, vol. 9, no. 5, pp. 448–453, 2006.
[199] X. Tan *et al.*, “Mechanism of auxin perception by the TIR1 ubiquitin ligase,” *Nature*, vol. 446, no. 7136, pp. 640–645, 2007.

[200] Y. Okushima *et al.*, “Functional Genomic Analysis of the AUXIN RESPONSE FACTOR Gene Family Members in Arabidopsis thaliana,” *Plant Cell*, vol. 17, no. February, pp. 444–463, 2005.
[201] A. M. Jones and M. A. Venis, “Photoaffinity labelling of indole-3-acetic acid-binding proteins in maize,” *Proc. Natl. Acad. Sci. U. S. A.*, vol. 86, no. 16, pp. 6153–6156, 1989.
[202] M. Sauer, S. Robert, and J. Kleine-Vehn, “Auxin: Simply complicated,” *J. Exp. Bot.*, vol. 64, no. 9, pp. 2565–2577, 2013.
[203] I. A. Paponov *et al.*, “Comprehensive transcriptome analysis of auxin responses in Arabidopsis,” *Mol. Plant*, vol. 1, no. 2, pp. 321–337, 2008.
[204] L. Gälweiler *et al.*, “Regulation of Polar Auxin Transport by AtPIN1 in *Arabidopsis* Vascular Tissue,” *Science (80-.).*, vol. 282, no. 5397, pp. 2226–2230, 1998.
[205] J. Friml, J. Wiśniewska, E. Benková, K. Mendgen, and K. Palme, “Lateral relocation of auxin efflux regulator PIN3 mediates tropism in Arabidopsis,” *Nature*, vol. 415, no. 6873, pp. 806–809, 2002.
[206] K. Sorefan *et al.*, “A regulated auxin minimum is required for seed dispersal in Arabidopsis,” *Nature*, vol. 459, no. 7246, pp. 583–586, 2009.
[207] E. M. Kramer and M. J. Bennett, “Auxin transport: a field in flux,” *Trends Plant Sci.*, vol. 11, no. 8, pp. 382–386, 2006.
[208] J. Wisniewska *et al.*, “Polar PIN localization directs auxin flow in plants,” *Science (80-.).*, vol. 312, no. 5775, p. 883, 2006.
[209] S. Vanneste and J. Friml, “Auxin: A Trigger for Change in Plant Development,” *Cell*, vol. 136, no. 6, pp. 1005–1016, 2009.
[210] M. Michniewicz *et al.*, “Antagonistic Regulation of PIN Phosphorylation by PP2A and PINOID Directs Auxin Flux,” *Cell*, vol. 130, no. 6, pp. 1044–1056, 2007.
[211] W. Grunewald and J. Friml, “The march of the PINs: Developmental plasticity by dynamic polar targeting in plant cells,” *EMBO J.*, vol. 29, no. 16, pp. 2700–2714, 2010.
[212] T. Viaene, C. F. Delwiche, S. A. Rensing, and J. Friml, “Origin and evolution of PIN auxin transporters in the green lineage,” *Trends Plant Sci.*, vol. 18, no. 1, pp. 5–10, 2013.
[213] C. Béziat, E. Barbez, M. I. Feraru, D. Lucyshyn, and J. Kleine-Vehn, “Light triggers PILS-dependent reduction in nuclear auxin signalling for growth transition,” *Nat. Plants*, vol. 3, no. July, 2017.
[214] E. Barbez *et al.*, “A novel putative auxin carrier family regulates intracellular auxin homeostasis in plants,” *Nature*, vol. 485, no. 7396, pp. 119–122, 2012.
[215] P. J. Jensen, R. P. Hangarter, and M. Estelle, “Auxin transport is required for hypocotyl elongation in light-grown but not dark-grown Arabidopsis,” *Plant Physiol.*, vol. 116, no. 2, pp. 455–462, 1998.
[216] T. Nishimura *et al.*, “Yucasin is a potent inhibitor of YUCCA, a key enzyme in auxin biosynthesis,” *Plant J.*, vol. 77, no. 3, pp. 352–366, 2014.
[217] J. Sánchez-Bravo, A. Ortuno, J. M. Botia, M. Acosta, and F. Sabater, “Lateral diffusion of polarly transported indoleacetic acid and its role in the growth of Lupinus albus L. hypocotyls,” *Planta*, vol. 185, no. 3, pp. 391–396, 1991.
[218] J. W. Reed *et al.*, *Three Auxin Response Factors Promote Hypocotyl Elongation.* 2018.
[219] Wikipedia, “Pectin.” [Online]. Available: https://en.wikipedia.org/wiki/Pectin.
[220] G. Levesque-Tremblay, J. Pelloux, S. A. Braybrook, and K. Müller, “Tuning of pectin methylesterification: consequences for cell wall biomechanics and development,” *Planta*, vol. 242, no. 4, pp. 791–811, 2015.
[221] W. G. T. Willats, L. Mccartney, W. Mackie, and J. P. Knox, “Pectin: Cell biology and prospects for functional analysis,” *Plant Mol. Biol.*, vol. 47, no. 1–2, pp. 9–27, 2001.
[222] S. Wolf, G. Mouille, and J. Pelloux, “Homogalacturonan methyl-esterification and plant development,” *Mol. Plant*, vol. 2, no. 5, pp. 851–860, 2009.

[223] S. Guénin *et al.*, “Identification of pectin methylesterase 3 as a basic pectin methylesterase isoform involved in adventitious rooting in Arabidopsis thaliana,” *New Phytol.*, vol. 192, no. 1, pp. 114–126, 2011.
[224] R. Louvet *et al.*, “Comprehensive expression profiling of the pectin methylesterase gene family during silique development in Arabidopsis thaliana,” *Planta*, vol. 224, no. 4, pp. 782–791, 2006.
[225] S. Wolf, T. Rausch, and S. Greiner, “The N-terminal pro region mediates retention of unprocessed type-I PME in the Golgi apparatus,” *Plant J.*, vol. 58, no. 3, pp. 361–375, 2009.
[226] L. Wang *et al.*, “Arabidopsis galacturonosyltransferase (GAUT) 13 and GAUT14 have redundant functions in pollen tube growth,” *Mol. Plant*, vol. 6, no. 4, pp. 1131–1148, 2013.
[227] D. Reinhardt, F. Wittwer, T. Mandel, and C. Kuhlemeier, “Localized upregulation of a new expansin gene predicts the site of leaf formation in the tomato meristem.,” *Plant Cell*, vol. 10, no. 9, pp. 1427–37, 1998.
[228] M. Bordenave and R. Goldberg, “Purification and characterization of pectin methylesterases from mung bean hypocotyl cell walls,” *Phytochemistry*, vol. 33, no. 5, pp. 999–1003, 1993.
[229] C. Scheler *et al.*, “Promotion of Testa Rupture during Garden Cress Germination Involves Seed Compartment-Specific Expression and Activity of Pectin Methylesterases,” *Plant Physiol.*, vol. 167, no. 1, pp. 200–215, 2015.
[230] S. H. An, K. H. Sohn, H. W. Choi, I. S. Hwang, S. C. Lee, and B. K. Hwang, “Pepper pectin methylesterase inhibitor protein CaPMEI1 is required for antifungal activity, basal disease resistance and abiotic stress tolerance,” *Planta*, vol. 228, no. 1, pp. 61–78, 2008.
[231] M. Hothorn, S. Wolf, P. Aloy, S. Greiner, and K. Scheffzek, “Structural insights into the target specificity of plant invertase and pectin methylesterase inhibitory proteins,” *Plant Cell*, vol. 16, no. 12, pp. 3437–3447, 2004.
[232] S. J. McQueen-Mason and D. J. Cosgrove, “Expansin mode of action on cell walls. Analysis of wall hydrolysis, stress relaxation, and binding.,” *Plant Physiol.*, vol. 107, no. 1, pp. 87–100, 1995.
[233] R. Huang, A. A. Becker, and I. A. Jones, “Modelling cell wall growth using a fibre-reinforced hyperelasticviscoplastic constitutive law,” *J. Mech. Phys. Solids*, vol. 60, no. 4, pp. 750–783, 2012.
[234] M. S. Doblin, I. Kurek, D. Jacob-Wilk, and D. P. Delmer, “Cellulose biosynthesis in plants: From genes to rosettes,” *Plant Cell Physiol.*, vol. 43, no. 12, pp. 1407–1420, 2002.
[235] N. G. Taylor, R. M. Howells, A. K. Huttly, K. Vickers, and S. R. Turner, “Interactions among three distinct CesA proteins essential for cellulose synthesis,” *Proc. Natl. Acad. Sci.*, vol. 100, no. 3, pp. 1450–1455, 2003.
[236] J. E. Burn, C. H. Hocart, R. J. Birch, A. C. Cork, and R. E. Williamson, “Functional Analysis of the Cellulose Synthase Genes,” *Society*, vol. 129, no. June, pp. 797–807, 2002.
[237] R. A. Burton, “The CesA Gene Family of Barley. Quantitative Analysis of Transcripts Reveals Two Groups of Co-Expressed Genes,” *Plant Physiol.*, vol. 134, no. 1, pp. 224–236, 2004.
[238] T. Desprez *et al.*, “Organization of cellulose synthase complexes involved in primary cell wall synthesis in Arabidopsis thaliana,” *Proc. Natl. Acad. Sci.*, vol. 104, no. 39, pp. 15572–15577, 2007.
[239] S. R. Turner, “Collapsed Xylem Phenotype of Arabidopsis Identifies Mutants Deficient in Cellulose Deposition in the Secondary Cell Wall,” *Plant Cell Online*, vol. 9, no. 5, pp. 689–701, 1997.
[240] T. Hamann, E. Osborne, H. L. Youngs, J. Misson, L. Nussaume, and C. Somerville, “Global expression analysis of CESA and CSL genes in Arabidopsis,” *Cellulose*, vol. 11, no. 3–4, pp. 279–286, 2004.
[241] R. Yokoyama and K. Nishitani, “A comprehensive expression analysis of all members of a gene family encoding cell-wall enzymes allowed us to predict cis-regulatory regions involved in

cell-wall construction in specific organs of Arabidopsis," *Plant Cell Physiol.*, vol. 42, no. 10, pp. 1025–1033, 2001.
[242] D. M. Cavalier *et al.*, "Disrupting Two Arabidopsis thaliana Xylosyltransferase Genes Results in Plants Deficient in Xyloglucan, a Major Primary Cell Wall Component," *Plant Cell Online*, vol. 20, no. 6, pp. 1519–1537, 2008.
[243] O. A. Zabotina *et al.*, "Arabidopsis XXT5 gene encodes a putative ??-1,6-xylosyltransferase that is involved in xyloglucan biosynthesis," *Plant J.*, vol. 56, no. 1, pp. 101–115, 2008.
[244] S. Vuttipongchaikij, D. Brocklehurst, C. Steele-King, D. A. Ashford, L. D. Gomez, and S. J. Mcqueen-Mason, "Arabidopsis GT34 family contains five xyloglucan α-1,6-xylosyltransferases," *New Phytol.*, vol. 195, no. 3, pp. 585–595, 2012.
[245] Y. Z. Shi, X. F. Zhu, J. G. Miller, T. Gregson, S. J. Zheng, and S. C. Fry, "Distinct catalytic capacities of two aluminium-repressed Arabidopsis thaliana xyloglucan endotransglucosylase/hydrolases, XTH15 and XTH31, heterologously produced in Pichia," *Phytochemistry*, vol. 112, no. 1, pp. 160–169, 2015.
[246] Z. Du, X. Zhou, Y. Ling, Z. Zhang, and Z. Su, "agriGO: A GO analysis toolkit for the agricultural community," *Nucleic Acids Res.*, vol. 38, no. SUPPL. 2, pp. 64–70, 2010.
[247] J. L. Pruneda-Paz and S. A. Kay, "An expanding universe of circadian networks in higher plants," *Trends Plant Sci.*, vol. 15, no. 5, pp. 259–265, 2010.
[248] N. Gregson, K. Sparrowhawk, J. Mauskopf, and J. Paul, "CIRCADIAN RHYTHMS FROM MULTIPLE OSCILLATORS: LESSONS FROM DIVERSE ORGANISMS," *Nat. Rev. Drug Discov.*, vol. 4, no. 2, pp. 121–130, 2005.
[249] Wikipedia, "Autophosphorylation." [Online]. Available: https://en.wikipedia.org/wiki/Autophosphorylation.
[250] P. J. Davies, *The plant hormones: their nature, occurrence, and functions*. Springer, Dordrecht, 2010.
[251] R. J. Cowling and N. P. Harberd, "Gibberellins control Arabidopsis hypocotyl growth via regulation of cellular elongation," *J. Exp. Bot.*, vol. 50, no. 337, pp. 1351–1357, 1999.
[252] N. P. Harberd, "Relieving DELLA restraint," *Science (80-.).*, vol. 299, no. 5614, pp. 1853–1854, 2003.
[253] A. L. Silverstone, "Repressing a Repressor: Gibberellin-Induced Rapid Reduction of the RGA Protein in Arabidopsis," *Plant Cell Online*, vol. 13, no. 7, pp. 1555–1566, 2001.
[254] P. Achard and P. Genschik, "Releasing the brakes of plant growth: How GAs shutdown della proteins," *J. Exp. Bot.*, vol. 60, no. 4, pp. 1085–1092, 2009.
[255] Y. B. Park and D. J. Cosgrove, "Xyloglucan and its interactions with other components of the growing cell wall," *Plant Cell Physiol.*, vol. 56, no. 2, pp. 180–194, 2015.
[256] Y. Osato, R. Yokoyama, and K. Nishitani, "A principal role for AtXTH18 in Arabidopsis thaliana root growth: A functional analysis using RNAi plants," *J. Plant Res.*, vol. 119, no. 2, pp. 153–162, 2006.
[257] V. Abraham, D. Taylor, and J. Haskins, "High content screening applied to large-scale cell biology," *Trends Biotechnol*, vol. 22 (1): 15, 2004.
[258] T. P. J. Dunkley, R. Watson, J. L. Griffin, P. Dupree, and K. S. Lilley, "Localization of Organelle Proteins by Isotope Tagging (LOPIT)," *Mol. Cell. Proteomics*, vol. 3, no. 11, pp. 1128–1134, 2004.
[259] H. C. Ishikawa-Ankerhold, R. Ankerhold, and G. P. C. Drummen, "Advanced fluorescence microscopy techniques-FRAP, FLIP, FLAP, FRET and FLIM," *Molecules*, vol. 17, no. 4, pp. 4047–4132, 2012.
[260] C. Sommer and D. W. Gerlich, "Machine learning in cell biology – teaching computers to recognize phenotypes," *J. Cell Sci.*, vol. 126, no. 24, pp. 5529–5539, 2013.
[261] M. Weigert *et al.*, "Content-Aware Image Restoration: Pushing the Limits of Fluorescence Microscopy," *bioRxiv*, p. 236463, 2018.

[262] S. Mei, W. Fei, and S. Zhou, “Gene ontology based transfer learning for protein subcellular localization,” *BMC Bioinformatics*, vol. 12, p. 44, 2011.
[263] Y. Long, I. Cheddadi, V. Mirabet, M. Dumond, C. Godin, and A. Boudaoud, “Cellular heterogeneity in pressure and growth emerges from tissue topology and geometry,” *bioRxiv*, p. 334664, 2018.

APPENDICES (Supplementary)

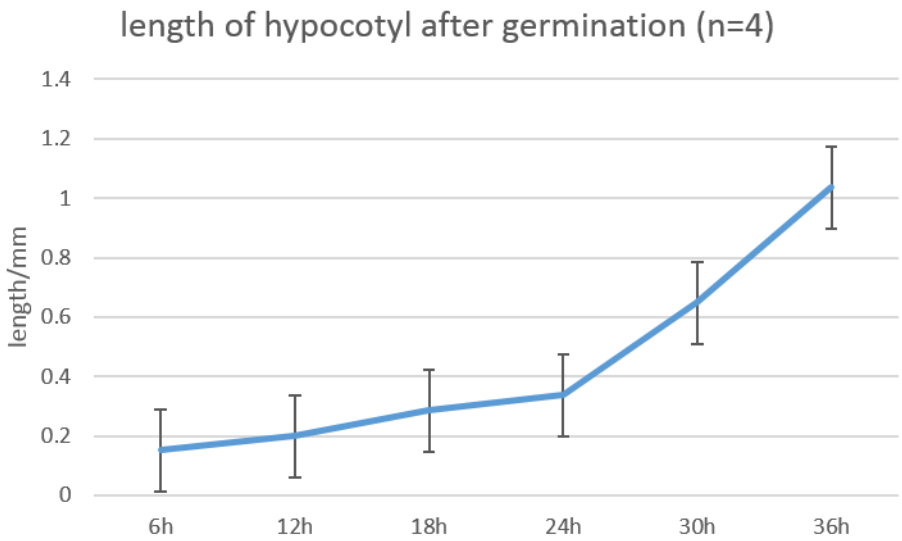

Supplementary Figure S1.1 The length of dark-grown hypocotyl in the first 36 HPG, measured using infra-red camera, n=4, error bar= standard deviation

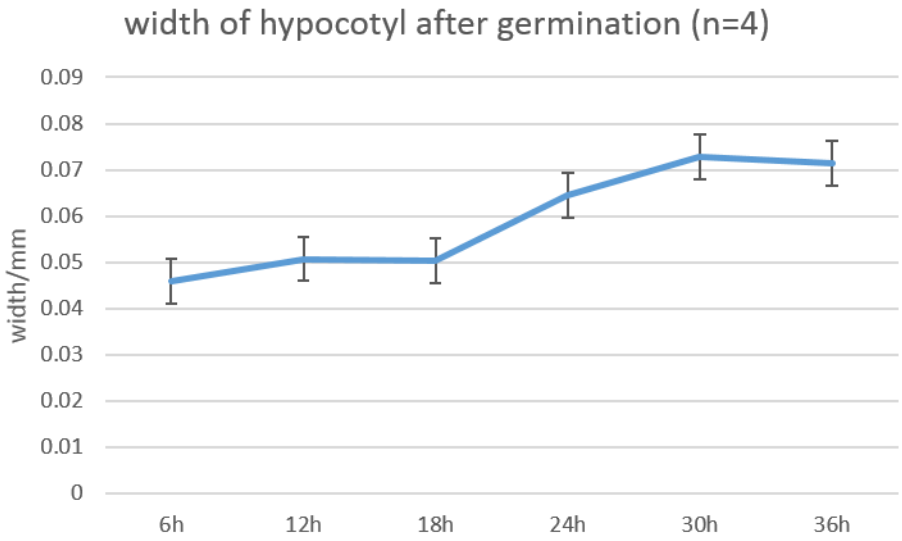

Supplementary Figure S1.2 The diameter (width) of dark-grown hypocotyl in the first 36 HPG, measured using infra-red camera, n=4, error bar= standard deviation

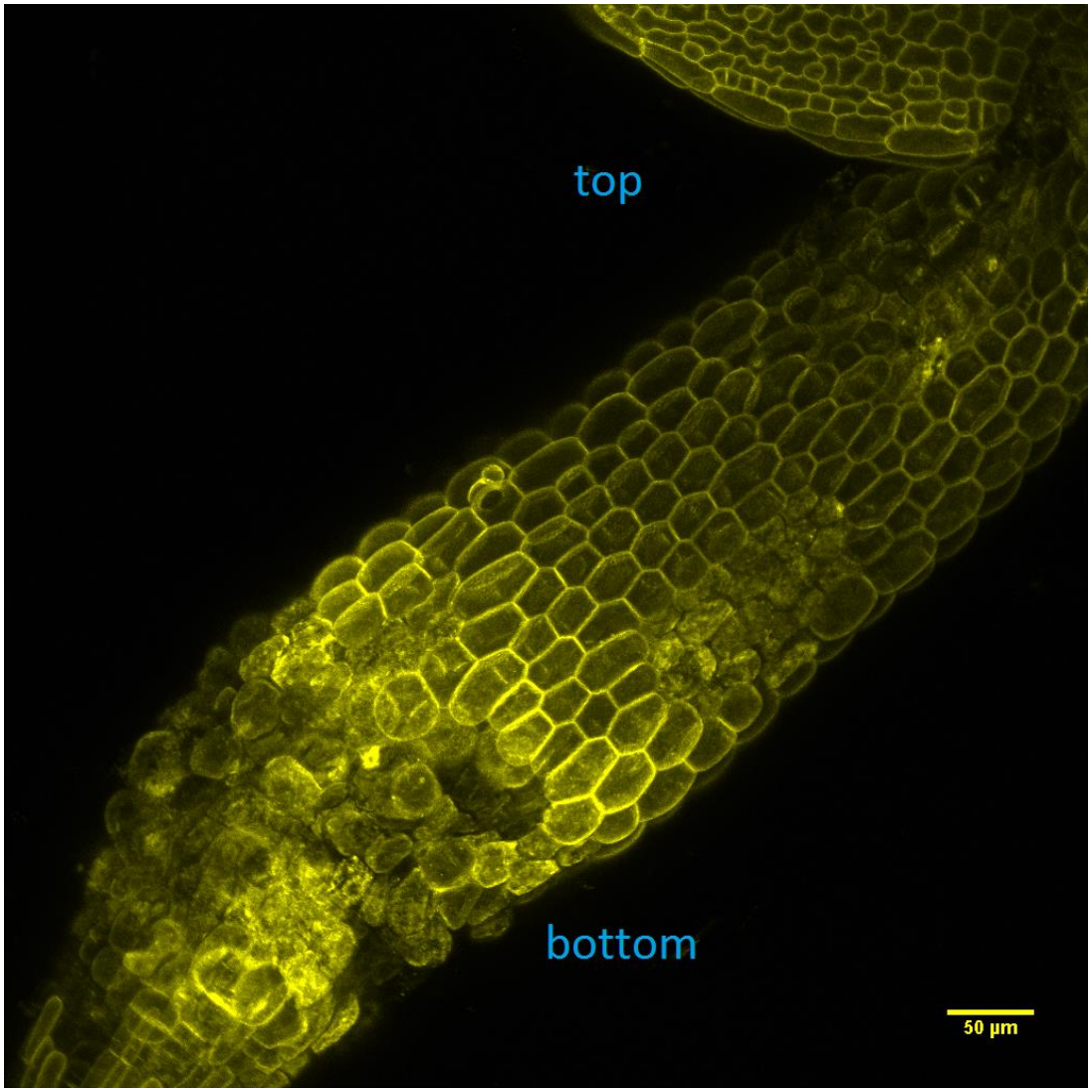

Supplementary Figure S1.3 Seedlings of A seedling of 24 HPG hypocotyl grown in dark, treated with 1 µm of isoxaben

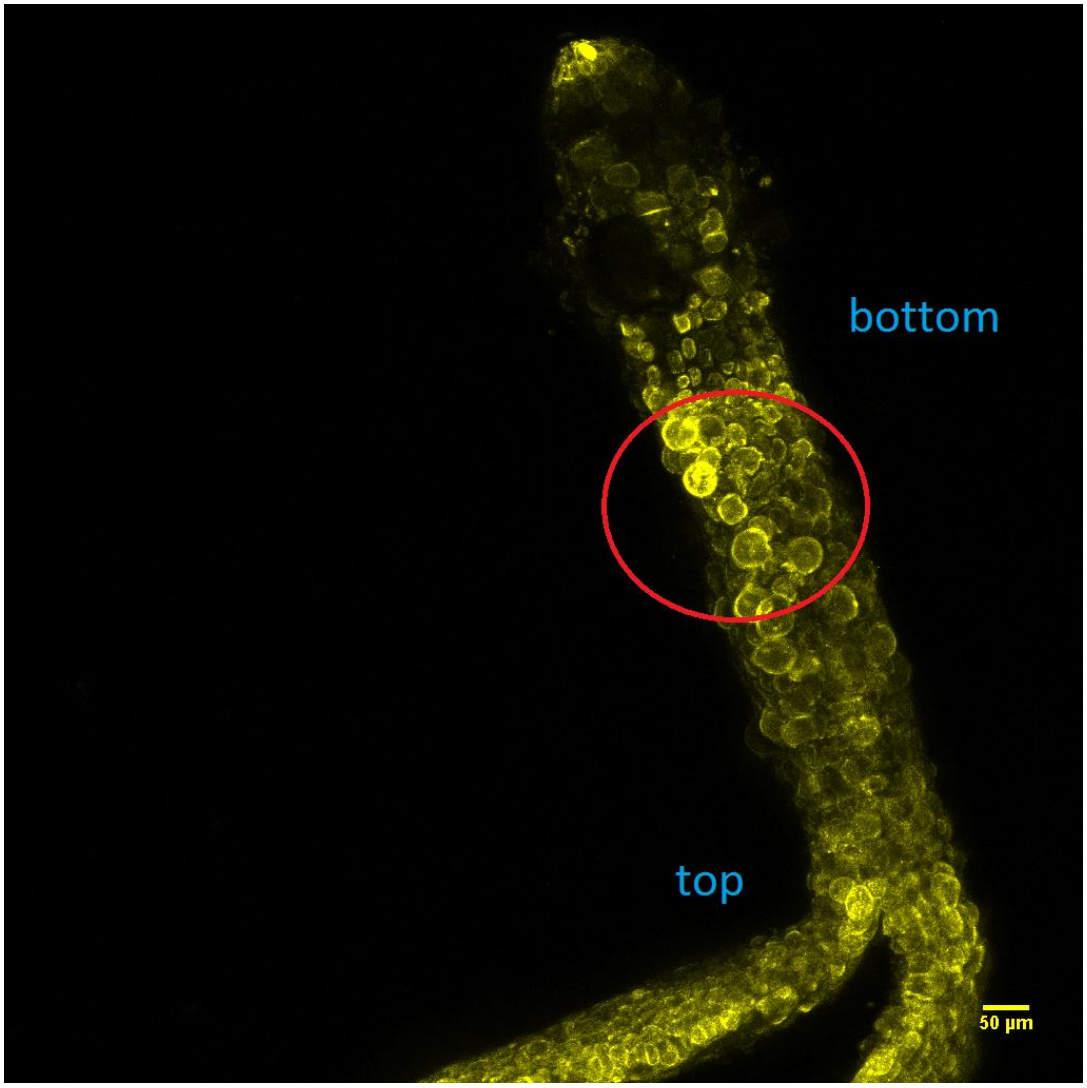

Supplementary Figure S1.4 Seedlings of A seedling of 96 HPG hypocotyl grown in dark, treated with 1 µm of isoxaben

Supplementary Figure S1.5 Quantification using Fibriltool, test image with noise had an anisotropy value of 0.38 but 0.9664 without noise

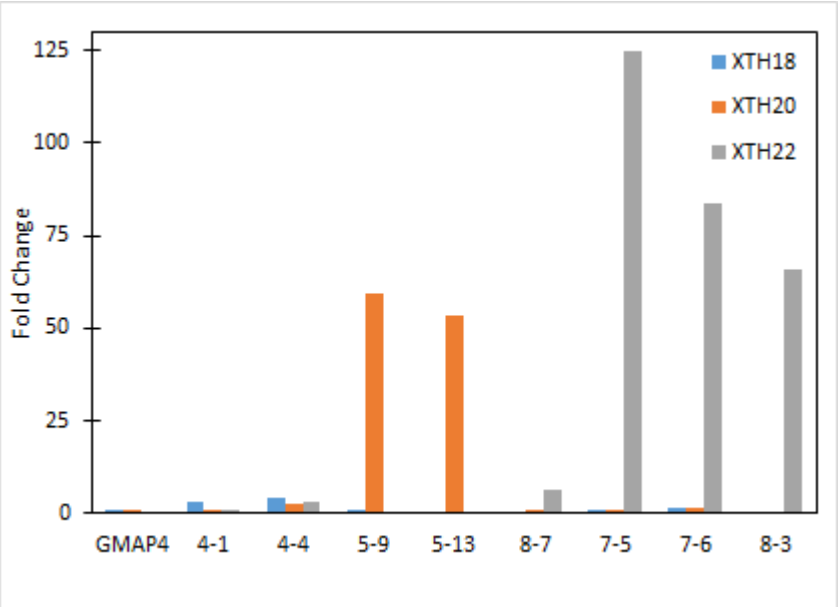

Supplementary Figure S1.6 Estradiol induction test of the XTH gene expression.

Calculating the osmotic potential and the turgor pressure (Chapter 2)

Molecular weight for sucrose: 342.2965 g/mol , so the concentration is: 0.0438 mol/L.

Use the formula :

$$\pi = i \cdot \phi \cdot C \cdot R \cdot T$$

Where pi is the osmotic potential, i is the ionization constant, phi is the osmotic coefficient (unitless, equals one in most cases), C is the concentration in mol/liter, R is the universal gas constant, 0.083145 L·bar/moles·K, and T is the absolute temperature in K

For the 1.5% sucrose solution: i=1 because sucrose does not ionize in water

Taking the room temperature to be 24 degree Celsius, i.e. 297.15 K

Osmotic potential is then 1.0821 bar=0.10821 MPa

Calculating the osmotic potential coming from other salts in the MS medium:

Major salts in 1/2MS media

- Ammonium nitrate (NH_4NO_3) 1,650 mg/l molecular weight: 80.0434 g/mol, i<=2
- Calcium chloride ($CaCl_2 \cdot 2H_2O$) 440 mg/l molecular weight: 110.98 g/mol, i<=3
- Magnesium sulphate ($MgSO_4 \cdot 7H_2O$) 370 mg/l molecular weight: 120.366 g/mol, i<=2
- Monopotassium phosphate (KH_2PO_4) 170 mg/l molecular weight: 136.086 g/mol, i<=2

- Potassium nitrate (KNO3) 1,900 mg/l. molecular weight: 101.1032 g/mol, i<=2

The maximum osmotic potential from those salts is therefore: 2.7227 bar=0.272 MPa

So psis, the original maximum osmotic pressure for the plant growing in the ½ MS media is

½*0.272+0.10821=0.2442

The formula for osmotic potential in the mannitol solution is:

PsiMAN=1*[MAN]*R*T

[MAN] in unit molar, mol/L, T in unit Kelvin

PsiMAN= -0.079[MAN]*T-22.67[MAN]

[MAN] in unit molal mol/kg. Since the water is the solvent, 1 molal= 1 molar, T in unit Celsius

The concentration of the mannitol solution to give plasmolysis varied with among seedlings, and the number of cells being plasmolysed per seedling also varied among seedlings. So the turgor pressure was estimated in terms of percentage of plasmolysed cells per seedling, and the calculated estimation was shown in the table below.

-P, the turgor pressure	**24h**	**48h**	**72h**	**96h**
mYFP	1.0528	Top: 0.6205 Bottom: <0.7441, >0.6205	Top: <0.497 Bottom: >0.497, <0.7441	Top: <0.2299- 0.497 Bottom: 0.497
mYFP+EtOH(control)	1.2378	1.1148	1.2378	>0.7441
PME	1.4853	1.1148-1.2378	1.2378	1.1147- 1.2378
PMEI	<1.2378 >0.9908	0.7441, <0.8676	0.7441 >0.6205	0.9911

Parameter	Meaning	Chosen method	value
LengthInitial	Initial cell length	From experimental data	20
WidthInitial	Initial cell width	From experimental data	16.17
PInitial	Initial turgor pressure	From experimental data	1.4

H1	Irreversible bond energy	arbitrarily	0.07
H2	Reversible bond energy	arbitrarily	0.01
alpha1	The linear parameter linking the synthesis rate (S) to the rate of increase in turgor pressure	arbitrary	1
psi	=R*T, linking the pressure difference to concentration difference	Calculated	24.7
theta1	Concentration of dissolved ions inside the cell	Calculated	0.0607
theta2	Concentration of dissolved ions outside the cell	Calculated	0.0099

Supplementary table S2.1 Initial values of some key parameters in the model

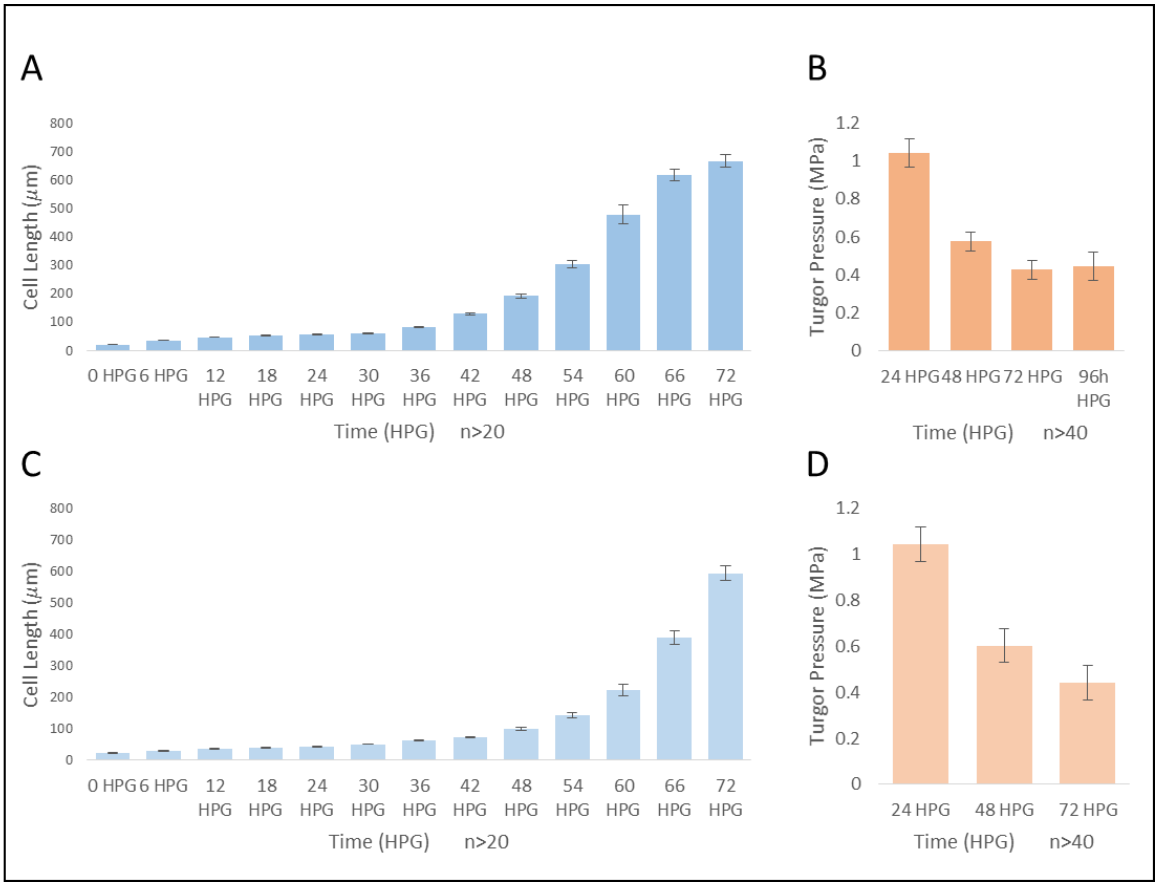

Supplementary Figure S2.1 The length and turgor pressure over for epidermal cells located in the middle (index 5-9) and upper (index 10-14) region of the hypocotyl shared very similar growth pattern with the basal cells, with a delay in time. **A:** Middle cell length over time. **B:** Middle cell pressure over time. **C:** Upper cell length over time. **D:** Upper cell pressure over time.

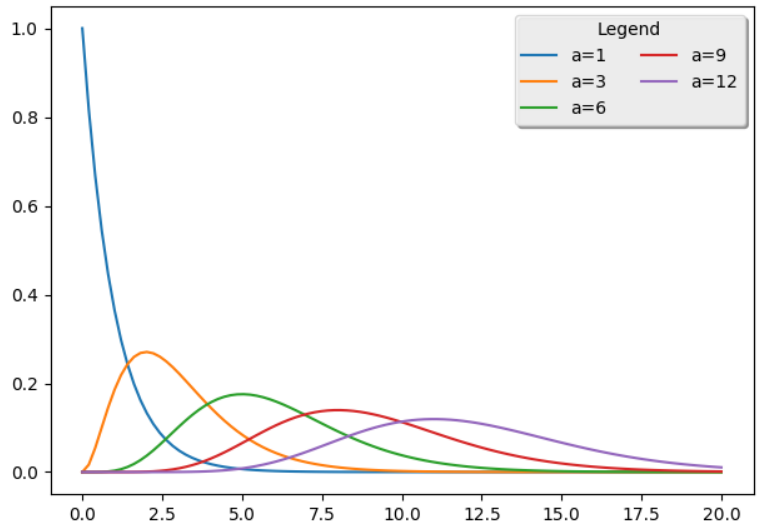

Supplementary Figure S2.2 Gamma distribution function with different parameters

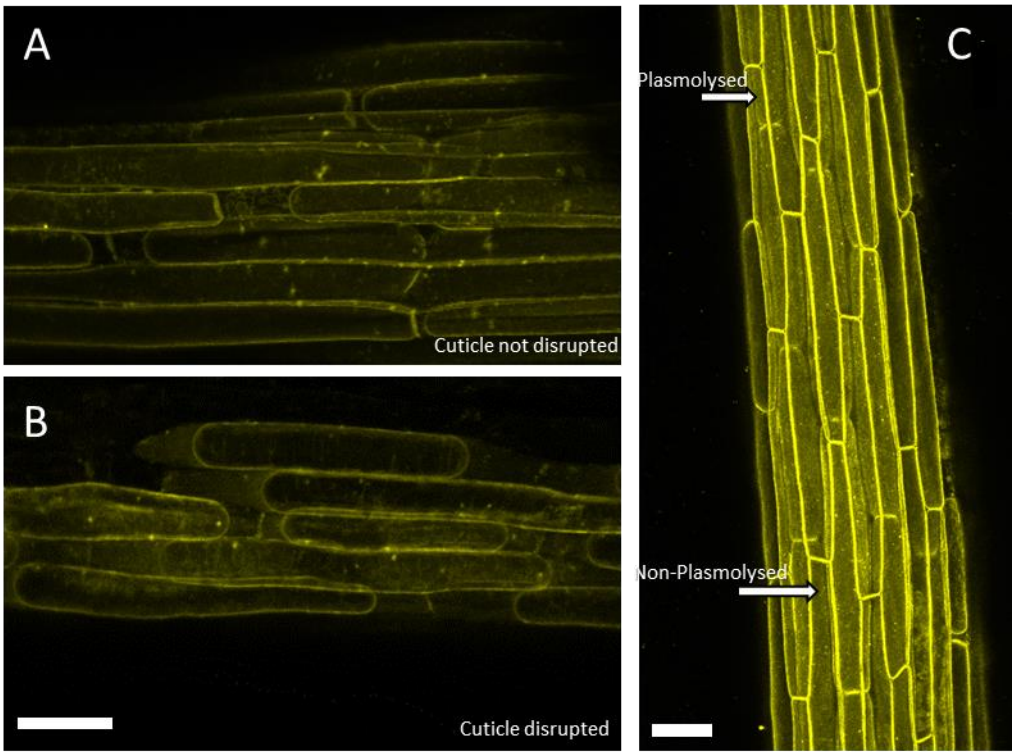

Supplementary Figure S2.3 A,B: Basal cells of M-YFP hypocotyl plasmolysed after immersed in the same concentration of mannitol solution, independent of the cuticle disruption. (bar=50 μm) **C:** A middle part of M-YFP hypocotyl imaged after 10 minutes in 0.35M Mannitol solution. Plasmolysed and non-plasmolysed cells can both be seen in the same region.

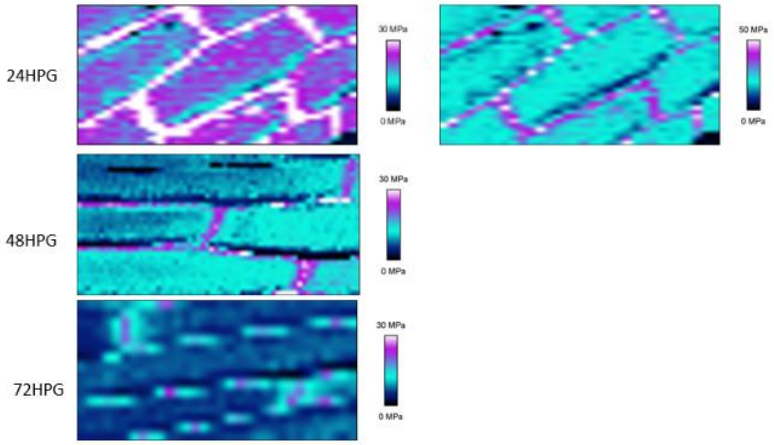

Supplementary Figure S2.4 Representative AFM images at 3 time points

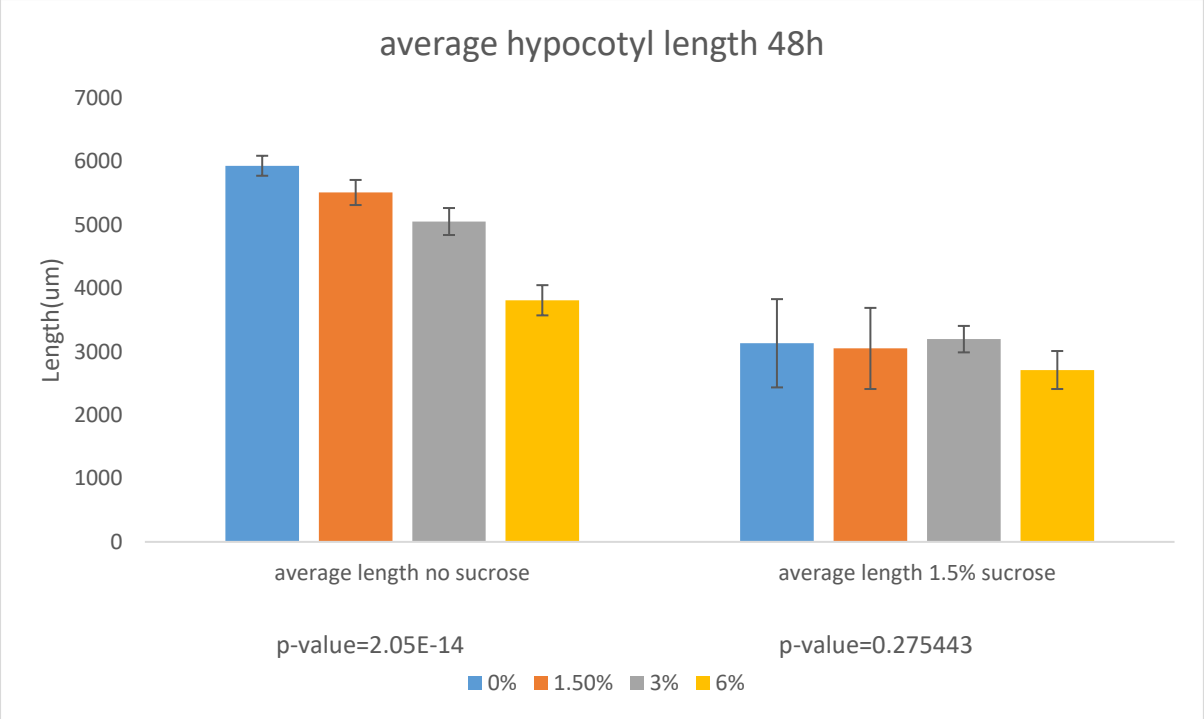

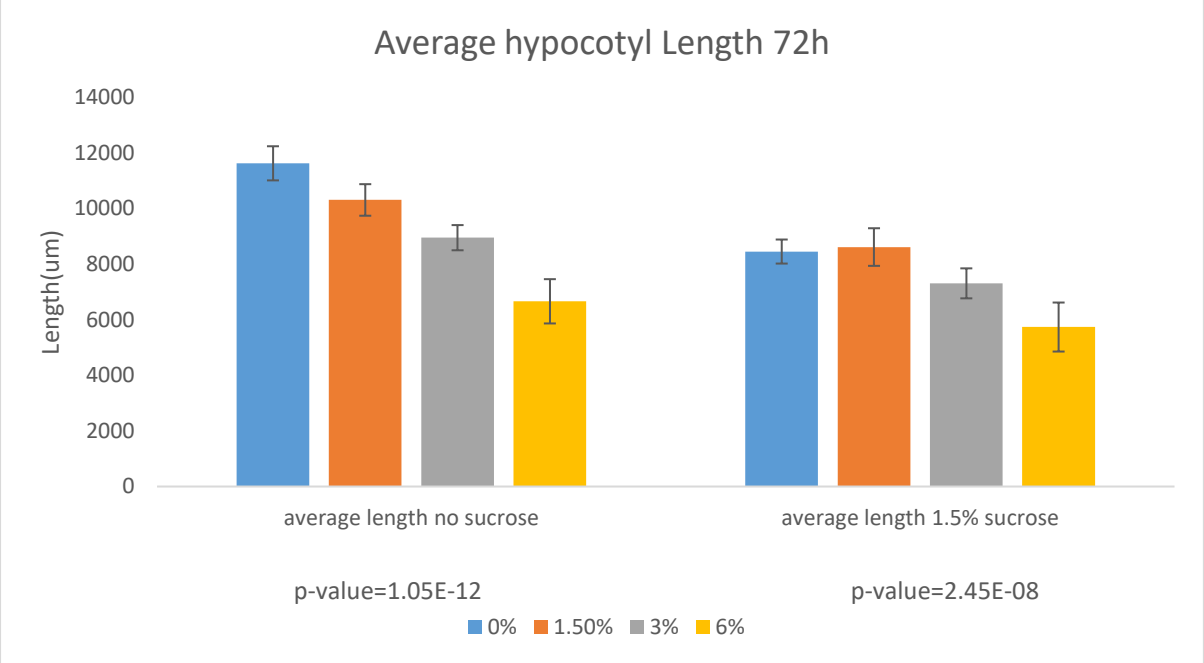

Supplementary Figure S2.5 Average hypocotyl length with different amount of sorbitol (concentration equivalent to sucrose) (n=8, ANOVA test). Except the seedlings grown with sucrose at 48 HPG, at all other three conditions the hypocotyl length varied significantly with the amount of sorbitol in the media. A higher concentration of sorbitol in the media caused reduced hypocotyl lengths.

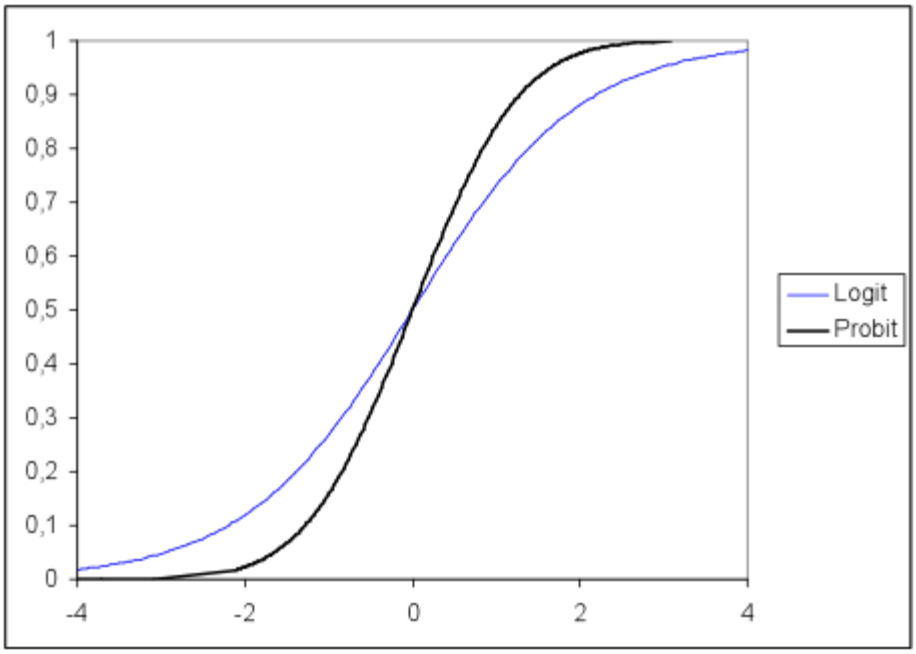

Supplementary Figure S3.1 The Logistic function has more flat tails than Probit function[128]

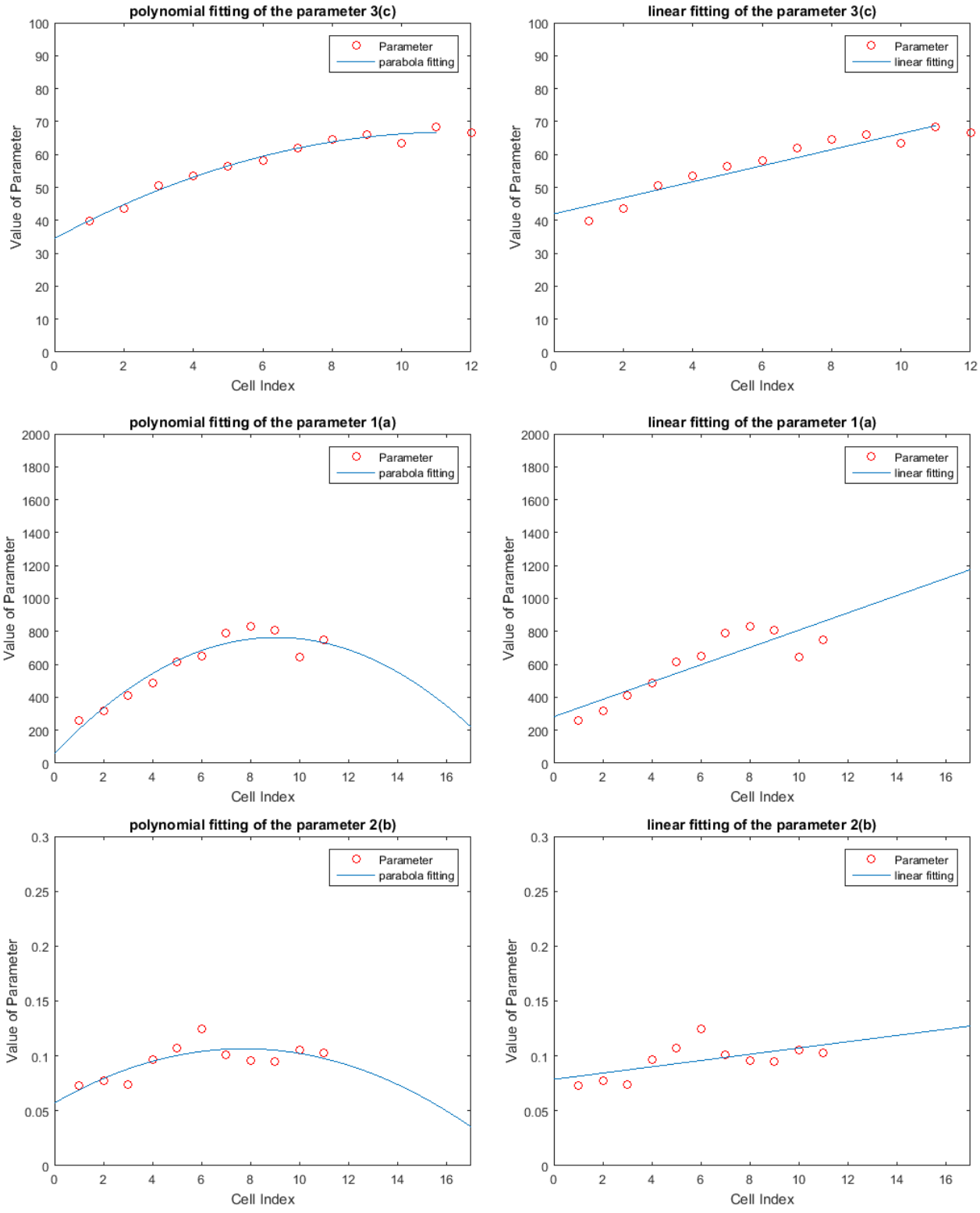

Supplementary Figure S3.2 The parameter extrapolations of the Log-log function

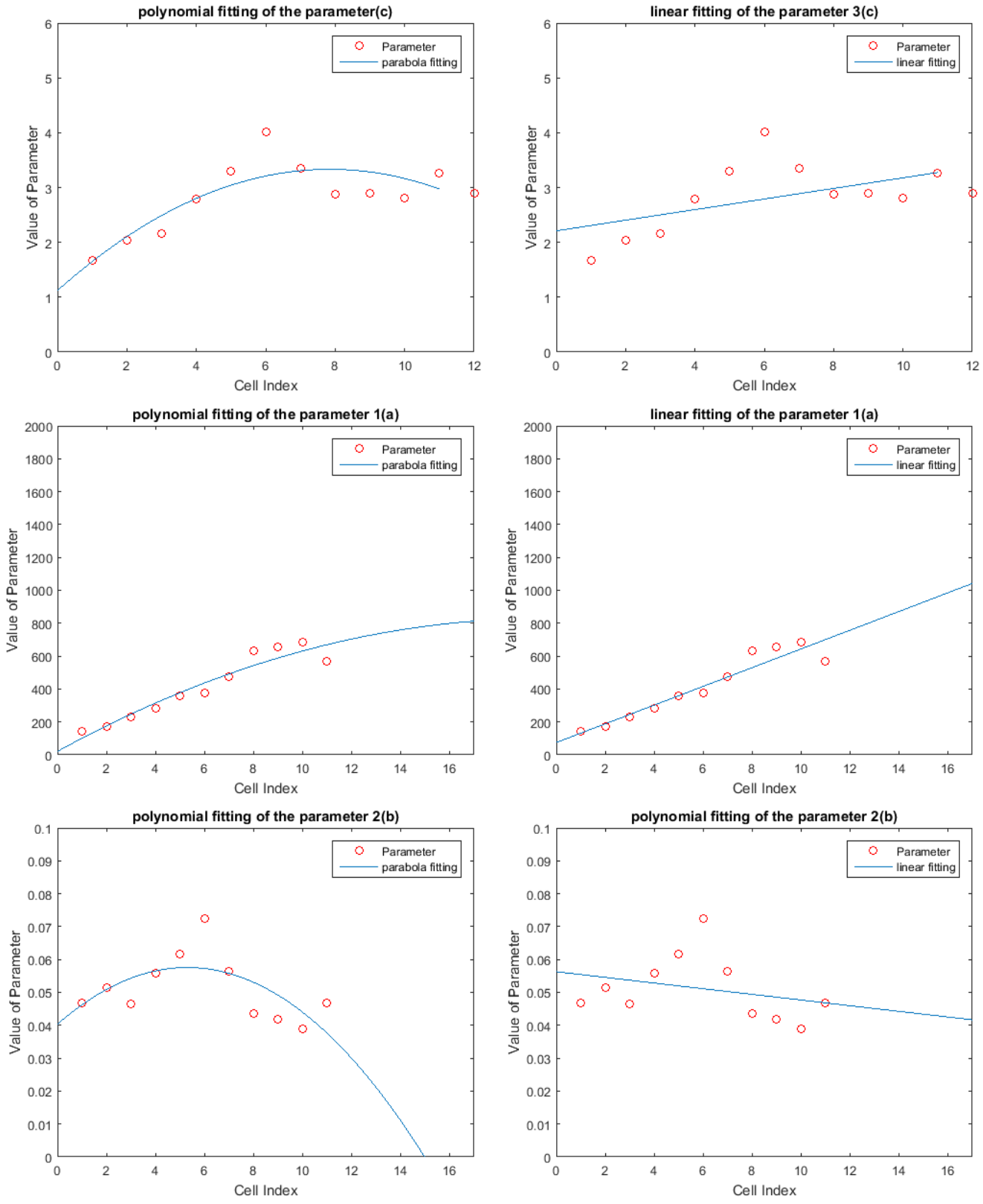

Supplementary Figure S3.3 The parameter extrapolations of the Probit function

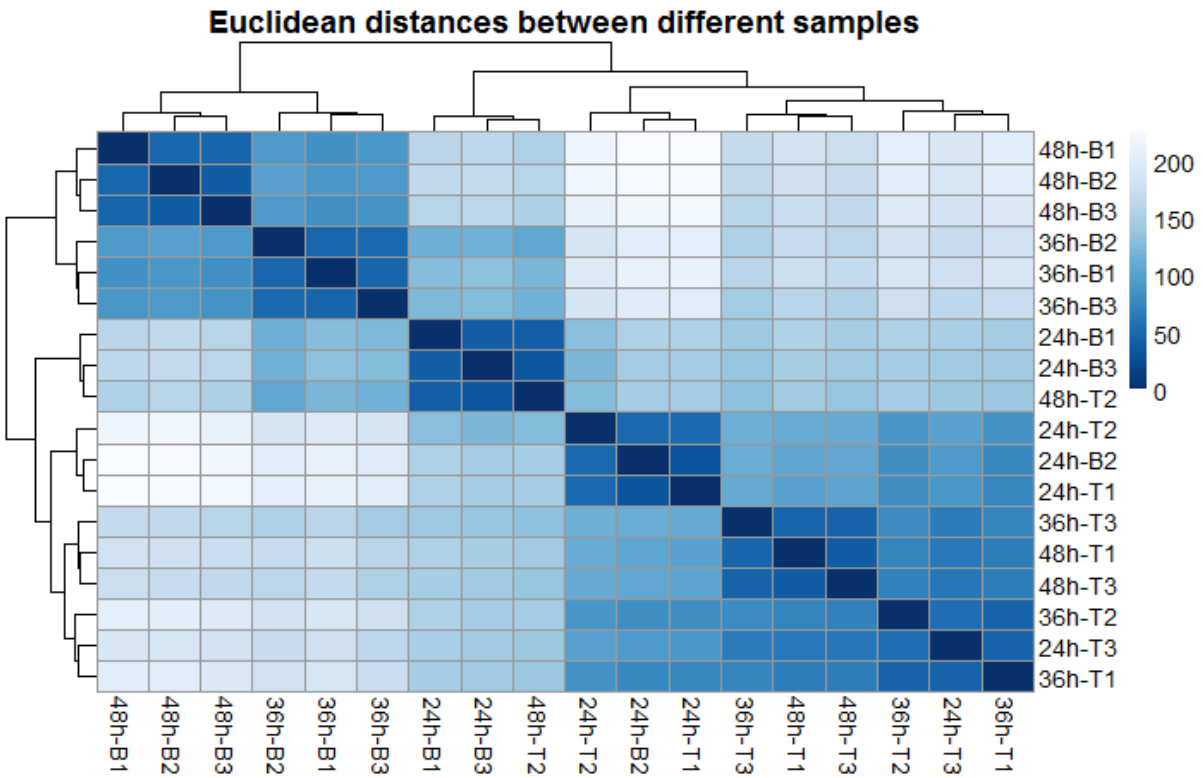

Supplementary Figure S4.1a The Euclidean distance among all 18 samples

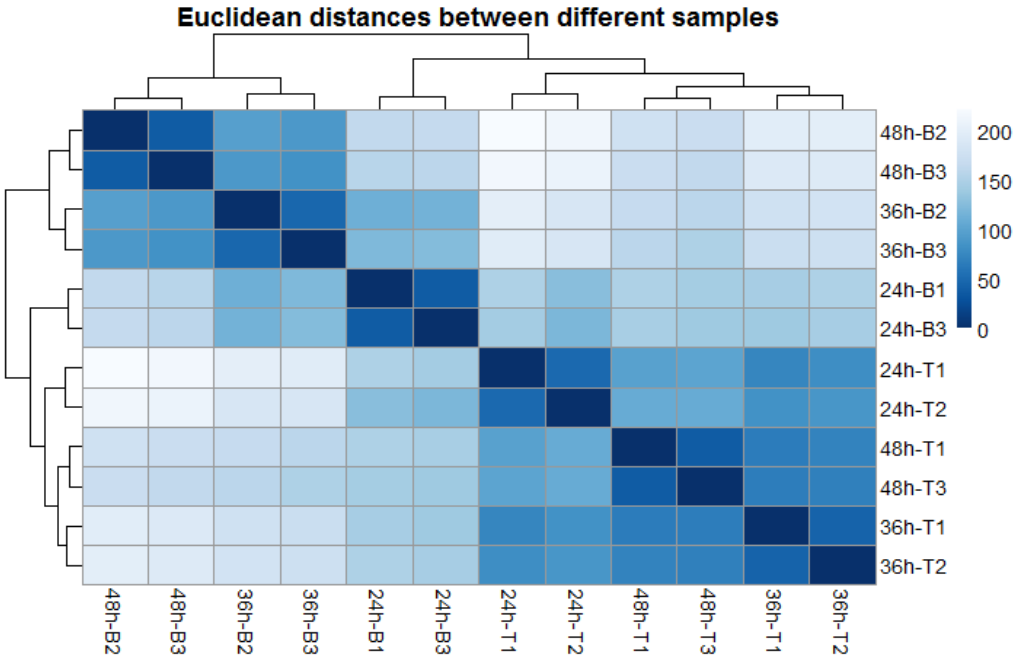

Supplementary Figure S4.1b The Euclidean distance among the 12 samples used in analysis

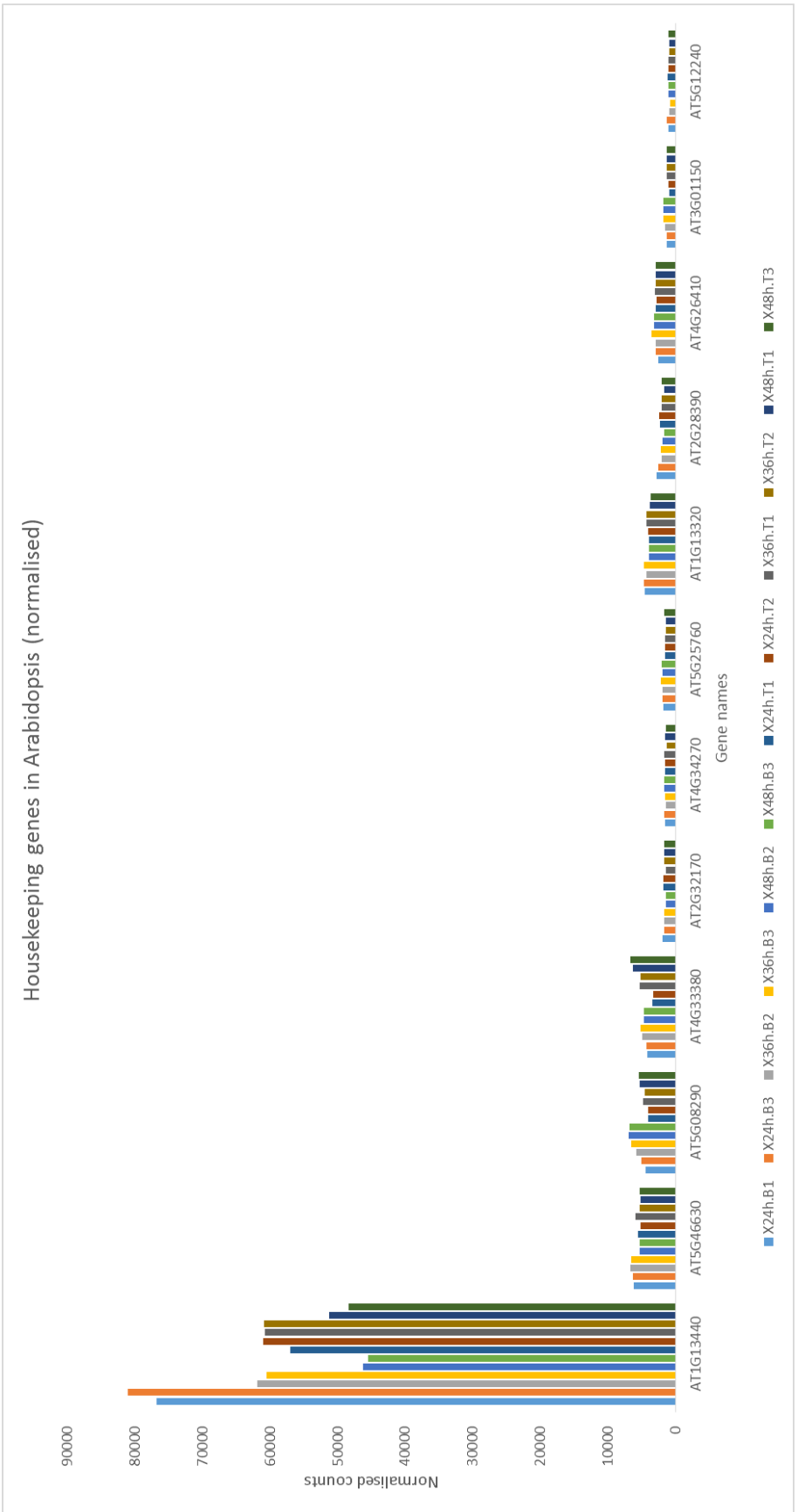

Supplementary Figure S4.2 Normalised counts for the *Arabidopsis* housekeeping genes

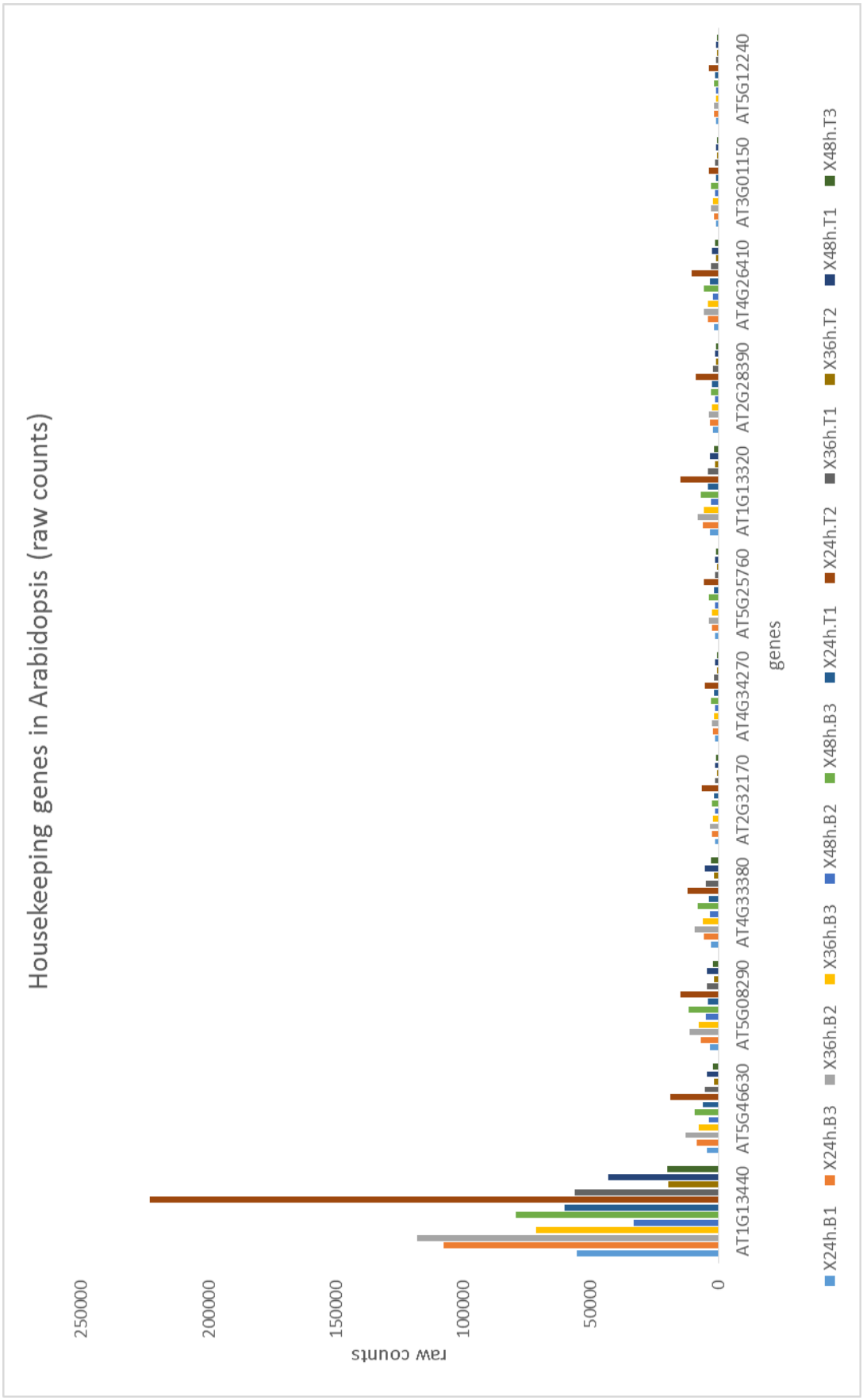

Supplementary Figure S4.3 Raw counts for the *Arabidopsis* housekeeping genes

Analysis Type:	PANTHER Overrepresentation Test (Released 20171205)
Annotation Version and Release Date:	GO Ontology database Released 2018-02-02
Analyzed List:	upload_1 (Arabidopsis thaliana)
Reference List:	Arabidopsis thaliana (all genes in database)
Test Type:	FISHER

GO biological process complete	Arabidopsis thaliana - REFLIST (27502)	upload_1 (189)	upload_1 (expected)	upload_1 (over/under)	upload_1 (fold Enrichment)	upload_1 (raw P-value)	upload_1 (FDR)
negative regulation of circadian rhythm (GO:0042754)	3	2	0.02	+	97.01	4.57E-04	4.29E-02
jasmonic acid biosynthetic process (GO:0009695)	23	4	0.16	+	25.31	3.26E-05	5.47E-03
regulation of systemic acquired resistance (GO:0010112)	20	3	0.14	+	21.83	5.01E-04	4.40E-02
jasmonic acid metabolic process (GO:0009694)	28	4	0.19	+	20.79	6.51E-05	9.47E-03
response to chitin (GO:0010200)	132	9	0.91	+	9.92	5.73E-07	1.86E-04
response to jasmonic acid (GO:0009753)	211	14	1.45	+	9.65	5.41E-10	3.32E-07
response to wounding (GO:0009611)	212	13	1.46	+	8.92	5.58E-09	3.09E-06
phenylpropanoid biosynthetic process (GO:0009699)	116	7	0.8	+	8.78	2.25E-05	4.01E-03
indole-containing compound metabolic process (GO:0042430)	89	5	0.61	+	8.17	4.72E-04	4.35E-02
response to organonitrogen compound (GO:0010243)	190	10	1.31	+	7.66	1.27E-06	3.50E-04
S-glycoside metabolic process (GO:0016143)	116	6	0.8	+	7.53	1.96E-04	2.36E-02
glucosinolate metabolic process (GO:0019760)	116	6	0.8	+	7.53	1.96E-04	2.31E-02
glycosinolate metabolic process (GO:0019757)	116	6	0.8	+	7.53	1.96E-04	2.26E-02
phenylpropanoid metabolic process (GO:0009698)	155	8	1.07	+	7.51	1.71E-05	3.16E-03
regulation of immune system process (GO:0002682)	117	6	0.8	+	7.46	2.05E-04	2.31E-02
response to salicylic acid (GO:0009751)	196	10	1.35	+	7.42	1.65E-06	4.16E-04
rhythmic process (GO:0048511)	122	6	0.84	+	7.16	2.54E-04	2.65E-02
response to drug (GO:0042493)	529	22	3.64	+	6.05	3.42E-11	4.73E-08
response to nitrogen compound (GO:1901698)	297	12	2.04	+	5.88	1.58E-06	4.15E-04
negative regulation of RNA biosynthetic process (GO:1902679)	204	8	1.4	+	5.71	1.10E-04	1.52E-02
negative regulation of nucleic acid-templated transcription (GO:1903507)	204	8	1.4	+	5.71	1.10E-04	1.48E-02
secondary metabolite biosynthetic process (GO:0044550)	311	12	2.14	+	5.61	2.49E-06	6.00E-04
negative regulation of RNA metabolic process (GO:0051253)	210	8	1.44	+	5.54	1.33E-04	1.64E-02
hormone biosynthetic process (GO:0042446)	184	7	1.26	+	5.54	3.54E-04	3.43E-02
secondary metabolic process (GO:0019748)	475	17	3.26	+	5.21	5.40E-08	2.13E-05
regulation of defense response (GO:0031347)	225	8	1.55	+	5.17	2.10E-04	2.32E-02

negative regulation of nucleobase-containing compound metabolic process (GO:0045934)	229	8	1.57	+	5.08	2.36E-04	2.51E-02
negative regulation of macromolecule biosynthetic process (GO:0010558)	257	8	1.77	+	4.53	4.96E-04	4.43E-02
response to ethylene (GO:0009723)	297	9	2.04	+	4.41	2.69E-04	2.76E-02
response to bacterium (GO:0009617)	425	12	2.92	+	4.11	5.06E-05	7.99E-03
response to organic cyclic compound (GO:0014070)	366	10	2.52	+	3.98	2.77E-04	2.79E-02
defense response to bacterium (GO:0042742)	331	9	2.27	+	3.96	5.78E-04	4.99E-02
response to acid chemical (GO:0001101)	1148	30	7.89	+	3.8	4.97E-10	3.44E-07
response to oxygen-containing compound (GO:1901700)	1506	39	10.35	+	3.77	1.01E-12	1.87E-09
response to oxidative stress (GO:0006979)	446	11	3.07	+	3.59	3.24E-04	3.20E-02
response to osmotic stress (GO:0006970)	618	15	4.25	+	3.53	3.22E-05	5.56E-03
defense response (GO:0006952)	1407	34	9.67	+	3.52	2.20E-10	2.03E-07
response to salt stress (GO:0009651)	545	13	3.75	+	3.47	1.29E-04	1.66E-02
response to inorganic substance (GO:0010035)	900	20	6.19	+	3.23	5.41E-06	1.25E-03
defense response to other organism (GO:0098542)	855	19	5.88	+	3.23	9.41E-06	1.93E-03
response to other organism (GO:0051707)	1155	25	7.94	+	3.15	5.29E-07	1.95E-04
response to external biotic stimulus (GO:0043207)	1157	25	7.95	+	3.14	5.45E-07	1.89E-04
response to external stimulus (GO:0009605)	1520	32	10.45	+	3.06	2.06E-08	8.76E-06
response to biotic stimulus (GO:0009607)	1195	25	8.21	+	3.04	9.70E-07	2.82E-04
response to organic substance (GO:0010033)	1947	40	13.38	+	2.99	4.90E-10	3.87E-07
response to hormone (GO:0009725)	1672	34	11.49	+	2.96	1.60E-08	8.04E-06
response to endogenous stimulus (GO:0009719)	1680	34	11.55	+	2.94	1.79E-08	8.27E-06
oxoacid metabolic process (GO:0043436)	1043	21	7.17	+	2.93	1.35E-05	2.66E-03
organic acid metabolic process (GO:0006082)	1046	21	7.19	+	2.92	1.41E-05	2.68E-03
response to stress (GO:0006950)	3283	64	22.56	+	2.84	4.09E-15	2.26E-11
multi-organism process (GO:0051704)	1616	30	11.11	+	2.7	8.38E-07	2.58E-04
response to chemical (GO:0042221)	2762	50	18.98	+	2.63	1.54E-10	1.70E-07
response to abiotic stimulus (GO:0009628)	1954	32	13.43	+	2.38	5.51E-06	1.22E-03
aromatic compound biosynthetic process (GO:0019438)	2285	35	15.7	+	2.23	7.96E-06	1.69E-03
small molecule metabolic process (GO:0044281)	1512	23	10.39	+	2.21	3.59E-04	3.43E-02
response to stimulus (GO:0050896)	5805	88	39.89	+	2.21	8.09E-15	2.24E-11
cell communication (GO:0007154)	1888	28	12.97	+	2.16	1.30E-04	1.64E-02
signal transduction (GO:0007165)	1625	24	11.17	+	2.15	4.96E-04	4.50E-02
signaling (GO:0023052)	1655	24	11.37	+	2.11	5.88E-04	5.00E-02
organic cyclic compound biosynthetic process (GO:1901362)	2419	34	16.62	+	2.05	8.19E-05	1.16E-02
cellular biosynthetic process (GO:0044249)	4040	49	27.76	+	1.76	5.21E-05	8.00E-03
biosynthetic process (GO:0009058)	4404	52	30.27	+	1.72	6.07E-05	9.07E-03

organic substance biosynthetic process (GO:1901576)	4140	48	28.45	+	1.69	2.15E-04	2.33E-02
cellular process (GO:0009987)	10706	102	73.57	+	1.39	3.45E-05	5.61E-03
metabolic process (GO:0008152)	9767	93	67.12	+	1.39	1.28E-04	1.69E-02

Supplementary Table S4.1 Enrichment analysis of genes with changed expression pattern (up-down or down-up) over time

Analysis Type:	PANTHER Overrepresentation Test (Released 20171205)
Annotation Version and Release Date:	GO Ontology database Released 2018-08-09
Analyzed List:	upload_1 (Arabidopsis thaliana)
Reference List:	Arabidopsis thaliana (all genes in database)
Test Type:	FISHER

GO biological process complete	Arabidopsis thaliana - REFLIST (27502)	upload_1 (1584)	upload_1 (expected)	upload_1 (over/under)	upload_1 (fold Enrichment)	upload_1 (raw P-value)	upload_1 (FDR)
camalexin metabolic process (GO:0052317)	11	7	0.63	+	11.05	2.62E-05	1.46E-03
camalexin biosynthetic process (GO:0010120)	11	7	0.63	+	11.05	2.62E-05	1.45E-03
defense response by callose deposition in cell wall (GO:0052544)	16	10	0.92	+	10.85	5.31E-07	5.31E-05
defense response by cell wall thickening (GO:0052482)	16	10	0.92	+	10.85	5.31E-07	5.22E-05
phytoalexin biosynthetic process (GO:0052315)	13	8	0.75	+	10.68	8.17E-06	5.74E-04
phytoalexin metabolic process (GO:0052314)	13	8	0.75	+	10.68	8.17E-06	5.68E-04
indole phytoalexin biosynthetic process (GO:0009700)	13	8	0.75	+	10.68	8.17E-06	5.61E-04
indole phytoalexin metabolic process (GO:0046217)	13	8	0.75	+	10.68	8.17E-06	5.55E-04
defense response by callose deposition (GO:0052542)	18	11	1.04	+	10.61	1.68E-07	1.91E-05
toxin biosynthetic process (GO:0009403)	21	10	1.21	+	8.27	3.45E-06	2.72E-04
indoleacetic acid biosynthetic process (GO:0009684)	11	5	0.63	+	7.89	1.25E-03	3.70E-02
indoleacetic acid metabolic process (GO:0009683)	12	5	0.69	+	7.23	1.70E-03	4.80E-02
protein autoubiquitination (GO:0051865)	15	6	0.86	+	6.94	6.90E-04	2.18E-02
cell wall thickening (GO:0052386)	28	11	1.61	+	6.82	4.91E-06	3.63E-04
indole-containing compound biosynthetic process (GO:0042435)	50	19	2.88	+	6.6	2.95E-09	4.70E-07
callose deposition in cell wall (GO:0052543)	27	10	1.56	+	6.43	2.01E-05	1.16E-03
response to insect (GO:0009625)	28	10	1.61	+	6.2	2.59E-05	1.46E-03
tryptophan biosynthetic process (GO:0000162)	23	8	1.32	+	6.04	1.94E-04	7.76E-03
indolalkylamine biosynthetic process (GO:0046219)	23	8	1.32	+	6.04	1.94E-04	7.71E-03

regulation of jasmonic acid mediated signaling pathway (GO:2000022)	29	10	1.67	+	5.99	3.32E-05	1.76E-03
indole glucosinolate metabolic process (GO:0042343)	35	12	2.02	+	5.95	5.75E-06	4.14E-04
callose localization (GO:0052545)	33	11	1.9	+	5.79	1.75E-05	1.06E-03
negative regulation of cell death (GO:0060548)	30	10	1.73	+	5.79	4.21E-05	2.12E-03
indolalkylamine metabolic process (GO:0006586)	31	10	1.79	+	5.6	5.29E-05	2.61E-03
tryptophan metabolic process (GO:0006568)	31	10	1.79	+	5.6	5.29E-05	2.58E-03
fatty acid derivative biosynthetic process (GO:1901570)	25	8	1.44	+	5.56	3.10E-04	1.12E-02
wax biosynthetic process (GO:0010025)	22	7	1.27	+	5.52	7.58E-04	2.37E-02
polysaccharide localization (GO:0033037)	36	11	2.07	+	5.31	3.42E-05	1.80E-03
indole-containing compound metabolic process (GO:0042430)	92	28	5.3	+	5.28	4.37E-11	8.33E-09
wax metabolic process (GO:0010166)	23	7	1.32	+	5.28	9.43E-04	2.89E-02
toxin metabolic process (GO:0009404)	71	20	4.09	+	4.89	7.43E-08	8.96E-06
defense response to bacterium, incompatible interaction (GO:0009816)	40	11	2.3	+	4.77	7.64E-05	3.53E-03
auxin biosynthetic process (GO:0009851)	41	11	2.36	+	4.66	9.22E-05	4.03E-03
fatty acid derivative metabolic process (GO:1901568)	38	10	2.19	+	4.57	2.18E-04	8.21E-03
response to nematode (GO:0009624)	74	18	4.26	+	4.22	2.01E-06	1.77E-04
jasmonic acid metabolic process (GO:0009694)	47	11	2.71	+	4.06	2.57E-04	9.39E-03
response to chitin (GO:0010200)	137	32	7.89	+	4.06	5.97E-10	1.01E-07
secondary metabolite biosynthetic process (GO:0044550)	198	46	11.4	+	4.03	1.32E-13	4.32E-11
phenol-containing compound metabolic process (GO:0018958)	44	10	2.53	+	3.95	5.93E-04	1.95E-02
S-glycoside biosynthetic process (GO:0016144)	53	12	3.05	+	3.93	1.79E-04	7.39E-03
glucosinolate biosynthetic process (GO:0019761)	53	12	3.05	+	3.93	1.79E-04	7.33E-03
glycosinolate biosynthetic process (GO:0019758)	53	12	3.05	+	3.93	1.79E-04	7.28E-03
negative regulation of defense response (GO:0031348)	54	12	3.11	+	3.86	2.08E-04	8.02E-03
glutathione metabolic process (GO:0006749)	57	12	3.28	+	3.66	3.20E-04	1.15E-02
cellular biogenic amine metabolic process (GO:0006576)	63	13	3.63	+	3.58	2.17E-04	8.27E-03
cellular amine metabolic process (GO:0044106)	63	13	3.63	+	3.58	2.17E-04	8.22E-03
lignin metabolic process (GO:0009808)	88	18	5.07	+	3.55	1.60E-05	1.02E-03
toxin catabolic process (GO:0009407)	49	10	2.82	+	3.54	1.22E-03	3.63E-02
lignin biosynthetic process (GO:0009809)	64	13	3.69	+	3.53	2.48E-04	9.11E-03
aromatic amino acid family metabolic process (GO:0009072)	84	17	4.84	+	3.51	3.07E-05	1.65E-03
oligopeptide transport (GO:0006857)	71	14	4.09	+	3.42	1.91E-04	7.66E-03
auxin metabolic process (GO:0009850)	66	13	3.8	+	3.42	3.22E-04	1.15E-02
benzene-containing compound metabolic process (GO:0042537)	51	10	2.94	+	3.4	1.58E-03	4.56E-02

phenylpropanoid biosynthetic process (GO:0009699)	123	24	7.08	+	3.39	1.38E-06	1.24E-04
phenylpropanoid metabolic process (GO:0009698)	162	31	9.33	+	3.32	6.26E-08	7.71E-06
aromatic amino acid family biosynthetic process (GO:0009073)	59	11	3.4	+	3.24	1.35E-03	3.96E-02
secondary metabolic process (GO:0019748)	403	75	23.21	+	3.23	1.28E-16	8.40E-14
regulation of cell death (GO:0010941)	78	14	4.49	+	3.12	4.43E-04	1.51E-02
defense response to oomycetes (GO:0002229)	67	12	3.86	+	3.11	1.13E-03	3.38E-02
S-glycoside metabolic process (GO:0016143)	147	26	8.47	+	3.07	2.56E-06	2.16E-04
glucosinolate metabolic process (GO:0019760)	147	26	8.47	+	3.07	2.56E-06	2.13E-04
glycosinolate metabolic process (GO:0019757)	147	26	8.47	+	3.07	2.56E-06	2.10E-04
regulation of innate immune response (GO:0045088)	119	21	6.85	+	3.06	2.35E-05	1.33E-03
response to wounding (GO:0009611)	216	38	12.44	+	3.05	1.57E-08	2.16E-06
regulation of immune response (GO:0050776)	126	22	7.26	+	3.03	1.75E-05	1.06E-03
detoxification (GO:0098754)	86	15	4.95	+	3.03	3.68E-04	1.28E-02
sulfur compound biosynthetic process (GO:0044272)	156	27	8.98	+	3.01	2.38E-06	2.07E-04
defense response to bacterium (GO:0042742)	388	67	22.35	+	3	1.24E-13	4.31E-11
antibiotic catabolic process (GO:0017001)	100	17	5.76	+	2.95	2.02E-04	7.85E-03
defense response, incompatible interaction (GO:0009814)	166	28	9.56	+	2.93	2.42E-06	2.08E-04
hydrogen peroxide catabolic process (GO:0042744)	95	16	5.47	+	2.92	3.37E-04	1.18E-02
regulation of defense response (GO:0031347)	246	41	14.17	+	2.89	1.68E-08	2.25E-06
regulation of immune system process (GO:0002682)	138	23	7.95	+	2.89	2.20E-05	1.26E-03
regulation of response to biotic stimulus (GO:0002831)	85	14	4.9	+	2.86	9.39E-04	2.89E-02
response to bacterium (GO:0009617)	487	80	28.05	+	2.85	5.72E-15	2.25E-12
response to jasmonic acid (GO:0009753)	214	35	12.33	+	2.84	2.72E-07	2.92E-05
response to oomycetes (GO:0002239)	86	14	4.95	+	2.83	1.04E-03	3.16E-02
response to organonitrogen compound (GO:0010243)	230	37	13.25	+	2.79	1.81E-07	2.01E-05
hydrogen peroxide metabolic process (GO:0042743)	102	16	5.87	+	2.72	6.73E-04	2.16E-02
regulation of response to external stimulus (GO:0032101)	90	14	5.18	+	2.7	1.53E-03	4.42E-02
protein autophosphorylation (GO:0046777)	202	31	11.63	+	2.66	6.16E-06	4.39E-04
innate immune response (GO:0045087)	306	46	17.62	+	2.61	4.03E-08	5.29E-06
immune system process (GO:0002376)	367	55	21.14	+	2.6	3.17E-09	4.94E-07
response to karrikin (GO:0080167)	134	20	7.72	+	2.59	4.51E-04	1.53E-02
amine metabolic process (GO:0009308)	115	17	6.62	+	2.57	8.43E-04	2.61E-02
immune response (GO:0006955)	312	46	17.97	+	2.56	1.01E-07	1.19E-05
leaf senescence (GO:0010150)	102	15	5.87	+	2.55	1.74E-03	4.86E-02

cell death (GO:0008219)	133	19	7.66	+	2.48	8.23E-04	2.56E-02
response to salicylic acid (GO:0009751)	203	29	11.69	+	2.48	2.96E-05	1.61E-03
aging (GO:0007568)	161	23	9.27	+	2.48	2.10E-04	8.07E-03
sulfur compound metabolic process (GO:0006790)	393	56	22.64	+	2.47	1.08E-08	1.51E-06
hormone biosynthetic process (GO:0042446)	183	26	10.54	+	2.47	8.36E-05	3.74E-03
cellular response to ethylene stimulus (GO:0071369)	200	28	11.52	+	2.43	5.42E-05	2.60E-03
response to drug (GO:0042493)	597	83	34.38	+	2.41	7.43E-12	1.69E-09
organic hydroxy compound biosynthetic process (GO:1901617)	175	24	10.08	+	2.38	2.40E-04	8.91E-03
glycosyl compound metabolic process (GO:1901657)	234	32	13.48	+	2.37	2.88E-05	1.58E-03
regulation of response to stress (GO:0080134)	352	48	20.27	+	2.37	3.14E-07	3.32E-05
reactive oxygen species metabolic process (GO:0072593)	133	18	7.66	+	2.35	1.70E-03	4.82E-02
phosphorelay signal transduction system (GO:0000160)	222	30	12.79	+	2.35	6.18E-05	2.90E-03
hormone metabolic process (GO:0042445)	259	35	14.92	+	2.35	1.38E-05	8.94E-04
ethylene-activated signaling pathway (GO:0009873)	180	24	10.37	+	2.31	4.63E-04	1.56E-02
post-embryonic plant morphogenesis (GO:0090698)	174	23	10.02	+	2.3	6.75E-04	2.16E-02
response to external biotic stimulus (GO:0043207)	1244	161	71.65	+	2.25	1.62E-19	4.79E-16
response to other organism (GO:0051707)	1244	161	71.65	+	2.25	1.62E-19	3.19E-16
response to nitrogen compound (GO:1901698)	350	45	20.16	+	2.23	3.08E-06	2.49E-04
response to ethylene (GO:0009723)	306	39	17.62	+	2.21	1.97E-05	1.15E-03
response to biotic stimulus (GO:0009607)	1282	162	73.84	+	2.19	1.41E-18	1.39E-15
organic hydroxy compound metabolic process (GO:1901615)	288	36	16.59	+	2.17	5.80E-05	2.76E-03
antibiotic metabolic process (GO:0016999)	192	24	11.06	+	2.17	1.24E-03	3.68E-02
abscisic acid-activated signaling pathway (GO:0009738)	216	27	12.44	+	2.17	4.98E-04	1.65E-02
response to toxic substance (GO:0009636)	205	25	11.81	+	2.12	1.06E-03	3.22E-02
protein phosphorylation (GO:0006468)	919	112	52.93	+	2.12	3.25E-12	8.00E-10
drug catabolic process (GO:0042737)	248	30	14.28	+	2.1	4.31E-04	1.48E-02
cellular response to abscisic acid stimulus (GO:0071215)	242	29	13.94	+	2.08	6.11E-04	1.98E-02
cellular response to alcohol (GO:0097306)	242	29	13.94	+	2.08	6.11E-04	1.97E-02
negative regulation of response to stimulus (GO:0048585)	201	24	11.58	+	2.07	1.65E-03	4.72E-02
defense response (GO:0006952)	1480	176	85.24	+	2.06	7.30E-18	6.16E-15
regulation of hormone levels (GO:0010817)	408	48	23.5	+	2.04	1.48E-05	9.48E-04
defense response to other organism (GO:0098542)	944	111	54.37	+	2.04	2.73E-11	5.55E-09

hormone-mediated signaling pathway (GO:0009755)	750	88	43.2	+	2.04	4.10E-09	6.21E-07
intracellular signal transduction (GO:0035556)	607	71	34.96	+	2.03	1.83E-07	2.00E-05
response to external stimulus (GO:0009605)	1636	191	94.23	+	2.03	1.30E-18	1.53E-15
cellular response to endogenous stimulus (GO:0071495)	877	102	50.51	+	2.02	4.07E-10	7.28E-08
cellular response to hormone stimulus (GO:0032870)	860	100	49.53	+	2.02	4.68E-10	8.13E-08
response to acid chemical (GO:0001101)	1196	135	68.88	+	1.96	2.36E-12	6.35E-10
response to organic cyclic compound (GO:0014070)	390	44	22.46	+	1.96	9.99E-05	4.34E-03
phosphorylation (GO:0016310)	1295	146	74.59	+	1.96	2.99E-13	9.29E-11
regulation of response to stimulus (GO:0048583)	666	74	38.36	+	1.93	6.18E-07	5.98E-05
response to antibiotic (GO:0046677)	307	34	17.68	+	1.92	6.78E-04	2.15E-02
response to endogenous stimulus (GO:0009719)	1738	192	100.1	+	1.92	2.38E-16	1.28E-13
response to hormone (GO:0009725)	1721	190	99.12	+	1.92	2.95E-16	1.45E-13
response to oxygen-containing compound (GO:1901700)	1605	177	92.44	+	1.91	4.15E-15	1.89E-12
multi-organism process (GO:0051704)	1761	194	101.43	+	1.91	1.65E-16	9.75E-14
response to oxidative stress (GO:0006979)	459	50	26.44	+	1.89	6.60E-05	3.07E-03
response to organic substance (GO:0010033)	2055	221	118.36	+	1.87	1.13E-17	8.34E-15
cellular response to lipid (GO:0071396)	382	41	22	+	1.86	3.36E-04	1.19E-02
cellular response to acid chemical (GO:0071229)	450	48	25.92	+	1.85	1.32E-04	5.67E-03
response to abscisic acid (GO:0009737)	572	61	32.94	+	1.85	1.74E-05	1.07E-03
response to alcohol (GO:0097305)	576	61	33.18	+	1.84	1.92E-05	1.14E-03
response to lipid (GO:0033993)	778	82	44.81	+	1.83	8.41E-07	7.76E-05
signal transduction (GO:0007165)	1727	178	99.47	+	1.79	1.09E-12	3.07E-10
cellular response to organic substance (GO:0071310)	1019	104	58.69	+	1.77	1.31E-07	1.51E-05
signaling (GO:0023052)	1756	178	101.14	+	1.76	3.46E-12	8.18E-10
cellular response to oxygen-containing compound (GO:1901701)	629	63	36.23	+	1.74	8.34E-05	3.76E-03
cellular response to chemical stimulus (GO:0070887)	1190	119	68.54	+	1.74	4.57E-08	5.86E-06
cell communication (GO:0007154)	2003	200	115.36	+	1.73	4.56E-13	1.35E-10
phosphate-containing compound metabolic process (GO:0006796)	1896	189	109.2	+	1.73	3.16E-12	8.12E-10
response to chemical (GO:0042221)	2895	288	166.74	+	1.73	1.23E-18	1.81E-15
phosphorus metabolic process (GO:0006793)	1939	190	111.68	+	1.7	1.05E-11	2.29E-09
transmembrane transport (GO:0055085)	850	78	48.96	+	1.59	1.62E-04	6.84E-03
response to stimulus (GO:0050896)	6214	567	357.9	+	1.58	9.77E-31	5.77E-27
response to stress (GO:0006950)	3539	316	203.83	+	1.55	2.41E-14	8.90E-12
cellular response to stimulus (GO:0051716)	2711	240	156.14	+	1.54	1.48E-10	2.73E-08
oxoacid metabolic process (GO:0043436)	1129	97	65.03	+	1.49	2.33E-04	8.72E-03
organic acid metabolic process (GO:0006082)	1132	97	65.2	+	1.49	2.40E-04	8.86E-03
protein modification process (GO:0036211)	2264	185	130.4	+	1.42	4.78E-06	3.62E-04

cellular protein modification process (GO:0006464)	2264	185	130.4	+	1.42	4.78E-06	3.57E-04
oxidation-reduction process (GO:0055114)	1429	116	82.3	+	1.41	4.29E-04	1.48E-02
response to abiotic stimulus (GO:0009628)	2076	166	119.57	+	1.39	4.53E-05	2.25E-03
small molecule metabolic process (GO:0044281)	1748	135	100.68	+	1.34	1.10E-03	3.32E-02
aromatic compound biosynthetic process (GO:0019438)	2424	185	139.61	+	1.33	1.71E-04	7.13E-03
organic cyclic compound biosynthetic process (GO:1901362)	2545	193	146.58	+	1.32	1.66E-04	6.97E-03
regulation of cellular process (GO:0050794)	4918	353	283.26	+	1.25	1.71E-05	1.06E-03
developmental process (GO:0032502)	3220	229	185.46	+	1.23	1.37E-03	4.01E-02
biological regulation (GO:0065007)	6175	437	355.65	+	1.23	3.65E-06	2.84E-04
regulation of biological process (GO:0050789)	5504	389	317.01	+	1.23	1.87E-05	1.12E-03
cellular process (GO:0009987)	12283	792	707.45	+	1.12	3.59E-05	1.88E-03
biological_process (GO:0008150)	22836	1368	1315.26	+	1.04	4.74E-04	1.58E-02
Unclassified (UNCLASSIFIED)	4666	216	268.74	-	0.8	4.74E-04	1.59E-02
cellular nitrogen compound metabolic process (GO:0034641)	4580	208	263.79	-	0.79	1.90E-04	7.68E-03
cellular component organization or biogenesis (GO:0071840)	3083	134	177.57	-	0.75	5.31E-04	1.75E-02
nucleobase-containing compound metabolic process (GO:0006139)	3720	161	214.26	-	0.75	8.90E-05	3.92E-03
nucleic acid metabolic process (GO:0090304)	3235	135	186.32	-	0.72	5.30E-05	2.57E-03
gene expression (GO:0010467)	3120	130	179.7	-	0.72	8.00E-05	3.66E-03
organelle organization (GO:0006996)	1605	51	92.44	-	0.55	3.37E-06	2.69E-04
cellular component biogenesis (GO:0044085)	1208	36	69.58	-	0.52	1.69E-05	1.06E-03
cellular component assembly (GO:0022607)	725	21	41.76	-	0.5	7.50E-04	2.36E-02
cellular amide metabolic process (GO:0043603)	807	22	46.48	-	0.47	1.29E-04	5.54E-03
peptide metabolic process (GO:0006518)	677	18	38.99	-	0.46	3.48E-04	1.22E-02
protein-containing complex subunit organization (GO:0043933)	589	12	33.92	-	0.35	3.65E-05	1.89E-03
chromatin organization (GO:0006325)	355	7	20.45	-	0.34	1.47E-03	4.28E-02
protein-containing complex assembly (GO:0065003)	501	9	28.86	-	0.31	4.42E-05	2.21E-03
mRNA metabolic process (GO:0016071)	479	7	27.59	-	0.25	1.08E-05	7.14E-04
DNA repair (GO:0006281)	300	4	17.28	-	0.23	3.23E-04	1.15E-02
chromosome organization (GO:0051276)	526	7	30.3	-	0.23	1.04E-06	9.46E-05
cellular response to DNA damage stimulus (GO:0006974)	330	4	19.01	-	0.21	8.49E-05	3.77E-03
amide biosynthetic process (GO:0043604)	670	8	38.59	-	0.21	8.79E-09	1.30E-06
DNA metabolic process (GO:0006259)	510	6	29.37	-	0.2	6.29E-07	5.99E-05
peptide biosynthetic process (GO:0043043)	599	6	34.5	-	0.17	1.02E-08	1.47E-06
cellular protein-containing complex assembly (GO:0034622)	443	4	25.51	-	0.16	4.80E-07	4.89E-05
RNA modification (GO:0009451)	366	3	21.08	-	0.14	4.15E-06	3.18E-04
macromolecule methylation (GO:0043414)	164	1	9.45	-	0.11	1.68E-03	4.79E-02

tRNA metabolic process (GO:0006399)	167	1	9.62	-	0.1	1.71E-03	4.81E-02
mRNA processing (GO:0006397)	353	2	20.33	-	0.1	8.21E-07	7.70E-05
translation (GO:0006412)	594	3	34.21	-	0.09	3.09E-11	6.08E-09
ncRNA metabolic process (GO:0034660)	405	2	23.33	-	0.09	6.12E-08	7.70E-06
photosynthesis (GO:0015979)	232	1	13.36	-	0.07	5.95E-05	2.81E-03
RNA processing (GO:0006396)	758	3	43.66	-	0.07	4.85E-15	2.04E-12
RNA splicing (GO:0008380)	267	1	15.38	-	0.07	8.90E-06	5.98E-04
ncRNA processing (GO:0034470)	327	1	18.83	-	0.05	4.47E-07	4.63E-05
ribonucleoprotein complex subunit organization (GO:0071826)	176	0	10.14	-	< 0.01	8.31E-05	3.77E-03
mitochondrion organization (GO:0007005)	167	0	9.62	-	< 0.01	1.98E-04	7.79E-03
rRNA processing (GO:0006364)	211	0	12.15	-	< 0.01	1.14E-05	7.51E-04
rRNA metabolic process (GO:0016072)	225	0	12.96	-	< 0.01	5.18E-06	3.77E-04
DNA replication (GO:0006260)	140	0	8.06	-	< 0.01	6.05E-04	1.98E-02
ribosome biogenesis (GO:0042254)	373	0	21.48	-	< 0.01	1.25E-09	2.05E-07
ribonucleoprotein complex assembly (GO:0022618)	167	0	9.62	-	< 0.01	1.98E-04	7.74E-03
ribonucleoprotein complex biogenesis (GO:0022613)	459	0	26.44	-	< 0.01	1.08E-11	2.27E-09
mRNA splicing, via spliceosome (GO:0000398)	174	0	10.02	-	< 0.01	1.33E-04	5.65E-03
RNA splicing, via transesterification reactions with bulged adenosine as nucleophile (GO:0000377)	191	0	11	-	< 0.01	3.77E-05	1.94E-03
RNA splicing, via transesterification reactions (GO:0000375)	191	0	11	-	< 0.01	3.77E-05	1.92E-03

Supplementary Table S4.2 Enrichment analysis of genes behaved like growth triggers

Analysis Type:	PANTHER Overrepresentation Test (Released 20171205)
Annotation Version and Release Date:	GO Ontology database Released 2018-08-09
Analyzed List:	upload_1 (Arabidopsis thaliana)
Reference List:	Arabidopsis thaliana (all genes in database)
Test Type:	FISHER

GO biological process complete	Arabidopsis thaliana - REFLIST (27502)	upload_1 (232)	upload_1 (expected)	upload_1 (over/under)	upload_1 (fold Enrichment)	upload_1 (raw P-value)	upload_1 (FDR)
response to gibberellin (GO:0009739)	154	8	1.3	+	6.16	6.95E-05	4.56E-02
unidimensional cell growth (GO:0009826)	273	13	2.3	+	5.64	9.79E-07	5.79E-03
developmental growth involved in morphogenesis (GO:0060560)	317	13	2.67	+	4.86	4.73E-06	1.40E-02
cell growth (GO:0016049)	357	13	3.01	+	4.32	1.60E-05	1.89E-02
cell morphogenesis (GO:0000902)	362	13	3.05	+	4.26	1.84E-05	1.82E-02

developmental growth (GO:0048589)	366	13	3.09	+	4.21	2.06E-05	1.74E-02
cellular component morphogenesis (GO:0032989)	397	14	3.35	+	4.18	1.07E-05	1.58E-02
growth (GO:0040007)	411	13	3.47	+	3.75	6.52E-05	4.81E-02
external encapsulating structure organization (GO:0045229)	553	15	4.66	+	3.22	9.70E-05	5.73E-02
cell wall organization or biogenesis (GO:0071554)	686	17	5.79	+	2.94	9.78E-05	5.25E-02
cellular developmental process (GO:0048869)	891	22	7.52	+	2.93	9.62E-06	1.89E-02
carbohydrate metabolic process (GO:0005975)	1045	22	8.82	+	2.5	9.89E-05	4.87E-02

Supplementary Table S4.3 Enrichment analysis of genes in category b23

Analysis Type:	PANTHER Overrepresentation Test (Released 20171205)
Annotation Version and Release Date:	GO Ontology database Released 2018-02-02
Analyzed List:	upload_1 (Arabidopsis thaliana)
Reference List:	Arabidopsis thaliana (all genes in database)
Test Type:	FISHER

GO biological process complete	Arabidopsis thaliana - REFLIST (27502)	upload_1 (372)	upload_1 (expected)	upload_1 (over/under)	upload_1 (fold Enrichment)	upload_1 (raw P-value)	upload_1 (FDR)
root hair initiation (GO:0048766)	13	4	0.18	+	22.75	6.47E-05	1.49E-02
plant-type cell wall loosening (GO:0009828)	36	5	0.49	+	10.27	2.08E-04	3.84E-02
root hair cell differentiation (GO:0048765)	104	10	1.41	+	7.11	3.16E-06	8.73E-03
trichoblast maturation (GO:0048764)	104	10	1.41	+	7.11	3.16E-06	5.82E-03
cell maturation (GO:0048469)	105	10	1.42	+	7.04	3.42E-06	4.73E-03
trichoblast differentiation (GO:0010054)	108	10	1.46	+	6.85	4.31E-06	3.98E-03
plant-type cell wall organization (GO:0009664)	129	11	1.74	+	6.3	3.01E-06	1.67E-02
root epidermal cell differentiation (GO:0010053)	124	10	1.68	+	5.96	1.34E-05	6.16E-03
plant epidermal cell differentiation (GO:0090627)	151	10	2.04	+	4.9	6.47E-05	1.56E-02
anatomical structure maturation (GO:0071695)	167	11	2.26	+	4.87	2.95E-05	9.58E-03
cell wall macromolecule metabolic process (GO:0044036)	149	9	2.02	+	4.47	2.86E-04	4.79E-02
developmental maturation (GO:0021700)	186	11	2.52	+	4.37	7.41E-05	1.58E-02

root morphogenesis (GO:0010015)	240	14	3.25	+	4.31	9.21E-06	5.09E-03
unidimensional cell growth (GO:0009826)	253	14	3.42	+	4.09	1.61E-05	6.37E-03
plant-type cell wall organization or biogenesis (GO:0071669)	236	13	3.19	+	4.07	3.37E-05	9.82E-03
cell morphogenesis (GO:0000902)	328	17	4.44	+	3.83	4.65E-06	3.67E-03
developmental growth involved in morphogenesis (GO:0060560)	294	15	3.98	+	3.77	2.01E-05	7.39E-03
plant epidermis development (GO:0090558)	237	12	3.21	+	3.74	1.43E-04	2.94E-02
cell growth (GO:0016049)	357	18	4.83	+	3.73	3.53E-06	3.90E-03
cellular component morphogenesis (GO:0032989)	361	17	4.88	+	3.48	1.53E-05	6.51E-03
developmental growth (GO:0048589)	344	16	4.65	+	3.44	3.13E-05	9.62E-03
cell development (GO:0048468)	287	13	3.88	+	3.35	2.19E-04	3.91E-02
root development (GO:0048364)	449	20	6.07	+	3.29	6.04E-06	4.18E-03
root system development (GO:0022622)	451	20	6.1	+	3.28	6.43E-06	3.95E-03
growth (GO:0040007)	433	19	5.86	+	3.24	1.26E-05	6.34E-03
plant organ morphogenesis (GO:1905392)	373	15	5.05	+	2.97	2.54E-04	4.39E-02
response to drug (GO:0042493)	529	20	7.16	+	2.8	5.70E-05	1.43E-02
cell wall organization or biogenesis (GO:0071554)	662	23	8.95	+	2.57	5.62E-05	1.48E-02
anatomical structure morphogenesis (GO:0009653)	801	26	10.83	+	2.4	6.81E-05	1.51E-02
cellular developmental process (GO:0048869)	906	29	12.25	+	2.37	2.92E-05	1.01E-02
plant organ development (GO:0099402)	892	27	12.07	+	2.24	1.72E-04	3.28E-02
response to stimulus (GO:0050896)	5805	112	78.52	+	1.43	5.35E-05	1.48E-02
organelle organization (GO:0006996)	1197	3	16.19	-	0.19	1.45E-04	2.87E-02

Supplementary Table S4.4 Enrichment analysis of genes in category b26 and b25

Analysis Type:	PANTHER Overrepresentation Test (Released 20171205)
Annotation Version and Release Date:	GO Ontology database Released 2018-02-02
Analyzed List:	upload_1 (Arabidopsis thaliana)
Reference List:	Arabidopsis thaliana (all genes in database)
Test Type:	FISHER

GO biological process complete	Arabidopsis thaliana - REFLIST (27502)	upload_1 (402)	upload_1 (expected)	upload_1 (over/under)	upload_1 (fold Enrichment)	upload_1 (raw P-value)	upload_1 (FDR)
histone phosphorylation (GO:0016572)	6	4	0.09	+	45.61	8.32E-06	2.00E-03
regulation of cytokinesis (GO:0032465)	6	4	0.09	+	45.61	8.32E-06	1.92E-03

mitotic spindle assembly checkpoint (GO:0007094)	8	4	0.12	+	34.21	1.92E-05	3.93E-03
negative regulation of mitotic sister chromatid separation (GO:2000816)	8	4	0.12	+	34.21	1.92E-05	3.79E-03
negative regulation of chromosome segregation (GO:0051985)	8	4	0.12	+	34.21	1.92E-05	3.66E-03
negative regulation of mitotic sister chromatid segregation (GO:0033048)	8	4	0.12	+	34.21	1.92E-05	3.53E-03
negative regulation of sister chromatid segregation (GO:0033046)	8	4	0.12	+	34.21	1.92E-05	3.42E-03
mitotic spindle checkpoint (GO:0071174)	8	4	0.12	+	34.21	1.92E-05	3.31E-03
spindle assembly checkpoint (GO:0071173)	8	4	0.12	+	34.21	1.92E-05	3.21E-03
negative regulation of metaphase/anaphase transition of cell cycle (GO:1902100)	8	4	0.12	+	34.21	1.92E-05	3.12E-03
negative regulation of mitotic metaphase/anaphase transition (GO:0045841)	8	4	0.12	+	34.21	1.92E-05	3.03E-03
spindle checkpoint (GO:0031577)	8	4	0.12	+	34.21	1.92E-05	2.94E-03
negative regulation of chromosome separation (GO:1905819)	8	4	0.12	+	34.21	1.92E-05	2.87E-03
negative regulation of mitotic nuclear division (GO:0045839)	9	4	0.13	+	30.41	2.74E-05	3.69E-03
mitotic spindle organization (GO:0007052)	8	3	0.12	+	25.65	4.49E-04	4.14E-02
negative regulation of mitotic cell cycle phase transition (GO:1901991)	11	4	0.16	+	24.88	5.11E-05	6.14E-03
negative regulation of cell cycle phase transition (GO:1901988)	11	4	0.16	+	24.88	5.11E-05	6.01E-03
regulation of mitotic sister chromatid separation (GO:0010965)	14	5	0.2	+	24.43	5.96E-06	1.94E-03
regulation of mitotic metaphase/anaphase transition (GO:0030071)	14	5	0.2	+	24.43	5.96E-06	1.83E-03
regulation of metaphase/anaphase transition of cell cycle (GO:1902099)	14	5	0.2	+	24.43	5.96E-06	1.73E-03
regulation of chromosome separation (GO:1905818)	14	5	0.2	+	24.43	5.96E-06	1.65E-03
regulation of mitotic sister chromatid segregation (GO:0033047)	15	5	0.22	+	22.8	7.85E-06	1.97E-03
negative regulation of nuclear division (GO:0051784)	12	4	0.18	+	22.8	6.73E-05	7.76E-03
regulation of sister chromatid segregation (GO:0033045)	19	6	0.28	+	21.6	1.21E-06	6.69E-04
regulation of chromosome segregation (GO:0051983)	20	6	0.29	+	20.52	1.55E-06	7.16E-04
regulation of mitotic nuclear division (GO:0007088)	17	5	0.25	+	20.12	1.30E-05	2.77E-03
mitotic cell cycle checkpoint (GO:0007093)	16	4	0.23	+	17.1	1.71E-04	1.93E-02

protein import into chloroplast stroma (GO:0045037)	17	4	0.25	+	16.1	2.09E-04	2.18E-02
regulation of mitotic cell cycle phase transition (GO:1901990)	30	7	0.44	+	15.96	8.67E-07	5.99E-04
cell cycle checkpoint (GO:0000075)	22	5	0.32	+	15.55	3.76E-05	4.73E-03
spindle organization (GO:0007051)	22	5	0.32	+	15.55	3.76E-05	4.62E-03
negative regulation of mitotic cell cycle (GO:0045930)	18	4	0.26	+	15.2	2.53E-04	2.54E-02
regulation of cell cycle phase transition (GO:1901987)	33	7	0.48	+	14.51	1.51E-06	7.61E-04
regulation of nuclear division (GO:0051783)	30	6	0.44	+	13.68	1.16E-05	2.57E-03
regulation of tetrapyrrole biosynthetic process (GO:1901463)	20	4	0.29	+	13.68	3.59E-04	3.48E-02
negative regulation of chromosome organization (GO:2001251)	22	4	0.32	+	12.44	4.94E-04	4.47E-02
negative regulation of cell cycle process (GO:0010948)	22	4	0.32	+	12.44	4.94E-04	4.40E-02
protein targeting to chloroplast (GO:0045036)	34	6	0.5	+	12.07	2.18E-05	3.10E-03
establishment of protein localization to chloroplast (GO:0072596)	34	6	0.5	+	12.07	2.18E-05	3.02E-03
thylakoid membrane organization (GO:0010027)	41	7	0.6	+	11.68	5.41E-06	1.87E-03
protein localization to chloroplast (GO:0072598)	36	6	0.53	+	11.4	2.91E-05	3.75E-03
regulation of cell cycle process (GO:0010564)	79	13	1.15	+	11.26	7.58E-10	1.40E-06
plastid membrane organization (GO:0009668)	43	7	0.63	+	11.14	7.16E-06	1.89E-03
microtubule-based movement (GO:0007018)	32	5	0.47	+	10.69	1.81E-04	2.00E-02
movement of cell or subcellular component (GO:0006928)	53	6	0.77	+	7.74	2.04E-04	2.17E-02
regulation of mitotic cell cycle (GO:0007346)	91	10	1.33	+	7.52	2.06E-06	8.15E-04
regulation of cell cycle (GO:0051726)	214	23	3.13	+	7.35	7.59E-13	4.19E-09
microtubule cytoskeleton organization (GO:0000226)	76	7	1.11	+	6.3	1.98E-04	2.15E-02
mitotic cell cycle process (GO:1903047)	144	13	2.1	+	6.18	4.96E-07	3.92E-04
regulation of chromosome organization (GO:0033044)	79	7	1.15	+	6.06	2.47E-04	2.53E-02
meiotic nuclear division (GO:0140013)	83	7	1.21	+	5.77	3.27E-04	3.23E-02
microtubule-based process (GO:0007017)	121	10	1.77	+	5.65	2.11E-05	3.08E-03
chromosome segregation (GO:0007059)	85	7	1.24	+	5.63	3.74E-04	3.57E-02
mitotic cell cycle (GO:0000278)	165	13	2.41	+	5.39	2.05E-06	8.74E-04
plastid organization (GO:0009657)	216	17	3.16	+	5.38	5.67E-08	5.22E-05
cell cycle process (GO:0022402)	282	21	4.12	+	5.09	3.87E-09	5.35E-06

protein import (GO:0017038)	113	8	1.65	+	4.84	3.78E-04	3.54E-02
cell cycle (GO:0007049)	440	30	6.43	+	4.66	1.31E-11	3.61E-08
RNA modification (GO:0009451)	232	15	3.39	+	4.42	3.43E-06	1.26E-03
cell division (GO:0051301)	300	18	4.39	+	4.1	1.01E-06	6.21E-04
ncRNA metabolic process (GO:0034660)	254	12	3.71	+	3.23	5.23E-04	4.59E-02
RNA processing (GO:0006396)	583	23	8.52	+	2.7	2.80E-05	3.69E-03
organelle organization (GO:0006996)	1197	44	17.5	+	2.51	5.12E-08	5.67E-05

Supplementary Table S4.5 Enrichment analysis of genes in category b2 and b3

Analysis Type:	PANTHER Overrepresentation Test (Released 20171205)
Annotation Version and Release Date:	GO Ontology database Released 2018-02-02
Analyzed List:	upload_1 (Arabidopsis thaliana)
Reference List:	Arabidopsis thaliana (all genes in database)
Test Type:	FISHER

GO biological process complete	Arabidopsis thaliana - REFLIST (27502)	upload_1 (1346)	upload_1 (expected)	upload_1 (over/under)	upload_1 (fold Enrichment)	upload_1 (raw P-value)	upload_1 (FDR)
indole glucosinolate biosynthetic process (GO:0009759)	6	4	0.29	+	13.62	7.90E-04	3.61E-02
pyrimidine-containing compound catabolic process (GO:0072529)	7	4	0.34	+	11.68	1.20E-03	5.09E-02
regulation of salicylic acid metabolic process (GO:0010337)	14	6	0.69	+	8.76	2.25E-04	1.22E-02
galactolipid metabolic process (GO:0019374)	12	5	0.59	+	8.51	8.48E-04	3.78E-02
detection of chemical stimulus (GO:0009593)	22	7	1.08	+	6.5	2.99E-04	1.58E-02
S-glycoside biosynthetic process (GO:0016144)	42	12	2.06	+	5.84	5.63E-06	5.76E-04
glucosinolate biosynthetic process (GO:0019761)	42	12	2.06	+	5.84	5.63E-06	5.66E-04
glycosinolate biosynthetic process (GO:0019758)	42	12	2.06	+	5.84	5.63E-06	5.56E-04
indole-containing compound biosynthetic process (GO:0042435)	53	14	2.59	+	5.4	2.08E-06	2.95E-04
negative regulation of cell death (GO:0060548)	27	7	1.32	+	5.3	8.41E-04	3.78E-02
defense response to bacterium, incompatible interaction (GO:0009816)	40	9	1.96	+	4.6	3.87E-04	2.00E-02
indole-containing compound metabolic process (GO:0042430)	89	18	4.36	+	4.13	2.20E-06	3.04E-04
auxin metabolic process (GO:0009850)	66	13	3.23	+	4.02	7.00E-05	4.56E-03
aromatic amino acid family metabolic process (GO:0009072)	72	14	3.52	+	3.97	4.22E-05	3.07E-03

cellular response to steroid hormone stimulus (GO:0071383)	76	14	3.72	+	3.76	7.07E-05	4.55E-03
response to steroid hormone (GO:0048545)	76	14	3.72	+	3.76	7.07E-05	4.49E-03
brassinosteroid mediated signaling pathway (GO:0009742)	76	14	3.72	+	3.76	7.07E-05	4.44E-03
steroid hormone mediated signaling pathway (GO:0043401)	76	14	3.72	+	3.76	7.07E-05	4.39E-03
cellular response to brassinosteroid stimulus (GO:0071367)	78	14	3.82	+	3.67	9.04E-05	5.55E-03
toxin metabolic process (GO:0009404)	68	12	3.33	+	3.61	3.23E-04	1.69E-02
oligopeptide transport (GO:0006857)	71	12	3.47	+	3.45	4.57E-04	2.24E-02
response to brassinosteroid (GO:0009741)	102	17	4.99	+	3.41	3.83E-05	2.87E-03
response to chitin (GO:0010200)	132	22	6.46	+	3.41	2.97E-06	3.64E-04
phenylpropanoid metabolic process (GO:0009698)	155	25	7.59	+	3.3	1.10E-06	1.69E-04
protein autophosphorylation (GO:0046777)	137	22	6.71	+	3.28	5.05E-06	5.37E-04
sulfur compound biosynthetic process (GO:0044272)	151	24	7.39	+	3.25	2.24E-06	3.03E-04
glycosyl compound biosynthetic process (GO:1901659)	82	13	4.01	+	3.24	4.65E-04	2.26E-02
membrane lipid metabolic process (GO:0006643)	88	13	4.31	+	3.02	8.41E-04	3.81E-02
phenylpropanoid biosynthetic process (GO:0009699)	116	17	5.68	+	2.99	1.57E-04	9.05E-03
protein dephosphorylation (GO:0006470)	103	15	5.04	+	2.98	3.98E-04	2.04E-02
cellular response to nutrient levels (GO:0031669)	153	21	7.49	+	2.8	6.58E-05	4.33E-03
response to organonitrogen compound (GO:0010243)	190	26	9.3	+	2.8	9.90E-06	8.83E-04
secondary metabolite biosynthetic process (GO:0044550)	311	42	15.22	+	2.76	2.97E-08	7.15E-06
transmembrane receptor protein tyrosine kinase signaling pathway (GO:0007169)	119	16	5.82	+	2.75	5.71E-04	2.70E-02
enzyme linked receptor protein signaling pathway (GO:0007167)	119	16	5.82	+	2.75	5.71E-04	2.68E-02
cell surface receptor signaling pathway (GO:0007166)	217	29	10.62	+	2.73	4.73E-06	5.23E-04
response to wounding (GO:0009611)	212	28	10.38	+	2.7	8.34E-06	7.56E-04
response to nutrient levels (GO:0031667)	183	24	8.96	+	2.68	3.97E-05	2.92E-03
defense response, incompatible interaction (GO:0009814)	153	20	7.49	+	2.67	1.76E-04	9.81E-03
S-glycoside metabolic process (GO:0016143)	116	15	5.68	+	2.64	1.20E-03	5.05E-02
glucosinolate metabolic process (GO:0019760)	116	15	5.68	+	2.64	1.20E-03	5.01E-02
glycosinolate metabolic process (GO:0019757)	116	15	5.68	+	2.64	1.20E-03	4.97E-02

cellular response to extracellular stimulus (GO:0031668)	188	24	9.2	+	2.61	5.83E-05	3.93E-03
cellular response to external stimulus (GO:0071496)	192	24	9.4	+	2.55	1.10E-04	6.55E-03
response to starvation (GO:0042594)	145	18	7.1	+	2.54	6.30E-04	2.93E-02
response to extracellular stimulus (GO:0009991)	219	27	10.72	+	2.52	4.34E-05	3.11E-03
secondary metabolic process (GO:0019748)	475	58	23.25	+	2.49	2.41E-09	8.90E-07
immune system process (GO:0002376)	320	38	15.66	+	2.43	2.94E-06	3.70E-04
cellular response to lipid (GO:0071396)	371	43	18.16	+	2.37	1.44E-06	2.15E-04
protein phosphorylation (GO:0006468)	783	89	38.32	+	2.32	4.46E-12	4.11E-09
innate immune response (GO:0045087)	273	31	13.36	+	2.32	4.88E-05	3.46E-03
hormone metabolic process (GO:0042445)	238	27	11.65	+	2.32	1.70E-04	9.61E-03
immune response (GO:0006955)	279	31	13.65	+	2.27	6.56E-05	4.37E-03
cellular response to abscisic acid stimulus (GO:0071215)	228	25	11.16	+	2.24	4.29E-04	2.17E-02
cellular response to alcohol (GO:0097306)	228	25	11.16	+	2.24	4.29E-04	2.16E-02
regulation of hormone levels (GO:0010817)	380	41	18.6	+	2.2	1.08E-05	9.36E-04
response to nitrogen compound (GO:1901698)	297	32	14.54	+	2.2	9.86E-05	5.99E-03
response to abscisic acid (GO:0009737)	549	59	26.87	+	2.2	1.47E-07	2.80E-05
response to lipid (GO:0033993)	748	80	36.61	+	2.19	8.52E-10	3.62E-07
response to alcohol (GO:0097305)	553	59	27.06	+	2.18	1.66E-07	3.06E-05
regulation of defense response (GO:0031347)	225	24	11.01	+	2.18	7.48E-04	3.45E-02
sulfur compound metabolic process (GO:0006790)	358	38	17.52	+	2.17	3.15E-05	2.42E-03
defense response to bacterium (GO:0042742)	331	34	16.2	+	2.1	1.39E-04	8.08E-03
response to organic cyclic compound (GO:0014070)	366	37	17.91	+	2.07	1.07E-04	6.44E-03
response to drug (GO:0042493)	529	53	25.89	+	2.05	3.70E-06	4.35E-04
response to bacterium (GO:0009617)	425	42	20.8	+	2.02	5.36E-05	3.71E-03
phosphorylation (GO:0016310)	1083	106	53	+	2	1.52E-10	9.34E-08
response to oxygen-containing compound (GO:1901700)	1506	143	73.71	+	1.94	6.51E-13	9.00E-10
response to water deprivation (GO:0009414)	329	31	16.1	+	1.93	9.90E-04	4.34E-02
cellular response to endogenous stimulus (GO:0071495)	846	77	41.4	+	1.86	9.93E-07	1.62E-04
cell communication (GO:0007154)	1888	170	92.4	+	1.84	2.05E-13	3.77E-10
hormone-mediated signaling pathway (GO:0009755)	746	67	36.51	+	1.84	6.59E-06	6.18E-04
response to acid chemical (GO:0001101)	1148	103	56.19	+	1.83	2.10E-08	5.53E-06
response to organic substance (GO:0010033)	1947	174	95.29	+	1.83	1.96E-13	5.41E-10

response to endogenous stimulus (GO:0009719)	1680	150	82.22	+	1.82	1.28E-11	1.01E-08
cellular response to hormone stimulus (GO:0032870)	838	74	41.01	+	1.8	4.38E-06	4.94E-04
cellular response to oxygen-containing compound (GO:1901701)	578	51	28.29	+	1.8	1.65E-04	9.40E-03
response to hormone (GO:0009725)	1672	147	81.83	+	1.8	5.67E-11	3.92E-08
phosphate-containing compound metabolic process (GO:0006796)	1556	136	76.15	+	1.79	4.54E-10	2.28E-07
phosphorus metabolic process (GO:0006793)	1621	141	79.33	+	1.78	3.06E-10	1.69E-07
signal transduction (GO:0007165)	1625	140	79.53	+	1.76	6.77E-10	3.12E-07
signaling (GO:0023052)	1655	141	81	+	1.74	9.81E-10	3.88E-07
cellular response to organic substance (GO:0071310)	940	80	46.01	+	1.74	6.85E-06	6.31E-04
response to external stimulus (GO:0009605)	1520	128	74.39	+	1.72	1.24E-08	3.42E-06
defense response (GO:0006952)	1407	117	68.86	+	1.7	1.27E-07	2.51E-05
regulation of biological quality (GO:0065008)	1096	89	53.64	+	1.66	1.12E-05	9.56E-04
oxoacid metabolic process (GO:0043436)	1043	84	51.05	+	1.65	2.59E-05	2.08E-03
response to chemical (GO:0042221)	2762	222	135.18	+	1.64	1.22E-12	1.34E-09
organic acid metabolic process (GO:0006082)	1046	84	51.19	+	1.64	2.68E-05	2.12E-03
cellular response to chemical stimulus (GO:0070887)	1099	88	53.79	+	1.64	2.19E-05	1.83E-03
response to biotic stimulus (GO:0009607)	1195	95	58.49	+	1.62	1.04E-05	9.09E-04
response to other organism (GO:0051707)	1155	91	56.53	+	1.61	2.51E-05	2.07E-03
response to external biotic stimulus (GO:0043207)	1157	91	56.63	+	1.61	2.57E-05	2.09E-03
protein modification process (GO:0036211)	1896	146	92.79	+	1.57	2.05E-07	3.66E-05
cellular protein modification process (GO:0006464)	1896	146	92.79	+	1.57	2.05E-07	3.55E-05
cellular response to stimulus (GO:0051716)	2466	188	120.69	+	1.56	5.65E-09	1.84E-06
multi-organism process (GO:0051704)	1616	123	79.09	+	1.56	4.25E-06	4.90E-04
defense response to other organism (GO:0098542)	855	65	41.85	+	1.55	1.05E-03	4.59E-02
response to stimulus (GO:0050896)	5805	425	284.11	+	1.5	3.23E-18	1.79E-14
response to stress (GO:0006950)	3283	237	160.68	+	1.48	3.47E-09	1.20E-06
macromolecule modification (GO:0043412)	2223	150	108.8	+	1.38	1.33E-04	7.84E-03
localization (GO:0051179)	2345	156	114.77	+	1.36	1.92E-04	1.06E-02
transport (GO:0006810)	2235	147	109.39	+	1.34	4.55E-04	2.25E-02
establishment of localization (GO:0051234)	2259	148	110.56	+	1.34	4.88E-04	2.35E-02
organonitrogen compound metabolic process (GO:1901564)	4132	265	202.23	+	1.31	6.44E-06	6.14E-04
biological regulation (GO:0065007)	5517	326	270.01	+	1.21	2.99E-04	1.59E-02
cellular process (GO:0009987)	10706	591	523.97	+	1.13	2.80E-04	1.50E-02

cellular nitrogen compound biosynthetic process (GO:0044271)	2763	97	135.23	-	0.72	4.53E-04	2.25E-02
heterocycle metabolic process (GO:0046483)	3566	124	174.53	-	0.71	3.39E-05	2.57E-03
cellular component organization (GO:0016043)	2211	76	108.21	-	0.7	1.11E-03	4.77E-02
cellular nitrogen compound metabolic process (GO:0034641)	4100	132	200.66	-	0.66	7.40E-08	1.57E-05
cellular component organization or biogenesis (GO:0071840)	2466	79	120.69	-	0.65	5.18E-05	3.63E-03
macromolecule biosynthetic process (GO:0009059)	2772	87	135.67	-	0.64	5.58E-06	5.82E-04
cellular macromolecule biosynthetic process (GO:0034645)	2721	84	133.17	-	0.63	3.66E-06	4.40E-04
RNA metabolic process (GO:0016070)	2541	76	124.36	-	0.61	2.28E-06	3.00E-04
nucleobase-containing compound metabolic process (GO:0006139)	3268	97	159.94	-	0.61	3.82E-08	8.81E-06
gene expression (GO:0010467)	2911	80	142.47	-	0.56	6.78E-09	2.08E-06
nucleic acid metabolic process (GO:0090304)	2876	79	140.76	-	0.56	7.56E-09	2.20E-06
organelle organization (GO:0006996)	1197	30	58.58	-	0.51	5.59E-05	3.82E-03
peptide metabolic process (GO:0006518)	639	14	31.27	-	0.45	9.56E-04	4.23E-02
mRNA metabolic process (GO:0016071)	374	5	18.3	-	0.27	5.33E-04	2.54E-02
amide biosynthetic process (GO:0043604)	618	8	30.25	-	0.26	4.90E-06	5.32E-04
peptide biosynthetic process (GO:0043043)	567	6	27.75	-	0.22	1.78E-06	2.59E-04
cellular response to DNA damage stimulus (GO:0006974)	286	3	14	-	0.21	1.08E-03	4.65E-02
translation (GO:0006412)	562	4	27.51	-	0.15	8.94E-08	1.83E-05
RNA processing (GO:0006396)	583	4	28.53	-	0.14	2.96E-08	7.44E-06
DNA metabolic process (GO:0006259)	455	3	22.27	-	0.13	9.99E-07	1.58E-04
mRNA processing (GO:0006397)	290	1	14.19	-	0.07	3.09E-05	2.41E-03
chromosome organization (GO:0051276)	428	1	20.95	-	0.05	4.63E-08	1.02E-05
covalent chromatin modification (GO:0016569)	189	0	9.25	-	< 0.01	1.93E-04	1.06E-02
chromatin organization (GO:0006325)	284	0	13.9	-	< 0.01	2.68E-06	3.45E-04
ribosome biogenesis (GO:0042254)	266	0	13.02	-	< 0.01	5.71E-06	5.54E-04
ribonucleoprotein complex biogenesis (GO:0022613)	310	0	15.17	-	< 0.01	8.52E-07	1.43E-04

Supplementary Table S4.6 Enrichment analysis of genes in category b18

Analysis Type:	PANTHER Overrepresentation Test (Released 20171205)
Annotation Version and Release Date:	GO Ontology database Released 2018-02-02
Analyzed List:	upload_1 (Arabidopsis thaliana)
Reference List:	Arabidopsis thaliana (all genes in database)

Test Type:	FISHER						
GO biological process complete	Arabidopsis thaliana - REFLIST (27502)	upload_1 (967)	upload_1 (expected)	upload_1 (over/under)	upload_1 (fold Enrichment)	upload_1 (raw P-value)	upload_1 (FDR)
mitotic DNA replication (GO:1902969)	4	4	0.14	+	28.44	8.30E-05	6.12E-03
nuclear DNA replication (GO:0033260)	5	4	0.18	+	22.75	1.45E-04	1.01E-02
leading strand elongation (GO:0006272)	5	4	0.18	+	22.75	1.45E-04	9.93E-03
regulation of double-strand break repair via homologous recombination (GO:0010569)	5	4	0.18	+	22.75	1.45E-04	9.81E-03
regulation of double-strand break repair (GO:2000779)	6	4	0.21	+	18.96	2.36E-04	1.52E-02
DNA replication initiation (GO:0006270)	20	13	0.7	+	18.49	2.26E-11	4.03E-09
valine biosynthetic process (GO:0009099)	8	5	0.28	+	17.78	4.59E-05	3.84E-03
DNA strand elongation involved in DNA replication (GO:0006271)	13	6	0.46	+	13.13	2.81E-05	2.59E-03
DNA strand elongation (GO:0022616)	13	6	0.46	+	13.13	2.81E-05	2.54E-03
isoleucine metabolic process (GO:0006549)	11	5	0.39	+	12.93	1.43E-04	1.01E-02
isoleucine biosynthetic process (GO:0009097)	11	5	0.39	+	12.93	1.43E-04	1.00E-02
DNA unwinding involved in DNA replication (GO:0006268)	9	4	0.32	+	12.64	7.40E-04	4.01E-02
glycogen metabolic process (GO:0005977)	17	7	0.6	+	11.71	1.06E-05	1.18E-03
energy reserve metabolic process (GO:0006112)	17	7	0.6	+	11.71	1.06E-05	1.15E-03
regulation of DNA recombination (GO:0000018)	13	5	0.46	+	10.94	2.65E-04	1.65E-02
DNA-dependent DNA replication (GO:0006261)	74	24	2.6	+	9.22	1.77E-14	3.77E-12
DNA replication (GO:0006260)	110	35	3.87	+	9.05	2.94E-20	9.03E-18
regulation of DNA replication (GO:0006275)	26	8	0.91	+	8.75	1.42E-05	1.51E-03
valine metabolic process (GO:0006573)	17	5	0.6	+	8.36	7.28E-04	3.98E-02
ribosomal large subunit assembly (GO:0000027)	24	7	0.84	+	8.3	6.57E-05	5.19E-03
DNA duplex unwinding (GO:0032508)	21	6	0.74	+	8.13	2.43E-04	1.54E-02
DNA geometric change (GO:0032392)	21	6	0.74	+	8.13	2.43E-04	1.52E-02
cell cycle DNA replication (GO:0044786)	25	7	0.88	+	7.96	8.16E-05	6.10E-03
mismatch repair (GO:0006298)	18	5	0.63	+	7.9	9.04E-04	4.81E-02
branched-chain amino acid biosynthetic process (GO:0009082)	22	6	0.77	+	7.76	3.00E-04	1.80E-02
starch biosynthetic process (GO:0019252)	26	7	0.91	+	7.66	1.01E-04	7.32E-03
DNA methylation (GO:0006306)	46	10	1.62	+	6.18	1.68E-05	1.72E-03
DNA alkylation (GO:0006305)	46	10	1.62	+	6.18	1.68E-05	1.69E-03
nucleosome assembly (GO:0006334)	33	7	1.16	+	6.03	3.57E-04	2.12E-02
double-strand break repair via homologous recombination (GO:0000724)	57	12	2	+	5.99	3.27E-06	4.10E-04
translation (GO:0006412)	562	116	19.76	+	5.87	3.11E-48	1.72E-44
ribosomal large subunit biogenesis (GO:0042273)	39	8	1.37	+	5.83	1.67E-04	1.11E-02

peptide biosynthetic process (GO:0043043)	567	116	19.94	+	5.82	6.79E-48	1.88E-44
recombinational repair (GO:0000725)	59	12	2.07	+	5.78	4.46E-06	5.36E-04
regulation of DNA metabolic process (GO:0051052)	79	16	2.78	+	5.76	1.24E-07	1.81E-05
amide biosynthetic process (GO:0043604)	618	120	21.73	+	5.52	1.67E-47	3.09E-44
starch metabolic process (GO:0005982)	52	10	1.83	+	5.47	4.23E-05	3.59E-03
DNA methylation or demethylation (GO:0044728)	53	10	1.86	+	5.37	4.87E-05	4.02E-03
ribosome assembly (GO:0042255)	48	9	1.69	+	5.33	1.21E-04	8.66E-03
aspartate family amino acid biosynthetic process (GO:0009067)	43	8	1.51	+	5.29	3.00E-04	1.82E-02
DNA modification (GO:0006304)	54	10	1.9	+	5.27	5.60E-05	4.55E-03
peptide metabolic process (GO:0006518)	639	117	22.47	+	5.21	4.65E-44	6.43E-41
DNA recombination (GO:0006310)	123	22	4.32	+	5.09	4.28E-09	6.96E-07
cellular amide metabolic process (GO:0043603)	716	121	25.18	+	4.81	1.94E-42	2.15E-39
double-strand break repair (GO:0006302)	84	14	2.95	+	4.74	5.71E-06	6.71E-04
DNA metabolic process (GO:0006259)	455	74	16	+	4.63	3.26E-25	1.50E-22
DNA conformation change (GO:0071103)	82	13	2.88	+	4.51	1.96E-05	1.94E-03
macromolecule methylation (GO:0043414)	120	19	4.22	+	4.5	2.61E-07	3.61E-05
translational elongation (GO:0006414)	57	9	2	+	4.49	3.78E-04	2.22E-02
ribosome biogenesis (GO:0042254)	266	42	9.35	+	4.49	1.93E-14	3.95E-12
protein-DNA complex assembly (GO:0065004)	64	9	2.25	+	4	8.03E-04	4.31E-02
ribonucleoprotein complex biogenesis (GO:0022613)	310	43	10.9	+	3.94	4.97E-13	9.47E-11
DNA repair (GO:0006281)	257	35	9.04	+	3.87	1.15E-10	1.99E-08
cellular response to DNA damage stimulus (GO:0006974)	286	36	10.06	+	3.58	4.43E-10	7.42E-08
organonitrogen compound biosynthetic process (GO:1901566)	1293	158	45.46	+	3.48	1.18E-39	1.09E-36
alpha-amino acid biosynthetic process (GO:1901607)	176	21	6.19	+	3.39	3.99E-06	4.90E-04
cellular amino acid biosynthetic process (GO:0008652)	198	21	6.96	+	3.02	2.05E-05	1.99E-03
chromosome organization (GO:0051276)	428	41	15.05	+	2.72	4.02E-08	6.17E-06
methylation (GO:0032259)	276	26	9.7	+	2.68	1.55E-05	1.62E-03
alpha-amino acid metabolic process (GO:1901605)	279	25	9.81	+	2.55	7.38E-05	5.59E-03
cellular macromolecular complex assembly (GO:0034622)	302	27	10.62	+	2.54	3.60E-05	3.11E-03
regulation of cell cycle (GO:0051726)	214	19	7.52	+	2.53	4.13E-04	2.40E-02
RNA modification (GO:0009451)	232	20	8.16	+	2.45	5.77E-04	3.26E-02
response to cadmium ion (GO:0046686)	337	29	11.85	+	2.45	2.76E-05	2.59E-03
cell cycle (GO:0007049)	440	35	15.47	+	2.26	2.82E-05	2.52E-03
cellular macromolecule biosynthetic process (GO:0034645)	2721	212	95.67	+	2.22	5.41E-27	3.74E-24

cellular amino acid metabolic process (GO:0006520)	388	30	13.64	+	2.2	1.71E-04	1.13E-02
macromolecule biosynthetic process (GO:0009059)	2772	214	97.47	+	2.2	8.28E-27	4.58E-24
macromolecular complex assembly (GO:0065003)	351	27	12.34	+	2.19	2.85E-04	1.75E-02
organic acid biosynthetic process (GO:0016053)	485	36	17.05	+	2.11	6.86E-05	5.34E-03
carboxylic acid biosynthetic process (GO:0046394)	485	36	17.05	+	2.11	6.86E-05	5.27E-03
cellular component biogenesis (GO:0044085)	944	69	33.19	+	2.08	4.55E-08	6.81E-06
cellular nitrogen compound metabolic process (GO:0034641)	4100	294	144.16	+	2.04	7.80E-33	6.16E-30
cellular nitrogen compound biosynthetic process (GO:0044271)	2763	198	97.15	+	2.04	4.06E-21	1.50E-18
small molecule biosynthetic process (GO:0044283)	599	42	21.06	+	1.99	5.66E-05	4.53E-03
response to metal ion (GO:0010038)	468	32	16.46	+	1.94	6.58E-04	3.64E-02
cellular biosynthetic process (GO:0044249)	4040	275	142.05	+	1.94	7.88E-27	4.84E-24
organic substance biosynthetic process (GO:1901576)	4140	277	145.57	+	1.9	4.75E-26	2.39E-23
organelle organization (GO:0006996)	1197	80	42.09	+	1.9	1.37E-07	1.94E-05
cellular response to stress (GO:0033554)	808	53	28.41	+	1.87	3.34E-05	2.93E-03
gene expression (GO:0010467)	2911	189	102.35	+	1.85	9.65E-16	2.22E-13
biosynthetic process (GO:0009058)	4404	284	154.85	+	1.83	2.09E-24	8.89E-22
cellular protein metabolic process (GO:0044267)	2677	170	94.13	+	1.81	2.22E-13	4.38E-11
cellular macromolecule metabolic process (GO:0044260)	5019	299	176.47	+	1.69	1.06E-20	3.66E-18
protein metabolic process (GO:0019538)	3073	182	108.05	+	1.68	7.90E-12	1.46E-09
organonitrogen compound metabolic process (GO:1901564)	4132	239	145.29	+	1.65	1.47E-14	3.26E-12
cellular component organization or biogenesis (GO:0071840)	2466	141	86.71	+	1.63	3.01E-08	4.76E-06
macromolecule metabolic process (GO:0043170)	6102	342	214.55	+	1.59	5.65E-20	1.64E-17
nitrogen compound metabolic process (GO:0006807)	6785	376	238.57	+	1.58	1.26E-21	4.97E-19
small molecule metabolic process (GO:0044281)	1512	82	53.16	+	1.54	1.99E-04	1.30E-02
primary metabolic process (GO:0044238)	7944	418	279.32	+	1.5	1.38E-20	4.48E-18
nucleic acid metabolic process (GO:0090304)	2876	150	101.12	+	1.48	2.09E-06	2.68E-04
cellular metabolic process (GO:0044237)	8072	420	283.82	+	1.48	1.07E-19	2.97E-17
nucleobase-containing compound metabolic process (GO:0006139)	3268	168	114.91	+	1.46	1.00E-06	1.32E-04
heterocycle metabolic process (GO:0046483)	3566	182	125.38	+	1.45	4.42E-07	5.96E-05

organic substance metabolic process (GO:0071704)	8574	434	301.47	+	1.44	2.17E-18	5.71E-16
cellular component organization (GO:0016043)	2211	109	77.74	+	1.4	5.13E-04	2.92E-02
organic cyclic compound metabolic process (GO:1901360)	3836	187	134.88	+	1.39	6.09E-06	7.02E-04
metabolic process (GO:0008152)	9767	475	343.42	+	1.38	1.85E-17	4.46E-15
cellular aromatic compound metabolic process (GO:0006725)	3706	178	130.31	+	1.37	2.59E-05	2.47E-03
cellular process (GO:0009987)	10706	510	376.43	+	1.35	1.59E-17	4.00E-15
growth (GO:0040007)	433	3	15.22	-	0.2	4.23E-04	2.44E-02
cell growth (GO:0016049)	357	2	12.55	-	0.16	6.28E-04	3.51E-02
vesicle-mediated transport (GO:0016192)	369	0	12.97	-	< 0.01	6.72E-06	7.58E-04

Supplementary Table S4.7 Enrichment analysis of genes in category b10

Analysis Type:	PANTHER Overrepresentation Test (Released 20171205)
Annotation Version and Release Date:	GO Ontology database Released 2018-08-09
Analyzed List:	upload_1 (Arabidopsis thaliana)
Reference List:	Arabidopsis thaliana (all genes in database)
Test Type:	FISHER

GO biological process complete	Arabidopsis thaliana - REFLIST (27502)	upload_1 (1790)	upload_1 (expected)	upload_1 (over/under)	upload_1 (fold Enrichment)	upload_1 (raw P-value)	upload_1 (FDR)
cell-cell junction assembly (GO:0007043)	5	4	0.33	+	12.29	1.37E-03	3.18E-02
cell junction assembly (GO:0034329)	6	4	0.39	+	10.24	2.17E-03	4.54E-02
fruit ripening (GO:0009835)	13	7	0.85	+	8.27	1.20E-04	4.08E-03
positive regulation of leaf development (GO:1905623)	15	6	0.98	+	6.15	1.26E-03	2.97E-02
positive regulation of leaf senescence (GO:1900057)	15	6	0.98	+	6.15	1.26E-03	2.96E-02
lignin catabolic process (GO:0046274)	18	7	1.17	+	5.97	5.69E-04	1.59E-02
phenylpropanoid catabolic process (GO:0046271)	18	7	1.17	+	5.97	5.69E-04	1.58E-02
water transport (GO:0006833)	29	11	1.89	+	5.83	1.91E-05	8.89E-04
fluid transport (GO:0042044)	29	11	1.89	+	5.83	1.91E-05	8.82E-04
brassinosteroid homeostasis (GO:0010268)	30	11	1.95	+	5.63	2.47E-05	1.09E-03
brassinosteroid metabolic process (GO:0016131)	36	13	2.34	+	5.55	5.23E-06	3.19E-04
lignan biosynthetic process (GO:0009807)	17	6	1.11	+	5.42	2.11E-03	4.49E-02
lignan metabolic process (GO:0009806)	17	6	1.11	+	5.42	2.11E-03	4.48E-02
brassinosteroid biosynthetic process (GO:0016132)	30	10	1.95	+	5.12	1.11E-04	3.82E-03
phytosteroid metabolic process (GO:0016128)	39	13	2.54	+	5.12	1.07E-05	5.78E-04
lignin metabolic process (GO:0009808)	88	27	5.73	+	4.71	1.06E-09	1.78E-07
hydrogen peroxide catabolic process (GO:0042744)	95	29	6.18	+	4.69	2.84E-10	5.42E-08

hydrogen peroxide metabolic process (GO:0042743)	102	31	6.64	+	4.67	7.66E-11	1.74E-08
phytosteroid biosynthetic process (GO:0016129)	33	10	2.15	+	4.66	2.12E-04	6.90E-03
antibiotic catabolic process (GO:0017001)	100	30	6.51	+	4.61	2.00E-10	4.08E-08
lignin biosynthetic process (GO:0009809)	64	19	4.17	+	4.56	4.64E-07	3.76E-05
xyloglucan metabolic process (GO:0010411)	55	15	3.58	+	4.19	1.73E-05	8.16E-04
response to chitin (GO:0010200)	137	37	8.92	+	4.15	2.14E-11	6.31E-09
cellular response to salt stress (GO:0071472)	34	9	2.21	+	4.07	9.89E-04	2.42E-02
hemicellulose metabolic process (GO:0010410)	100	26	6.51	+	3.99	3.76E-08	3.90E-06
auxin polar transport (GO:0009926)	77	20	5.01	+	3.99	1.38E-06	1.02E-04
phenylpropanoid metabolic process (GO:0009698)	162	41	10.54	+	3.89	1.03E-11	3.38E-09
phenylpropanoid biosynthetic process (GO:0009699)	123	31	8.01	+	3.87	3.59E-09	5.44E-07
reactive oxygen species metabolic process (GO:0072593)	133	33	8.66	+	3.81	1.59E-09	2.61E-07
cellular response to osmotic stress (GO:0071470)	45	11	2.93	+	3.76	4.99E-04	1.43E-02
cell wall polysaccharide metabolic process (GO:0010383)	128	31	8.33	+	3.72	8.01E-09	1.08E-06
cofactor catabolic process (GO:0051187)	122	29	7.94	+	3.65	3.41E-08	3.60E-06
xylan metabolic process (GO:0045491)	47	11	3.06	+	3.6	6.83E-04	1.82E-02
auxin transport (GO:0060918)	86	20	5.6	+	3.57	5.82E-06	3.47E-04
lipid homeostasis (GO:0055088)	52	12	3.38	+	3.55	4.41E-04	1.27E-02
response to auxin (GO:0009733)	401	91	26.1	+	3.49	1.54E-21	1.52E-18
toxin catabolic process (GO:0009407)	49	11	3.19	+	3.45	9.19E-04	2.26E-02
cellular response to auxin stimulus (GO:0071365)	183	41	11.91	+	3.44	2.55E-10	5.02E-08
secondary metabolite biosynthetic process (GO:0044550)	198	44	12.89	+	3.41	7.16E-11	1.69E-08
hormone transport (GO:0009914)	90	20	5.86	+	3.41	1.04E-05	5.74E-04
cell wall polysaccharide biosynthetic process (GO:0070592)	55	12	3.58	+	3.35	6.80E-04	1.82E-02
hyperosmotic salinity response (GO:0042538)	62	13	4.04	+	3.22	5.73E-04	1.57E-02
secondary metabolic process (GO:0019748)	403	83	26.23	+	3.16	1.46E-17	8.62E-15
negative regulation of defense response (GO:0031348)	54	11	3.51	+	3.13	1.81E-03	3.97E-02
cellular component macromolecule biosynthetic process (GO:0070589)	59	12	3.84	+	3.12	1.16E-03	2.82E-02
cell wall macromolecule biosynthetic process (GO:0044038)	59	12	3.84	+	3.12	1.16E-03	2.81E-02
auxin-activated signaling pathway (GO:0009734)	164	33	10.67	+	3.09	1.26E-07	1.20E-05
antibiotic metabolic process (GO:0016999)	192	38	12.5	+	3.04	2.12E-08	2.46E-06
cell wall macromolecule metabolic process (GO:0044036)	172	34	11.19	+	3.04	1.18E-07	1.14E-05
toxin metabolic process (GO:0009404)	71	14	4.62	+	3.03	6.10E-04	1.66E-02
response to salicylic acid (GO:0009751)	203	38	13.21	+	2.88	7.58E-08	7.72E-06
steroid metabolic process (GO:0008202)	107	20	6.96	+	2.87	8.85E-05	3.15E-03

drug catabolic process (GO:0042737)	248	46	16.14	+	2.85	4.33E-09	6.40E-07
sterol metabolic process (GO:0016125)	77	14	5.01	+	2.79	1.22E-03	2.91E-02
response to drug (GO:0042493)	597	107	38.86	+	2.75	2.14E-18	1.58E-15
cellular response to phosphate starvation (GO:0016036)	73	13	4.75	+	2.74	2.11E-03	4.52E-02
hyperosmotic response (GO:0006972)	73	13	4.75	+	2.74	2.11E-03	4.51E-02
detoxification (GO:0098754)	86	15	5.6	+	2.68	1.20E-03	2.87E-02
response to organonitrogen compound (GO:0010243)	230	40	14.97	+	2.67	2.32E-07	2.08E-05
cellular response to drug (GO:0035690)	95	16	6.18	+	2.59	1.16E-03	2.80E-02
aging (GO:0007568)	161	27	10.48	+	2.58	3.82E-05	1.56E-03
response to antibiotic (GO:0046677)	307	51	19.98	+	2.55	1.97E-08	2.33E-06
cell wall biogenesis (GO:0042546)	215	35	13.99	+	2.5	6.42E-06	3.79E-04
response to wounding (GO:0009611)	216	35	14.06	+	2.49	6.68E-06	3.91E-04
response to oxidative stress (GO:0006979)	459	74	29.87	+	2.48	4.96E-11	1.22E-08
plant organ senescence (GO:0090693)	107	17	6.96	+	2.44	1.85E-03	4.01E-02
plant-type cell wall organization (GO:0009664)	152	24	9.89	+	2.43	2.05E-04	6.72E-03
inorganic anion transport (GO:0015698)	115	18	7.48	+	2.4	1.47E-03	3.37E-02
S-glycoside metabolic process (GO:0016143)	147	23	9.57	+	2.4	3.09E-04	9.36E-03
glucosinolate metabolic process (GO:0019760)	147	23	9.57	+	2.4	3.09E-04	9.31E-03
glycosinolate metabolic process (GO:0019757)	147	23	9.57	+	2.4	3.09E-04	9.27E-03
cell wall organization (GO:0071555)	517	80	33.65	+	2.38	3.69E-11	9.92E-09
response to toxic substance (GO:0009636)	205	31	13.34	+	2.32	5.52E-05	2.10E-03
response to gibberellin (GO:0009739)	154	23	10.02	+	2.29	6.89E-04	1.80E-02
external encapsulating structure organization (GO:0045229)	553	82	35.99	+	2.28	1.46E-10	3.08E-08
cell wall modification (GO:0042545)	162	24	10.54	+	2.28	5.40E-04	1.51E-02
cellular response to starvation (GO:0009267)	149	22	9.7	+	2.27	1.02E-03	2.48E-02
regulation of hormone levels (GO:0010817)	408	60	26.56	+	2.26	8.13E-08	8.14E-06
organic hydroxy compound metabolic process (GO:1901615)	288	42	18.74	+	2.24	7.29E-06	4.22E-04
response to nitrogen compound (GO:1901698)	350	51	22.78	+	2.24	8.18E-07	6.28E-05
response to water (GO:0009415)	346	50	22.52	+	2.22	1.25E-06	9.31E-05
cell wall organization or biogenesis (GO:0071554)	686	98	44.65	+	2.19	2.09E-11	6.48E-09
organic hydroxy compound biosynthetic process (GO:1901617)	175	25	11.39	+	2.19	8.61E-04	2.17E-02
plant-type cell wall organization or biogenesis (GO:0071669)	268	38	17.44	+	2.18	3.30E-05	1.41E-03
response to water deprivation (GO:0009414)	339	48	22.06	+	2.18	3.08E-06	2.02E-04
cellular response to extracellular stimulus (GO:0031668)	205	29	13.34	+	2.17	2.87E-04	8.79E-03
hormone metabolic process (GO:0042445)	259	36	16.86	+	2.14	7.34E-05	2.69E-03
lipid transport (GO:0006869)	209	29	13.6	+	2.13	3.57E-04	1.06E-02
cellular response to external stimulus (GO:0071496)	209	29	13.6	+	2.13	3.57E-04	1.05E-02

defense response, incompatible interaction (GO:0009814)	166	23	10.8	+	2.13	1.85E-03	4.02E-02
response to organic cyclic compound (GO:0014070)	390	53	25.38	+	2.09	3.05E-06	2.03E-04
response to jasmonic acid (GO:0009753)	214	29	13.93	+	2.08	6.17E-04	1.67E-02
cellular response to nutrient levels (GO:0031669)	170	23	11.06	+	2.08	2.15E-03	4.53E-02
cellular polysaccharide metabolic process (GO:0044264)	259	35	16.86	+	2.08	1.86E-04	6.15E-03
response to hormone (GO:0009725)	1721	232	112.01	+	2.07	2.85E-23	4.21E-20
response to osmotic stress (GO:0006970)	654	88	42.57	+	2.07	3.37E-09	5.23E-07
response to endogenous stimulus (GO:0009719)	1738	233	113.12	+	2.06	4.43E-23	5.24E-20
response to ethylene (GO:0009723)	306	41	19.92	+	2.06	6.03E-05	2.25E-03
developmental growth involved in morphogenesis (GO:0060560)	317	42	20.63	+	2.04	5.33E-05	2.06E-03
anion transport (GO:0006820)	303	40	19.72	+	2.03	9.18E-05	3.23E-03
response to salt stress (GO:0009651)	581	76	37.82	+	2.01	9.19E-08	9.05E-06
oxidation-reduction process (GO:0055114)	1429	185	93.01	+	1.99	6.94E-17	3.41E-14
response to organic substance (GO:0010033)	2055	265	133.75	+	1.98	4.34E-24	8.55E-21
cell growth (GO:0016049)	357	46	23.24	+	1.98	5.41E-05	2.07E-03
unidimensional cell growth (GO:0009826)	273	35	17.77	+	1.97	4.36E-04	1.27E-02
response to extracellular stimulus (GO:0009991)	250	32	16.27	+	1.97	6.78E-04	1.82E-02
response to acid chemical (GO:0001101)	1196	153	77.84	+	1.97	1.09E-13	4.59E-11
defense response to bacterium (GO:0042742)	388	49	25.25	+	1.94	4.56E-05	1.81E-03
lipid localization (GO:0010876)	238	30	15.49	+	1.94	1.25E-03	2.96E-02
response to oxygen-containing compound (GO:1901700)	1605	202	104.46	+	1.93	2.56E-17	1.37E-14
developmental growth (GO:0048589)	366	46	23.82	+	1.93	1.03E-04	3.60E-03
polysaccharide metabolic process (GO:0005976)	457	57	29.74	+	1.92	1.52E-05	7.36E-04
root morphogenesis (GO:0010015)	249	31	16.21	+	1.91	1.49E-03	3.39E-02
response to bacterium (GO:0009617)	487	60	31.7	+	1.89	1.22E-05	6.07E-04
cellular response to hormone stimulus (GO:0032870)	860	105	55.97	+	1.88	9.78E-09	1.20E-06
intracellular signal transduction (GO:0035556)	607	74	39.51	+	1.87	1.47E-06	1.07E-04
growth (GO:0040007)	411	50	26.75	+	1.87	7.88E-05	2.85E-03
cellular response to endogenous stimulus (GO:0071495)	877	106	57.08	+	1.86	1.34E-08	1.61E-06
response to chemical (GO:0042221)	2895	347	188.42	+	1.84	1.55E-26	4.58E-23
response to lipid (GO:0033993)	778	93	50.64	+	1.84	1.76E-07	1.60E-05
response to abscisic acid (GO:0009737)	572	68	37.23	+	1.83	1.17E-05	5.86E-04
response to alcohol (GO:0097305)	576	68	37.49	+	1.81	1.25E-05	6.16E-04
hormone-mediated signaling pathway (GO:0009755)	750	88	48.81	+	1.8	7.52E-07	5.92E-05
cell morphogenesis (GO:0000902)	362	41	23.56	+	1.74	1.52E-03	3.46E-02
immune system process (GO:0002376)	367	41	23.89	+	1.72	1.70E-03	3.75E-02
cellular carbohydrate metabolic process (GO:0044262)	389	43	25.32	+	1.7	1.61E-03	3.64E-02

response to inorganic substance (GO:0010035)	929	102	60.47	+	1.69	1.60E-06	1.15E-04
root development (GO:0048364)	467	51	30.4	+	1.68	8.02E-04	2.06E-02
response to biotic stimulus (GO:0009607)	1282	140	83.44	+	1.68	2.14E-08	2.43E-06
root system development (GO:0022622)	469	51	30.53	+	1.67	8.37E-04	2.14E-02
cellular response to organic substance (GO:0071310)	1019	109	66.32	+	1.64	2.34E-06	1.59E-04
response to external biotic stimulus (GO:0043207)	1244	133	80.97	+	1.64	1.36E-07	1.27E-05
response to other organism (GO:0051707)	1244	133	80.97	+	1.64	1.36E-07	1.25E-05
cellular response to chemical stimulus (GO:0070887)	1190	127	77.45	+	1.64	3.49E-07	2.95E-05
defense response (GO:0006952)	1480	156	96.33	+	1.62	2.74E-08	2.99E-06
response to external stimulus (GO:0009605)	1636	172	106.48	+	1.62	6.13E-09	8.43E-07
response to stimulus (GO:0050896)	6214	632	404.45	+	1.56	5.93E-32	3.50E-28
cell communication (GO:0007154)	2003	201	130.37	+	1.54	8.31E-09	1.09E-06
response to abiotic stimulus (GO:0009628)	2076	208	135.12	+	1.54	4.88E-09	6.86E-07
signal transduction (GO:0007165)	1727	171	112.4	+	1.52	2.95E-07	2.56E-05
response to stress (GO:0006950)	3539	347	230.34	+	1.51	7.50E-14	3.41E-11
signaling (GO:0023052)	1756	171	114.29	+	1.5	7.78E-07	6.05E-05
carbohydrate metabolic process (GO:0005975)	1045	101	68.02	+	1.48	2.49E-04	7.94E-03
plant organ development (GO:0099402)	931	89	60.6	+	1.47	8.38E-04	2.13E-02
defense response to other organism (GO:0098542)	944	90	61.44	+	1.46	7.22E-04	1.88E-02
anatomical structure morphogenesis (GO:0009653)	843	80	54.87	+	1.46	1.63E-03	3.66E-02
protein phosphorylation (GO:0006468)	919	87	59.81	+	1.45	1.25E-03	2.97E-02
multi-organism process (GO:0051704)	1761	160	114.62	+	1.4	6.27E-05	2.33E-03
regulation of biological quality (GO:0065008)	1151	104	74.91	+	1.39	1.68E-03	3.74E-02
cellular response to stimulus (GO:0051716)	2711	239	176.45	+	1.35	4.46E-06	2.83E-04
developmental process (GO:0032502)	3220	263	209.58	+	1.25	2.52E-04	7.96E-03
anatomical structure development (GO:0048856)	3039	242	197.8	+	1.22	1.72E-03	3.78E-02
macromolecule metabolic process (GO:0043170)	7023	394	457.1	-	0.86	8.39E-04	2.13E-02
organonitrogen compound metabolic process (GO:1901564)	4849	264	315.6	-	0.84	1.63E-03	3.65E-02
nitrogen compound metabolic process (GO:0006807)	7813	422	508.52	-	0.83	8.45E-06	4.71E-04
protein metabolic process (GO:0019538)	3624	184	235.87	-	0.78	3.25E-04	9.70E-03
cellular component organization or biogenesis (GO:0071840)	3083	154	200.66	-	0.77	5.27E-04	1.48E-02
cellular protein metabolic process (GO:0044267)	3237	160	210.68	-	0.76	2.16E-04	7.00E-03
heterocycle metabolic process (GO:0046483)	4029	194	262.23	-	0.74	5.20E-06	3.20E-04
gene expression (GO:0010467)	3120	150	203.07	-	0.74	7.61E-05	2.77E-03
nucleic acid metabolic process (GO:0090304)	3235	155	210.55	-	0.74	4.40E-05	1.76E-03
nucleobase-containing compound metabolic process (GO:0006139)	3720	170	242.12	-	0.7	4.62E-07	3.79E-05

cellular nitrogen compound metabolic process (GO:0034641)	4580	207	298.09	-	0.69	4.87E-09	7.02E-07
reproductive process (GO:0022414)	1763	79	114.75	-	0.69	5.13E-04	1.45E-02
reproduction (GO:0000003)	1773	79	115.4	-	0.68	4.38E-04	1.27E-02
reproductive system development (GO:0061458)	1235	54	80.38	-	0.67	2.38E-03	4.92E-02
reproductive structure development (GO:0048608)	1235	54	80.38	-	0.67	2.38E-03	4.91E-02
proteolysis (GO:0006508)	984	37	64.04	-	0.58	4.05E-04	1.19E-02
cellular component biogenesis (GO:0044085)	1208	45	78.62	-	0.57	6.48E-05	2.39E-03
peptide transport (GO:0015833)	797	29	51.87	-	0.56	8.81E-04	2.18E-02
organonitrogen compound biosynthetic process (GO:1901566)	1550	53	100.88	-	0.53	2.33E-07	2.05E-05
nucleobase-containing small molecule metabolic process (GO:0055086)	502	16	32.67	-	0.49	2.17E-03	4.54E-02
protein catabolic process (GO:0030163)	632	20	41.13	-	0.49	4.83E-04	1.39E-02
cell cycle (GO:0007049)	538	17	35.02	-	0.49	1.62E-03	3.65E-02
cellular macromolecule localization (GO:0070727)	675	21	43.93	-	0.48	2.16E-04	6.98E-03
regulation of protein metabolic process (GO:0051246)	488	15	31.76	-	0.47	1.83E-03	3.99E-02
cellular localization (GO:0051641)	901	27	58.64	-	0.46	7.41E-06	4.25E-04
cellular protein localization (GO:0034613)	643	19	41.85	-	0.45	1.48E-04	4.94E-03
protein localization (GO:0008104)	815	24	53.05	-	0.45	1.93E-05	8.86E-04
seed development (GO:0048316)	720	21	46.86	-	0.45	4.80E-05	1.89E-03
intracellular protein transport (GO:0006886)	560	16	36.45	-	0.44	2.90E-04	8.83E-03
nucleotide metabolic process (GO:0009117)	397	11	25.84	-	0.43	2.34E-03	4.86E-02
nucleoside phosphate metabolic process (GO:0006753)	399	11	25.97	-	0.42	1.76E-03	3.86E-02
cell cycle process (GO:0022402)	370	10	24.08	-	0.42	2.39E-03	4.91E-02
cellular macromolecule catabolic process (GO:0044265)	667	18	43.41	-	0.41	3.31E-05	1.41E-03
establishment of protein localization (GO:0045184)	746	20	48.55	-	0.41	7.93E-06	4.50E-04
cellular amide metabolic process (GO:0043603)	807	21	52.52	-	0.4	2.02E-06	1.40E-04
proteolysis involved in cellular protein catabolic process (GO:0051603)	539	14	35.08	-	0.4	1.06E-04	3.70E-03
intracellular transport (GO:0046907)	695	18	45.23	-	0.4	1.12E-05	5.75E-04
establishment of localization in cell (GO:0051649)	736	19	47.9	-	0.4	4.70E-06	2.95E-04
protein transport (GO:0015031)	738	19	48.03	-	0.4	4.75E-06	2.96E-04
cellular protein catabolic process (GO:0044257)	548	14	35.67	-	0.39	8.08E-05	2.91E-03
generation of precursor metabolites and energy (GO:0006091)	363	9	23.63	-	0.38	1.43E-03	3.29E-02
embryo development (GO:0009790)	576	13	37.49	-	0.35	1.12E-05	5.73E-04
modification of morphology or physiology of other organism (GO:0035821)	311	7	20.24	-	0.35	1.96E-03	4.21E-02
peptide metabolic process (GO:0006518)	677	15	44.06	-	0.34	1.12E-06	8.48E-05

regulation of transcription by RNA polymerase II (GO:0006357)	332	7	21.61	-	0.32	5.73E-04	1.58E-02
ribose phosphate metabolic process (GO:0019693)	305	6	19.85	-	0.3	7.47E-04	1.93E-02
embryo development ending in seed dormancy (GO:0009793)	560	11	36.45	-	0.3	2.24E-06	1.54E-04
regulation of reproductive process (GO:2000241)	364	7	23.69	-	0.3	1.72E-04	5.72E-03
ubiquitin-dependent protein catabolic process (GO:0006511)	443	8	28.83	-	0.28	1.56E-05	7.51E-04
cell killing (GO:0001906)	280	5	18.22	-	0.27	6.85E-04	1.82E-02
disruption of cells of other organism (GO:0044364)	280	5	18.22	-	0.27	6.85E-04	1.81E-02
killing of cells of other organism (GO:0031640)	280	5	18.22	-	0.27	6.85E-04	1.80E-02
organophosphate biosynthetic process (GO:0090407)	399	7	25.97	-	0.27	3.65E-05	1.50E-03
modification-dependent protein catabolic process (GO:0019941)	456	8	29.68	-	0.27	8.25E-06	4.64E-04
modification-dependent macromolecule catabolic process (GO:0043632)	467	8	30.4	-	0.26	4.26E-06	2.73E-04
organelle organization (GO:0006996)	1605	27	104.46	-	0.26	3.30E-19	2.79E-16
cellular component assembly (GO:0022607)	725	11	47.19	-	0.23	1.06E-09	1.84E-07
positive regulation of transcription by RNA polymerase II (GO:0045944)	204	3	13.28	-	0.23	1.96E-03	4.22E-02
mRNA metabolic process (GO:0016071)	479	7	31.18	-	0.22	7.33E-07	5.85E-05
plastid organization (GO:0009657)	275	4	17.9	-	0.22	2.23E-04	7.17E-03
purine-containing compound metabolic process (GO:0072521)	287	4	18.68	-	0.21	1.14E-04	3.91E-03
protein localization to organelle (GO:0033365)	291	4	18.94	-	0.21	1.17E-04	4.00E-03
photosynthesis (GO:0015979)	232	3	15.1	-	0.2	5.11E-04	1.45E-02
peptidyl-amino acid modification (GO:0018193)	318	4	20.7	-	0.19	3.04E-05	1.32E-03
nucleotide biosynthetic process (GO:0009165)	244	3	15.88	-	0.19	2.54E-04	7.99E-03
nucleoside phosphate biosynthetic process (GO:1901293)	246	3	16.01	-	0.19	2.59E-04	8.11E-03
establishment of protein localization to organelle (GO:0072594)	247	3	16.08	-	0.19	2.63E-04	8.11E-03
protein-containing complex subunit organization (GO:0043933)	589	7	38.34	-	0.18	2.17E-09	3.46E-07
DNA metabolic process (GO:0006259)	510	6	33.19	-	0.18	2.58E-08	2.87E-06
protein folding (GO:0006457)	257	3	16.73	-	0.18	1.27E-04	4.26E-03
mitotic cell cycle (GO:0000278)	263	3	17.12	-	0.18	8.94E-05	3.16E-03
amide biosynthetic process (GO:0043604)	670	7	43.61	-	0.16	3.28E-11	9.23E-09
DNA repair (GO:0006281)	300	3	19.53	-	0.15	1.62E-05	7.73E-04
protein-containing complex assembly (GO:0065003)	501	5	32.61	-	0.15	9.49E-09	1.19E-06
cellular response to DNA damage stimulus (GO:0006974)	330	3	21.48	-	0.14	2.61E-06	1.76E-04
RNA modification (GO:0009451)	366	3	23.82	-	0.13	2.95E-07	2.52E-05

purine ribonucleotide metabolic process (GO:0009150)	253	2	16.47	-	0.12	3.14E-05	1.35E-03
purine nucleotide metabolic process (GO:0006163)	262	2	17.05	-	0.12	1.47E-05	7.18E-04
ncRNA metabolic process (GO:0034660)	405	3	26.36	-	0.11	3.29E-08	3.53E-06
ribonucleotide metabolic process (GO:0009259)	272	2	17.7	-	0.11	1.04E-05	5.69E-04
DNA replication (GO:0006260)	140	1	9.11	-	0.11	2.36E-03	4.88E-02
translation (GO:0006412)	594	4	38.66	-	0.1	5.47E-12	2.02E-09
DNA recombination (GO:0006310)	149	1	9.7	-	0.1	1.66E-03	3.70E-02
peptide biosynthetic process (GO:0043043)	599	4	38.99	-	0.1	5.92E-12	2.06E-09
nuclear division (GO:0000280)	157	1	10.22	-	0.1	1.18E-03	2.82E-02
nucleoside monophosphate biosynthetic process (GO:0009124)	161	1	10.48	-	0.1	7.78E-04	2.01E-02
ncRNA processing (GO:0034470)	327	2	21.28	-	0.09	3.65E-07	3.03E-05
chromosome organization (GO:0051276)	526	3	34.24	-	0.09	4.30E-11	1.10E-08
purine-containing compound biosynthetic process (GO:0072522)	180	1	11.72	-	0.09	2.52E-04	8.00E-03
organelle fission (GO:0048285)	201	1	13.08	-	0.08	8.34E-05	2.98E-03
nucleoside monophosphate metabolic process (GO:0009123)	213	1	13.86	-	0.07	3.86E-05	1.55E-03
cellular protein-containing complex assembly (GO:0034622)	443	2	28.83	-	0.07	4.11E-10	7.35E-08
RNA splicing (GO:0008380)	267	1	17.38	-	0.06	1.97E-06	1.39E-04
chromatin organization (GO:0006325)	355	1	23.11	-	0.04	8.80E-09	1.13E-06
RNA processing (GO:0006396)	758	2	49.34	-	0.04	2.32E-18	1.52E-15
ATP metabolic process (GO:0046034)	163	0	10.61	-	< 0.01	5.31E-05	2.08E-03
ribonucleoprotein complex subunit organization (GO:0071826)	176	0	11.46	-	< 0.01	2.40E-05	1.09E-03
protein import (GO:0017038)	136	0	8.85	-	< 0.01	4.15E-04	1.21E-02
histone modification (GO:0016570)	171	0	11.13	-	< 0.01	3.60E-05	1.50E-03
covalent chromatin modification (GO:0016569)	176	0	11.46	-	< 0.01	2.40E-05	1.08E-03
ATP biosynthetic process (GO:0006754)	112	0	7.29	-	< 0.01	2.13E-03	4.49E-02
ribonucleotide biosynthetic process (GO:0009260)	187	0	12.17	-	< 0.01	1.76E-05	8.23E-04
purine ribonucleoside triphosphate biosynthetic process (GO:0009206)	119	0	7.75	-	< 0.01	8.69E-04	2.18E-02
purine ribonucleoside triphosphate metabolic process (GO:0009205)	172	0	11.19	-	< 0.01	3.65E-05	1.51E-03
ribonucleoside triphosphate biosynthetic process (GO:0009201)	127	0	8.27	-	< 0.01	5.88E-04	1.61E-02
mitochondrion organization (GO:0007005)	167	0	10.87	-	< 0.01	5.59E-05	2.12E-03
ribonucleoside triphosphate metabolic process (GO:0009199)	180	0	11.72	-	< 0.01	2.55E-05	1.12E-03
purine ribonucleoside monophosphate biosynthetic process (GO:0009168)	139	0	9.05	-	< 0.01	2.63E-04	8.18E-03
purine ribonucleoside monophosphate metabolic process (GO:0009167)	190	0	12.37	-	< 0.01	1.09E-05	5.87E-04

ribonucleoside monophosphate metabolic process (GO:0009161)	206	0	13.41	-	< 0.01	5.36E-06	3.23E-04
ribonucleoside monophosphate biosynthetic process (GO:0009156)	154	0	10.02	-	< 0.01	1.23E-04	4.14E-03
purine ribonucleotide biosynthetic process (GO:0009152)	169	0	11	-	< 0.01	3.57E-05	1.51E-03
purine nucleoside triphosphate biosynthetic process (GO:0009145)	119	0	7.75	-	< 0.01	8.69E-04	2.17E-02
purine nucleoside triphosphate metabolic process (GO:0009144)	175	0	11.39	-	< 0.01	2.40E-05	1.07E-03
nucleoside triphosphate biosynthetic process (GO:0009142)	131	0	8.53	-	< 0.01	6.44E-04	1.74E-02
nucleoside triphosphate metabolic process (GO:0009141)	190	0	12.37	-	< 0.01	1.09E-05	5.82E-04
purine nucleoside monophosphate biosynthetic process (GO:0009127)	139	0	9.05	-	< 0.01	2.63E-04	8.13E-03
purine nucleoside monophosphate metabolic process (GO:0009126)	190	0	12.37	-	< 0.01	1.09E-05	5.76E-04
electron transport chain (GO:0022900)	118	0	7.68	-	< 0.01	1.41E-03	3.26E-02
organelle assembly (GO:0070925)	170	0	11.06	-	< 0.01	3.57E-05	1.50E-03
mRNA processing (GO:0006397)	353	0	22.98	-	< 0.01	3.49E-10	6.43E-08
rRNA processing (GO:0006364)	211	0	13.73	-	< 0.01	3.46E-06	2.25E-04
rRNA metabolic process (GO:0016072)	225	0	14.64	-	< 0.01	1.64E-06	1.17E-04
peptidyl-lysine modification (GO:0018205)	115	0	7.48	-	< 0.01	1.32E-03	3.08E-02
ribosome biogenesis (GO:0042254)	373	0	24.28	-	< 0.01	1.08E-10	2.36E-08
ribonucleoprotein complex assembly (GO:0022618)	167	0	10.87	-	< 0.01	5.59E-05	2.10E-03
ribonucleoprotein complex biogenesis (GO:0022613)	459	0	29.87	-	< 0.01	3.86E-13	1.52E-10
purine nucleotide biosynthetic process (GO:0006164)	175	0	11.39	-	< 0.01	2.40E-05	1.06E-03
ribose phosphate biosynthetic process (GO:0046390)	192	0	12.5	-	< 0.01	1.14E-05	5.73E-04
nuclear transport (GO:0051169)	121	0	7.88	-	< 0.01	8.79E-04	2.19E-02
mRNA splicing, via spliceosome (GO:0000398)	174	0	11.32	-	< 0.01	3.83E-05	1.55E-03
nucleocytoplasmic transport (GO:0006913)	121	0	7.88	-	< 0.01	8.79E-04	2.18E-02
RNA splicing, via transesterification reactions with bulged adenosine as nucleophile (GO:0000377)	191	0	12.43	-	< 0.01	1.11E-05	5.80E-04
RNA splicing, via transesterification reactions (GO:0000375)	191	0	12.43	-	< 0.01	1.11E-05	5.75E-04
regulation of DNA metabolic process (GO:0051052)	117	0	7.62	-	< 0.01	1.37E-03	3.18E-02
macromolecule methylation (GO:0043414)	164	0	10.67	-	< 0.01	5.33E-05	2.07E-03

Supplementary Table S4.8 Enrichment analysis of genes in category b27

Analysis Type:	PANTHER Overrepresentation Test (Released 20171205)
Annotation Version and Release Date:	GO Ontology database Released 2018-02-02
Analyzed List:	upload_1 (Arabidopsis thaliana)
Reference List:	Arabidopsis thaliana (all genes in database)
Test Type:	FISHER

GO biological process complete	Arabidopsis thaliana - REFLIST (27502)	upload_1 (1563)	upload_1 (expected)	upload_1 (over/under)	upload_1 (fold Enrichment)	upload_1 (raw P-value)	upload_1 (FDR)
chloroplast ribulose bisphosphate carboxylase complex biogenesis (GO:0080158)	4	4	0.23	+	17.6	4.90E-04	1.48E-02
plastid translation (GO:0032544)	12	11	0.68	+	16.13	7.80E-09	6.63E-07
photosynthesis, light harvesting in photosystem I (GO:0009768)	23	19	1.31	+	14.54	9.31E-14	1.78E-11
chloroplast rRNA processing (GO:1901259)	10	8	0.57	+	14.08	1.85E-06	9.48E-05
photosynthetic electron transport in photosystem I (GO:0009773)	15	11	0.85	+	12.9	3.83E-08	2.79E-06
plastid transcription (GO:0042793)	10	7	0.57	+	12.32	1.55E-05	6.54E-04
photosynthesis, light harvesting (GO:0009765)	45	31	2.56	+	12.12	6.06E-20	2.24E-17
photosystem II repair (GO:0010206)	15	10	0.85	+	11.73	3.05E-07	1.80E-05
PSII associated light-harvesting complex II catabolic process (GO:0010304)	8	5	0.45	+	11	4.00E-04	1.24E-02
DNA-templated transcription, termination (GO:0006353)	10	6	0.57	+	10.56	1.20E-04	4.37E-03
photosynthesis, light harvesting in photosystem II (GO:0009769)	10	6	0.57	+	10.56	1.20E-04	4.34E-03
photosystem II stabilization (GO:0042549)	7	4	0.4	+	10.05	2.03E-03	4.75E-02
photosystem I assembly (GO:0048564)	14	8	0.8	+	10.05	1.11E-05	4.89E-04
photosystem II assembly (GO:0010207)	21	12	1.19	+	10.05	6.92E-08	4.84E-06
cytochrome b6f complex assembly (GO:0010190)	7	4	0.4	+	10.05	2.03E-03	4.73E-02
reductive pentose-phosphate cycle (GO:0019253)	16	9	0.91	+	9.9	3.42E-06	1.65E-04
chloroplast RNA processing (GO:0031425)	20	11	1.14	+	9.68	3.27E-07	1.91E-05
photosynthesis, light reaction (GO:0019684)	120	65	6.82	+	9.53	1.21E-35	3.34E-32
photosynthesis, dark reaction (GO:0019685)	17	9	0.97	+	9.32	4.99E-06	2.32E-04
chlorophyll biosynthetic process (GO:0015995)	40	21	2.27	+	9.24	2.95E-12	4.08E-10
photosynthesis (GO:0015979)	216	113	12.28	+	9.21	4.36E-60	2.41E-56
energy quenching (GO:1990066)	10	5	0.57	+	8.8	8.52E-04	2.37E-02
negative regulation of photosynthesis, light reaction (GO:0043155)	14	7	0.8	+	8.8	7.65E-05	2.84E-03
chromosome condensation (GO:0030261)	10	5	0.57	+	8.8	8.52E-04	2.36E-02

regulation of shoot apical meristem development (GO:1902183)	10	5	0.57	+	8.8	8.52E-04	2.34E-02
guard mother cell differentiation (GO:0010444)	10	5	0.57	+	8.8	8.52E-04	2.33E-02
photoinhibition (GO:0010205)	14	7	0.8	+	8.8	7.65E-05	2.82E-03
nonphotochemical quenching (GO:0010196)	10	5	0.57	+	8.8	8.52E-04	2.32E-02
response to low light intensity stimulus (GO:0009645)	18	9	1.02	+	8.8	7.12E-06	3.20E-04
chlorophyll metabolic process (GO:0015994)	58	28	3.3	+	8.49	3.69E-15	8.51E-13
chloroplast RNA modification (GO:1900865)	17	8	0.97	+	8.28	3.26E-05	1.34E-03
tetrapyrrole biosynthetic process (GO:0033014)	51	24	2.9	+	8.28	5.22E-13	8.75E-11
negative regulation of photosynthesis (GO:1905156)	17	8	0.97	+	8.28	3.26E-05	1.33E-03
porphyrin-containing compound biosynthetic process (GO:0006779)	47	22	2.67	+	8.24	5.25E-12	6.92E-10
Group II intron splicing (GO:0000373)	18	8	1.02	+	7.82	4.49E-05	1.72E-03
regulation of photosynthesis, light reaction (GO:0042548)	25	11	1.42	+	7.74	1.81E-06	9.36E-05
tetrapyrrole metabolic process (GO:0033013)	72	31	4.09	+	7.58	1.51E-15	3.64E-13
porphyrin-containing compound metabolic process (GO:0006778)	70	30	3.98	+	7.54	4.76E-15	1.05E-12
carbon fixation (GO:0015977)	21	9	1.19	+	7.54	1.88E-05	7.81E-04
photosynthetic electron transport chain (GO:0009767)	42	18	2.39	+	7.54	1.37E-09	1.30E-07
protein-chromophore linkage (GO:0018298)	38	16	2.16	+	7.41	1.37E-08	1.08E-06
regulation of ubiquitin protein ligase activity (GO:1904666)	12	5	0.68	+	7.33	1.60E-03	3.93E-02
meiotic chromosome separation (GO:0051307)	12	5	0.68	+	7.33	1.60E-03	3.91E-02
protein import into chloroplast stroma (GO:0045037)	17	7	0.97	+	7.25	1.98E-04	6.50E-03
protein targeting to chloroplast (GO:0045036)	34	14	1.93	+	7.25	1.37E-07	9.13E-06
establishment of protein localization to chloroplast (GO:0072596)	34	14	1.93	+	7.25	1.37E-07	9.02E-06
anthocyanin-containing compound biosynthetic process (GO:0009718)	17	7	0.97	+	7.25	1.98E-04	6.47E-03
protoporphyrinogen IX biosynthetic process (GO:0006782)	15	6	0.85	+	7.04	6.46E-04	1.90E-02
'de novo' protein folding (GO:0006458)	15	6	0.85	+	7.04	6.46E-04	1.89E-02

protoporphyrinogen IX metabolic process (GO:0046501)	15	6	0.85	+	7.04	6.46E-04	1.88E-02
regulation of generation of precursor metabolites and energy (GO:0043467)	28	11	1.59	+	6.91	4.35E-06	2.04E-04
protein localization to chloroplast (GO:0072598)	36	14	2.05	+	6.84	2.41E-07	1.50E-05
chloroplast organization (GO:0009658)	160	62	9.09	+	6.82	1.08E-27	8.51E-25
regulation of ubiquitin-protein transferase activity (GO:0051438)	13	5	0.74	+	6.77	2.12E-03	4.90E-02
protein repair (GO:0030091)	26	10	1.48	+	6.77	1.38E-05	5.87E-04
regulation of photosynthesis (GO:0010109)	41	15	2.33	+	6.44	1.71E-07	1.10E-05
plastid organization (GO:0009657)	216	79	12.28	+	6.44	1.49E-33	2.06E-30
anthocyanin-containing compound metabolic process (GO:0046283)	23	8	1.31	+	6.12	1.78E-04	5.94E-03
thylakoid membrane organization (GO:0010027)	41	14	2.33	+	6.01	8.68E-07	4.85E-05
pigment biosynthetic process (GO:0046148)	108	36	6.14	+	5.87	5.29E-15	1.12E-12
chloroplast fission (GO:0010020)	18	6	1.02	+	5.87	1.39E-03	3.55E-02
plastid membrane organization (GO:0009668)	43	14	2.44	+	5.73	1.39E-06	7.44E-05
pigment metabolic process (GO:0042440)	130	42	7.39	+	5.68	7.25E-17	1.82E-14
stomatal complex development (GO:0010374)	44	14	2.5	+	5.6	1.74E-06	9.06E-05
response to high light intensity (GO:0009644)	79	25	4.49	+	5.57	1.85E-10	2.17E-08
regulation of chlorophyll biosynthetic process (GO:0010380)	19	6	1.08	+	5.56	1.75E-03	4.23E-02
plastid fission (GO:0043572)	19	6	1.08	+	5.56	1.75E-03	4.21E-02
regulation of tetrapyrrole biosynthetic process (GO:1901463)	20	6	1.14	+	5.28	2.18E-03	4.95E-02
chaperone-mediated protein folding (GO:0061077)	27	8	1.53	+	5.21	4.39E-04	1.33E-02
adaxial/abaxial pattern specification (GO:0009955)	32	9	1.82	+	4.95	2.69E-04	8.61E-03
adaxial/abaxial axis specification (GO:0009943)	25	7	1.42	+	4.93	1.32E-03	3.41E-02
stomatal complex morphogenesis (GO:0010103)	25	7	1.42	+	4.93	1.32E-03	3.39E-02
glyceraldehyde-3-phosphate metabolic process (GO:0019682)	40	11	2.27	+	4.84	6.82E-05	2.57E-03
response to red light (GO:0010114)	66	18	3.75	+	4.8	4.10E-07	2.34E-05
glucose metabolic process (GO:0006006)	37	10	2.1	+	4.76	1.64E-04	5.56E-03
regulation of isoprenoid metabolic process (GO:0019747)	26	7	1.48	+	4.74	1.60E-03	3.92E-02
response to blue light (GO:0009637)	77	20	4.38	+	4.57	1.85E-07	1.16E-05
heme metabolic process (GO:0042168)	27	7	1.53	+	4.56	1.92E-03	4.55E-02

RNA secondary structure unwinding (GO:0010501)	27	7	1.53	+	4.56	1.92E-03	4.53E-02
regulation of tetrapyrrole metabolic process (GO:1901401)	27	7	1.53	+	4.56	1.92E-03	4.51E-02
response to far red light (GO:0010218)	58	15	3.3	+	4.55	6.46E-06	2.95E-04
mitochondrial RNA metabolic process (GO:0000959)	47	12	2.67	+	4.49	5.95E-05	2.25E-03
rRNA processing (GO:0006364)	110	28	6.25	+	4.48	1.03E-09	1.08E-07
rRNA metabolic process (GO:0016072)	115	29	6.54	+	4.44	6.29E-10	6.82E-08
response to light intensity (GO:0009642)	148	37	8.41	+	4.4	3.54E-12	4.78E-10
RNA modification (GO:0009451)	232	56	13.19	+	4.25	4.00E-17	1.05E-14
generation of precursor metabolites and energy (GO:0006091)	336	79	19.1	+	4.14	5.18E-23	2.20E-20
axis specification (GO:0009798)	44	10	2.5	+	4	5.38E-04	1.61E-02
mRNA modification (GO:0016556)	46	10	2.61	+	3.83	7.25E-04	2.05E-02
cellular protein complex assembly (GO:0043623)	148	32	8.41	+	3.8	2.27E-09	2.09E-07
electron transport chain (GO:0022900)	98	21	5.57	+	3.77	1.40E-06	7.47E-05
protein complex biogenesis (GO:0070271)	203	40	11.54	+	3.47	2.65E-10	2.99E-08
ribosome biogenesis (GO:0042254)	266	52	15.12	+	3.44	7.45E-13	1.18E-10
ncRNA processing (GO:0034470)	187	35	10.63	+	3.29	1.08E-08	9.03E-07
protein complex assembly (GO:0006461)	197	36	11.2	+	3.22	1.15E-08	9.51E-07
ncRNA metabolic process (GO:0034660)	254	46	14.44	+	3.19	1.45E-10	1.75E-08
cytokinetic process (GO:0032506)	61	11	3.47	+	3.17	1.54E-03	3.89E-02
mitotic cytokinetic process (GO:1902410)	61	11	3.47	+	3.17	1.54E-03	3.87E-02
cytokinesis by cell plate formation (GO:0000911)	61	11	3.47	+	3.17	1.54E-03	3.86E-02
cellular aldehyde metabolic process (GO:0006081)	73	13	4.15	+	3.13	6.65E-04	1.91E-02
flavonoid metabolic process (GO:0009812)	74	13	4.21	+	3.09	7.44E-04	2.09E-02
response to cytokinin (GO:0009735)	236	41	13.41	+	3.06	4.15E-09	3.64E-07
flavonoid biosynthetic process (GO:0009813)	64	11	3.64	+	3.02	2.16E-03	4.93E-02
ribonucleoprotein complex biogenesis (GO:0022613)	310	53	17.62	+	3.01	3.92E-11	4.82E-09
DNA conformation change (GO:0071103)	82	14	4.66	+	3	6.08E-04	1.80E-02
meiotic nuclear division (GO:0140013)	83	14	4.72	+	2.97	6.76E-04	1.93E-02
protein complex subunit organization (GO:0071822)	232	39	13.19	+	2.96	2.17E-08	1.66E-06
regulation of cell proliferation (GO:0042127)	72	12	4.09	+	2.93	1.74E-03	4.23E-02
mitotic cytokinesis (GO:0000281)	87	14	4.94	+	2.83	1.02E-03	2.67E-02
tRNA metabolic process (GO:0006399)	128	20	7.27	+	2.75	1.36E-04	4.81E-03
cytoskeleton-dependent cytokinesis (GO:0061640)	90	14	5.11	+	2.74	1.36E-03	3.47E-02
gynoecium development (GO:0048467)	84	13	4.77	+	2.72	2.06E-03	4.78E-02

response to radiation (GO:0009314)	726	112	41.26	+	2.71	6.31E-19	2.05E-16
mitotic cell cycle process (GO:1903047)	144	22	8.18	+	2.69	8.64E-05	3.16E-03
mitotic cell cycle (GO:0000278)	165	25	9.38	+	2.67	3.33E-05	1.34E-03
pattern specification process (GO:0007389)	172	26	9.78	+	2.66	2.42E-05	1.00E-03
RNA processing (GO:0006396)	583	88	33.13	+	2.66	1.16E-14	2.28E-12
response to light stimulus (GO:0009416)	699	105	39.73	+	2.64	3.19E-17	8.81E-15
nuclear division (GO:0000280)	114	17	6.48	+	2.62	6.72E-04	1.93E-02
cellular macromolecular complex assembly (GO:0034622)	302	45	17.16	+	2.62	5.04E-08	3.62E-06
meiotic cell cycle (GO:0051321)	141	21	8.01	+	2.62	1.70E-04	5.72E-03
regionalization (GO:0003002)	141	21	8.01	+	2.62	1.70E-04	5.69E-03
organelle fission (GO:0048285)	156	23	8.87	+	2.59	1.46E-04	5.12E-03
DNA replication (GO:0006260)	110	16	6.25	+	2.56	1.21E-03	3.15E-02
meiotic cell cycle process (GO:1903046)	117	17	6.65	+	2.56	8.71E-04	2.36E-02
cofactor biosynthetic process (GO:0051188)	234	34	13.3	+	2.56	3.55E-06	1.69E-04
cell division (GO:0051301)	300	43	17.05	+	2.52	3.46E-07	1.99E-05
macromolecular complex assembly (GO:0065003)	351	49	19.95	+	2.46	7.81E-08	5.40E-06
response to red or far red light (GO:0009639)	208	29	11.82	+	2.45	3.45E-05	1.38E-03
cell cycle process (GO:0022402)	282	39	16.03	+	2.43	2.21E-06	1.10E-04
response to cold (GO:0009409)	375	51	21.31	+	2.39	9.95E-08	6.79E-06
cell cycle (GO:0007049)	440	59	25.01	+	2.36	1.66E-08	1.29E-06
translation (GO:0006412)	562	75	31.94	+	2.35	2.00E-10	2.31E-08
macromolecular complex subunit organization (GO:0043933)	399	53	22.68	+	2.34	1.31E-07	8.80E-06
peptide biosynthetic process (GO:0043043)	567	75	32.22	+	2.33	2.68E-10	2.96E-08
shoot system morphogenesis (GO:0010016)	160	21	9.09	+	2.31	1.26E-03	3.28E-02
embryo development ending in seed dormancy (GO:0009793)	548	71	31.14	+	2.28	2.17E-09	2.03E-07
embryo development (GO:0009790)	565	72	32.11	+	2.24	3.77E-09	3.41E-07
amide biosynthetic process (GO:0043604)	618	78	35.12	+	2.22	1.25E-09	1.24E-07
cellular component biogenesis (GO:0044085)	944	116	53.65	+	2.16	3.39E-13	6.05E-11
peptide metabolic process (GO:0006518)	639	78	36.32	+	2.15	3.90E-09	3.48E-07
fruit development (GO:0010154)	734	88	41.71	+	2.11	8.22E-10	8.74E-08
seed development (GO:0048316)	700	83	39.78	+	2.09	4.18E-09	3.61E-07
cellular amide metabolic process (GO:0043603)	716	82	40.69	+	2.02	2.53E-08	1.92E-06
cofactor metabolic process (GO:0051186)	537	61	30.52	+	2	2.14E-06	1.08E-04
cellular component assembly (GO:0022607)	534	60	30.35	+	1.98	3.19E-06	1.56E-04
organelle organization (GO:0006996)	1197	134	68.03	+	1.97	2.60E-12	3.69E-10
response to temperature stimulus (GO:0009266)	545	61	30.97	+	1.97	2.66E-06	1.31E-04
mRNA processing (GO:0006397)	290	32	16.48	+	1.94	1.05E-03	2.74E-02

organonitrogen compound biosynthetic process (GO:1901566)	1293	140	73.48	+	1.91	6.50E-12	8.36E-10
mRNA metabolic process (GO:0016071)	374	40	21.26	+	1.88	3.79E-04	1.18E-02
nucleic acid metabolic process (GO:0090304)	2876	302	163.45	+	1.85	1.05E-23	5.27E-21
heterocycle metabolic process (GO:0046483)	3566	374	202.66	+	1.85	5.00E-30	5.53E-27
cellular nitrogen compound metabolic process (GO:0034641)	4100	428	233.01	+	1.84	1.22E-34	2.24E-31
RNA metabolic process (GO:0016070)	2541	263	144.41	+	1.82	1.05E-19	3.62E-17
DNA metabolic process (GO:0006259)	455	47	25.86	+	1.82	2.81E-04	8.93E-03
cellular aromatic compound metabolic process (GO:0006725)	3706	381	210.62	+	1.81	5.84E-29	5.38E-26
nucleobase-containing compound metabolic process (GO:0006139)	3268	329	185.73	+	1.77	3.00E-23	1.38E-20
reproductive system development (GO:0061458)	1194	119	67.86	+	1.75	2.74E-08	2.05E-06
reproductive structure development (GO:0048608)	1194	119	67.86	+	1.75	2.74E-08	2.02E-06
organic cyclic compound metabolic process (GO:1901360)	3836	380	218.01	+	1.74	4.82E-26	3.33E-23
gene expression (GO:0010467)	2911	285	165.44	+	1.72	2.70E-18	8.31E-16
phyllome development (GO:0048827)	443	43	25.18	+	1.71	1.52E-03	3.86E-02
response to abiotic stimulus (GO:0009628)	1954	189	111.05	+	1.7	9.30E-12	1.17E-09
post-embryonic development (GO:0009791)	1426	137	81.04	+	1.69	1.33E-08	1.06E-06
cellular nitrogen compound biosynthetic process (GO:0044271)	2763	261	157.03	+	1.66	5.74E-15	1.17E-12
cellular component organization or biogenesis (GO:0071840)	2466	231	140.15	+	1.65	7.17E-13	1.17E-10
developmental process involved in reproduction (GO:0003006)	1407	126	79.96	+	1.58	2.16E-06	1.09E-04
shoot system development (GO:0048367)	746	66	42.4	+	1.56	8.72E-04	2.35E-02
reproductive process (GO:0022414)	1637	143	93.03	+	1.54	1.27E-06	6.93E-05
cellular component organization (GO:0016043)	2211	193	125.66	+	1.54	1.29E-08	1.05E-06
reproduction (GO:0000003)	1644	143	93.43	+	1.53	1.71E-06	9.01E-05
cellular macromolecule biosynthetic process (GO:0034645)	2721	234	154.64	+	1.51	1.09E-09	1.12E-07
macromolecule biosynthetic process (GO:0009059)	2772	237	157.54	+	1.5	1.16E-09	1.17E-07
heterocycle biosynthetic process (GO:0018130)	2205	187	125.32	+	1.49	1.73E-07	1.10E-05
organic substance biosynthetic process (GO:1901576)	4140	350	235.29	+	1.49	9.73E-14	1.79E-11
system development (GO:0048731)	1779	149	101.1	+	1.47	6.59E-06	2.99E-04
cellular biosynthetic process (GO:0044249)	4040	337	229.6	+	1.47	1.83E-12	2.74E-10

aromatic compound biosynthetic process (GO:0019438)	2285	190	129.86	+	1.46	4.48E-07	2.53E-05
biosynthetic process (GO:0009058)	4404	365	250.29	+	1.46	3.75E-13	6.48E-11
cellular metabolic process (GO:0044237)	8072	659	458.75	+	1.44	1.60E-25	9.84E-23
regulation of metabolic process (GO:0019222)	3038	246	172.66	+	1.42	5.34E-08	3.79E-06
multicellular organism development (GO:0007275)	2569	207	146	+	1.42	1.06E-06	5.86E-05
regulation of cellular metabolic process (GO:0031323)	2833	228	161.01	+	1.42	2.75E-07	1.64E-05
oxidation-reduction process (GO:0055114)	1331	107	75.64	+	1.41	7.56E-04	2.11E-02
nitrogen compound metabolic process (GO:0006807)	6785	544	385.61	+	1.41	4.59E-18	1.34E-15
organic cyclic compound biosynthetic process (GO:1901362)	2419	193	137.48	+	1.4	5.12E-06	2.36E-04
macromolecule metabolic process (GO:0043170)	6102	471	346.79	+	1.36	1.47E-12	2.26E-10
regulation of nucleobase-containing compound metabolic process (GO:0019219)	2401	185	136.45	+	1.36	5.62E-05	2.14E-03
regulation of macromolecule metabolic process (GO:0060255)	2830	218	160.84	+	1.36	9.76E-06	4.32E-04
regulation of RNA metabolic process (GO:0051252)	2350	181	133.56	+	1.36	7.04E-05	2.63E-03
regulation of primary metabolic process (GO:0080090)	2741	211	155.78	+	1.35	1.60E-05	6.70E-04
metabolic process (GO:0008152)	9767	748	555.08	+	1.35	2.85E-22	1.13E-19
regulation of gene expression (GO:0010468)	2625	201	149.18	+	1.35	3.56E-05	1.40E-03
nucleic acid-templated transcription (GO:0097659)	1780	136	101.16	+	1.34	9.37E-04	2.52E-02
transcription, DNA-templated (GO:0006351)	1780	136	101.16	+	1.34	9.37E-04	2.50E-02
regulation of nitrogen compound metabolic process (GO:0051171)	2686	205	152.65	+	1.34	3.53E-05	1.40E-03
regulation of transcription, DNA-templated (GO:0006355)	2307	176	131.11	+	1.34	1.34E-04	4.77E-03
RNA biosynthetic process (GO:0032774)	1783	136	101.33	+	1.34	9.48E-04	2.52E-02
regulation of RNA biosynthetic process (GO:2001141)	2309	176	131.23	+	1.34	1.60E-04	5.53E-03
regulation of nucleic acid-templated transcription (GO:1903506)	2309	176	131.23	+	1.34	1.60E-04	5.50E-03
cellular process (GO:0009987)	10706	816	608.45	+	1.34	6.17E-25	3.41E-22
nucleobase-containing compound biosynthetic process (GO:0034654)	1992	151	113.21	+	1.33	5.85E-04	1.74E-02
multicellular organismal process (GO:0032501)	2804	212	159.36	+	1.33	4.12E-05	1.62E-03

regulation of biosynthetic process (GO:0009889)	2564	192	145.72	+	1.32	1.87E-04	6.20E-03
regulation of cellular macromolecule biosynthetic process (GO:2000112)	2457	183	139.64	+	1.31	3.42E-04	1.08E-02
regulation of macromolecule biosynthetic process (GO:0010556)	2467	183	140.21	+	1.31	4.16E-04	1.27E-02
anatomical structure development (GO:0048856)	2855	211	162.26	+	1.3	1.61E-04	5.49E-03
regulation of cellular biosynthetic process (GO:0031326)	2542	187	144.47	+	1.29	4.99E-04	1.50E-02
developmental process (GO:0032502)	3057	223	173.74	+	1.28	2.12E-04	6.85E-03
organic substance metabolic process (GO:0071704)	8574	623	487.28	+	1.28	1.99E-12	2.89E-10
primary metabolic process (GO:0044238)	7944	566	451.48	+	1.25	1.28E-09	1.25E-07
cellular macromolecule metabolic process (GO:0044260)	5019	344	285.24	+	1.21	2.56E-04	8.23E-03
regulation of cellular process (GO:0050794)	4465	306	253.76	+	1.21	6.57E-04	1.90E-02
regulation of biological process (GO:0050789)	4949	338	281.26	+	1.2	3.97E-04	1.23E-02
response to stimulus (GO:0050896)	5805	386	329.91	+	1.17	9.50E-04	2.51E-02
biological_process (GO:0008150)	21684	1299	1232.35	+	1.05	4.21E-05	1.64E-03
Unclassified (UNCLASSIFIED)	5818	264	330.65	-	0.8	4.21E-05	1.63E-03
protein modification process (GO:0036211)	1896	76	107.75	-	0.71	1.58E-03	3.92E-02
cellular protein modification process (GO:0006464)	1896	76	107.75	-	0.71	1.58E-03	3.91E-02
organic substance transport (GO:0071702)	1151	38	65.41	-	0.58	3.73E-04	1.17E-02
cellular catabolic process (GO:0044248)	1126	37	63.99	-	0.58	4.15E-04	1.27E-02
proteolysis (GO:0006508)	859	28	48.82	-	0.57	1.88E-03	4.47E-02
nitrogen compound transport (GO:0071705)	874	27	49.67	-	0.54	7.02E-04	1.99E-02
macromolecule catabolic process (GO:0009057)	716	22	40.69	-	0.54	2.15E-03	4.94E-02
response to fungus (GO:0009620)	540	14	30.69	-	0.46	1.58E-03	3.89E-02
cellular macromolecule catabolic process (GO:0044265)	530	11	30.12	-	0.37	1.52E-04	5.29E-03
protein catabolic process (GO:0030163)	470	9	26.71	-	0.34	2.00E-04	6.51E-03
cellular protein catabolic process (GO:0044257)	446	8	25.35	-	0.32	1.38E-04	4.87E-03
response to nitrogen compound (GO:1901698)	297	5	16.88	-	0.3	1.84E-03	4.40E-02
protein ubiquitination (GO:0016567)	519	8	29.5	-	0.27	8.71E-06	3.89E-04
protein modification by small protein conjugation (GO:0032446)	542	8	30.8	-	0.26	3.36E-06	1.63E-04
protein modification by small protein conjugation or removal (GO:0070647)	598	8	33.99	-	0.24	2.41E-07	1.48E-05
modification of morphology or physiology of other organism (GO:0035821)	292	3	16.6	-	0.18	1.33E-04	4.78E-03

vesicle-mediated transport (GO:0016192)	369	3	20.97	-	0.14	4.06E-06	1.92E-04
modification-dependent macromolecule catabolic process (GO:0043632)	387	3	21.99	-	0.14	1.35E-06	7.29E-05
proteolysis involved in cellular protein catabolic process (GO:0051603)	437	3	24.84	-	0.12	1.64E-07	1.07E-05
ubiquitin-dependent protein catabolic process (GO:0006511)	380	2	21.6	-	0.09	2.72E-07	1.65E-05
modification-dependent protein catabolic process (GO:0019941)	381	2	21.65	-	0.09	2.74E-07	1.65E-05
cell killing (GO:0001906)	261	1	14.83	-	0.07	1.29E-05	5.61E-04
disruption of cells of other organism (GO:0044364)	261	1	14.83	-	0.07	1.29E-05	5.57E-04
killing of cells of other organism (GO:0031640)	261	1	14.83	-	0.07	1.29E-05	5.53E-04
nucleobase-containing compound transport (GO:0015931)	123	0	6.99	-	< 0.01	2.03E-03	4.71E-02

Supplementary Table S4.9 Enrichment analysis of genes in category b1

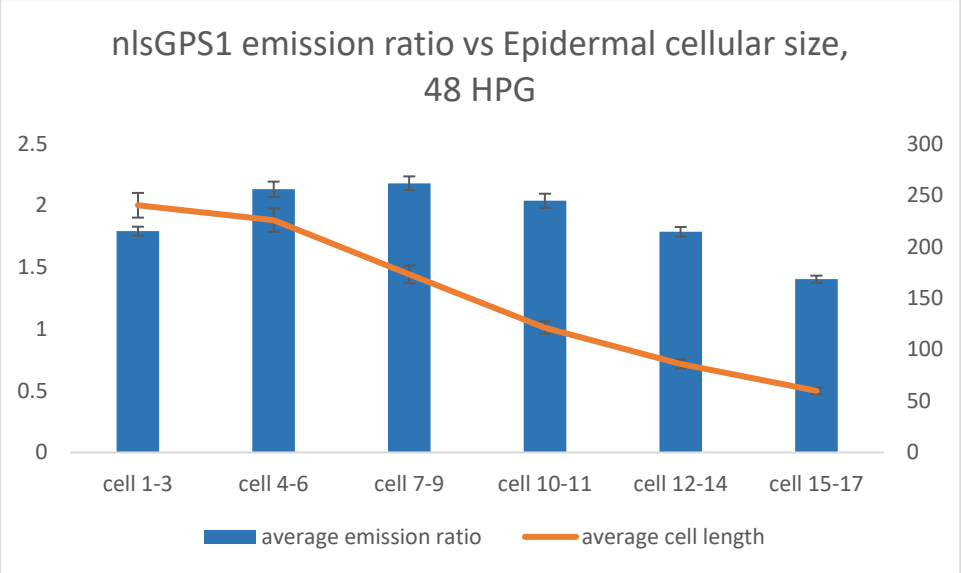

Supplementary S5.1. At 48 HPG, the nlsGPS1 emission ratio was peaked at hypocotyl region with epidermal cell 7-9, but those cells were not the largest in size. Hence the emission ratio and cellular size were unlikely to be correlated.

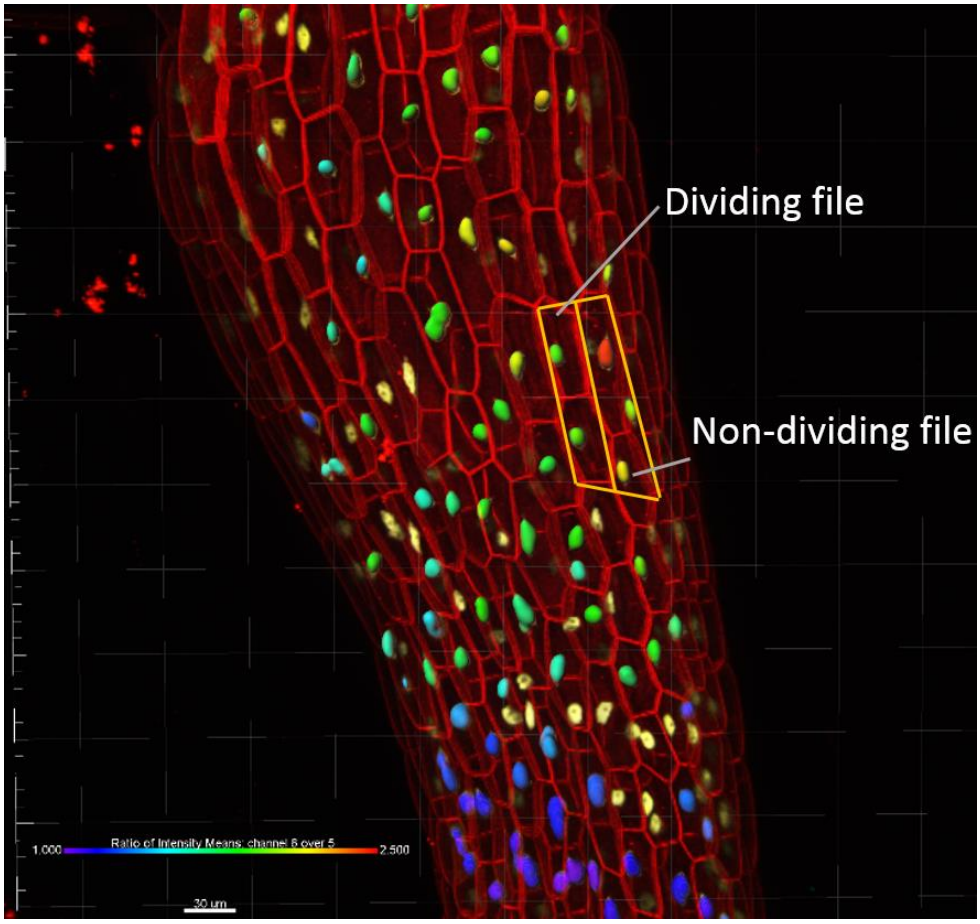

Supplementary S5.2. At 24 HPG, the nlsGPS1 emission ratio along the dark-grown hypocotyl has a gradient, the colour bar represents level of the emission ratio, and bar=30μm. From the picture, the non-dividing cells appear to have higher emission ratio (not quantified)

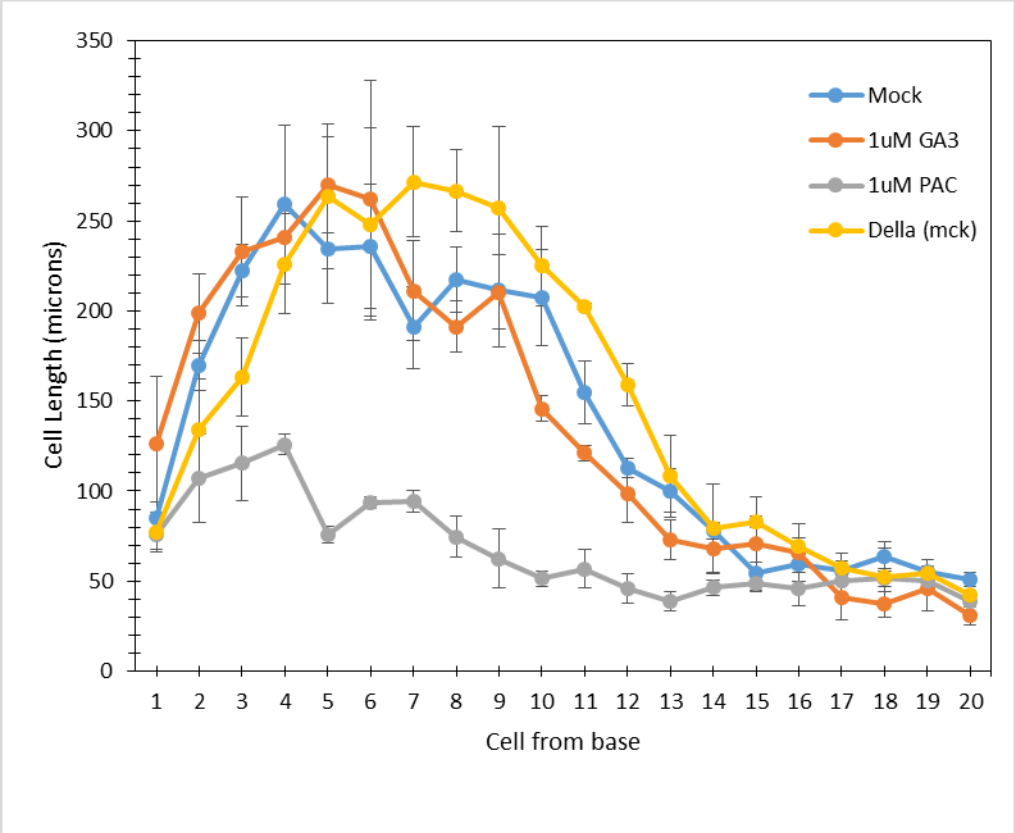

Supplementary S5.3. Cell length over cell indices at 48HPG, like the mock (col-0), the DELLA mutant show heterogeneous cell sizes (Siobhan Braybrook, UCLA, personal communication, Fig. S5.3)